FINAL REPORT ~ FHWA-OK-19-08

COMPILATION OF LOCAL STUDIES AND REGIONAL CALIBRATION OF PAVEMENT ME DESIGN FOR RIGID AND FLEXIBLE PAVEMENTS IN OKLAHOMA

Maryam S. Sakhaeifar, Ph.D.
Mahmood Tabesh, Graduate Research Assistant
Robert Lytton, Ph.D., P.E., D.GE, F. ASCE
Dan Zollinger, Ph.D., P.E.

Zachry Department of Civil Engineering
Texas A&M University

David Newcomb, Ph.D. P.E.
Isaa Mahmoud Issa, Graduate Research Assistant

Texas A&M Transportation Institute

College Station, Texas

November 2019

OKLAHOMA
Transportation

The Oklahoma Department of Transportation (ODOT) ensures that no person or groups of persons shall, on the grounds of race, color, sex, religion, national origin, age, disability, retaliation or genetic information, be excluded from participation in, be denied the benefits of, or be otherwise subjected to discrimination under any and all programs, services, or activities administered by ODOT, its recipients, sub-recipients, and contractors. To request an accommodation please contact the ADA Coordinator at 405-521-4140 or the Oklahoma Relay Service at 1-800-722-0353. If you have any ADA or Title VI questions email ODOT-ada-titlevi@odot.org.

COMPILATION OF LOCAL STUDIES AND REGIONAL CALIBRATION OF PAVEMENT ME DESIGN FOR RIGID AND FLEXIBLE PAVEMENTS IN OKLAHOMA

FINAL REPORT ~ FHWA-OK-19-08
ODOT SPR ITEM NUMBER 2277

Submitted to:
Office of Research and Implementation
Oklahoma Department of Transportation

Submitted by:
Maryam S. Sakhaeifar, Ph.D. [1]
Assistant Professor

Mahmood Tabesh [1]
Graduate Research Assistant

David Newcomb, Ph.D. P.E. [2]
Senior Research Scientist

Robert Lytton, Ph.D., P.E., D.GE, F. ASCE [1]
Professor

Dan Zollinger, Ph.D., P.E. [1]
Professor

Isaa Mahmoud Issa [2]
Graduate Research Assistant

[1]Texas A&M University
[2]Texas A&M Transportation Institute

OKLAHOMA
Transportation

November 2019

TECHNICAL REPORT DOCUMENTATION PAGE

1. REPORT NO. FHWA-OK-2277	2. GOVERNMENT ACCESSION NO.	3. RECIPIENT'S CATALOG NO.
4. TITLE AND SUBTITLE Compilation of Local Studies and Regional Calibration of Pavement ME design for Rigid and Flexible Pavements in Oklahoma		5. REPORT DATE Nov 2019 6. PERFORMING ORGANIZATION CODE
7. AUTHOR(S) Maryam S. Sakhaeifar, Mahmood Tabesh, David Newcomb, Robert Lytton , Dan Zollinger, Isaa Mahmoud Issa		8. PERFORMING ORGANIZATION REPORT
9. PERFORMING ORGANIZATION NAME AND ADDRESS Texas A&M University, Zachry Department of Civil Engineering, 3136 TAMU, College Station, TX 77843-3136		10. WORK UNIT NO. 11. CONTRACT OR GRANT NO. ODOT SPR Item Number 2277
12. SPONSORING AGENCY NAME AND ADDRESS Oklahoma Department of Transportation Office of Research and Implementation 200 N.E. 21st Street, Room G18 Oklahoma City, OK 73105		13. TYPE OF REPORT AND PERIOD COVERED Final Report Example: May 2017 – Nov 2019 14. SPONSORING AGENCY CODE
15. SUPPLEMENTARY NOTES		

16. ABSTRACT

The AASHTOWare Pavement ME Design software was developed as an advanced pavement design tool based on the mechanistic-empirical pavement design guide (MEPDG). The existing performance prediction models utilized in this design guide are nationally calibrated, and it is essential to calibrate these models based on the specific regional materials and environmental conditions and pavement performance information. In this study, the Pavement ME design prediction models were calibrated using local inputs and performance data for the state of Oklahoma. Also, to facilitate using Pavement ME, an interface software named INput ME was developed. This software can be used to process and compile the required pavement ME input data based on the Oklahoma material, traffic, and climate properties gathered from long term pavement performance and Oklahoma and national cooperative highway research program datasets. The material input data were evaluated, and the most accurate available data was selected. The predictions from distress and international roughness index (IRI) models were evaluated and compared with the measured distress values, and the accuracy and bias of each model were determined. The nationally calibrated models showed large errors and significant bias values, which asserts the need for local calibration. The locally calibrated coefficients for the distress and IRI models for the Oklahoma pavement system were determined. The predictions from calibrated models show that the use of calibrated coefficients improves the accuracy of the pavement ME predictions and the design of flexible pavements in Oklahoma.

17. KEY WORDS	18. DISTRIBUTION STATEMENT		
AASHTOWare Pavement ME Design, local calibration, Material Database, Flexible Pavement, Rigid Pavement	No restrictions. This publication is available from the Office of Research and Implementation, Oklahoma DOT.		
19. SECURITY CLASSIF. (OF THIS REPORT) Unclassified	20. SECURITY CLASSIF. (OF THIS PAGE) Unclassified	21. NO. OF PAGES 186	22. PRICE N/A

Form DOT F 1700.7 (08/72)

SI* (MODERN METRIC) CONVERSION FACTORS

APPROXIMATE CONVERSIONS TO SI UNITS

SYMBOL	WHEN YOU KNOW	MULTIPLY BY	TO FIND	SYMBOL
		LENGTH		
in	inches	25.4	millimeters	mm
ft	feet	0.305	meters	m
yd	yards	0.914	meters	m
mi	miles	1.61	kilometers	km
		AREA		
in^2	square inches	645.2	square millimeters	mm^2
ft^2	square feet	0.093	square meters	m^2
yd^2	square yard	0.836	square meters	m^2
ac	acres	0.405	hectares	ha
mi^2	square miles	2.59	square kilometers	km^2
		VOLUME		
fl oz	fluid ounces	29.57	milliliters	mL
gal	gallons	3.785	liters	L
ft^3	cubic feet	0.028	cubic meters	m^3
yd^3	cubic yards	0.765	cubic meters	m^3
		NOTE: volumes greater than 1000 L shall be shown in m^3		
		MASS		
oz	ounces	28.35	grams	g
lb	pounds	0.454	kilograms	kg
T	short tons (2000 lb)	0.907	megagrams (or "metric ton")	Mg (or "t")
		TEMPERATURE (exact degrees)		
°F	Fahrenheit	5 (F-32)/9 or (F-32)/1.8	Celsius	°C
		ILLUMINATION		
fc	foot-candles	10.76	lux	lx
fl	foot-Lamberts	3.426	$candela/m^2$	cd/m^2
		FORCE and PRESSURE or STRESS		
lbf	poundforce	4.45	newtons	N
lbf/in^2	poundforce per square inch	6.89	kilopascals	kPa

APPROXIMATE CONVERSIONS FROM SI UNITS

SYMBOL	WHEN YOU KNOW	MULTIPLY BY	TO FIND	SYMBOL
		LENGTH		
mm	millimeters	0.039	inches	in
m	meters	3.28	feet	ft
m	meters	1.09	yards	yd
km	kilometers	0.621	miles	mi
		AREA		
mm^2	square millimeters	0.0016	square inches	in^2
m^2	square meters	10.764	square feet	ft^2
m^2	square meters	1.195	square yards	yd^2
ha	hectares	2.47	acres	ac
km^2	square kilometers	0.386	square miles	mi^2
		VOLUME		
mL	milliliters	0.034	fluid ounces	fl oz
L	liters	0.264	gallons	gal
m^3	cubic meters	35.314	cubic feet	ft^3
m^3	cubic meters	1.307	cubic yards	yd^3
		MASS		
g	grams	0.035	ounces	oz
kg	kilograms	2.202	pounds	lb
Mg (or "t")	megagrams (or "metric ton")	1.103	short tons (2000 lb)	T
		TEMPERATURE (exact degrees)		
°C	Celsius	1.8C+32	Fahrenheit	°F
		ILLUMINATION		
lx	lux	0.0929	foot-candles	fc
cd/m^2	$candela/m^2$	0.2919	foot-Lamberts	fl
		FORCE and PRESSURE or STRESS		
N	newtons	0.225	poundforce	lbf
kPa	kilopascals	0.145	poundforce per square inch	lbf/in^2

*SI is the symbol for the International System of Units. Appropriate rounding should be made to comply with Section 4 of ASTM E380. (Revised March 2003)

Table of Contents

Table of Figures

List of Tables

EXECUTIVE SUMMARY

Pavement Mechanistic-Empirical (ME) design is one of the AAHSHTOWare Design software which has been built to design new and rehabilitated pavement with a flexible, rigid, and composite structure. The performance prediction models in Pavement ME were calibrated and validated using performance data from hundreds of pavement sections across the nation. However, nationally calibrated performance models in Pavement ME do not precisely reflect local pavement performance. Many state agencies are trying to improve the software outcomes by implementing different local materials, construction, climate, and traffic characteristics in evaluating and calibrating the performance models. To reach this goal, a comprehensive study of all input modulus was conducted, and initial properties required for all pavement layers to execute the AASHTOWare Pavement ME design were determined in this study. The tests and experimental methods required in providing level 1 for hot mix asphalt (HMA) material, unbound material, and bedrock properties were presented. Level 2 predictive models provided for material inputs of Pavement ME for the state of Oklahoma were gathered, and the performance was evaluated. In addition, appropriate level 3 data values for each input were determined.

In this study, the Pavement ME design prediction models were calibrated using local inputs and performance data for the state of Oklahoma. A total number of 66 sections from Long-term pavement performance (LTPP) and few more asphalt pavement sections in Oklahoma were identified for the purpose of this project. The selected projects are representatives of Oklahoma's flexible pavement construction practices and include various pavement conditions, construction age, and environmental conditions. The material, structural, and traffic data were gathered from LTPP, Oklahoma, and national cooperative highway research program (NCHRP) datasets. The material input data were evaluated, and the most accurate available date was selected. The prediction models were used to estimate level 2 and 3 material properties to generate the database.

After reviewing the input data and running a sensitivity analysis for each parameter, a master input database was developed. For each section, the Pavement ME design analysis was conducted. The predicted distresses, and international roughness index (IRI) models were evaluated and compared with the measured distress values, and the accuracy and bias of each model were determined.

The nationally calibrated models show an improper performance and a significant bias, which asserts the need for local calibration. The rutting and IRI models show better performance compared to fatigue bottom-up and top-down and thermal cracking models. The reason for bias and error in measured versus predicted distresses mainly comes from inaccurate input data, error in the distress survey, and accuracy of prediction models. In this effort, the error in prediction models was reduced through the calibration process. This process includes two steps for reducing bias and increasing accuracy. An iterative narrow-down approach was used to determine the calibration coefficient values corresponding to the minimum prediction bias. In this approach, starting from a wide range of coefficients' combinations, the best range was determined, and in the next steps, the identified ranges were narrowed down to the optimum combination of coefficients. In the next step, the standard error of prediction was decreased by optimizing the coefficients related to the accuracy of models. Finally, the locally calibrated coefficients for the distress and IRI models were determined for the Oklahoma pavement system. The distress and IRI models show that the calibrated coefficients improve the pavement ME predictions and design of flexible pavements in Oklahoma. After completing the calibration effort of the Pavement ME software, it is essential to consider the next step of the implementation process, which is adopting the locally calibrated models for some routine

pavement designs. For this reason, the Pavement ME was used to design the asphalt pavements using the typical material and design parameters for the state of Oklahoma. Three types of conventional flexible pavement design, as well as one perpetual design, were compared in this study. Generally, using calibration coefficients yields lower rutting and higher fatigue cracking. However, the pavement roughness at the end of design life is using the Oklahoma calibration coefficients.

The high sensitivity of the pavement performance prediction to the dynamic modulus highlights the importance of providing this input at different levels. In this study, the results of dynamic modulus tests in previous studies of Oklahoma were collected for the Pavement ME calibration database. Five common prediction models were applied to evaluate their precision in estimating the dynamic modulus from the job mix formula (JMF) HMA properties. The performance of each model in predicting Oklahoma's typical mixture dynamic modulus values were evaluated and compared. So, the best prediction models which can be applied in Pavement ME analysis were introduced.

The rigid pavement calibration process in Oklahoma is limited to the Jointed Plain Concrete Pavement (JPCP) and the Continuously Reinforced Concrete Pavement (CRCP). It is well known that the rigid pavement is a durable pavement type, which reduces the number and extent of distresses in the LTPP survey records. In Oklahoma, there was only limited performance data available in the General Pavement Studies (GPS) database for CRC and JPC pavements. The type of data utilized in local calibration, as adopted in NCHRP 1-37A, requires considerable visual performance damages to validate the calibrated coefficients. For CRCP, this set of circumstances required a different approach as to the type of data used for calibration. Therefore, the researchers proposed a new methodology to calibrate the punchout damage in CRC pavements. Non-observable damage (i.e., erosion) was found of a greater value for the new calibration methodology as it represents the deterioration process required to produce the visual manifestation of punchouts. The proposed methodology requires estimating erosion percentage damage using Falling Weight Deflectometer data (FWD), which depends on the type of base and subbase, determining the percentage of punchout from the Long-Term Performance Program (LTPP) records, and establishing the relationship between both components to estimate the existing punchout distresses. The same circumstances were encountered in the calibration for JPC pavement. However, the new methodology was not applicable for the transverse cracking distress prediction as pavement ME depends mainly on the traffic for estimating fatigue damage. Therefore, the national calibration coefficients for transverse cracking and faulting models were assessed for sections in Oklahoma and Arkansas (As a neighbor state). The national calibration coefficients were found sufficient for predicting the main distresses in JPCP.

A database including traffic, climatic, structure, material property, and the corresponding pavement performance/distress data has been developed. In this database, the material property data has three hierarchical input levels based on the Pavement ME Design Guide. The INput-ME software program was developed to convert the traffic data, climatic data, structure data, and material property data from the developed ODOT database into the input format of the Pavement ME Design software. This software has a user-friendly interface, which facilitates the ODOT employees to conduct the local calibration periodically.

INTRODUCTION

Pavement ME design is one of the AAHSHTOWare Design software which has been built to design the new and rehabilitated pavement with a flexible, rigid, and composite structure. Mechanistic empirical (ME) design supports AASHTO's mechanistic-empirical pavement design guide (MEPDG), which was generated under the National Cooperative Highway Research Program (NCHRP) 1-37A project (*1*). MEPDG, compared to the 1993 American Association of strategic highway transportation officials (AASHTO) Guide, by an update from an empirical approach to a combined mechanistic-empirical approach, provides a more realistic understanding of designing pavements. A formal review of the 1-37A project presented in NCHRP 1-40 A, resulted in an improvement in the MEPDG procedure. Further efforts in the 1-40D project brought out the first version of MEPDG software. In April 2007, version 1.0 was taken under consideration by NCHRP, federal highway administration (FHWA), and AASHTO as an AASHTO provisional standard, which resulted in Version 2.0 (*2*). This software predicts the pavement condition, including fatigue, rutting, thermal cracking, and IRI in flexible pavements and cracking, faulting, and IRI in concrete pavements. It allows the consideration of different environmental and loading states and provides new approaches for evaluating design variability and reliability.

MEPDG Approach

The MEPDG approach comprises three stages (*3*). In the first phase, all the input properties, including the unbound and paving material properties, environmental and climatic conditions, traffic data, and design criteria, are evaluated. The methods of data collection and precision of collected data can dramatically affect the software analysis and results. For this reason, three distinguished levels of inputs based on the criticality of the project and the availability of data were determined. The second stage is the confluence of empirical and mechanistic analysis. In this phase, by using the pavement response and distress models, incremental damages are calculated, and pavement performance under the designed features will be determined. The M-E design optimization allows the users to find the appropriate pavement structure, which satisfies all of the distress below the failure criteria (*4*). In stage 3 of the MEPDG approach, viable design alternatives based on engineering judgment, life cycle analysis, and national and local pavement construction policy are evaluated, and a final strategy will be determined.

Hierarchical Design Input Levels

The hierarchical input levels are features of AASHTOWare Pavement ME Design, which categorizes the input parameters in three distinct levels. Designers can provide their input values from different levels based on the availability of required data, the importance of the project, and allocated design time and budget. The hierarchical theme applies to material, traffic, and climate inputs.

- **Level 1**: level 1 data is calculated directly by in-situ or lab tests. This level provides the most precise data for input parameters with the highest data collection cost and the lowest uncertainty. Also, designers should apply level 1 data in new and unusual pavement conditions, which is far from the conditions used for establishing level 2 and 3 default data (*4*).

- **Level 2**: level 2 data has an intermediate level of accuracy and certainty. These data do not project-specific and can be estimated from correlation equations or an agency's database. Considering the needed level of knowledge and the impact of parameters on the final design strategy, designers may choose level 2 data for the input values.

- **Level 3**: level 3 data have the lowest level of accuracy and are based on global or regional surveyed values. This level of data provides the least information about the input values in a specific project but is available at the lowest cost. In some input parameter values which have low variance concerning the change in location and time, the level 3 data are excellent and reliable sources for designers.

Designers, in any given project, may choose a combination of different levels of input parameters. Pavement ME estimation algorithm provides the capability of pavement performance prediction with varying combinations of input parameter levels. Each input level for different parameters will have an associated standard error in pavement performance design (*4*).

Material Characterization

The input properties for all asphalt mixtures are divided into volumetric and engineering inputs. The volumetric properties are mostly air voids, effective binder content, aggregate sieve analysis results, different types of density, and asphalt binder type. The engineering or mechanistic properties for asphalt materials examples are dynamic modulus, resilient modulus, creep compliance, and tensile strength (*2*). As discussed before, a hierarchical approach is a practical method for providing input data. For material parameters, level 1 data can be obtained by comprehensive sets of laboratory tests. However, level 2 and level 3 data can be estimated by a series of correlation equations or default values.

FLEXIBLE PAVEMENTS
HMA MIXTURES

For all asphalt mixture types or layers, primary properties are required to run the AASHTOWare Pavement ME Design. Significant HMA mixtures considered in Pavement ME design are Stone Matrix Asphalt (SMA), asphalt treated or stabilized based or asphalt permeable treated base mix (*4*). Providing Level 1 data is sophisticated, time-consuming, and costly, and most agencies cannot acquire them through test protocols for most analyses. However, the use of a combination of Level 1, 2, and 3 material inputs are allowed. Therefore, designers, based on the specific qualifications and the state agency needs, can combine levels 1, 2, and 3 material inputs in Pavement ME. In the following, recommended procedures and correlation equations to estimate levels 2 and 3 material properties for HMA mixtures are presented.

Dynamic Modulus ($|E^*|_{HMA}$)

Pavement ME design predicts the dynamic modulus of an HMA mixture, $|E^*|_{HMA}$ using predictive equations, including the NCHRP 1-37A viscosity based model or 1-40D $|G^*|$ based model known as original and modified Witczak models respectively (*4*). Furthermore, other researchers have also tried to develop new predictive models that, in some cases, can give more realistic estimates for dynamic modulus. Hirsch and Al-Khateeb models are samples of these efforts which have gained national interests. However, some researchers believe that these regression models have disadvantages that make restraints when applied to a broad range of mixture types and at the critical very high and low temperatures. To improve these disadvantages, North Carolina State University (NCSU) Global Model and NCSU Simplified Global model have been developed (*5*). These models can predict $|E^*|_{HMA}$ in a broader range of

testing conditions and estimate more accurate dynamic modulus values with less deviation compared to previous existing models.

Original Witczak Model

Revised Witczak dynamic modulus predictive equation developed under NCHRP 1- 37A project is as follows (*6*):

$$Log\left|E^*\right| = -1.249937 + 0.02923p_{200} - 0.001767\left(p_{200}\right)^2 - 0.002841p_4 - 0.05809V_a$$
$$-0.802208\frac{V_{beff}}{V_{beff}+V_a} + \frac{3.871977 - 0.0021p_4 + 0.003958p_{3/8} - 0.000017\left(p_{3/8}\right)^2 + 0.00547p_{3/4}}{1+\exp\left(-0.603313 - 0.31335\log f - 0.393532\log\eta\right)} \quad (1)$$

where:

$|E^*|$ = dynamic modulus, 10^5 psi;
P_{200} = Percentage of aggregate passing #200 sieve;
P_4 = Percentage of cumulative aggregate retained on #4 sieve;
$P_{3/8}$ = Percentage of cumulative aggregate retained on 3/8-inch (9.56-mm) sieve;
$P_{3/4}$ = Percentage of cumulative aggregate retained in 3/4-inch (19.01-mm) sieve;
V_a = Percentage of air voids (by volume of the mix);
V_{beff} = Percentage of effective asphalt content (by volume of the mix).
f = Loading frequency (HZ); and
η = Binder viscosity at the required temperature (10^6 Poise).

For the viscosity term in equation(1), the designed program converts all levels 2 and 3 inputs into the regression intercept (A) - regression slope (VTS) of viscosity-temperature relationship for the formulation of the |*E**| master curve. This relationship is commonly referred to as the "*A-VTS* relationship" (*6*).

$$\log\left(\eta\right) = \begin{cases} A + VTS\log\left(T_R\right) & T_R > T_{critical} \\ 1.095 & T_R \le T_{critical} \end{cases} \quad (2)$$

where:

η = Viscosity (cP);
A = Intercept of the relationship;
VTS = slope of the relationship;
T_R = Temperature in Rankine; and
$T_{Critical}$ = Temperature in Rankine, where the viscosity is equal to 2.7 x 1012 cP (0.0027 x 10^{12} Pas).

A and *VTS* typical values for different types of binders were recommended following by NCHRP 1-37A effort (*6*, *7*).

|G*| Based Witczak Model

Modified Witczak dynamic modulus predictive equation including $|G^*|$ and developed under NCHRP 1- 40D project is as follows (*6*):

$$Log|E^*| = -0.349 + 0.754\left(|G^*|_b^{-0.0052}\right)\left(\begin{array}{l} 6.65 - 0.032p_{200} + 0.0027(p_{200})^2 + 0.011p_4 - 0.0001(p_4)^2 \\ +0.006p_{3/8} - 0.00014(p_{3/8})^2 - 0.08V_a - 1.06\left(\frac{V_{beff}}{V_{beff}+V_a}\right) \end{array}\right) \quad (3)$$
$$+\frac{2.558 + 0.032V_a + 0.713\left(\frac{V_{beff}}{V_{beff}+V_a}\right) + 0.0124p_{3/8} - 0.0001(p_{3/8})^2 + 0.0098p_{3/4}}{1+\exp\left(-0.7814 - 0.5785\log|G^*|_b + 0.8834\log\delta_b\right)}$$

where,

$|G^*|_b$ = dynamic shear modulus of asphalt binder (psi);

δ_b = binder phase angle associated with $|G^*|_b$ (degrees).

These two, original and $|G^*|$ based Witczak equations currently are used in Pavement ME design for predicting level 2 and 3 dynamic moduli. If some of the mixture databases do not have $|G^*|_b$ data, the Cox-Mertz rule, can be used to calculate $|G^*|_b$ from A-VTS values as follows (*6*).

$$|G^*|_b = 0.0051 f_s \eta_{f_s,T} (\sin\delta_b)^{7.1542 - 0.4929 f_s + 0.0211 f_s^2} \quad (4)$$

$$\delta_b = 90 + (-7.3146 - 2.6162 * VTS') * \log\left(f_s * \eta_{f_s,T}\right) + \left(0.1124 + 0.2029 * VTS'\right) * \log\left(f_s * \eta_{f_s,T}\right)^2 \quad (5)$$

$$\log\eta_{f_s,T} = 0.9699 f_s^{-0.0527} * A + 0.9668 f_s^{-0.0525} * VTS \log T_R \quad (6)$$

where:

f_s = Dynamic shear frequency;

δ_b = binder phase angle predicted from equation(5) (degrees);

$\eta_{fs,T}$ = viscosity of binder at a specific loading frequency (f_s) and temperature (T) determined from equation(6) (cP); and

T_R = Temperature in Rankine unit.

Hirsch Model

Hirsch model is the incorporation of binder modulus and volumetric properties, including voids in mineral aggregate (*VMA*) and voids filled by aggregate (*VFA*). One of the advantages of the Hirsch Model is the phase angle of HMA, which is applied in the calculation of creep compliance and relaxation modulus from dynamic modulus. However, this model developed based on a low number of data point and did not show good results at low *VFA* and V_a values

Al-Khateeb Model

The law of mixtures parallel model, Al-Khateeb Model, was developed based on the Hirsch model. The strengths of this model include the improved prediction of high-temperature and low-frequency $|E^*|$ data for mixtures used in the FHWA accelerated loading facility (ALF) test sections. The weaknesses include the lack of model verification and the fact that the researchers who developed this model used $|E^*|$ values obtained from tests at higher than recommended strain amplitudes (200 *με* versus the recommended maximum of 75–150 *με*) (*6*).

NSCU Global and Simplified Global model

The NCSU models can be used to estimate the HMA dynamic modulus for a wide range of temperatures suggested by (AASHTO) TP62-03 test protocol. These models are generated based on merging the master-curves from both binder and HMA mixture (*5*).
The collected data for generating these models includes 20,209 data points from 1008 mixes with different aging conditions that consist of modified and unmodified asphalt binders (*5*).

Tensile strength (TS)

Tensile strength at level 1 can be determined by the AASHTO T322 test, "*Determining the Creep Compliance and Strength of HMA using the Indirect Tensile Test Device*." At Level 3, the Pavement ME design guide suggested the same regression equation(14), which has been developed for MEPDG under NCHRP 1-37A. The tensile strength can be determined by the following equations (*4, 7*)

$$TS = 7416.712 - 114.016 * V_a - 0.304 * V_a^2 - 122.592 * VFA + 0.704 * VFA^2 + 405.71 * \log(Pen77) - 2039.296 * \log(A) \quad (7)$$

where,

TS = Indirect tensile strength at 14 ºF, (psi);
VFA = Voids filled with asphalt, as constructed, (percent);
V_a = HMA air voids, as constructed, (percent);
A = Asphalt viscosity-temperature susceptibility intercept and,
$Pen77$ = Asphalt penetration at 77 ºF, (mm/10);

Creep Compliance

Creep Compliance can be determined at level 1 by AASHTO T 322 test protocol. The data should be provided at testing temperatures of -4, 14, and 32 ºF and time of loading of 1, 2, 5, 10, 20, 50, and 100 HZ. At Level 3, the Pavement ME design guide suggested the same regression equation, which has been developed for MEPDG under NCHRP 1-37A. The Creep Compliance can be determined by the following equation (*4, 7*):

$$D(t) = D_1 * t^m$$

$$\log(D_1) = -8.524 + 0.01306 * Temp + 0.7957 * \log V_a + 2.0103 \log VFA - 1.923 * \log A \quad (8)$$

$$m = 1.1628 - 0.00185 * Temp - 0.04596 * V_a - 0.01126 * VFA + 0.00247 * Pen77 + 0.001683 * Temp * Pen77^{0.4605}$$

where,

t = Time, (months);
$Temp$ = Temperature at which creep compliance is measured, (ºF);
V_a = HMA air voids, as constructed, (%);
VFA = Aggregate Voids filled with asphalt binder, as constructed, (%); and
$Pen77$ = Asphalt penetration test result at 77 ºF, (mm/10).

Coefficient of Thermal Contraction (CTC)

The coefficient of thermal contraction can be determined neither by ASTM nor by AASHTO standards. Pavement ME calculates CTC from HMA volumetric properties like VMA and the volumetric coefficient of thermal contraction of the aggregate (7). The model used by pavement ME for predicting CTC for HMA mixtures is shown in equation(9).

$$L_{MIX} = \frac{VMA * B_{ac} + V_{AGG} * B_{AGG}}{3 * V_{TOTAL}} \quad (9)$$

where,

L_{MIX} = Linear coefficient of thermal contraction of the HMA (1/oC);
B_{ac} = Volumetric coefficient of thermal contraction of the asphalt binder in the solid state (1/oC);
B_{AGG} = Volumetric coefficient of thermal contraction of the aggregate (1/oC);
V_{MA} = Voids in the mineral aggregate (percent %);
V_{AGG} = Volume of aggregate in the mixture (percent %); and
V_{TOTAL} = 100 percent.

Table 1 represents the Pavement ME design guide suggested typical values for parameters used in calculating CTC for HMA mixtures.

Table 1- Suggested values for estimating coefficients of thermal contraction (*4*, *7*)

Parameter	Suggested value
L_{MIX}	2.2 to 3.4*10^{-5}/°C (linear)
B_{ac}	3.5 to 4.3*10-4 /°C (cubic)
B_{AGG}	21 to 37*10 -6 /°C (cubic)

Poisson's Ratio

Poisson's ratio of asphalt concrete materials ranges typically between 0.15 and 0.50 and changes at different temperatures (7). For Poisson's ratio, using recommended typical values are suitable for new HMA materials. The following equation(10) can provide an estimation of Poisson's ratio (7).

$$\mu_{ac} = 0.15 + \frac{0.35}{1 + \exp(-1.63 + 3.84 * 10^{-6} E_{ac})} \quad (10)$$

where,

μ_{ac} = Poisson's ratio of asphalt concrete at a required temperature; and
E_{ac} = Modulus of asphalt concrete at a required temperature, (psi).

Furthermore, Pavement ME design provides level 3 typical values of Poisson's ratio at different temperatures that are presented in Table 2 for the existing dense and open-graded HMA layers.

Table 2- Typical level 3 values of Poisson's ratio for aged HMA (*4*)

Temperature °F	Dense-Graded HMA	Open-Graded HMA
<0 °F	0.15	0.35
0 –40 °F	0.2	0.35

Temperature °F	Dense-Graded HMA	Open-Graded HMA
41 –70 °F	0.25	0.4
71 –100 °F	0.35	0.4
101 –130 °F	0.45	0.45
>130 °F	0.48	0.45

Other Parameters

For air voids, (*Va*), volumetric asphalt content, (*Vb*), and total unit weight for different mix types obtained from previous work, the databases are suggested by Pavement ME design to be applied in the software (*4*).

For surface shortwave absorptivity, the following typical values are suggested (*4*):

- Weathered asphalt concrete (gray): 0.8-0.9
- Fresh asphalt concrete (black): 0.9-0.98

Thermal conductivity (*k*) can be measured at level 1 by ASTM E 1952, "*Standard Test Method for Thermal Conductivity and Thermal Diffusivity by Modulated Temperature Differential Scanning Calorimetry*" or can be chosen at level 3 by typical values range from 0.44 to 0.81 Btu/(ft)(hr)(°F) (*7*).

Heat capacity can be measured at level 1 by ASTM D 2766, "*Specific Heat of Liquids and Solids,*" or can be chosen at level 3 by typical values that range from 0.22 to 0.4 Btu/(lb)(°F) (*7*).

Unbound Material

Pavement ME requires physical and engineering features of unbound base and subbase layers. The material properties which are required in Pavement ME design of unbound granular material, subgrade, and bedrock are classified into three groups (*7*):

- Material inputs required for pavement response models such as resilient modulus (M_r) and poison's ratio represent the response behavior of the unbound material under cyclic wheel loads.

- Enhanced Integrated Climatic Model (EICM) material inputs that are required for prediction of temperature and moisture content within a pavement. Gradation, Atterberg limits, and saturated hydraulic conductivity are examples of EICM inputs.

- Other inputs such as lateral pressure (K_0) coefficient which are required in design approaches used in Pavement ME.

In the following, the recommended input parameters for the unbound material are presented.

Resilient Modulus

Resilient modulus is calculated by the ratio of applied deviator stress to recoverable or resilient strain. It can be determined by using cyclic stress on the cylindrical sample under consistent confining pressure (σ_3 or σ_c) and gauging the axial recoverable strain (ε_r) (*8*).

$$Mr = \frac{\sigma_{cyclic}}{\varepsilon_r} \tag{11}$$

where,

Mr = resilient modulus;

σ_{cyclic} = cyclic (deviatoric) stress; and

ε_r = resilient (recoverable) axial strain.

Resilient modulus can be determined by laboratory tests as level 1 or can be estimated by different properties of unbound materials as level 2 or default values as level 3 for different types of unbound materials recommended by Pavement ME Design. For rehabilitation and reconstruction projects, the resilient modulus can be estimated by empirical test methods such as Dynamic Cone Penetration (DCP), California Bearing Ratio (CBR), or Plate Load Test or back-calculated by elastic layer modulus values from deflection basin test (*4*).

Level 1 Test Procedures and Models

Test procedures developed by AASHTO include AASHTO T, AASHTO T 294 and AASHTO T 307 (previous AASHTO TP46). NCHRP Project 1-28 A was developed to improve earlier AASHTO methods, and the product of this project is "*Harmonized test methods for laboratory determination of resilient modulus for flexible pavement design*." The test protocols of AASHTO T307 and NCHRP 1-28A are comparable but have some differences in material classification methods, load cell's location, and loading test order (*9*). The Pavement ME design recommends M_r to be measured from the AASHTO T 307 or NCHPR 1-28 A (*4*).

Based on AASHTO T 307, the resilient modulus is measured in 15 sequences with different levels of confining and deviatoric stresses. In order to find the amount of M_r at different stress conditions caused by cyclic wheel loads, it is necessary to find a relationship between resilient modulus and stress states.

MEPDG Model

Pavement ME design guide proposes a stress-based model that was developed based on NCHRP 1-28 A project (*7*). This model can be applied to all types of subgrade layers and unbound granular materials. The main equation includes six regression constants. The basic form of the model has three constants (equation(12)), which K_1 has a positive value since M_r cannot be negative. By increasing the bulk stress, the amount of M_r will increase due to the hardening behavior of unbound material; thus, the K_2 parameter should have a positive value. Increasing the shear stress leads to softening behavior and lowers M_r, which means K_3 should have a negative value (*9*).

$$M_r = K_1 P_a \left(\frac{\theta}{P_a}\right)^{K_2} \left(\frac{\tau_{oct}}{P_a} + 1\right)^{K_3} \quad (12)$$

K_1, K_2, and K_3 coefficients differ for various types of material and should be determined for each soil type. Yau et al. (*10*) evaluated the resilient modulus test results obtained from measured data on recovered samples from LTPP sections. Hussein et al. performed a study on different types of level 1 and evaluated different models for the estimation of resilient modulus. This study includes various types of the state of Oklahoma unbound soil and coarse aggregate. Based on this study, the Uzan model shows a better estimation for Oklahoma subgrade soils, and the MEPDG model gives an acceptable fit for coarse aggregate (*11*). Table 3 shows recommended regression coefficients for estimating M_r by Uzan and MEPG models for subgrade soil and aggregates of Oklahoma DOT, respectively.

Table 3- Regression coefficients of M_r predictive models for the state of Oklahoma (*11*)

Layer	Soil Type	K_1 Mean	K_1 SD	K_2 Mean	K_2 SD	K_3 Mean	K_3 SD
Subgrade soils	A-2-4	511.54	118.05	0.208	0.412	-0.378	0.314
Subgrade soils	A-2-6	486.69	N/A	0.562	N/A	-0.544	N/A
Subgrade soils	A-4	440.96	130.88	0.383	0.334	-0.42	0.207
Subgrade soils	A-6	449.05	216.8	0.141	0.231	-0.547	0.27
Subgrade soils	A-7-6	434.36	240.95	0.051	0.147	-0.604	0.326
Coarse aggregate	lime stone	860.56	612.11	-0.0217	0.487	0.939	0.919
Coarse aggregate	Sand stone	637.49	255.23	0.298	0.386	0.433	0.702

Level 2 – Correlation with other Material Features

Measuring level 1 resilient modulus from the recommended test protocols needs special equipment and is a time-consuming procedure, which makes some DOTs unwilling to perform it. In this situation, level 2 estimation can be selected for calculating the resilient modulus using typical correlations with other soil properties such as water content, gradation, Atterberg limit, etc.Many researchers tried to find the estimation relations for regression constants (K_1, K_2, K_3) from unbound material properties. Yau et al. provide the following models for unbound aggregate base/subbase materials and subgrade soils (*10*).

Kim et al. reported a reasonably high correlation by predicting material constants for the MEPDG model by using 12 soil indices for a total of fourteen fine-grained soils and five coarse-grained soils at Indiana State (*12*). Hossein et al. (*11*) provided correlation relations for estimating Level 2 M_r for subgrade soil and coarse aggregates, which generally are used in the state of Oklahoma. Two methods of direct estimation and indirect estimation with regression coefficients (K_1, K_2, K_3) were provided. Six parameters (*UCS, MDD, MC, PI, DR, MCR*) were used to establish the correlation equations for material constants. The strength of the established correlation was found to be fair; the R^2 and F values of the model were found to be 0.44, and 16.13, respectively, indicating significantly lesser fit than the stress-based model. The level 2 value of resilient modulus can be estimated using strength properties such as CBR, R-value, and AASHTO layer coefficient and can be calculated by direct or indirect methods. The resilient modulus can be estimated from CBR test results, and in indirect methods, some material properties are used for estimating CBR values (*7*). Based on a study on cohesionless subgrade soils in Mississippi State (*13*), the resilient modulus can be estimated from standard California Bearing Ratio (CBR). The results of correlation relation with CBR showed no significant change in the resilient modulus if soils are within ± 1.5 % of optimum moisture content.

$$M_r = 3116(CBR)^a \quad (13)$$

where,
a=0.4779707

Yeh and Su of the Colorado Department of Highways tested the resilient properties of Colorado soils with the objective of establishing a correlation between resilient modulus and stabilometer R-value (*14*). The equation finally derived between M_r and R-value is as follows:

$$Mr = 3500 + 125(R - value) \quad (14)$$

where *Mr* is expressed in psi. Level 1 and 2 procedures described can be used in all pavement construction projects. In rehabilitation and reconstruction projects, material specimens can be sampled by coring. In addition, level 2 resilient modulus, M_r, can be measured from falling weight reflectometers results obtained from existing pavement layers (7).

Level 3 – Typical Values of Resilient Modulus

For typical values of Level 3, M_r values are suggested by NCHRP 1-28 project. In this condition, M_r values are required at optimum moisture content. Also, the typical values are represented for AASHTO and USCS Soil classification (7). The typical values of resilient modulus suggested by Hussein et al. for the state of Oklahoma are presented in Table 4. The default M_r values for finer soil types (i.e., A-7-6) tend to be close to or within those of the MEPDG recommended ranges. In the case of A-6 soil, typical values were found to be on the conservative ends compared to the MEPDG recommended range. In the cases of other soil types (A-2-4, A-2-6, and A-4) in Oklahoma, the default M_r values were found to be on the more conservative ends. The predicted default M_r values corresponding to limestone and sandstone aggregates for Oklahoma were found to be 124% and 136% lower than those of the MEPDG recommended typical values (11).

Table 4-Resilient modulus typical values for the state of Oklahoma (11)

Material Classification	Average Level 3 *Mr* values (psi)	The midpoint of MEPDG vs. Oklahoma
A-2-4	10800	203%
A-2-6	10100	193%
A-4	8900	184%
A-6	10300	83%
A-7-6	9900	-7%
Limestone	14200	--
Sandstone	9300	--

Enhanced Integrated Climatic Model (EICM)

The enhanced integrated climatic model considers variations of temperature and moisture content of unbound layers in Pavement ME analysis. The EICM consists of three distinct elements (7):

- Climatic-Materials-Structure Model (CMS Model)
- CRREL Frost-Heave and Thaw Settlement Model (CRREL Model)
- Infiltration and Drainage Model (ID Model)

Environmental information related to weather, groundwater, drainage, and pavement structure and material properties are inputs for the ELCM model. Considering the variation in temperature and environmental characteristics, the EICM model modifies the resilient modulus through adjustment factors (F_F, F_R, F_U) over the design period. The effect of environmental parameters like moisture content variation, freezing, thawing, and also recovery from thawing are determined by adjustment factors introduced by the EICM model. The environmental factor, F_{env} is a composite weighted factor, which could generally represent a combination of the factors suitable in different climatic conditions (7).

- F_F = factor for frozen material and calculated based on the temperature;
- F_R = factor of recovered materials from thawing before freezing cycle; and
- F_U = factor for unfrozen materials. This is used for materials that never freeze or are fully recovered from the frozen condition.

These factors incorporate the effect of moisture variation and freeze/thaw cycles on the resilient modulus value of pavement layers at any specific point during the period of pavement analysis. The resilient modulus, M_r, can be measured at each time or location from the following equation:

$$M_r = F_{env} \times M_{r_{opt}} \tag{15}$$

where,
F_{env} = adjustment factor; and
M_{ropt} = resilient modulus at optimum conditions (maximum dry density and optimum moisture content)

The EICM accounts for unsaturated soil conditions based on the soil-water characteristic curve (SWCC), saturated and unsaturated hydraulic conductivity, hourly climatic information from 800 weather stations including sunshine hours, daily rainfall data, wind speed, daily air temperature and relative humidity (7).

The SWCC is a function of the relationship between matric suction to the moisture content of generally unsaturated soils. This relationship shows the suction versus the variation of water content indices like gravimetric, volumetric, or degree of saturation *n*. The degree of saturation in equilibrium condition (S_{equil}) can be calculated from SWCC (7).

$$Sequil = C(h) \times \frac{1}{\left[\ln\left[EXP(1) + \left(\frac{h}{a_f}\right)^{b_f}\right]\right]^{c_f}}$$
$$C(h) = 1 - \frac{\ln\left(1 + \frac{h}{h_r}\right)}{\ln\left(1 + \frac{1.45 \times 10^5}{h_r}\right)} \tag{16}$$

where,
h = matric suction (psi); and
h_r, a_f, b_f, c_f = regression coefficients.

Resilient Modulus and Soil Moisture
The resilient behavior of soils depends on moisture content as well as the stress state conditions. By increasing the moisture content in soils with similar dry density, the resilient modulus will increase. Pavement ME modifies the resilient modulus values of subgrade soils due to moisture variation through the EICM model. The resilient modulus as a function of soil moisture in the M-E Design Guide is as follows:

$$\log \frac{Mr}{Mr_{opt}} = a + \frac{b-a}{1+EXP\left(\ln \frac{-b}{a} + k_m\left(S - S_{opt}\right)\right)} \quad (17)$$

where,

Mr/Mr_{opt} = resilient modulus ratio; M_r is the resilient modulus at a required time and $(M_r)_{opt}$ is the resilient modulus at the optimum moisture content;

a = minimum of $\log \frac{Mr}{Mr_{opt}}$;

b = maximum of $\log \frac{Mr}{Mr_{opt}}$;

k_m = regression parameter; and

$(S\text{-}S_{opt})$ = variation in the degree of saturation expressed in decimal.

The M-E Design Guide suggests that the range of modulus ratio, Mr/Mr_{opt} value, for coarse-grained soils are from 2 to 0.5, and for fine-grained soils are from 2.5 to 0.5. It can be concluded that the fine-grained soils are more susceptible to changing moisture content than the coarse-grained soils. The degree of saturation in subgrade soil (particularly for fine-grained materials) increases over the design period; as a consequence, the resilient modulus will gradually decrease with time, reaching the minimum resilient modulus (*7*).

Moisture Dependent Model

Lytton et al. developed a new resilient modulus of unbound aggregates model, which incorporates the moisture dependency and stress dependency of the resilient modulus in the used models (*15*). Furthermore, to predict the constant coefficients, a series of predictive models are presented by the researcher. In this model, the degree of saturation and the matric suction are proposed to discriminate the effect of moisture variations. The multiple regression analysis was performed to generate the predictive models for the constant coefficients in the resilient modulus model using a set of performance-related base course properties. The dry density, shape, angularity, and texture of the aggregates and the percent fine content are used in the predictive models.

Poisson's Ratio

Pavement performance responses are less susceptible to Poisson's ratio compared to other soil properties. Thus, instead of testing procedures, recommended values can be used (*7*). Also, the Pavement ME design guide typical values are suggested to be used in new and rehabilitation pavement analysis (*4*).Typical values for unbound granular and subgrade soils range from 0.2 to 0.45. Furthermore, the Poisson's ratio has different values in cohesive and non-cohesive unbound materials (*7*).

Other Properties

AASHTO T 88 test procedure is used for the gradation of the unbound aggregate or subgrade soil. In the case of an inadequate soil sample, the default values included in the AASHTO Pavement ME design for the material classification could be used.

The liquid limit can be calculated by AASHTO T 89, and the plastic limit and plasticity index measured by AASHTO T 90. The default values included in the AASHTOWare Pavement ME

design for the material classification could be used as level 3. AASHTO T 215 can be used to measure Saturated Hydraulic Conductivity for new and existing unbound layers (*4*).

The coefficient of lateral pressure, k_o, is the ratio of the lateral earth pressure to the vertical earth pressure. The typical in-situ k_o ranges between 0.4 to 0.6, for unbound granular and subgrade soil, and bedrock layers (*7*). This procedure applies to a new design, reconstruction, and rehabilitation pavement design.

Bedrock Inputs Properties

Modulus of Elasticity

Shallow bedrock layers, the same as the subgrade soils, have a considerable influence on the pavement's responses and should be evaluated in the pavement performance design. For rehabilitation design, which back-calculation of layer moduli is considered, the modulus of elasticity has vital importance. The stiffness is rarely measured precisely as level 1; however, bedrock layer stiffness must be considered into the pavement design (*7*).

Poisson's Ratio

Pavement performance responses are not significantly susceptible to Poisson's ratio of bedrock. Thus, instead of testing procedures, the recommended values can be used. Pavement ME design guide typical values are suggested to be used in new and rehabilitation pavement analysis. The typical Poisson's ratio for bedrock ranges between 0.1 to 0.26 for Solid, massive bedrock, and 0.25 to 0.4 for highly fractured and weathered bedrock layers (*7*).

Chemically Stabilized Materials

Chemically stabilized subgrade soils increase the pavement performance by providing better support in the pavement structure.

In the Pavement ME design, the chemically stabilized materials include:

- lean concrete;
- cement stabilized;
- open grade cement stabilized;
- soil cement;
- lime-cement-fly ash; and
- lime-treated materials.

The cement mixed materials (e.g., lean concrete, cement stabilized, and soil cement) involve natural coarse or fine aggregate combined with cement, and the mix design can control the amount of strength. The combination of lime, cement (more often cement kiln dust, CKD), and fly ash are typically applied in fine-grained soils (*16*). Using cementitious chemical additives with fine grain soils generate a new type of materials with different properties in Pavement ME inputs (*4*).

Resilient Modulus (M_r)

Although Level 1 data provides the most accurate results for the pavement design, Pavement ME characterizes chemically stabilized material properties in levels 2 and 3 for the situation when the limited testing capability is recognized. Designers can combine different levels of data based on the priority of tests and the capability of agencies. Level 3 typical values for the chemically stabilized material modulus and deteriorated chemically stabilized materials are shown in Table 5.

Table 5- Level 3 typical values of chemically stabilize materials modulus (*4*)

Material	*E* or M_r typical value (psi)	Deteriorated *E* or M_r value (psi)
Lean concrete	2,000,000	300,000
cement treated aggregate	1,000,000	100,000
Lime-Cement-fly ash	1,500,000	40,000
Soil Cement	500,000	25,000
Open graded cement stabilized aggregate	750,000	50,000
Lime stabilized soil	45,000	15,000

To evaluate the stabilized subgrade soils, Hossain et al. (*11*) conducted a series of M_r tests on Oklahoma soils. This dataset represents four different types of Oklahoma soil (Carnasaw (*C*), Port (*P*), Kingfisher (*K*), and Vernon (V) series) modified with different types of additives (lime: 3%, 6%, and 9%, *CFA*: 5%, 10%, and 15%, and *CKD*: 5%, 10%, and 15%). Besides the Pavement ME model, M_r was calculated using the correlation with chemical components (e.g., silica, alumina, ferrous oxide, free lime, loss of ignition) of the additives used in Oklahoma (*11*).

Other Parameters

Table 6 and Table 7 present the level 3 typical values of modulus of rupture and Poisson's ratio for the chemically stabilized materials, respectively.

Table 6-Typical flexural strength (*MR*) values for chemically stabilized materials (*4*)

Material	Typical *MR* value (psi)
Lean concrete	450
cement treated aggregate	200
Open-graded cement stabilized aggregate	200
Lime-Cement-fly ash	150
Soil Cement	100
Lime stabilized soil	25

Table 7- Poisson's ratio range for chemically stabilized materials (*4*)

Material	Poisson's Ratio
Cement Stabilized Aggregate (including Lean Cement)	0.1 - 0.2
Soil Cement	0.15 - 0.35
Lime-Fly Ash Materials	0.1 - 0.15
Lime stabilized soil	0.15 - 0.2

Snethen et al. (*16*) conducted a series of laboratory and field tests on the susceptibility of subgrade soil strength to cementitious additives, which improve the soil supports in Oklahoma.

The additives used in this study include lime, fly ash, cement kiln dust (CKD), and Portland cement or their combination, which are the most commonly utilized additives in Oklahoma.

Traffic Input

Among Pavement ME inputs, truck traffic is a key data element that has a dramatic influence on the structural design and analysis of pavement structures. AASHTO 1993 Design Guide characterizes traffic using Equivalent Single Axle Load (ESAL). AASHTOWare Pavement ME design implements the full axle-load spectrum information for each axle type (*4*). Traffic volume, lane distribution, volume adjustment factors (e.g., class distribution, traffic growth factors, etc.) and weight data are used as inputs along with some miscellaneous data such as tire pressure.

Common traffic data collected by highway agencies include weight in motion(WIM), automatic vehicle classification (AVC), and vehicle counts (*17*). Comparing to the WIM and AVC methods, traffic counts have the least information about the traffic, and only record AADT (Annual Average Daily Traffic). Many DOTs use this kind of data to build state traffic counts maps or interactive live traffic maps (*17*). AVC system identifies the vehicle class as it passes through a series of detection devices

Weigh-In-Motion can be defined as the static equivalent load of a dynamic tire load for a moving vehicle (*18*). In this method, by using testing equipment in pavement layers, the weight of the vehicle, axle load, wheel load, and the axle types are estimated. Among three types of gathering traffic data, only WIM data is appropriate to generate both truck classification and axle loading spectra data required in Pavement ME (*17*). However, collecting high-quality WIM data is expensive, and analyzing the data requires extensive efforts and expertise.

Analyzing WIM and AVC collected data can determine the required truck traffic information for state agencies. Level 1 traffic data can be determined from WIM, or AVC sites settled along the roadways can be collected as level 2 from similar traffic roads. Input parameters required in the traffic module of Pavement ME are site-specific and can be determined by state agencies or traffic departments.

Initial Two-Way Average Annual Daily Truck Traffic (AADTT)

AADTT is a product of the Annual Average Daily Traffic (AADT) and percent trucks. AADTT might be obtained from WIM, AVC, or manual traffic count and includes the truck traffic in both directions and all lanes (*4*). AADTT should be calculated for the base year at the beginning of a roadway opening or rehabilitation completion.

Lane and Directional Distributions

Lane distribution of traffic can be determined by predicting the portion of the traffic in separate lanes and directions. The most heavily used lane is referred to as the design lane. Generally, the outside lanes are the design lanes (*4*), and the directional distribution factor is a 50/50 percent split.

Growth Factors for Trucks

The number of trucks mostly increases over time. The future truck traffic prediction and the rate of increase are difficult to be determined due to large various known and unknown parameters. AASHTOWare Pavement ME design program can get a specific growth rate for each type of truck during the design year; however, for most analysis, the amount of growth rate remains the same during the analysis time (*4*). A simple growth rate assumes the AADT is increased by the same amount each year. A compound growth rate assumes an accumulative growth for the AADT amount.

The growth factor can be calculated by equation(18) considering the compound growth rate (*19*).

$$T_f = (1+r)^n \quad (18)$$

where,

T_f = growth factor;
r = rate, if growth expressed as a fraction; and
n = number of years.

The roadway system is divided into subsystems that are believed to have approximately similar growth rates. AASHTO guideline for traffic data program (*20*) gave several observations which can be useful in forming the growth-factor groups, including:

- The growth factor is different in urban and rural areas
- Outlying parts of an urban area are likely to have traffic volumes that are growing faster than central cities.
- Traffic on the interstate system in rural areas and small urban areas have a less affected growth rate by the local economy.
- In large states, rural growth rates may vary regionally, and different growth rates may be estimated in different urbanized areas.

Based on the observations found through AASHTO, a basic set of growth factor group might consist of central cities and older suburbs, newer suburbs, the rural and small urban interstate system, and other small rural roadways.

Operational Speed

Dynamic modulus of HMA mixtures is susceptible to the dynamic load frequency, which is a function of the truck speeds. Based on Pavement ME design, lower speed trucks bring out a higher amount of fatigue and a deeper amount of rut depth. The speed limit can be used in all design efforts unless the pavements are located in a special low-speed area (*4*).

Vehicle Classification

M-E Design traffic input requires the distribution percentage of truck classes 4 to 13 for the base year of design, which named vehicle class distribution. The vehicle class distribution can be determined from WIM or AVC data, and the sum of the distribution percentage is equal to 100.

In a case where level 1 data is not available, designers may use an appropriate default Truck Traffic Class (TTC) group in the M-E Design software. TTC factors were developed using traffic data from over 100 WIM and AVC sites located nationwide. The Truck class distribution for each TTC group recommended by Pavement ME Design. By using these typical values, the truck distribution for each specific road can be estimated.

Monthly Distribution Factors

The distribution of each vehicle class through a year is defined as the monthly distribution factor. Since most of the calibration sites are located near the interstate system or primary arterials, it is recommended by the Pavement ME guide to using values of 1.0 for these factors. In the case of local routes, monthly distribution factors in truck traffic operations should be

considered. The seasonal or monthly distribution factors can be estimated through the WIM, AVC, or manual traffic count data analysis.

Hourly Distribution Factors
During a day, total truck traffic varies from an early hour to the end of a day. The hourly distribution factors can be estimated through the WIM, AVC, or manual traffic count data analysis. The variance of total traffic can affect more on rigid pavements, which are susceptible to temperature change during a day. In the case of flexible pavements, the monthly distribution factor satisfies the pavement performance analysis models (*4*).

Axle-Load Configurations
WIM database records the spacing of the axles for passing vehicles. Based on the recorded data, the values of axle spacing for each truck class are approximately the same and can be considered as 51.6 and 49.2 (in) for tandem and tridem axles, respectively (*4*). Axle width is the distance between the outer edges of an axle. The recommended value of axle width for trucks is 8.5 feet. Center to center distance for two tires in a dual tire configuration is named as dual tire spacing. The recommended value of dual tire spacing for trucks is 12 inches (*19*).

The wheelbase is the distance between the centers of the front and rear axles. This is used in determining the number of load applications for JPCP top-down cracking. The wheelbase is recorded in the WIM database.

Tire Pressure
AASHTOWare Pavement ME design program assumes a tire pressure of 120 psi for all types of truck classes and loading conditions. The hot inflation pressure for specific designs should be studied, or the default value should be used.

Lateral Wander of Axle Loads
The inputs required for characterizing the lateral wander include the following (*4*):

- **Mean Wheel Location:** is the distance from the outer edge of the wheel to the pavement marking. The M-E Design software provides a default value of 18 inches, which is recommended unless a measured value is available.

- **Traffic Wander Standard Deviation:** is the standard deviation of lateral traffic wander. For a standard lane width, the standard deviation amount of 10 inches is recommended unless a defined value is available. A lower or higher lateral wander value is suggested for narrower or wider lanes, respectively.

- **Design Lane Width**: is the distance between the lane markings on each side of the design lane and has a typical value of 10-12 ft.

Climate Input
Climatic data inputs that contribute to the prediction of pavement distress of AASHTOWare Pavement ME design include hourly temperature, relative humidity, precipitation, cloud cover, and wind speed. The climate data determines the amount of temperature and moisture content of different layers in pavement structure and provides some of the parameters of predictive models in the analysis procedure (*4*).

For states with higher variance in climate conditions such as hourly temperature, separate regions with similar climate condition can be a candidate for collecting the required data. It is important to understand that proximity is not the best indicator of similar weather conditions. In

order to attain a more accurate analysis, it is recommended to create a weather station by importing a new climatic file created with locally collected climatic data (*4*).

Performance Models

Rutting

Surface distress in the form of rutting is caused by plastic or permanent vertical deformation in HMA, unbound layers, and foundation soil. The approach utilized in the Pavement ME is based upon calculating the incremental rutting within each sublayer. Rutting is estimated for each season in the middle of each layer in the pavement structure. The plastic deformation for any season is the summation of plastic vertical deformations in each layer.

The model for calculating the total permanent deformation uses the plastic vertical strain under specific pavement conditions for the total number of trucks. Conditions vary from month to month, so the "strain hardening" approach can be used to incorporate those plastic vertical strains within each month in a cumulative deformation. The rate of accumulation of plastic deformation is measured in the laboratory using repeated load permanent deformation triaxial tests for both HMA mixtures and unbound materials. The laboratory-derived relationship is calibrated by the rut depth measured on the roadway. For all HMA mixtures, the MEPDG calibrated relationship from repeated load permanent deformation tests is shown in equation (19) (*4*).

$$\Delta_{p(HMA)} = \varepsilon_{p(HMA)} h_{HMA} = \beta_{1r} k_z \varepsilon_{r(HMA)} 10^{k_{1r}} n^{k_{2r}\beta_{2r}} T^{k_{3r}\beta_{3r}} \quad (19)$$

where,

$\Delta_{p(HMA)}$ = Accumulated permanent or plastic vertical deformation in the HMA layer/sublayer, (in);

$\varepsilon_{p(HMA)}$ = Accumulated permanent or plastic axial strain in the HMA layer/sublayer, (in /in);

h_{HMA} = Thickness of the HMA layer/sublayer, (in);

$\varepsilon_{r(HMA)}$ = Resilient or elastic strain calculated by the structural response model at the mid-depth of each HMA sublayer, (in/in);

n = Number of axle-load repetitions;

T = Mix or pavement temperature, (°F);

k_z = Depth confinement factor;

$k_{r1, r2, r3}$ = Global field calibration parameters (k_{r1} = –3.35412, k_{r2} = 0.4791, k_{r3} = 1.5606); and

$\beta_{1r,2r,3r}$ = Local or mixture field calibration constants, (for the global calibration, these constants were all set to 1).

and,

$$k_z = (C_1 + C_2 D)0.328196^D \quad (20)$$

$$C_1 = -0.1039(H_{HMA})^2 + 2.4868 H_{HMA} - 17.342$$

$$C_2 = 0.0172(H_{HMA})^2 - 1.7331 H_{HMA} + 27.428$$

where,

D = Depth below the surface, (in); and

H_{HMA} = Total HMA thickness (in).

The equation(21) shows the field-calibrated mathematical equation used to calculate the plastic vertical deformation within all unbound pavement sublayers and the foundation or embankment soil (*4*).

$$\Delta_{p(soil)} = \beta_{s1} k_{s1} \varepsilon_v h_{soil} \left(\frac{\varepsilon_\circ}{\varepsilon_r} \right) e^{-\left(\frac{\rho}{n}\right)^{\beta}} \quad (21)$$

$\Delta_{p(soil)}$ = Permanent or plastic deformation for the layer/sublayer, (in);
n = Number of axle-load applications;
$\varepsilon_\circ$ = Intercept determined from laboratory repeated load permanent deformation tests, (in/in);
ε_r = Resilient strain imposed in a laboratory test to obtain material properties, (in/in);
ε_v = Average vertical resilient or elastic strain in the layer/sublayer and calculated by the structural response model, (in/in);
h_{soil} = Thickness of the unbound layer/sublayer, (in);
k_{s1} = Global calibration coefficients; recommended 2.03 for granular materials and 1.35 for fine-grained materials; and
β_{s1} = Local calibration constant for the rutting in the unbound layers; the local calibration constant was set to 1 for the global calibration effort.

and

$$\log \beta = -0.61119 - 0.017638(W_C)$$

$$\rho = 10^9 \left(\frac{C_\circ}{(1 - (\left(10^9\right)^{\beta})} \right)^{\frac{1}{\beta}} \quad (22)$$

$$C_\circ = Ln\left(\frac{a_1 M_r^{b1}}{a_9 M_r^{b9}} \right)$$

Wc = Water content, (%);
Mr = Resilient modulus of the unbound layer or sublayer, (psi);
$a_{1,9}$ = Regression constants; a_1=0.15 and a_9=20; and
$b_{1,9}$ = Regression constants; b_1=1 and b_9=1;

The regression coefficients or plastic deformation coefficients were determined from lab tests and adjusted to the field measured values. The k_{3r} factor is the slope in the steady-state or the secondary range, while k_{1r} is the intercept of the log-log relationship between the number of load applications and cumulative plastic strain. The k_{2r} factor is the effect of temperature on the intercept (*21*).

The pavement ME uses an incremental thickness and time approach in calculating total HMA rut depth. The depth function (equation(20)), is included to consider the effect of confinement from the upper HMA thickness increments in calculating the incremental rut depths through all of the HMA layers. A time-hardening scheme is included to accumulate plastic deformation

over multiple load levels and seasons. The depth function has received extensive criticism from industry regarding its applicability, while the time hardening scheme has been used by others in calculating total HMA rutting with time (22).

Fatigue Cracking

Two types of load-related cracks, which are predicted by AASHTOWare Pavement ME Design, include alligator cracking and longitudinal cracking. The Pavement ME Design assumes that alligator cracks are triggered at the bottom of HMA layers and propagate to the surface under cyclic traffic load, while longitudinal cracks are assumed to initiate at the surface. The allowable number of axle-load applications to predict both types of load-related cracks (i.e., alligator and longitudinal) is shown in equation(23) (2).

$$N_{f-HMA} = k_{f1}(C)(C_H)\beta_{f1}(\varepsilon_t)^{k_{f2}\beta_{f2}}(E_{HMA})^{k_{f3}\beta_{f3}} \quad (23)$$

where

$N_{f\text{-}HMA}$ = Allowable number of axle-load applications for a flexible pavement;
ε_t = Tensile strain calculated by the structural response model, (in/in);
E_{HMA} = Dynamic modulus of the HMA (psi);
$k_{f1, f2, f3}$ = Global field calibration coefficients (k_{f1} = 0.007566, k_{f2} = 3.9492, and k_{f3}= 1.281); and
$\beta_{f1, f2, f3}$ = Local or mixture specific field calibration constants.

and;

$$C = 10^M$$

$$M = 4.84\left(\frac{V_{be}}{V_a + V_{be}} - 0.69\right) \quad (24)$$

where,

V_{be} = Effective asphalt content by volume, (%);
V_a = Percent air voids in the HMA mixture.

C_H can be defined as a thickness correction term which depends on the type of cracking. For bottom-up or alligator cracking:

$$C_H = \frac{1}{0.000398 + \frac{0.003602}{1 + e^{(11.02 - 3.49 H_{HMA})}}} \quad (25)$$

For top-down or longitudinal cracking:

$$C_H = \frac{1}{0.01 + \frac{12}{1 + e^{(15.676 - 2.8186 H_{HMA})}}} \quad (26)$$

where

H_{HMA} = Total HMA thickness (in).

AASHTOWare Pavement ME Design calculates the incremental damage as specified throughout the HMA layers at critical depths. The incremental damage index (ΔDI) is calculated by dividing the actual number of axles' loads by the allowable number of axles' loads in a time period for each axle type. The cumulative damage index (DI) for each critical depth is determined by equation (27)(2).

$$DI = \sum (\Delta DI)_{j,m,l,p,T} = \sum \left(\frac{n}{N_{f-HMA}} \right)_{j,m,l,p,T} \quad (27)$$

where,

n = Actual number of axle-load applications within a specific time period;
j = Axle-load interval;
m = Axle-load type (single, tandem, tridem, or quad);
l = Truck type using the truck classification groups;
p = Month, and
T = Median temperature for the five temperature intervals.

The area of alligator cracking and length of longitudinal cracking are calculated from the total damage over time. The equation(28) shows a relationship used to predict the amount of alligator cracking on the surface.

$$FC_{Bottom} = \left(\frac{1}{60} \right) \left(\frac{C_4}{1 + e^{\left(C_1 C_1^* + C_2 C_2^* \log(DI_{bottom} * 100) \right)}} \right) \quad (28)$$

where,

FC_{Bottom} = Area of alligator cracking that initiates at the bottom of the HMA layers, (% of total lane area);
DI_{Bottom} = Cumulative damage index at the bottom of the HMA layers, and
$C_{1,2,3,4}$ = Transfer function regression constants; (Global calibration values: C_4 = 6000; C_1 =1; and C_2 =1).

and,

$$C_1^* = -2C_2^*$$
$$C_2^* = -2.40874 - 39.748(1 + H_{HMA})^{-2.856} \quad (29)$$

The equation (30) is the relationship used to predict the length of longitudinal fatigue cracks.

$$FC_{Top} = 10.56 \left(\frac{C_4}{1 + e^{\left(C_1 - C_2 \log(DI_{Top}) \right)}} \right) \quad (30)$$

where,

FC_{Top} = Length of longitudinal cracks that initiate at the top of the HMA layer, (ft/mile);
DI_{Top} = Cumulative damage index near the top of the HMA surface; and
$C_{1,2,3}$ = Transfer function regression constants; (Global calibration values: C_1 = 7; C_2 =3.5; and C_4=1000).

For fatigue cracks in CTB layers, the allowable number of load applications, N_{f-CTB}, is determined using equation (31) , and the amount of fatigue cracking area is calculated using

equation (32). These damage and distress transfer functions were never calibrated under any of NCHRP projects and are not recommended for use until the transfer function has been calibrated (*4*).

$$N_{f-CTB} = 10^{\left[\frac{k_{c1}\beta_{c1}\left(\frac{\sigma_t}{MOR}\right)}{k_{c2}\beta_{c2}}\right]} \quad (31)$$

$$FC_{CTB} = C_1 + \frac{C_2}{1+e^{(C_3 - C_4 \log(DI_{CTB}))}} \quad (32)$$

where

$N_{f\text{-}CTB}$ = Allowable number of axle-load applications for a semi-rigid pavement;
σ_t =Tensile stress at the bottom of the CTB layer, (psi);
MOR = 28-day modulus of rupture for the CTB layer, (psi);
DI_{CTB} = Cumulative damage index of the CTB or cementitious layer;
$k_{c1,c2}$ = Calibration coefficients;
$\beta_{c1,\ c2}$ =Local calibration constants;
FC_{CTB} = Area of fatigue cracking, (sq. ft), and
$C_{1,2,3,4}$ =Transfer function regression constants.

Thermal Cracking

The thermal cracking model is presented below in the following equation.

$$\Delta C = A\left(\Delta K\right)^n \quad (33)$$

where,

ΔC = Change in the crack depth due to a cooling cycle.
ΔK = Change in the stress intensity factor due to a cooling cycle, and
A,n = Fracture parameters for the HMA mixture.

Experimental results indicate that reasonable estimates of *A* and *n* can be obtained from the indirect tensile creep-compliance and strength of the HMA.

$$A = k_1\beta_1 10^{\left[4.389 - 2.52\log(E_{HMA}\,\sigma_m\,n)\right]}$$

$$n = 0.8\left[1 + \frac{1}{m}\right] \quad (34)$$

where

k_t = Coefficient determined through the global calibration for each input level (Level 1 = 1.5; Level 2 = 0.5; and Level 3 = 1.5);
E_{HMA} = HMA indirect tensile modulus, (psi);
σ_m = Mixture tensile strength, (psi);
m =The *m*-value derived from the indirect tensile creep compliance curve measured in the laboratory; and
β_t = Local or mixture calibration factor.

The stress intensity factor, *K*, has been incorporated in AASHTOWare Pavement ME Design using a simplified equation shown below:

$$K = \sigma_{tip}\left[0.45 + 1.99\left(C_{\circ}\right)^{0.56}\right] \quad (35)$$

where,

σ_{tip} = far-field stress from pavement response model at a depth of crack tip, (psi); and

$C_{\circ}$ = initial crack length, (ft).

AASHTOWare Pavement ME Design predicts the degree of cracking by using an assumed relationship between the probability distribution of the log of crack depth to the HMA-layer thickness ratio and the percent of cracking. The equation (36) shows the expression used to determine the extent of thermal cracking.

$$TC = \beta_{t1} N\left[\frac{1}{\sigma_d}\log\left(\frac{C_d}{H_{HMA}}\right)\right] \quad (36)$$

where,

TC = Observed amount of thermal cracking, (ft/mi);

β_t = Regression coefficient determined through global calibration;

N = Standard normal distribution;

σ_d = Standard deviation of the log of the depth of cracks in pavement (0.769 in);

C_d = Crack depth, (in); and

H_{HMA} = Thickness of HMA layers (in).

Smoothness

AASHTOWare Pavement ME Design utilizes the International Roughness Index (IRI) for estimating the smoothness of a pavement due to different surface distresses. Equations (37) through (39) were developed from the LTPP data and inserted in AASHTOWare Pavement ME design to predict IRI for HMA pavements (*4*).

$$IRI = IRI_{\circ} + C_1(RD) + C_2(FC_{Total}) + C_3(TC) + C_4(SF) \quad (37)$$

where,

IRI_o = Initial IRI after construction, (in/mi);

SF = Site factors;

FC_{Total} = Area of fatigue cracking (combined alligator, longitudinal, and reflection cracking), percent of total lane area. All load related cracks are combined on an area basis.

TC = Length of transverse cracking, (ft/mile); and

RD = Average rut depth

$C_{1,2,3,4}$ = Calibration factors; Global values: C_1 =40, C_2 =0.4, C_3 =0.008, and C_4=0.015.

The site factor (SF) can be calculated for different site conditions using equation (38).

$$SF = Age^{1.5}\left\{\ln\left[(Precip+1)(FI+1)_{P02}\right]\right\} + \left\{\ln\left[(Precip+1)(PI+1)_{P200}\right]\right\} \quad (38)$$

where,

Age = Pavement age, year;

PI = Percent plasticity index of the soil;
$Precip$ = Average annual precipitation or rainfall, (in);
FI = Average annual freezing index, (°F-days);
P_{02} = Percent passing the 0.02 mm sieve;
P_{200} = Percent passing the 0.075 mm sieve.

The equation (39) shows the amount of IRI for HMA overlays of rigid pavements.

$$IRI = IRI_{\circ} + PCC\_C_1(RD) + PCC\_C_2(FC_{Total}) + PCC\_C_3(TC) + PCC\_C_4(SF) \quad (39)$$

where,
$PCC\_C_{1,2,3,4}$= Calibration factors; Global values: PCC_C_1 = 40.8; PCC_C_2 =0.575; PCC_C_3 = 0.0014; PCC_C_4 =0.00825.

RIGID PAVEMENTS

In the Pavement ME, different material properties are incorporated to characterize Portland Cement Concrete (PCC) materials for the design of jointed plain concrete pavement (JPCP) and continuously reinforced concrete pavement (CRCP). Key parameters for PPC mixture, such as compressive strength and flexural strength, can be determined through laboratory testing or correlation with other properties. These parameters are crucial to perform the analytical model for response calculation, damage determination, and performance prediction. The effect of climate is also modeled by the MEPDG procedure by using PCC slab depth and additional parameters. Default values for the additional parameters, in climatic modeling, are usually used.

Static Modulus of Elasticity over Time
The modulus of elasticity in PCC materials is a complicated parameter, which is usually influenced by many factors such as mix design and mode of testing. In general, modulus of elasticity for a given concrete mixture can be determined in the elastic part of the stress-strain curve by calculating the ratio of stress to strain (*23*). The following parameters have a significant effect on determining the elastic modulus:

1. Water to cementitious materials ratio (*w/(cm)*)
2. Paste and aggregate features.
3. Type of aggregate.

In the mechanistic pavement response, the concrete mixture modulus of elasticity (E_c) has a significant role in deflection and stress development throughout the pavement structure. In the Pavement ME, the characterization of the PCC elastic modulus depends mainly on the pavement design type and structure. Thus, the PCC material modulus characterization falls into three distinct groups:

- PCC modulus for new or reconstruction JPCP and CRCP projects and PCC overlays.
- Existing PCC pavement layer modulus being considered for rehabilitation with overlays or for restoration (applicable for JPCP only).
- Fractured PCC pavements.

PCC Modulus Characterization for New/Reconstruction JPCP and CRCP and PCC Overlays

For Modulus of elasticity determination, the designer should provide an estimate of modulus development or degradation over time. For level 1 input, for instance, the relationship can be built through the testing results at different ages. For level 3, typical materials relationships are usually used.

For new PCC slabs, the modulus of elasticity, Ec, can be measured as level 1 by using ASTM C 469 at 7, 14, 28, 90 days. By predicting the ratio of the 20-year value of elastic modulus to the 28-days value, a modulus curve can be determined, and the value of E_c at any time of the design period will be calculated.

The modulus of elasticity can be determined from compressive strength values obtained by AASHTO T22 at 7, 14, 28, and 90 days. The level 2 E_C can be calculated using equation (40). By knowing the amount of compressive strength at any time of design life.

$$E_c = 33 * \rho^{\frac{3}{2}} * \left(f_c^{'}\right)^{\frac{1}{2}} \tag{40}$$

If the data of compressive strength is not available, the value of compressive strength can be estimated from the modulus of rupture values. The modulus of rupture at any given time can be estimated using equation (41) by having the typical or tested values of *MR* at 28 days. Equation (42) converts the modulus of rupture at any given time to compressive strength, which can be used as input in equation(41).

$$MR_{(t)} = \left(1 + \log\left(\frac{t}{0.0767}\right) - 0.01566\log\left(\frac{t}{0.0767}\right)^2\right) \times MR_{28d} \tag{41}$$

$$f_c^{'} = \left(\frac{MR}{9.5}\right)^2 \tag{42}$$

Level 3 data obtained from this method shows the least accuracy and level of confidence.

PCC Elastic Modulus Characterization of Existing Intact PCC Pavement Layers

In the case of rehabilitation design with an overlay or restoration of an existing JPCP, the modulus of existing shall be characterized for design and performance reasons. The primary difference in characterizing new PCC layer and existing layers can be summarized by the following:

- For overly on existing layers, the performance of concrete pavements under the traffic and environmental loads should be considered. Thus, the estimated intact slab modulus of existing layers is considered the main component in developing damage in pavements.

- In the case of restoration, the modulus gain is not considered overtime as it does not increase in old PCC.

For level 1, the core of existing PCC layer is acquired and tested for elastic modulus using ASTM C 469 or nondestructive testing using FWD data for CRCP or JPCP can be used to back-calculate the estimated mean of the modulus E_{test} using the best fit method (7, 24). The back-calculated modulus can be, then, used to determine the static elastic modulus for the uncracked section by multiplying E_{test} by a factor of 0.8. Additionally, the overall condition of the existing PCC should be determined by following a specific evaluation methodology presented in chapter 5-Part II of the Pavement ME guideline. By multiplying the E_{test} with C_{BD} , the $E_{BASE/DESIGN}$ of the existing PCC layer can be estimated.

$$E_{base/design} = C_{BD} * E_{Test} \quad (43)$$

For level 2, cores along the existing PCC layer are acquired and tested for compressive strength using AASHTO T22. The tested elastic modulus can be estimated by incorporating the uncracked compressive strength of the cores using the equation (40). Again, the overall condition of the existing PCC should be determined by following a specific evaluation methodology presented in chapter 5-Part II of the Pavement ME guideline. For level 3, one should determine the total condition of the existing PCC by following a specific evaluation methodology presented in chapter 5-Part II of the Pavement ME guideline.

PCC Elastic Modulus Characterization of Fractured PCC Pavement Layers

In the case of fractured PCC pavement layers, Level 1 and 2 data inputs are not applicable because it is based on obtaining uncracked cores from the site to test for elastic modulus and compressive strength respectively. The typical methods of fracturing existing pavements are crack and seat, break and seat, and rubblization. However, rubblization in terms of material featuring can be placed in a separate category from cracked or broken and seated PCC layers. Thus, level 3 typical values of the elastic modulus can be used as indicated by the FHWA part II- Material Characterization (7).

Poisson's Ratio of PCC Materials

Poisson's ratio has no critical impact on the efficiency of the PCC pavement. However, it is still required for the computation of the structural response models. Therefore, this parameter is usually not measured by testing. In the case of level 1 requirement, Poisson's ratio may be estimated along with the determination of the elastic modulus through the ASTM C 469 procedure. Input level 2 is not applicable in the case of Poisson's ratio because there is no correlation or relationship between Poisson's ratio and material characteristics or other test parameters. Generally, for normal concrete, Poisson's ratio ranges from 0.11 and 0.21 while in PCC pavement design, a value between a range of 0.15 and 0.18 can be assumed.

Flexural Strength (*MR*) of PCC Materials

The flexural strength, *MR,* can be obtained by evaluating the tensile stress at the rupture of the bottom fiber of a supported plain concrete beam through the third point loading flexural test. The *MR* is significantly affected by many parameters such as mix design (i.e., mix constituents, cement type, presence of chemical or mineral admixtures, w/c ratio, and aggregate properties which include; type, maximum particle size, gradation, particle shape, and texture as well as curing technique, age, and testing condition). *MR* is highly significant in determining fatigue cracking potential under repeated flexural stresses. Thus, special care should be practiced determining the most accurate value of the *MR* for use in rigid pavement design. The same other important concrete properties, *MR* determination, can be categorized into (I) new or reconstruction JPCP and CRCP projects and PCC overlays; and (II) existing PCC pavement

layers considered for overlay rehabilitation or for restoration which is applicable only in case of JPCP.

PCC Flexural Strength Characterization for New or Reconstruction JPCP and CRCP Projects and PCC Overlays

For the design cases, the strength gain over time is basically considered to provide a more sensitive gathering of incremental damage. This can be established using the level 1 input procedure of compressive strength characterization provided earlier. For level 3 inputs, typical relationships are used to determine *MR* from other PCC mix properties. For new PCC slabs, the modulus of rupture, *MR*, can be measured as level 1 by using ASTM T 97 at 7, 14, 28, 90 days. By predicting the ratio of the 20-year value of *MR* to the 28-day value, a develop modulus curve can be determined, and the value of flexural strength at any time of the design period will be calculated.

The modulus of rupture can be determined from compressive strength values obtained by AASHTO T22 at 7, 14, 28, and 90 days. The level 2 *MR* can be calculated through equation (44) by knowing the amount of compressive strength at any time of design life.

$$MR = 9.5 * \left(f_c^{'}\right)^{\frac{1}{2}} \quad (44)$$

Indirect Tensile Strength of PCC Materials

This parameter is considered one of the basics of the CRCP pavement design, as it is significant to predict the aggregation of damage and the development of punchouts. Indirect tensile strength factors are also the main factors for the flexural strength; thus, these two parameters are well related. Defining the indirect tensile strength of PCC can be grouped into new or reconstruction CRCP projects and existing PCC pavement layers that require overlay rehabilitation.

Compressive Strength of PCC Materials

The compressive strength is usually required to determine other parameters such as the elastic modulus, flexural strength, and indirect tensile strength. The protocol used to determine compressive strength can be found in the previous sections.

PCC Coefficient of Thermal Expansion

The coefficient of thermal expansion (α_{PCC}) is significantly under the influence of the hardened cement content and other mix parameters. The α_{PCC} can be predicted using the weight portion of concrete mix components. Thus, the aggregate dictates the α_{PCC} as it comprises 70 to 80% of the total volume. However, other factors such as the volume of cement paste, moisture content, porosity, and degree of hydration (age) of the paste also participate in the determination of $\alpha_{PCC.}$

As the coefficient of thermal expansion is considered as a new parameter in pavement design, the Pavement M-E design guideline lists the procedures to determine this coefficient at the different input levels. For level 1 input, α_{PCC} can be measured following the AASHTO TP 60 “Standard Test Method for the Coefficient of Thermal Expansion of Hydraulic Cement Concrete.” Through this protocol, a direct change of the length in the lab specimens can be determined. This procedure is also used for all pavement sections in the LTPP or for the calibration of the Pavement ME Design.

Level 2 input, Pavement ME guide uses a linear, weighted average of the constituent such as aggregate and paste coefficient of thermal expansion values based on the volume of each

constituent. The equation (45) is usually used to determine the specified average of the thermal coefficient.

$$\alpha_{pcc} = \alpha_{agg} \times V_{agg} + \alpha_{paste} \times V_{paste} \quad (45)$$

where,
α = the thermal coefficients of aggregate and paste; and
V = the volumetric proportion of the aggregate and paste in the concrete constituent.

For Level 3 input, historical averages of the thermal expansion are used to estimate the $\alpha_{pcc.}$ In this procedure, the LTPP records of concrete pavement subjected to the AASHTO TP 60 protocol are collected, and the linear average is determined. To estimate a reasonable thermal coefficient, concrete pavements that contain typical concrete mixes in terms of aggregate and paste volume are preferable.

PCC Shrinkage
Drying shrinkage in concrete pavement is an essential factor in determining the crack development in CRCP slabs. On the other hand, the JPCP can be affected by slab warping due to the deferential moisture throughout the slab thickness that yields to cracking.

Inputs required to drying shrinkage based on the Pavement ME guide include ultimate shrinkage strain in micro-strain, the time needed to reach 50% of the ultimate shrinkage strains in days, expected amount of reversible shrinkage in percent and the average monthly surrounding relative humidity for the pavement which can be established through EICM model and weather data.

AASHTO T 160 test procedure can be used for determining level 1 shrinkage strain at 40% humidity. Also, by using mix parameters such as the type of the cement, cement content and water-cement ratio, and compressive strength, the level 2 PCC shrinkage value can be measured by applying equation (46).

$$\varepsilon_{su} = C_1 C_2 \left[26w^{2.1} \left(f_c' \right)^{-0.28} + 270 \right] \quad (46)$$

where,
ε_{su} = ultimate shrinkage strain, x 10^{-6};
C_1 = cement type factor:
1.0 for type I cement
0.85 for type II cement
1.1 for type III cement

C_2 = type of curing factor:
0.75 if steam cured
1.0 if cured in water or 100% relative humidity
1.2 if sealed during curing (curing compound
w = water content, lb/ft^3 for the PCC mix under consideration.
f'_c = 28-day PCC compressive strength, psi (determined from AASHTO T22).

For level 3 cases, by having typical recorded values of compressive strength and water content, equation (46) can be used.

For all design cases, the recommended amount for 50% shrinkage by ACI committee 209 is 35 days, and the anticipated amount of reversible shrinkage in performance models can be considered 50%.

Literature Review of Unbound Layer and Subgrade Characteristics and Models

The main concern of this section of the literature review is to determine the probable root causes for the problems associated with Pavement ME methodology and the solutions that target the identified causes. To answer these concerns, the following items should be addressed:

1. Review the characteristics of unbound layers and subgrade used in the AASHTOWare Pavement ME Design software and MEPDG.
2. Collect and review the influence of unbound layer and subgrade characteristics on the performance of rigid pavements.
3. Collect and identify mechanistic-empirical models of unbound layers and subgrade that address such influence.

Characteristics of Unbound Layers and Subgrade Used in Pavement ME Design

Pavement ME Design software and MEPDG are practical tools for the pavement design and analysis based on mechanistic-empirical principles. They predict multiple performance indicators for rigid pavements, including the following (8):

Rigid pavements:

- Transverse cracking in the jointed plain concrete pavement (JPCP)
- Faulting in JPCP
- Punchouts in the continuously reinforced concrete pavement (CRCP)
- Crack spacing and crack width in CRCP
- Smoothness (IRI) in JPCP and CRCP

For each performance indicator above, Pavement ME Design has a distress prediction model that requires inputs from different layers in a pavement structure. The inputs from unbound layers and subgrade are shown in Table 8 to account for the influence of these underlying layers.

Table 8- Inputs from Unbound Layers and Subgrade in Pavement ME Design-Rigid Pavement

Performance Indicator	Unbound Layer	Subgrade
Transverse Cracking (JPCP)	Thickness Resilient Modulus Erodibility index Loss of friction	Groundwater depth Resilient Modulus
Faulting (JPCP)	Resilient Modulus Erodibility index Thickness Load transfer efficiency (LTE)	Resilient Modulus

Performance Indicator	Unbound Layer	Subgrade
Punchouts (CRCP)	Resilient Modulus Base slab friction Thickness	Resilient Modulus Groundwater depth
Crack Width (CRCP)	Base slab friction Resilient Modulus Thickness LTE	Resilient Modulus Groundwater depth
Smoothness (IRI) (JPCP)	Resilient Modulus Erodibility index Base slab friction Thickness	Resilient Modulus
Smoothness (IRI) (CRCP)	Resilient Modulus Base slab friction Thickness	Resilient Modulus

However, recent investigations indicate that the performance predicted by Pavement ME Design generally shows low or no sensitivity to these underlying layers. A recent study conducted in the NCHRP Project 01-47 (54) reveals the following major problems in the rigid pavement:

- Faulting in JPCP is marginally sensitive to resilient modulus and erodibility, non-sensitive to a thickness of unbound layers.
- Transverse cracking in JPCP is marginally sensitive to resilient modulus, thickness, and erodibility of unbound layers.

In order to find the reasons for these problems, a better understanding of how the properties/thickness of unbound layers and subgrade affect pavement performance is needed, which is discussed in the next section.

Influence of Unbound Layers and Subgrade on Performance of Rigid Pavements

Table 8 presents the inputs of unbound layers and subgrade required in Pavement ME Design for predicting the performance of flexible and rigid pavements. However, besides these parameters, recent studies have identified the pavement performance to be significantly affected by other characteristics of the underlying layers. According to a comprehensive literature review, the Research Team divided the factors into the following categories:

- Material properties (e.g., modulus, shear strength)
- Material behaviors responding to traffic and environmental (temperature and moisture) conditions (e.g., permanent deformation and erosion)
- Structural characteristics (e.g., the thickness of unbound layers)

LOCAL CALIBRATION OF FLEXIBLE PAVEMENT

The AASHTO Guide for the local calibration of the Mechanical-Empirical pavement design guide defines a guideline for calibration of Pavement ME design according to the local material, climate, and pavement structural design. The guideline includes the following steps:

- Estimating sample size for each distress type.
- Selecting a roadway segment.
- Selecting Hierarchical Input Levels for use in local calibration.
- Extracting and evaluating test section Data.
- Analyzing the sections with Pavement ME.
- Assessing bias for experimental sections.
- Determining local calibration coefficient to eliminate bias.

The calibration effort for the state of Oklahoma follows the defined guideline. This chapter describes each step in detail regarding the Oklahoma pavement conditions.

Minimum Sample Size for Different Distress and IRI Prediction Models

Pavement sections should represent the agency standard specifications, construction, design practices, and climatic and traffic conditions. The selected sections represent a variety of design types for new, reconstruction, and rehabilitation. In addition, the proper number of pavement sections should be included in the calibration effort. The Pavement ME calibration design recommends a number of pavement segments for each type of HMA distress which includes (*25*):

- Rut depth and faulting: 20 pavement segments.
- Alligator and longitudinal cracking: 30 pavement segments.
- Transverse slab cracking: 30 pavement segments
- Transverse cracking: 26 pavement segments
- Reflection cracking: 26 pavement segments

The minimum number of required projects for Pavement ME distress and IRI model validation and calibration efforts depends on design reliability level and standard error estimate (*SEE*) for each type of distress (*21*).

$$n = \left(\frac{z_{\alpha/2}\sigma}{E} \right)^2 \quad (47)$$

where

n = Number of the sample;
σ = standard deviation of the true values;
E = The tolerable bias; and
$z_{\alpha/2}$ = 1.282 for a 90 percent confidence interval.

Table 9 shows the distress/IRI threshold values and *SEE* for the global Pavement ME models. The minimum number of projects required for calibration effort was estimated using equation (47).

Table 9- Estimated number of pavement projects required for Pavement ME validation and local calibration

Pavement Type	Performance Prediction Models	Threshold Values	Global Standard Error Estimate (SEE)	Tolerable Bias	Minimum Number of Project
HMA	Alligator cracking	20% lane area	5.01	2.5	13
HMA	Transverse cracking	630 ft/mi	250	100	16
HMA	Rut depth	0.4 inch	0.107	0.05	14
HMA	IRI	169 inch/mi	18.9	10	12
Rigid	Transverse Cracking-JPCP	<10% slabs	4.52	1.23	24
Rigid	Joint Faulting-JPCP	<0.15 inch	0.033	0.008	26
Rigid	Punchouts-CRCP	15 per mi	3.6	2.2	10
Rigid	IRI	169 inch/mi	17.1	10	11

Based on the statistical model, the minimum number of sample size for the calibration of flexible and rigid pavements are respectively 16 and 26 pavement segments. However, the local calibration guideline recommends using at least 30 pavement segments for the flexible pavements.

Selection of Roadway Segment

The experimental pavement sections should satisfy the recommendations from the Local Calibration Guide of the Pavement ME design:

- Projects should be representative of the typical Oklahoma pavement design and construction efforts.
- The project should cover different pavements in poor, moderate, and good conditions.
- Projects age should cover different construction ages and practices of newly constructed, older existing, and rehabilitated sections.
- The sample projects must be located throughout the state of Oklahoma and cover different climate conditions.

There are 59 sections in the LTPP database, which covers typical Oklahoma's flexible pavement design. These sections spanned the construction age from newly constructed to older constructed pavements and rehabilitated sections. In addition, 9 sections from a different research study about rehabilitation design (*26*) were added to the LTPP flexible pavement samples of Oklahoma to cover different pavement conditions. Pavement sections should be located throughout the state of Oklahoma to cover different climate conditions. The selected LTPP sections and the ones from the rehabilitation project cannot be representative of all the climate conditions in Oklahoma. For this reason, 3 LTPP sections from Sherman and Ochiltree counties located in an uppermost part of Texas and one section from Norton County in Kansas

were also added to the existing sections for calibration effort. Table 10 summarizes the selected experimental sections for the Oklahoma calibration effort.

Table 10 – Total experimental sections selected for calibration effort

Types	Status	Composite	Flexible
Oklahoma LTPP	Active	1	27
Oklahoma LTPP	Out of study	6	26
Neighbor states' LTPP	TX –KN	NA	4
ODOT Rehabilitation Project	NA	NA	9
Total	NA	7	66

The state of Oklahoma has been split by the interstate highway of I-35 into two regions of east and west Oklahoma. The east region has higher precipitation, and the average annual temperature and the west region have lower precipitation and average annual temperature. The annual average temperature is between 56 to 63 ˚F which put the two regions in the Non-Freeze climate category. Thus, to have better calibration results, the flexible pavement sections were divided into two groups of the west and east regions.

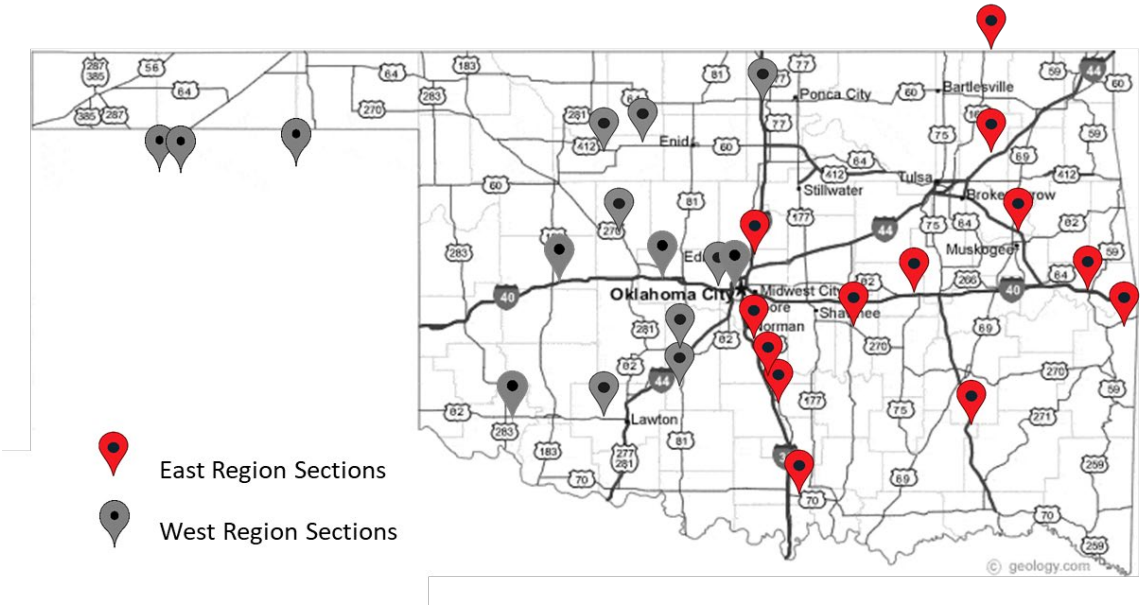

Figure 1- Location of roadway sections identified for local calibration effort of flexible pavements in Oklahoma

LTPP sections include two types of studies, General Pavement Studies (GPS) and Specific Pavement Studies (SPS). The GPS sections include commonly used structural design, and their performances are monitored against climatic, geologic, maintenance, rehabilitation, traffic, and other service conditions. The SPS sites have multiple sections with different design structure which provide the influence of each design factor on pavement performance (27).

The required Pavement ME input data were collected for each section and gathered in a database. The collected data were reviewed, and questionable data were corrected using

typical values or specific information in similar sections. A summary of experimental sections is included in Appendix A. The following data were assembled, reviewed, and cleaned up, and two sets of projects were selected with adequate detailed information for model verification and local calibration. The distress and IRI data of the new and aged constructed pavements will be used for the new pavement construction calibration, and the pavement performance after the treatment process will be used for the calibration of rehabilitation projects,

Data Extraction and Evaluation

Extracting and evaluating LTPP data and preparing the master calibration database is an important and vital objective for this project. Figure 2 shows the common flexible pavement groups used in the Pavement ME calibration effort in this study.

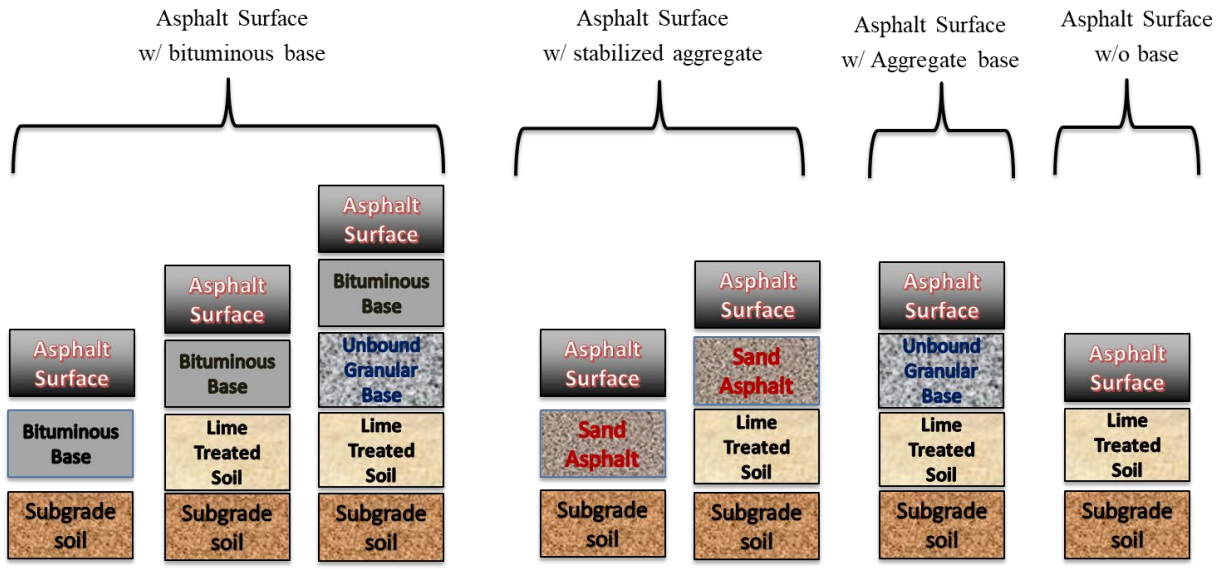

Figure 2 – Representative flexible pavements' structures used in Oklahoma calibration effort

The selected pavement sections cover different types of roads and construction age. The majority of segments were constructed during the 1980s, and they experienced various kinds of rehabilitation and treatments. In addition, the selected sections mostly are parts of the principal arterial roads, which carry the majority of traffics in Oklahoma. Figure 3 shows the distribution of the pavement construction year, and Figure 4 shows the road, functional class of the selected sections, for the Pavement ME calibration effort for the state of Oklahoma.

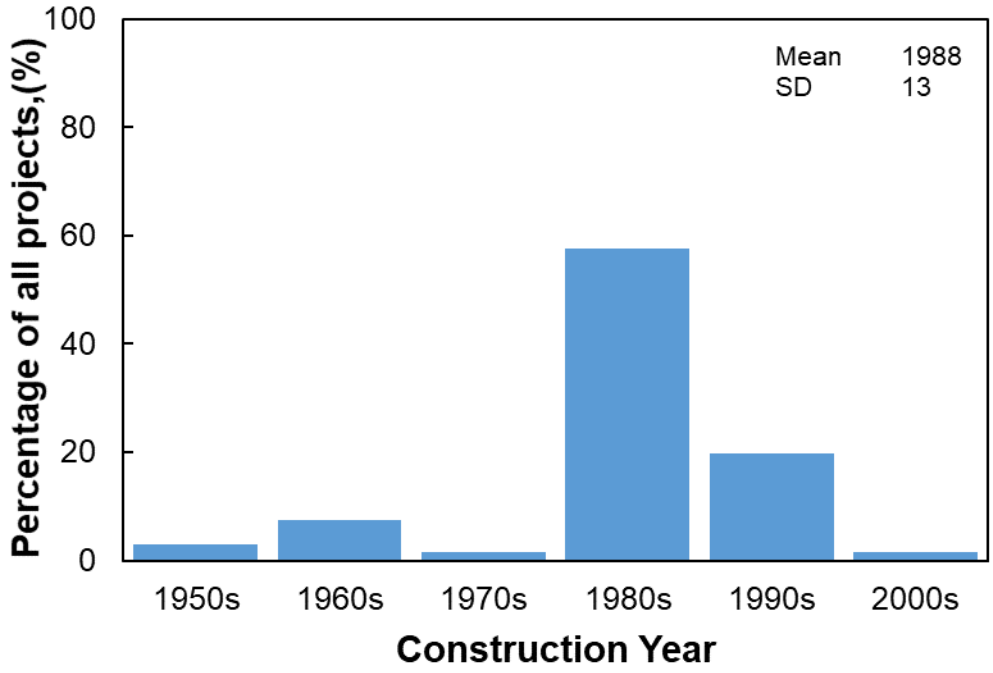

Figure 3- Construction year of Projects selected for the ODOT Pavement ME calibration database

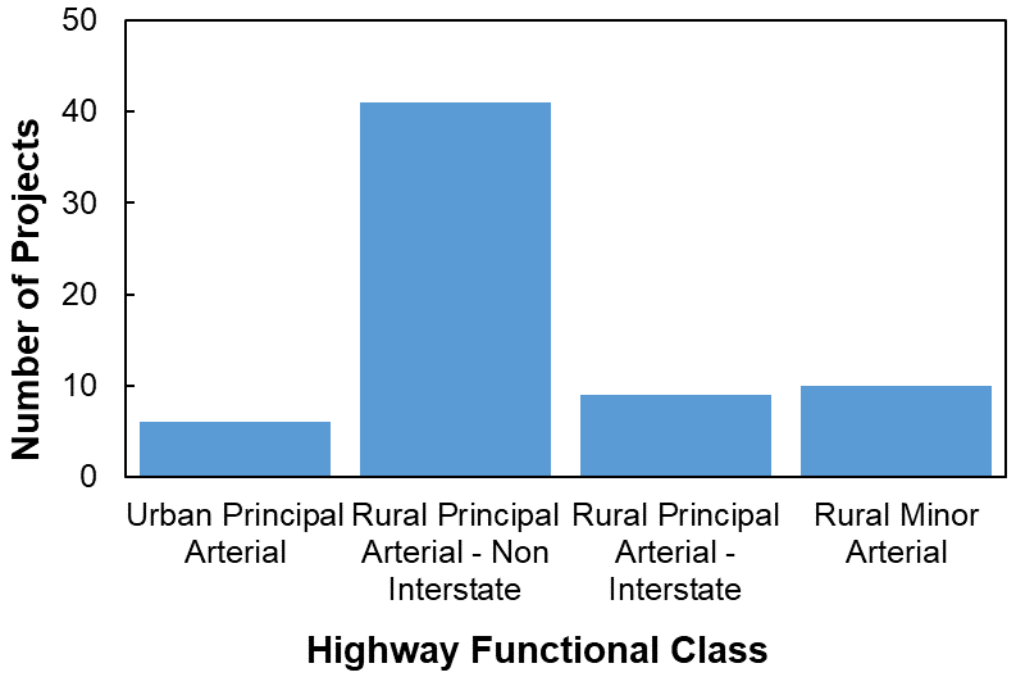

Figure 4- Highway functional class of Projects selected for the ODOT Pavement ME calibration database

The required data for calibration of Pavement ME include:

- Asphalt concrete material inputs
- Base and Subgrade/foundation field conditions and design inputs
- Environmental inputs

- Traffic loading inputs
- Climate data
- Performance/pavement distress data.

As shown before, the Pavement ME design requires several categories of input data. For this implementation project, pavement data were obtained from the LTPP and previous research reports. The researcher team also collected additional data, as needed, from climate and soil databases, including the Oklahoma water resource board and the U.S. Department of Agriculture (USDA) Natural Resources Conservation Service (NRCS) database. The following table shows a summary of the input data's level and source. The first objective of the data collection is finding reliable and accurate data for each of the input modules. LTPP data is not complete for all the sections, and some sections lack important information. For the missing data, typical values from the developed database were used and unreliable, and out of range data were replaced by reliable level 2 and 3 data.

Table 11- Summary of level and source of input data for the Pavement ME calibration effort for the state of Oklahoma

Pavement ME Input Variable	Input Level	Source of Data
HMA thickness	Level 1	LTPP database, ODOT design and Construction reports, ODOT SPR No. 2261 (*26*)
HMA coefficient of thermal contraction	Level 3	Pavement ME typical value
HMA dynamic modulus	Level 2 & 3	LTPP database, ODOT SPR No. 2177 (*28*), ODOT SPR No. 2261 (*26*)
Asphalt binder shear modulus	Level 2	ODOT SPR No. 2209 (*11*)
HMA air voids	Level 1&2	LTPP database
Effective HMA binder content	Level 1 & 2	LTPP database, ODOT design and Construction reports
HMA creep compliance	Level 2	LTPP database, ODOT SPR No. 2261(*26*)
HMA tensile strength	Level 2 & 3	Pavement ME typical value, ODOT SPR No. 2261
Base type/modulus	Level 2 & 3	LTPP database, ODOT SPR No. 2209 (*11*), Sajib et al. 2018 (*29*)
Base thickness	Level 1	LTPP database, ODOT design and Construction reports, ODOT SPR No. 2261(*26*)
Subgrade type	Level 1 & 2	LTPP database, USDA soil survey (*30*)
Subgrade modulus	Level 2 & 3	LTPP database, ODOT SPR No. 2209, ODOT SPR No. 2261, NCHRP 9-23 (*31*),
Groundwater table	Level 2	Oklahoma water resource board (*32*)
Climate	Level 1 & 2	Oklahoma Weather stations (*30*)
Traffic Data	Level 1 & 2	LTPP database, Oklahoma Traffic Database

AC Material Inputs

Asphalt concrete material inputs include the binder, aggregate, and mix properties. The AC layer thickness and mix properties such as mix air voids and binder content were extracted from the LTPP and ODOT PMS database. Figure 5 through Figure 8 shows the HMA layer properties of the experimental sections.

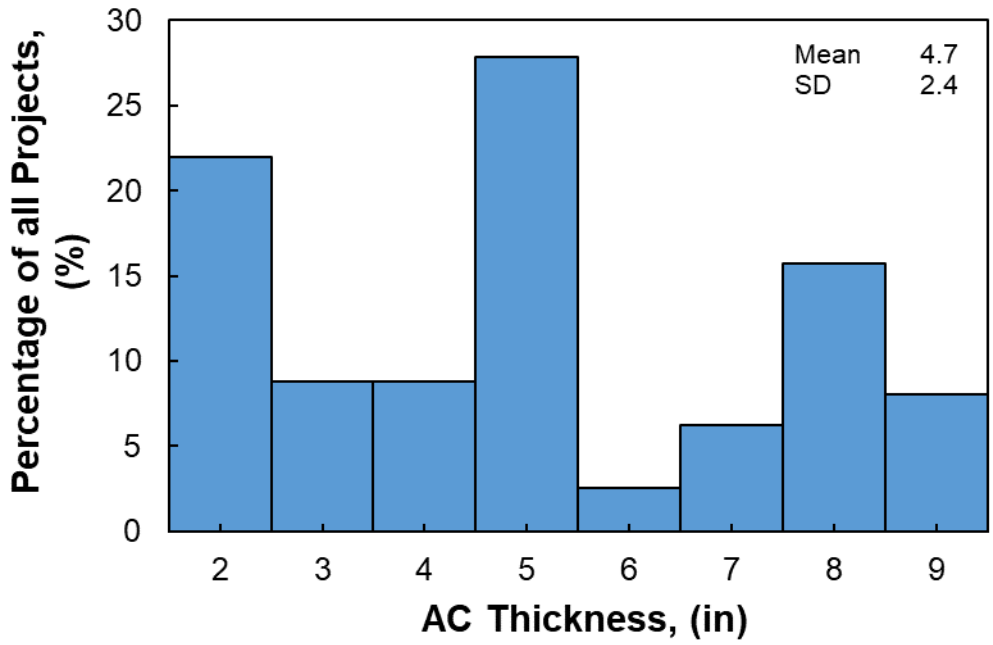

Figure 5- HMA thickness of selected projects for the ODOT Pavement ME calibration database

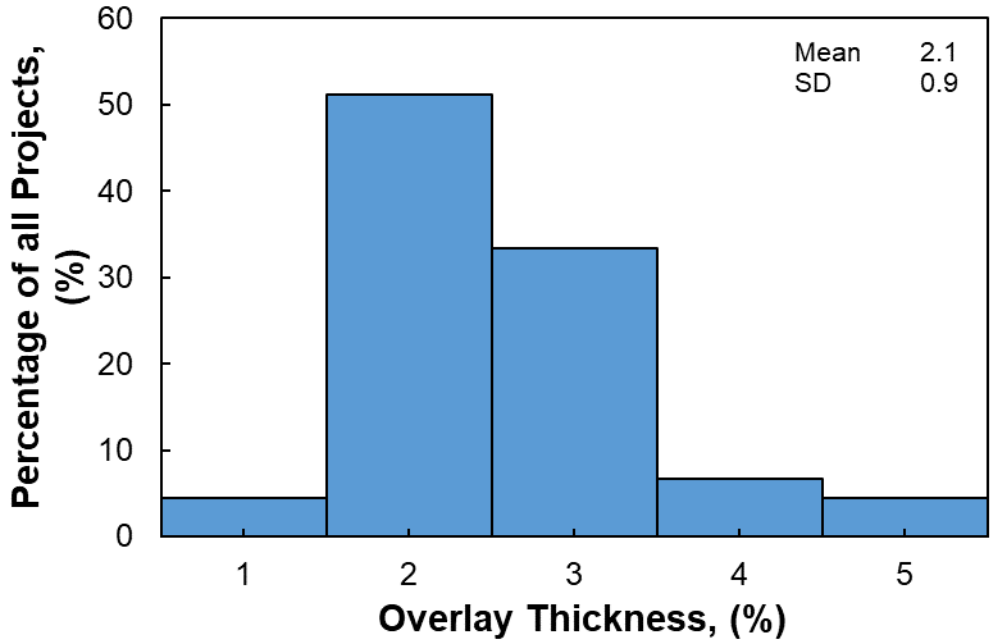

Figure 6- Overlay AC thickness of selected projects for the ODOT Pavement ME calibration database

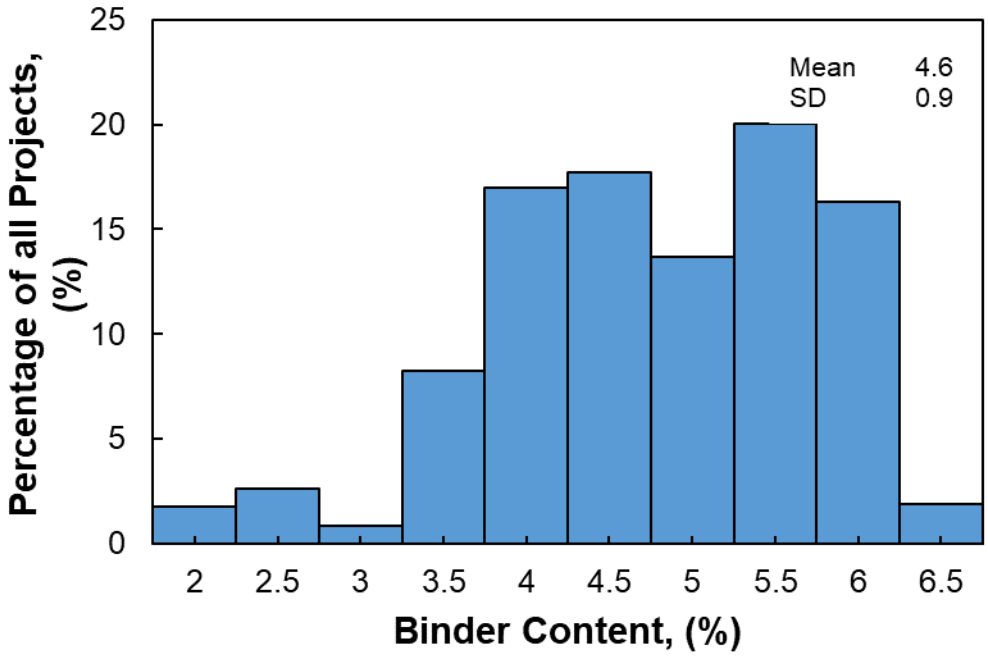

Figure 7-Binder content of HMA of selected projects for the ODOT Pavement ME calibration database

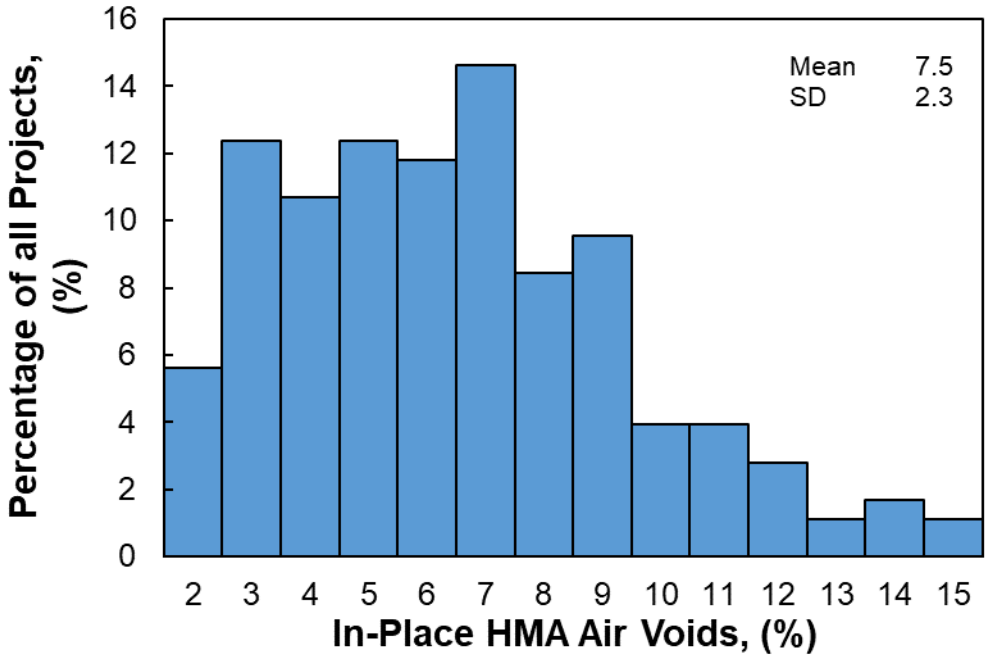

Figure 8- In-Place air voids of selected projects for the ODOT Pavement ME calibration database

The LTPP Infopave database provided the level 1 binder mechanical properties for some of the sections. Some of the previous ODOT research studies provided Oklahoma's typical binders and HMA mixture properties (*33*). Level 2 and level 3 binder's mechanical properties were extracted from different ODOT research studies and were used as the input set for the identified sections. Also, the dynamic modulus of HMA mixtures was calculated by using different predictive models.

Dynamic Modulus

Dynamic modulus, |*E**|, is one of the critical material input properties in Pavement ME Design. The NCHRP 1-47 study on the sensitivity of input variables on performance predictions in Pavement ME design shows that dynamic modulus data has a consistently high impact on all performance predictions except the thermal cracking (*34*). The high sensitivity of the pavement performance prediction to dynamic modulus highlights the importance of providing this input with high accuracy at different levels.

Oklahoma DOT has collected the dynamic modulus of commonly used mix designs in Oklahoma pavement construction projects through different research efforts (*26, 33, 35*). Cross et al. (*33, 35*) evaluated ODOT HMA mixtures and determined mix design's effect on dynamic modulus. A total of 21 mixtures include predominant aggregate types used in Oklahoma, Limestone, sandstone, granite/rhyolite, and crushed gravel, and three mix designations, S-2, S-3, and S-4. Three main asphalt cement in Oklahoma, PG 64-22, 70-28, and 76-28 used with each mix design, which provides a comprehensive source of level 1 data for evaluating dynamic modulus. Furthermore, Cross et al. (*35*) evaluated the performance of stone matrix asphalt (SMA) compared to conventional ODOT S-4 mixes. All mixtures were only mixed with PG 76-28 asphalt cement. Sakhaei Far et al. (*26*) measured dynamic modulus of S3, S4, and S5 mixture designs used in the Oklahoma pavement project combined with PG 64-22, PG 70-28, and PG 76-28.

In this study, the results of dynamic modulus tests in the previous research study were collected for the Pavement ME calibration database. Table 12 shows the type of mixtures and asphalt cement and the total number of mix design used in each study.

Table 12- Dynamic Modulus (|*E|) database**

Data	Sourec	Mixture Type	Asphalt Cement Type	Total Number of Mix Design	Replicate
Source A	Cross et al. (2007)	S-2 S-3 S-4	PG 64-22 PG 70-28 PG 76-28	63	2
Source B	Cross et al. (2011)	S-4 SMA	PG 76-28	7	2
Source C	Sakhaeifar et al. (2015)	S-3 S-4 S-5	PG 64-22 PG 70-28 PG 76-28	5	3

For each set of results, by using the time-temperature superposition concept, a master-curve at a reference temperature of 20°C, which covers a full range of temperature and frequency, was created.

Dynamic modulus can be estimated as level 2 or 3 by using existing predictive models. For this reason, five common existing predictive models were applied to evaluate their precision in estimating |*E**| from different HMA properties. Original Witczak model (equation (1)), |*G**| based Witczak model (equation (3)), NSCU model, Hirsch model, and Al-Khateeb Model were used, and their performance was compared. Level 2 predictive models of dynamic modulus need information on viscosity parameters and binder complex shear modulus (|*G**|) and phase angle (δ) of Oklahoma asphalts mixed in tested HMA mixtures. This information was presented as level 3 typical values in source A and B, which decreases the precision of the predictive models. Level 1 binder complex shear modulus and phase angle were tested in different temperatures

for PG 64-22, PG 70-28, PG 76-28 Oklahoma asphalt binders used in tested mixtures and the results were presented in source C. Due to increasing the precision of predictions, the level 1 binder properties information presented in source C were used as input for prediction of dynamic modulus of source A and B mixtures.

The results of predictive models by using collected HMA mixtures properties from source A are shown in the arithmetic scale in Figure 9 (a) through (e) and in the logarithmic scale in Figure 10 (a) through (e).

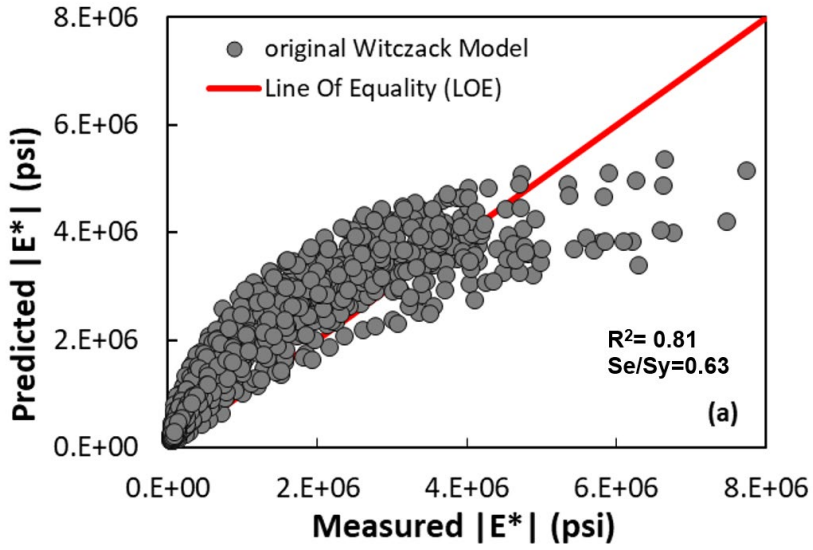

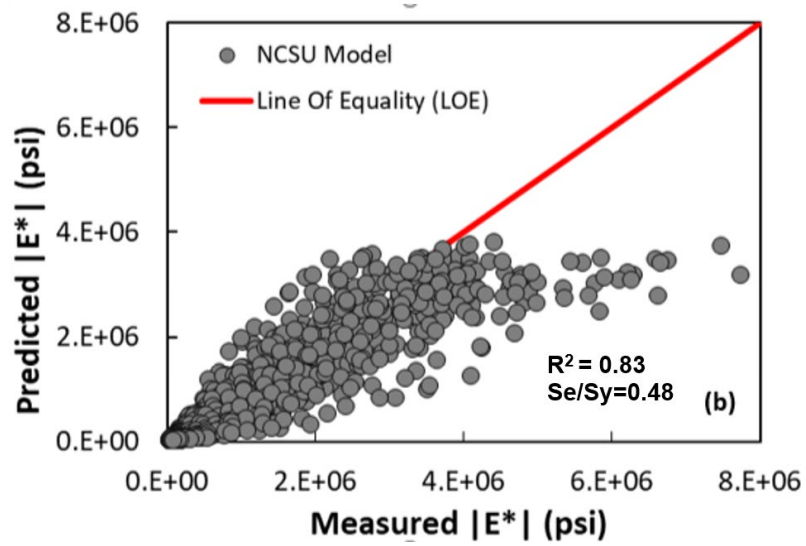

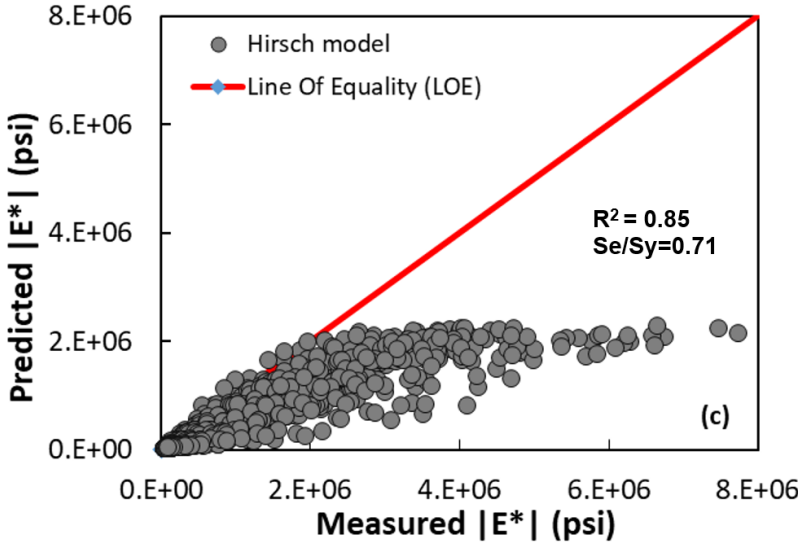
Hirsch model
Line Of Equality (LOE)
R² = 0.85
Se/Sy=0.71
(c)
Predicted |E*| (psi)
Measured |E*| (psi)
0.E+00
2.E+06
4.E+06
6.E+06
8.E+06

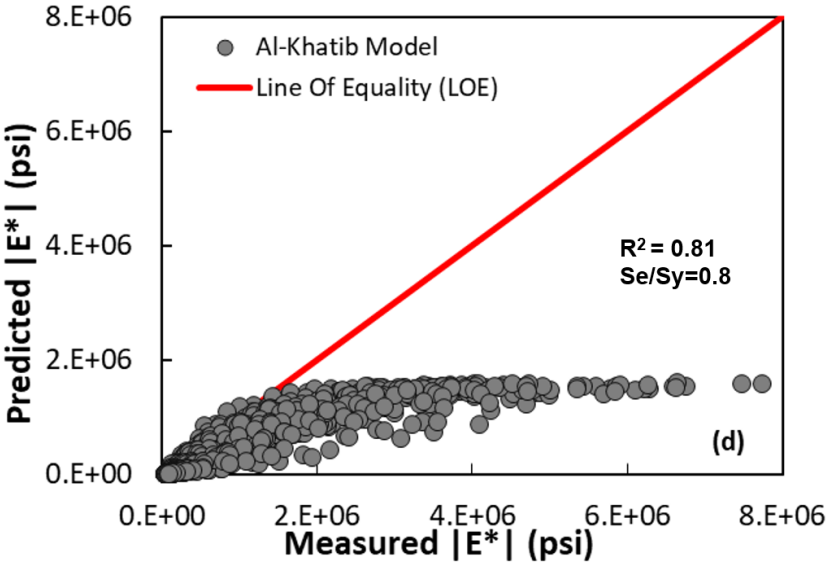
Al-Khatib Model
Line Of Equality (LOE)
R² = 0.81
Se/Sy=0.8
(d)
Predicted |E*| (psi)
Measured |E*| (psi)
0.E+00
2.E+06
4.E+06
6.E+06
8.E+06

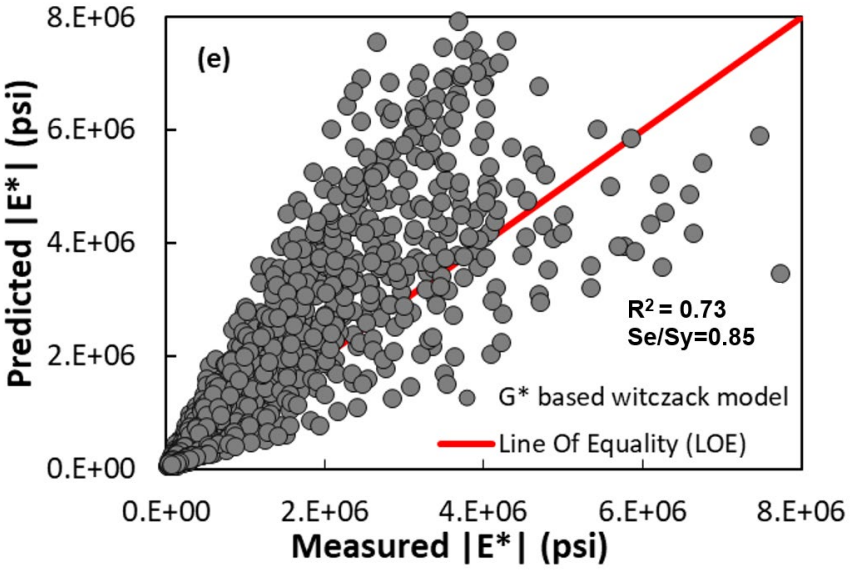

Figure 9- Predicted versus measured dynamic modulus in arithmetic scale using HMA mixture properties of Source A using: (a) original Witcsack model, (b) NCSU model, (d) (c) Hirsch model, and (d) Al-Khatib model, (e) Gstar based Witczak model

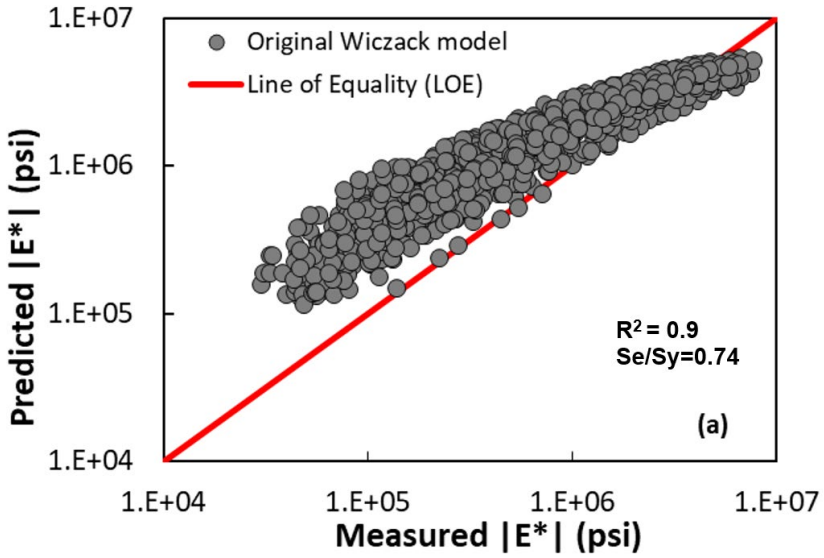

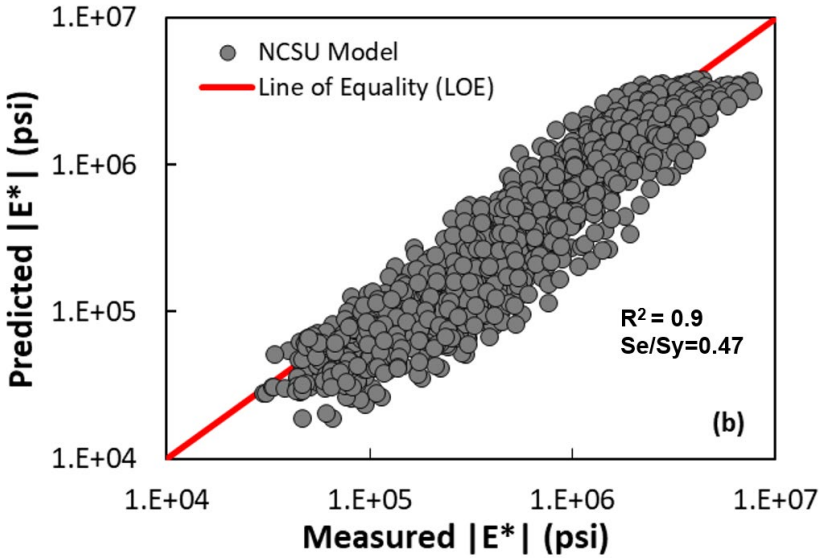
1.E+07
1.E+06
1.E+05
1.E+04
Predicted |E*| (psi)
NCSU Model
Line of Equality (LOE)
R² = 0.9
Se/Sy=0.47
(b)
1.E+04
1.E+05
1.E+06
1.E+07
Measured |E*| (psi)

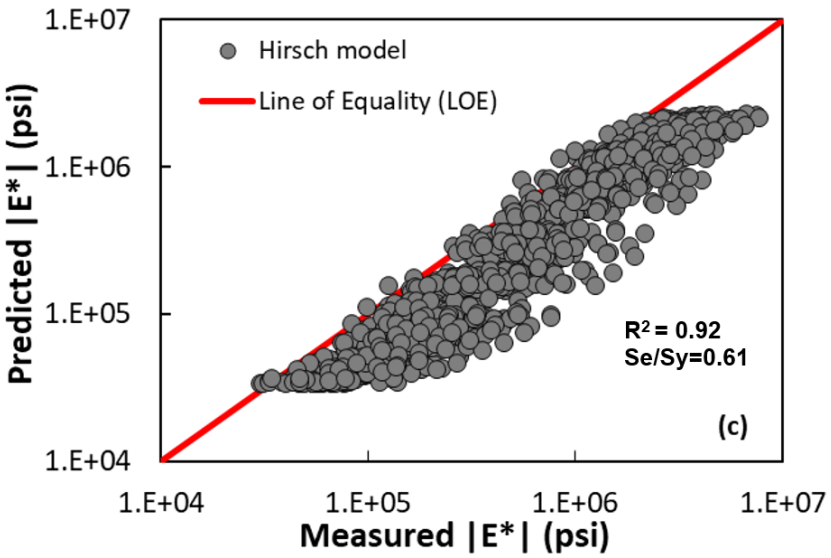
1.E+07
1.E+06
1.E+05
1.E+04
Predicted |E*| (psi)
Hirsch model
Line of Equality (LOE)
R² = 0.92
Se/Sy=0.61
(c)
1.E+04
1.E+05
1.E+06
1.E+07
Measured |E*| (psi)

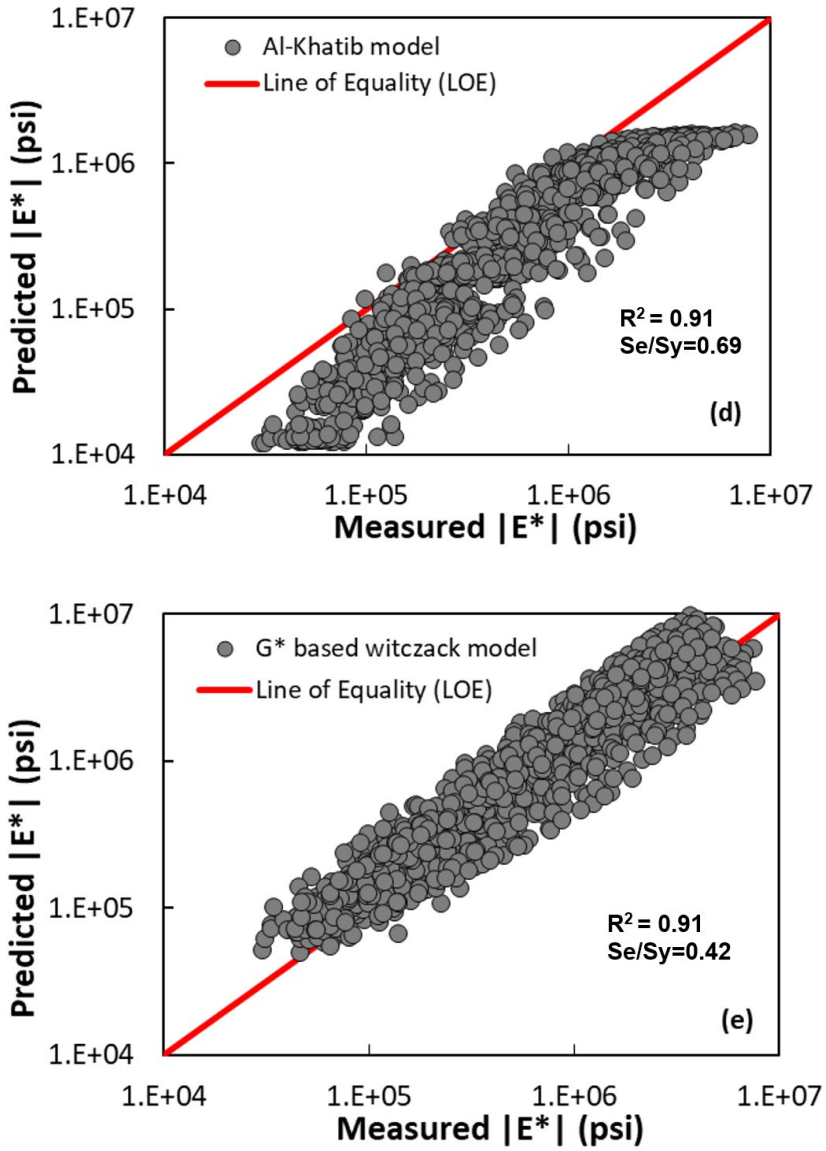

Figure 10- Predicted versus measured dynamic modulus in logarithmic scale for HMA mixtures in Source A using: (a) original Witcsack, (b) Gstar based Witczak, (c) NCSU, (d) Hirsch, and (e) Al-Khatib models

The results of predictive models by using collected HMA mixture properties from source B are shown in the arithmetic scale in Figure 11 (a) through (e) and in the logarithmic scale in Figure 12 (a) through (e).

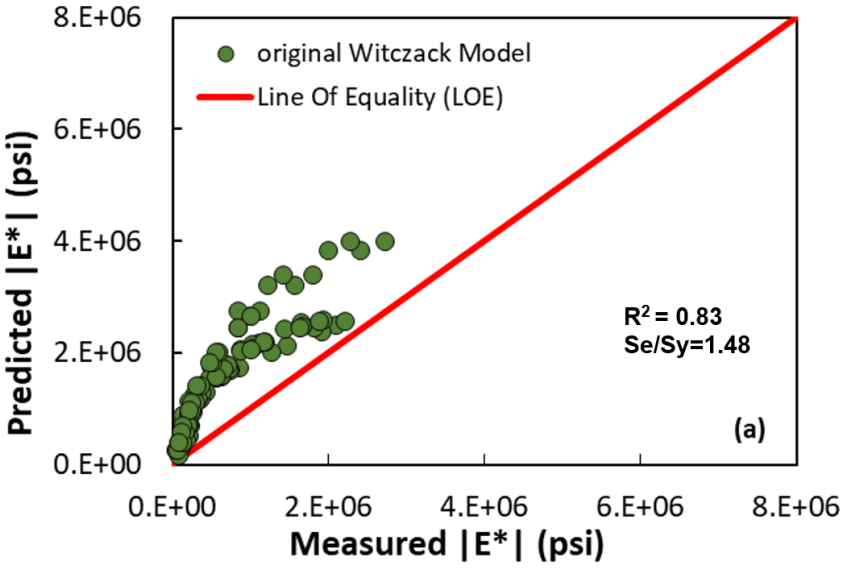
8.E+06
6.E+06
4.E+06
2.E+06
0.E+00
Predicted |E*| (psi)
original Witczack Model
Line Of Equality (LOE)
R2 = 0.83
Se/Sy=1.48
(a)
0.E+00
2.E+06
4.E+06
6.E+06
8.E+06
Measured |E*| (psi)

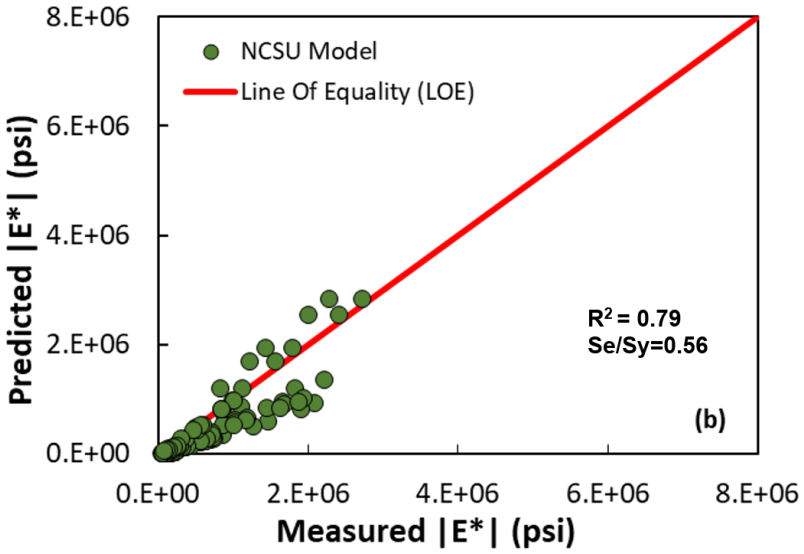
8.E+06
6.E+06
4.E+06
2.E+06
0.E+00
Predicted |E*| (psi)
NCSU Model
Line Of Equality (LOE)
R2 = 0.79
Se/Sy=0.56
(b)
0.E+00
2.E+06
4.E+06
6.E+06
8.E+06
Measured |E*| (psi)

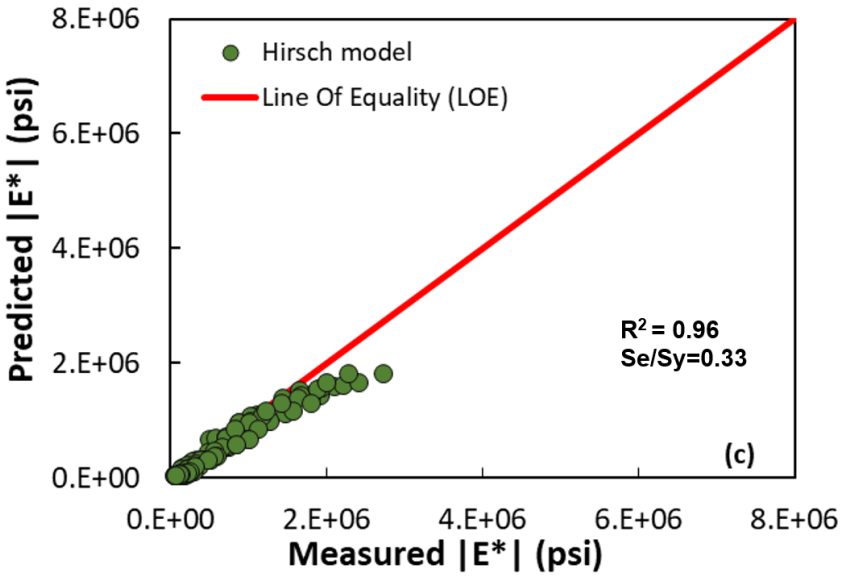
Hirsch model
Line Of Equality (LOE)
R2 = 0.96
Se/Sy=0.33
(c)
Predicted |E*| (psi)
Measured |E*| (psi)
0.E+00
2.E+06
4.E+06
6.E+06
8.E+06

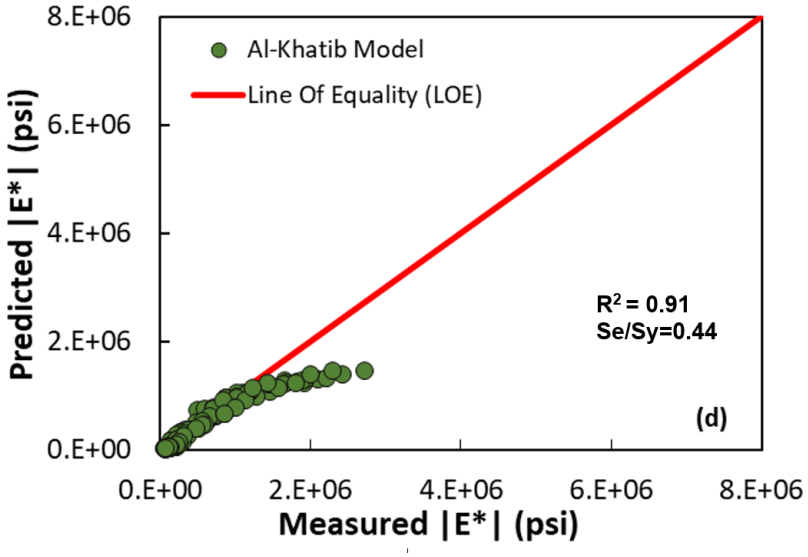
Al-Khatib Model
Line Of Equality (LOE)
R2 = 0.91
Se/Sy=0.44
(d)
Predicted |E*| (psi)
Measured |E*| (psi)
0.E+00
2.E+06
4.E+06
6.E+06
8.E+06

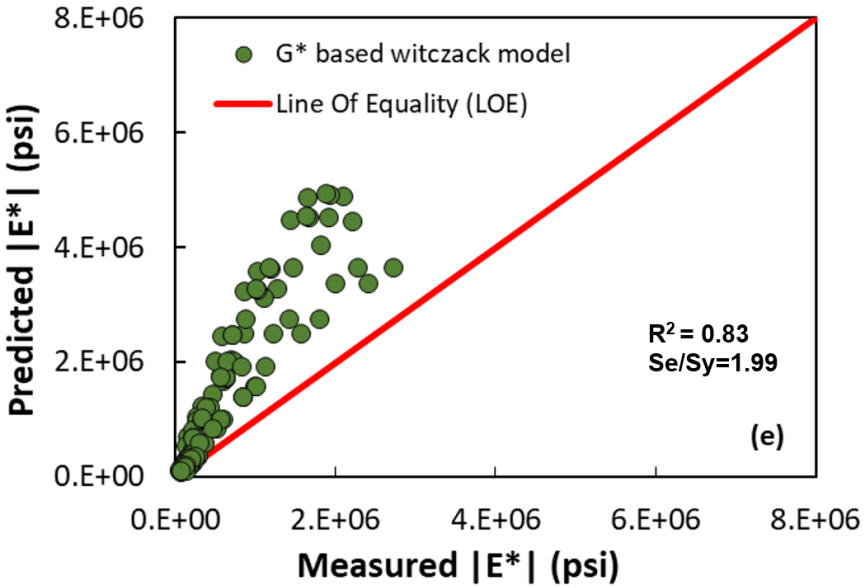

Figure 11- Predicted versus measured dynamic modulus in arithmetic scale for HMA mixtures in Source B using: (a) original Witcsack, (b) Gstar based Witczak, (c) NCSU, (d) Hirsch, and (e) Al-Khatib models

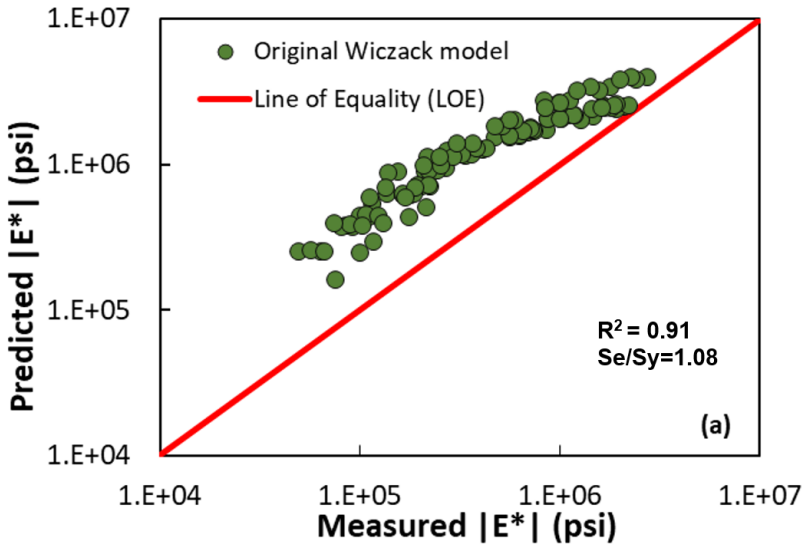

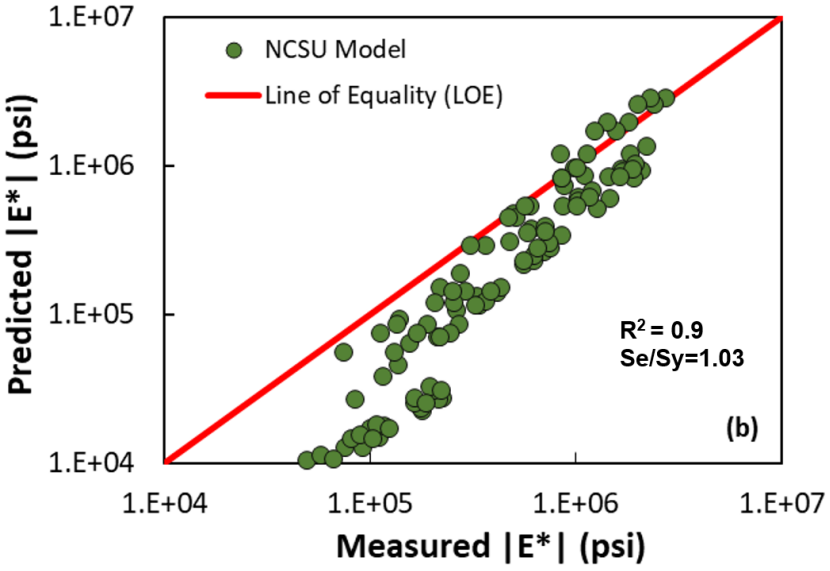
1.E+07
1.E+06
1.E+05
1.E+04
Predicted |E*| (psi)
NCSU Model
Line of Equality (LOE)
R² = 0.9
Se/Sy=1.03
(b)
1.E+04
1.E+05
1.E+06
1.E+07
Measured |E*| (psi)

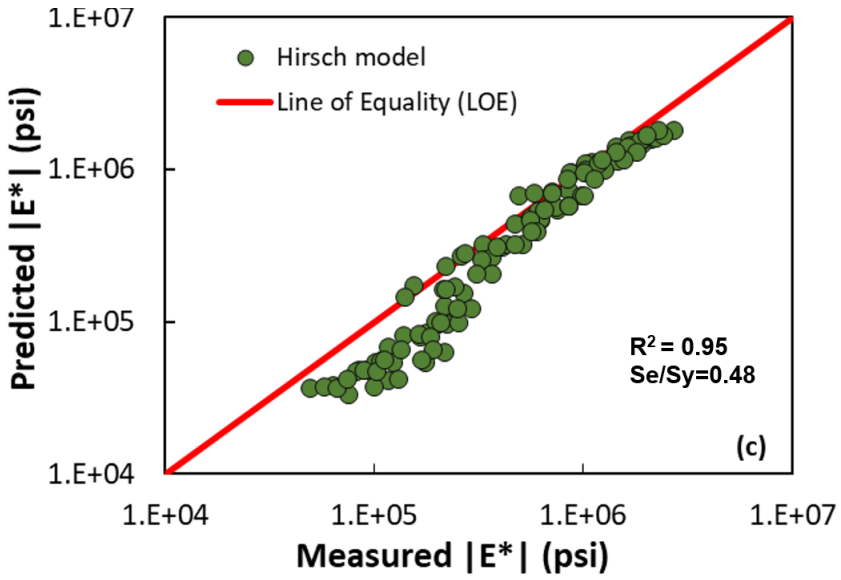
1.E+07
1.E+06
1.E+05
1.E+04
Predicted |E*| (psi)
Hirsch model
Line of Equality (LOE)
R² = 0.95
Se/Sy=0.48
(c)
1.E+04
1.E+05
1.E+06
1.E+07
Measured |E*| (psi)

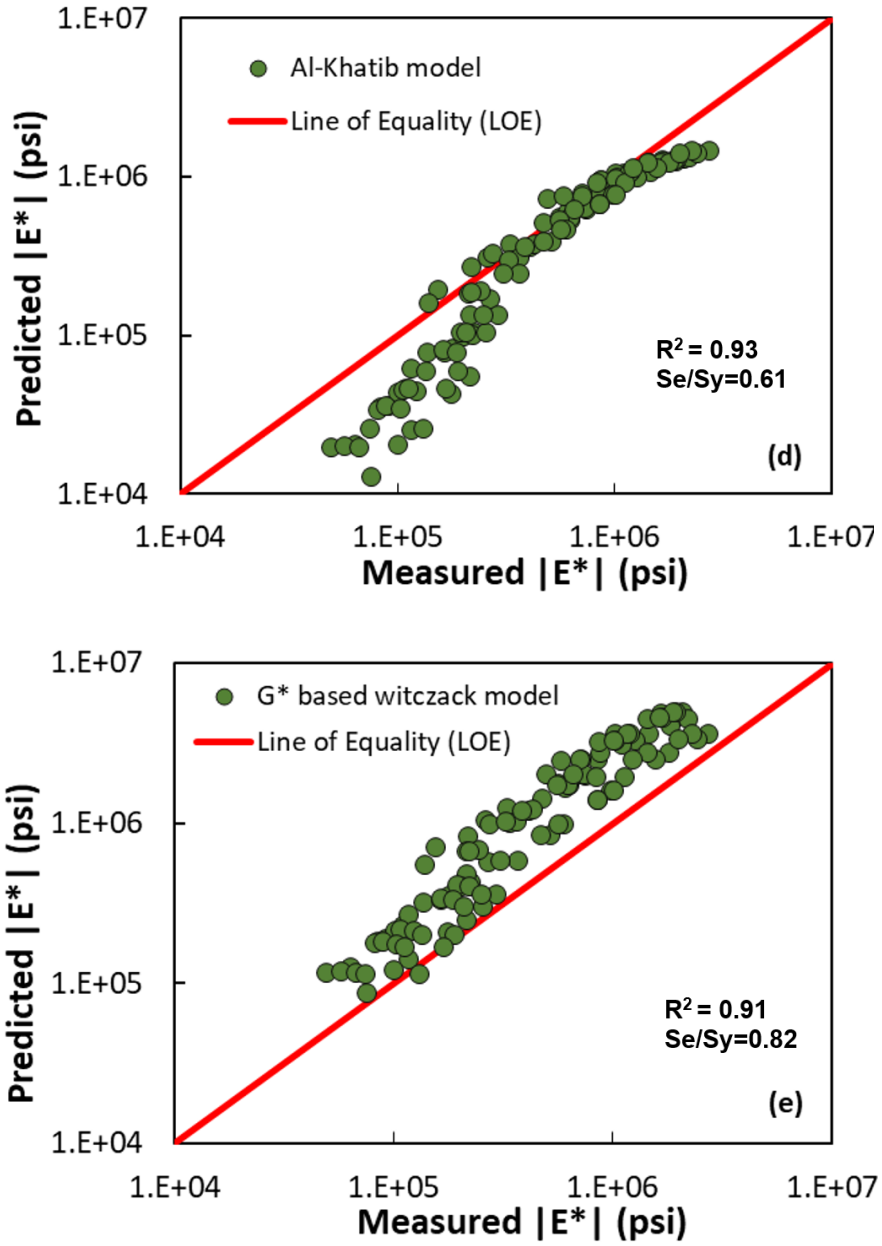

Figure 12- Predicted versus measured dynamic modulus in logarithmic scale for HMA mixtures in Source B using: (a) original Witczak, (b) Gstar based Witczak, (c) NCSU, (d) Hirsch, and (e) Al-Khatib models

The results of predictive models by using collected HMA mixture properties from source C are shown in the arithmetic scale in Figure 13 (a) through (e) and in the logarithmic scale in Figure 14 (a) through (e).

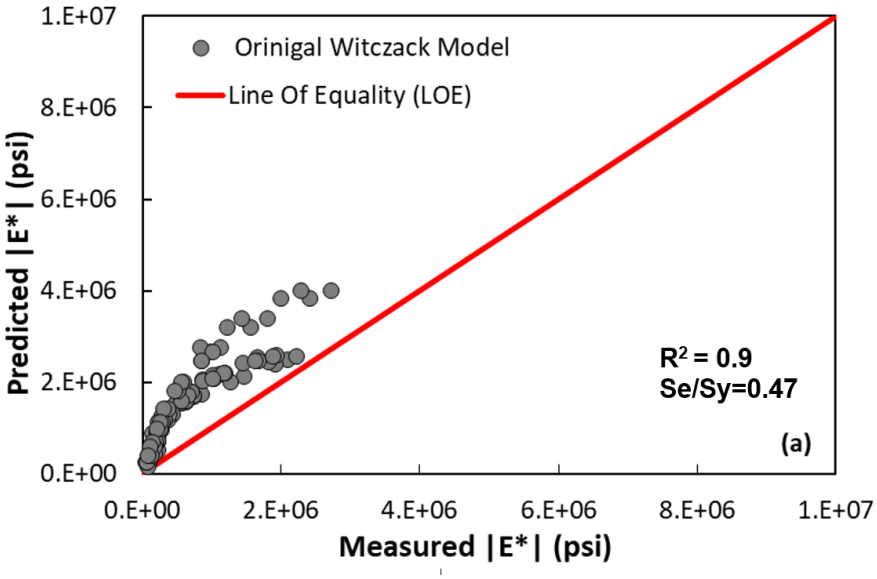
Orinigal Witczack Model
Line Of Equality (LOE)
R² = 0.9
Se/Sy=0.47
(a)
Predicted |E*| (psi)
Measured |E*| (psi)
1.E+07
8.E+06
6.E+06
4.E+06
2.E+06
0.E+00

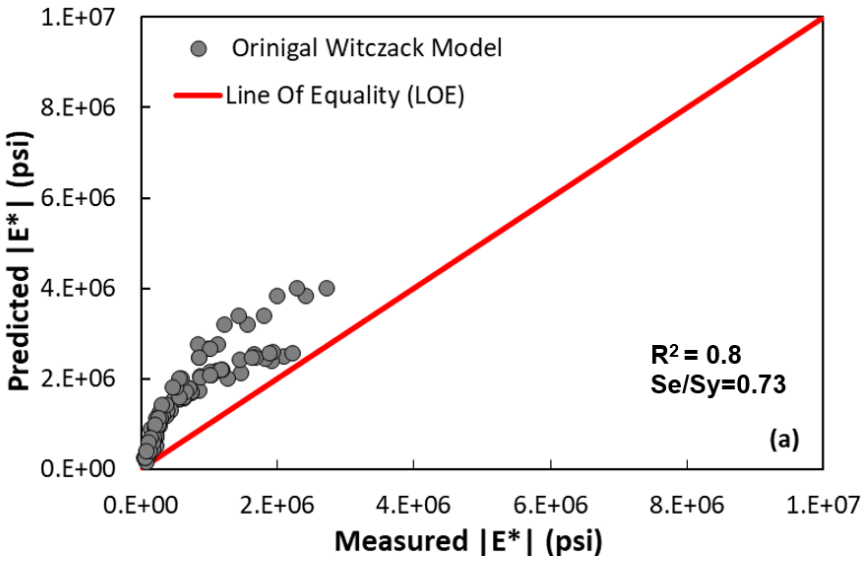
Orinigal Witczack Model
Line Of Equality (LOE)
R² = 0.8
Se/Sy=0.73
(a)
Predicted |E*| (psi)
Measured |E*| (psi)
1.E+07
8.E+06
6.E+06
4.E+06
2.E+06
0.E+00

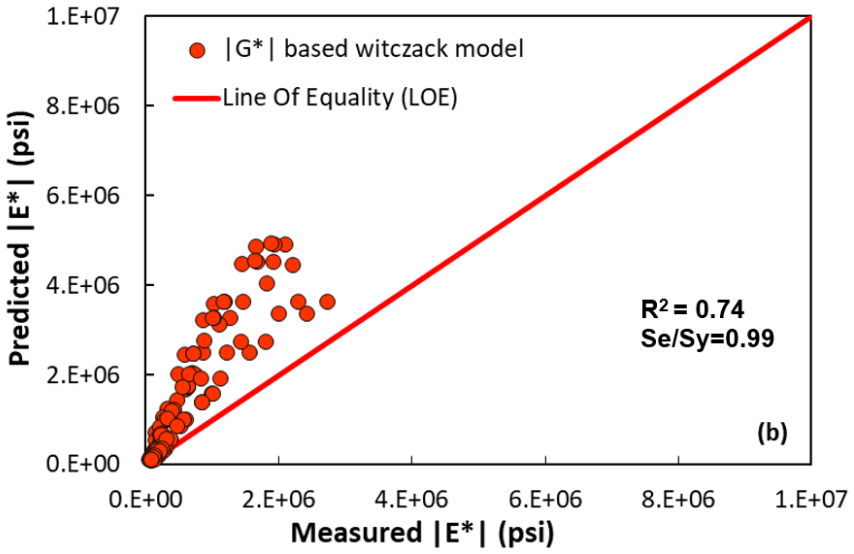
|G*| based witczack model
Line Of Equality (LOE)
R² = 0.74
Se/Sy=0.99
(b)
Predicted |E*| (psi)
Measured |E*| (psi)
0.E+00
2.E+06
4.E+06
6.E+06
8.E+06
1.E+07

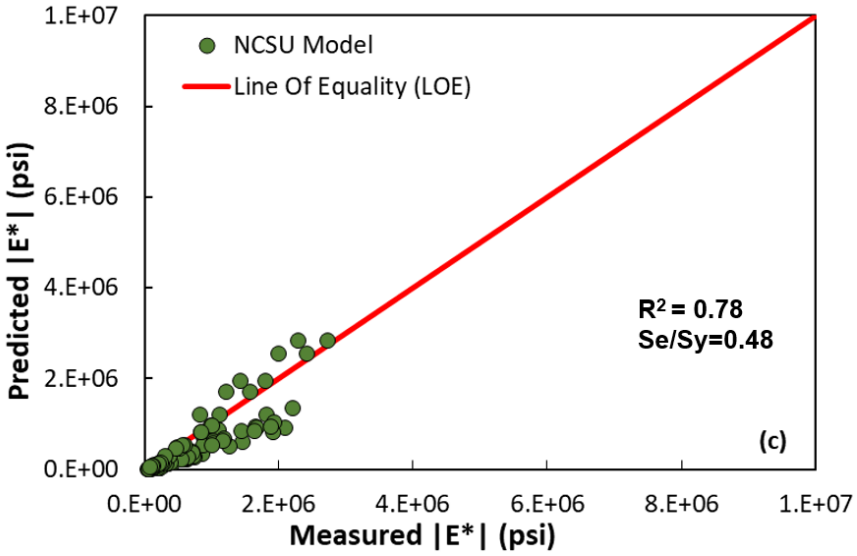
NCSU Model
Line Of Equality (LOE)
R² = 0.78
Se/Sy=0.48
(c)
Predicted |E*| (psi)
Measured |E*| (psi)
0.E+00
2.E+06
4.E+06
6.E+06
8.E+06
1.E+07

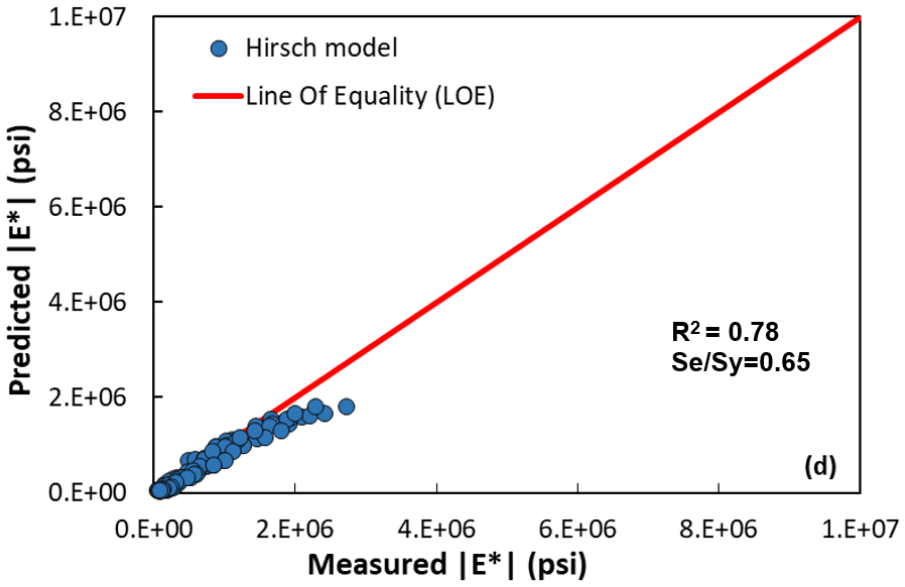

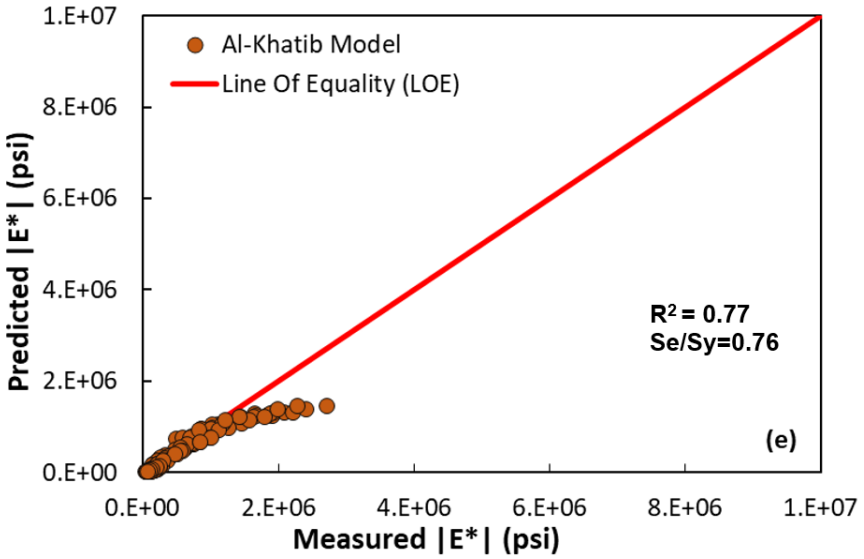

Figure 13- Predicted versus measured dynamic modulus in arithmetic scale for HMA mixtures in Source C using (a) original Witczak, (b) Gstar based Witczak, (c) NCSU, (d) Hirsch, and (e) Al-Khatib models

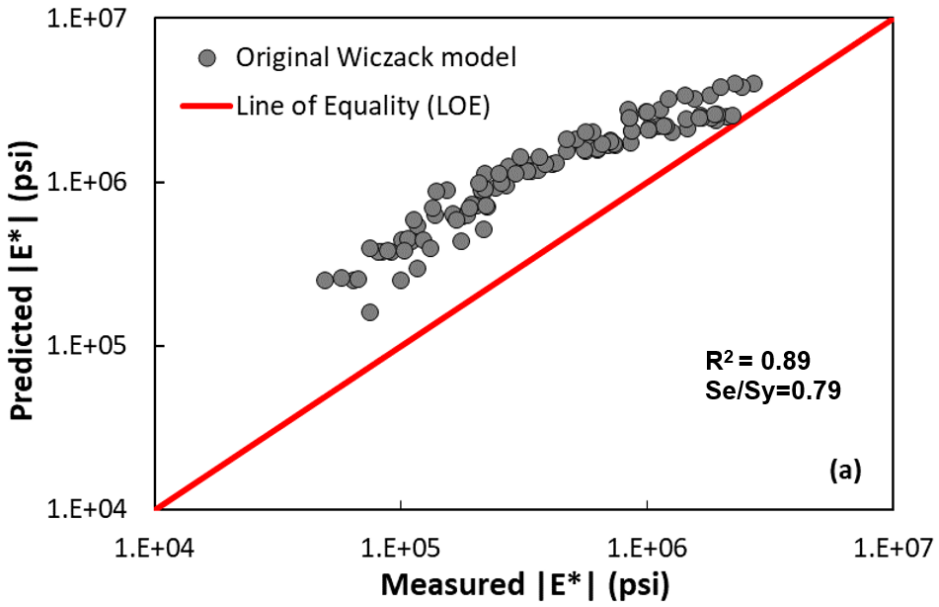
1.E+07
1.E+06
1.E+05
1.E+04
Predicted |E*| (psi)
Original Wiczack model
Line of Equality (LOE)
R² = 0.89
Se/Sy=0.79
(a)
1.E+04
1.E+05
1.E+06
1.E+07
Measured |E*| (psi)

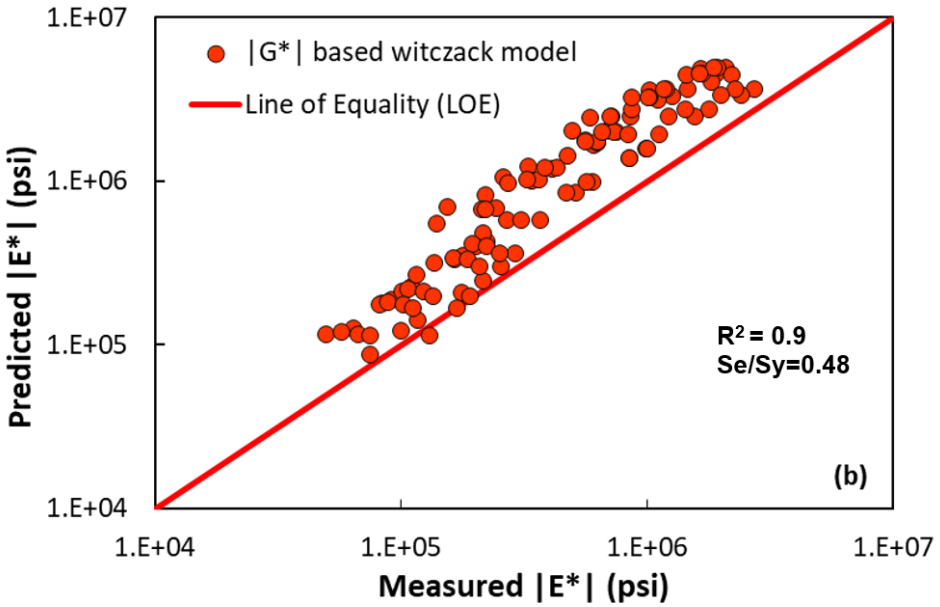
1.E+07
1.E+06
1.E+05
1.E+04
Predicted |E*| (psi)
|G*| based witczack model
Line of Equality (LOE)
R² = 0.9
Se/Sy=0.48
(b)
1.E+04
1.E+05
1.E+06
1.E+07
Measured |E*| (psi)

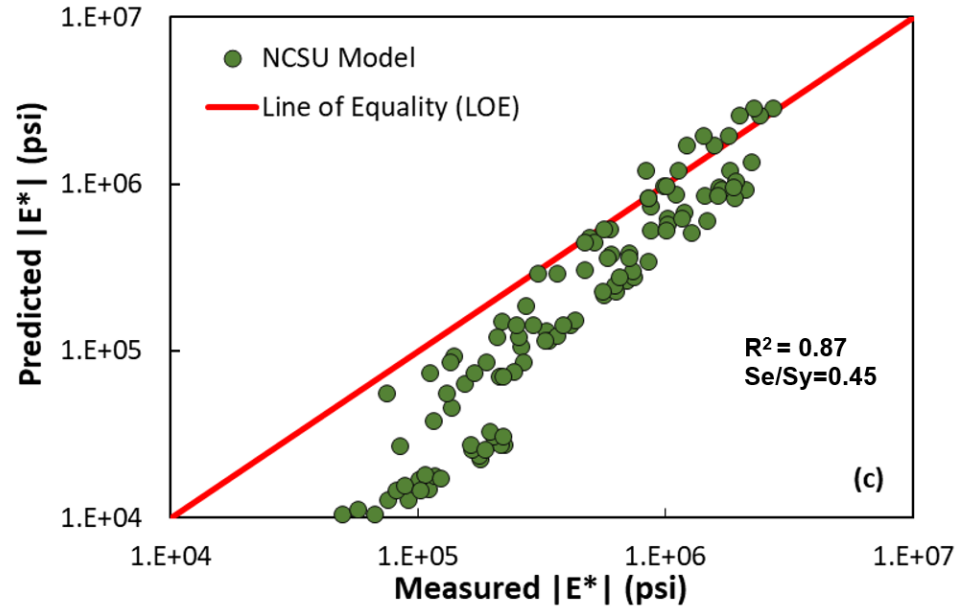
1.E+07
1.E+06
1.E+05
1.E+04
Predicted |E*| (psi)
NCSU Model
Line of Equality (LOE)
R² = 0.87
Se/Sy=0.45
(c)
1.E+04
1.E+05
1.E+06
1.E+07
Measured |E*| (psi)

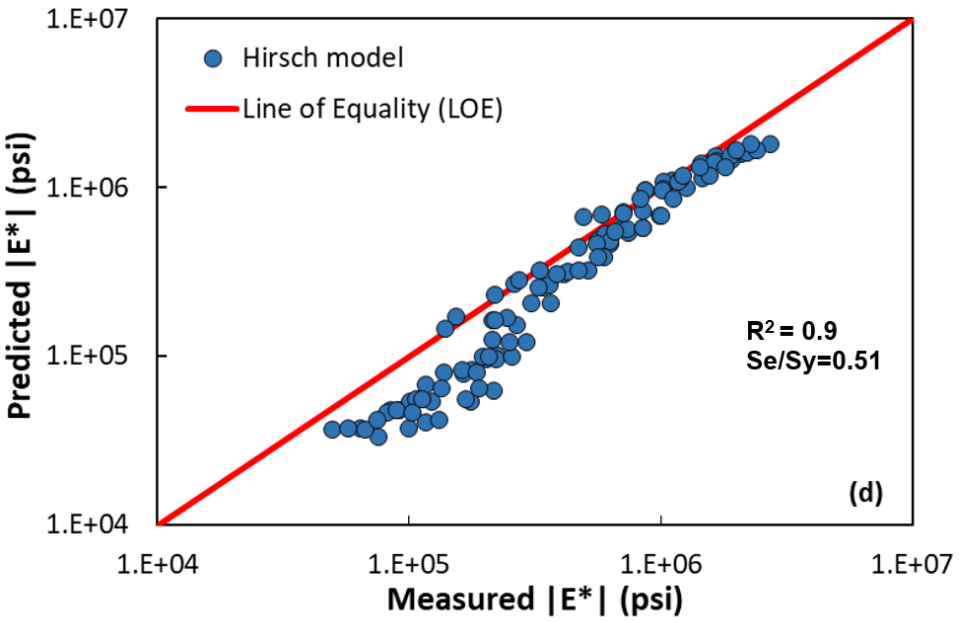
1.E+07
1.E+06
1.E+05
1.E+04
Predicted |E*| (psi)
Hirsch model
Line of Equality (LOE)
R² = 0.9
Se/Sy=0.51
(d)
1.E+04
1.E+05
1.E+06
1.E+07
Measured |E*| (psi)

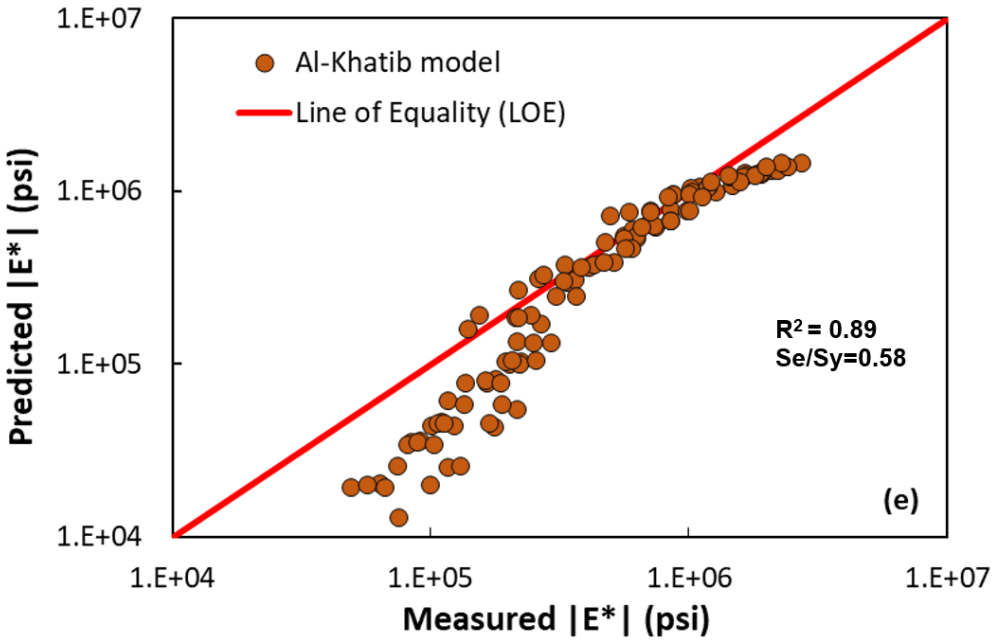

Figure 14- Predicted versus measured dynamic modulus in logarithmic scale for HMA mixtures in Source C using (a) original Witczak, (b) Gstar based Witczak, (c) NCSU, (d) Hirsch, and (e) Al-Khatib models

The goodness-of-fit statistics and line of equality (LOE) were used to evaluate the performance of each predictive model. The ratio of the standard error of estimate (S_e) to the standard deviation (S_y) and the coefficient of determination (R^2) represents the accuracy of a model (6). A predictive model with higher values of R^2 and lower amounts of S_e/S_y has a better performance. Figure 15 summarizes S_e/S_y and R^2 values for each predictive model.

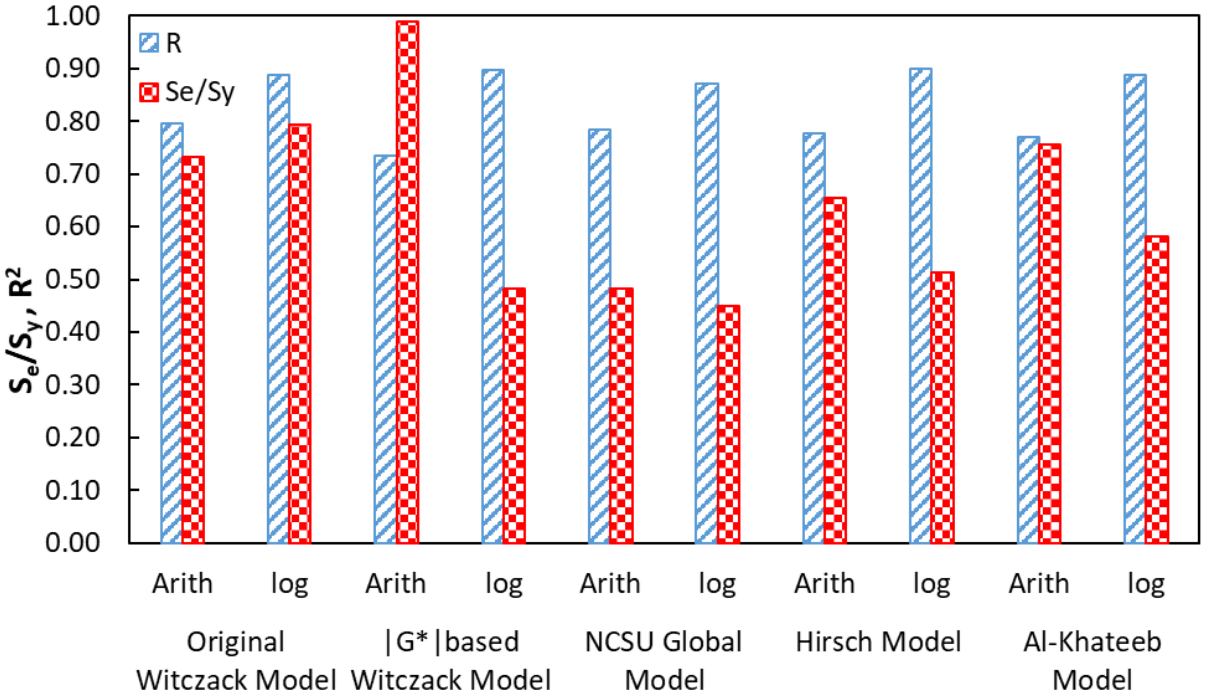

Figure 15- Overall performance of different predictive models

Based on the goodness of fit statistics results, the NCSU model, in comparison to Pavement ME predictive models, represents better performance. Also, predictions of the NCSU model are tightly clustered around the line of equality, which is an indication of proper matching between predicted and measured values. Hirsch's model performance, which is shown in Figure 9(d) to Figure 14(d), has a poor performance in lower and higher stiffness values. Al-Khateeb Model gives a significant bias in all predictions and shows a significant deviation from the LOE plot (high bias). The performance results are inconsistent with the previous studies on dynamic modulus predictive models (*6*, *36*)

Base and Subgrade Design Inputs

The LTPP infopave provided information for base and subgrade materials for LTPP sections. In addition, NCHRP 9-23A provides a national database of the subgrade soil's material properties. This database includes the soil-water characteristic curve (SWCC) parameters, grain-size distribution, Atterberg limits, hydraulic conductivity, porosity, and water content of the subgrade soil throughout the US. This database was used together with the LTPP database to generate Pavement ME subgrade properties. Figure 16 to Figure 20 shows the properties of subgrade soils in the experimental sections.

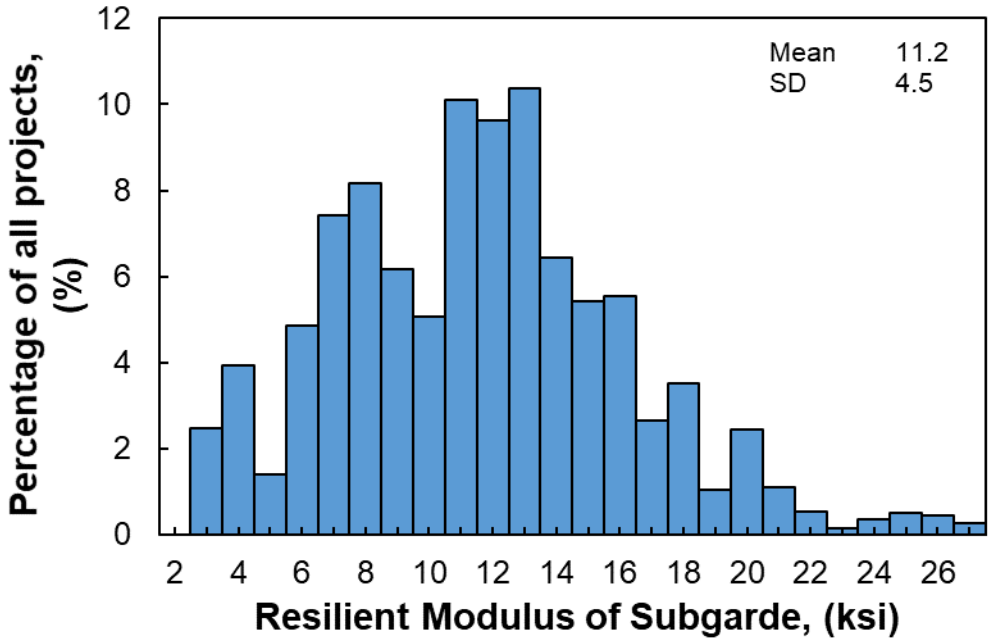

Figure 16- Resilient modulus of subgrade for selected projects in ODOT Pavement ME calibration database

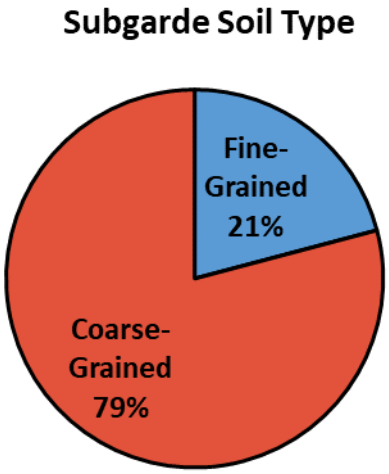

Figure 17- Subgrade soil type of projects selected for ODOT Pavement ME calibration database

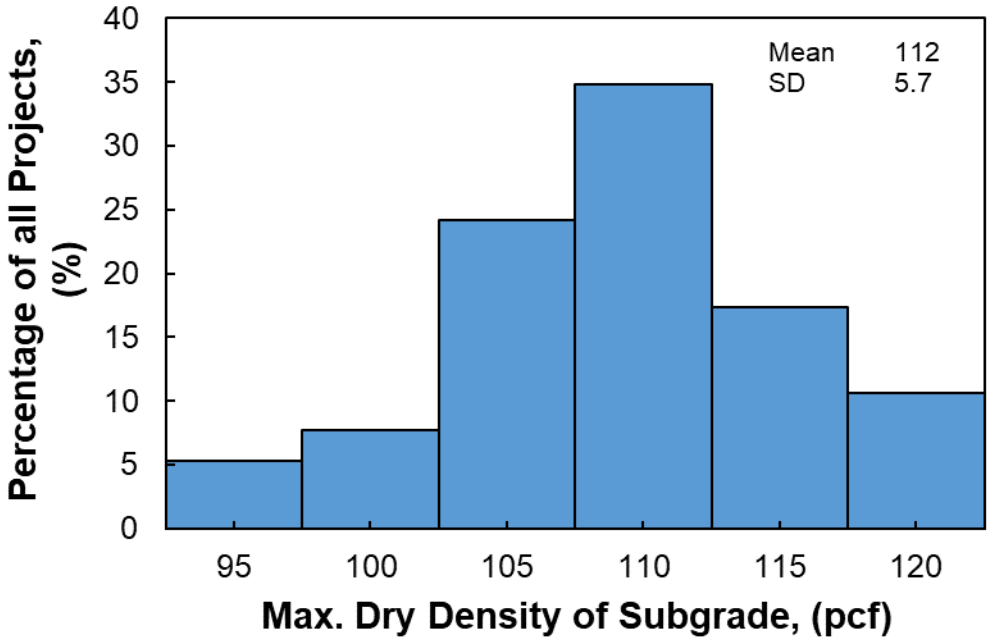

Figure 18- Maximum dry density of subgrades for selected projects in ODOT Pavement ME calibration database

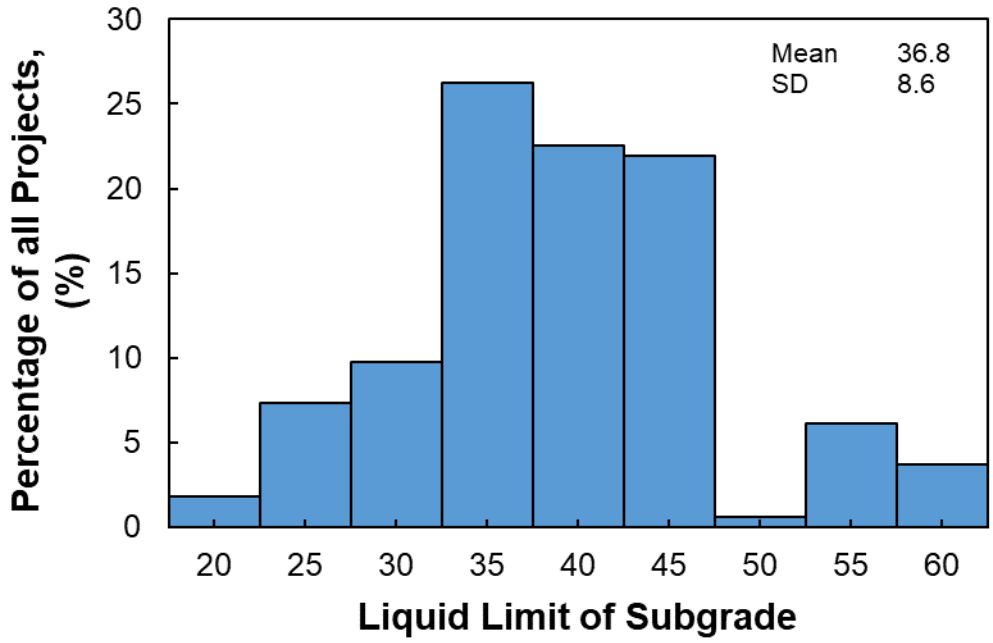

Figure 19- Liquid limit of subgrades for selected projects in ODOT Pavement ME calibration database

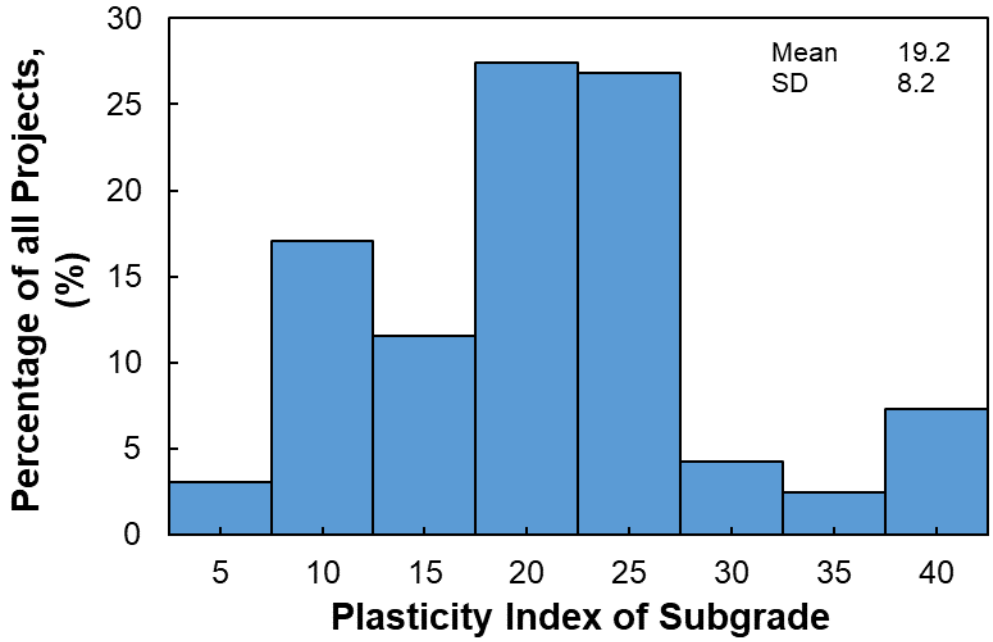

Figure 20- Plasticity index of subgrades for selected projects in ODOT Pavement ME calibration database

SWCC Properties

The resilient modulus (M_r) is one of the primary material input properties in Pavement ME design, which mainly affects the analysis of pavement structures. Zahid et al. Provided level 1 resilient modulus data for Oklahoma unbound materials. Also, level 2 and level 3 stress-dependent predictive models were evaluated, and correlation coefficients were calculated for

the Pavement ME model (*11*). However, the resilient modulus of unbound materials is not only stress-dependent but also moisture dependent (*37*). Some researchers proposed moisture dependent resilient modulus models for unbound aggregates and subgrade soils (*15*). In this model, moisture and suction, as well as the state of stress, are used to characterize M_r in different soil types.

In this study, by using available data on Oklahoma unbound materials collected from ODOT, the moisture dependence model was used to predict the values of resilient modulus in different stress states. The application of moisture dependent model requires the moisture content, saturation factor, and suction information of tested specimen and correlation coefficients of K_1, K_2, and K_3. Volumetric water content, θ, and saturation factor, f, for each type of test specimen were calculated from the collected moisture content, *MC*, maximum dry density, *MDD*, and specific gravity, *G*, using equation (48) and equation (49) (*15*, *38*).

$$\theta = w \frac{\rho_b}{\rho_w} \tag{48}$$

where,

θ = volumetric water content, %;
w = gravimetric water content, %;
ρ_b = bulk specific gravity, pcf, and
ρ_w = water specific gravity = 62.43 pcf.

and

$$f = 1 + \frac{S - 85}{15}\left(\frac{1}{\theta} - 1\right) \tag{49}$$

where,

f = saturation factor;
S = degree of saturation, %; and
θ = volumetric water content, decimal.

Matric suction, h_m, of unbound materials can be calculated from the soil-water characteristic curve (SWCC). SWCC is a relationship between the suction and moisture content, which can be determined by conducting experimental tests to measure matric suction in different water contents. This laboratory test requires specialized equipment and expert operators, which has a time-consuming procedure. The alternative method is an indirect method of predicting model parameters that can be used for generating SWCC of unbound materials. Equation (50) Shows the Fredlund-Xing model used for making the soil-water characteristic curve (*38*).

$$S = C_{(h)} \left(\frac{1}{\left(\ln\left[e + \left(\frac{h}{a_f} \right)^{b_f} \right] \right)^{c_f}} \right) \qquad (50)$$

$$C_{(h)} = 1 - \frac{\ln\left(1 + \frac{h}{h_r} \right)}{\ln\left(1 + \left(\frac{1.45 \times 10^5}{h_r} \right) \right)}$$

where
S = degree of saturation, decimal;
h = total matric suction, psi;
a_f, b_f, c_f and h_r =soil fitting parameters.

Sajib et al. developed an ANN model to predict fitting coefficients of a_f, b_f, c_f, and h_r by using a large database collected from the NCHRP 9-23 A (*39*). The proposed ANN model compared to existing predictive models showed higher prediction accuracy in predicting Fredlund-Xing fitting parameters. The input variables of this model include the material percent passing sieve size No.4, material passing sieve size No. 200, Liquid Limit (LL), plasticity index (PI), saturated volumetric water content, and local mean annual air temperature.

Using the developed ANN model, SWCC was predicted for each soil type presented in the Oklahoma M_r database. Table 13 represents the fitting coefficients of Fredlund-Xing equation for A-2-4, A-2-6, A-4, A-6, and A-7-6 soils in the state of Oklahoma.

Table 13- Fredlund-Xing fitting coefficients for the Oklahoma subgrade soils

Soil Type	a_f	b_f	c_f	h_r
A-2-4	4.25	1.20	0.90	2999.86
A-2-6	4.43	1.01	1.00	2999.83
A-4	5.88	0.97	0.74	2999.81
A-6	11.27	0.92	0.57	2999.85
A-7-6	4.61	0.93	0.40	2999.88

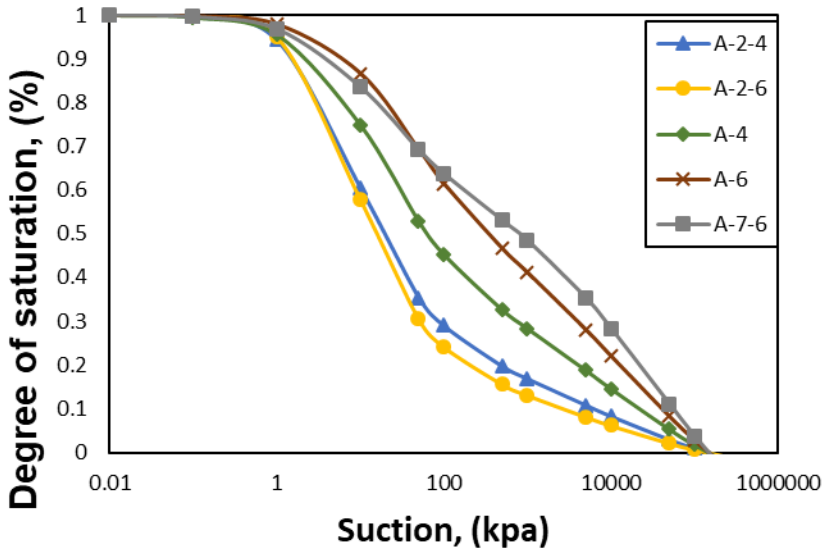

Figure 21- Soil Water Characteristic Curve (SWCC) for Oklahoma subgrade soils

Soil water characteristic curve can provide the value of suction in a different amount of soil water content. The obtained values will be used as an input in the moisture dependence model. The next step for using this model is predicting the correlation coefficients of K_1, K_2, and K_3 for different soil types in Oklahoma. The correlation coefficients can be determined by predictive models using other soil properties (*39*).

Traffic Loading Inputs

The required traffic input data were collected for each section and compiled in a database. The collected data were reviewed, and questionable data were corrected, corresponding to typical values or specific information in similar sections. Figure 22 shows the annual average daily truck traffic in experimental sections. The data was extracted from WIM, and traffic volume count information was provided by LTPP.

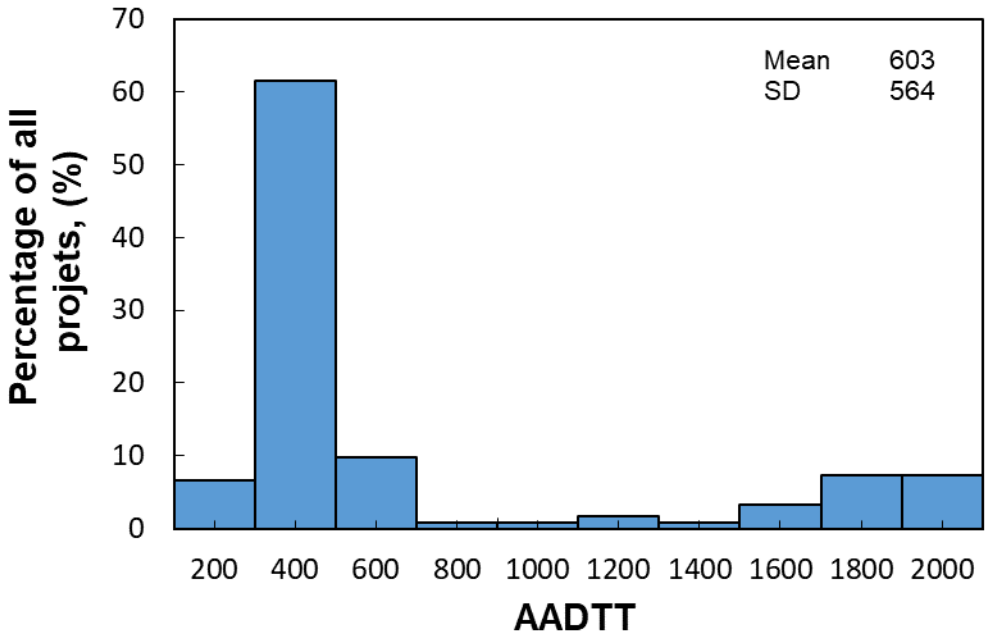

Figure 22- Annual average daily traffic of the selected projects for ODOT Pavement ME calibration database

There were missing data for some of the sections in different years. The required parameters can be estimated using the average rate of traffic growth for each road class. Table 14 shows the average rate of truck traffic growth for each type of road class in the state of Oklahoma, which is calculated using LTPP traffic data.

Table 14- Average growth rate of truck traffic compound for each road functional class

Road Functional Class	Traffic Compound Growth Rate (%)
Urban Principal Arterial	1.15%
Rural Principal Arterial - Non Interstate	2.47%
Rural Principal Arterial -Interstate	1.89%
Rural Minor Arterial	2.63%

The truck class distribution is another important traffic input in Pavement ME Design. These data are extracted from the LTPP traffic data for each section and used in the design effort. Figure 23 and Table 15 show the average distribution factors of truck classes for each cluster of roads in Oklahoma. The truck classes number 9 and 5 have the highest distribution factor in the state.

Table 15- Vehicle class distribution factors used in calibration effort

Class Type	Rural Principle Arterial	Urban Principal Arterial	Rural Major Collector
Class 4	2.08	1.56	2.05
Class 5	20.29	27.55	25.86

Class Type	Rural Principle Arterial	Urban Principal Arterial	Rural Major Collector
Class 6	3.74	9.72	4.82
Class 7	0.86	0.81	0.28
Class 8	8.67	12.83	7.89
Class 9	61.09	41.88	55.78
Class 10	1.37	1.69	1.27
Class 11	0.77	1.04	1.02
Class 12	0.38	0.70	0.45
Class 13	0.75	2.22	0.58

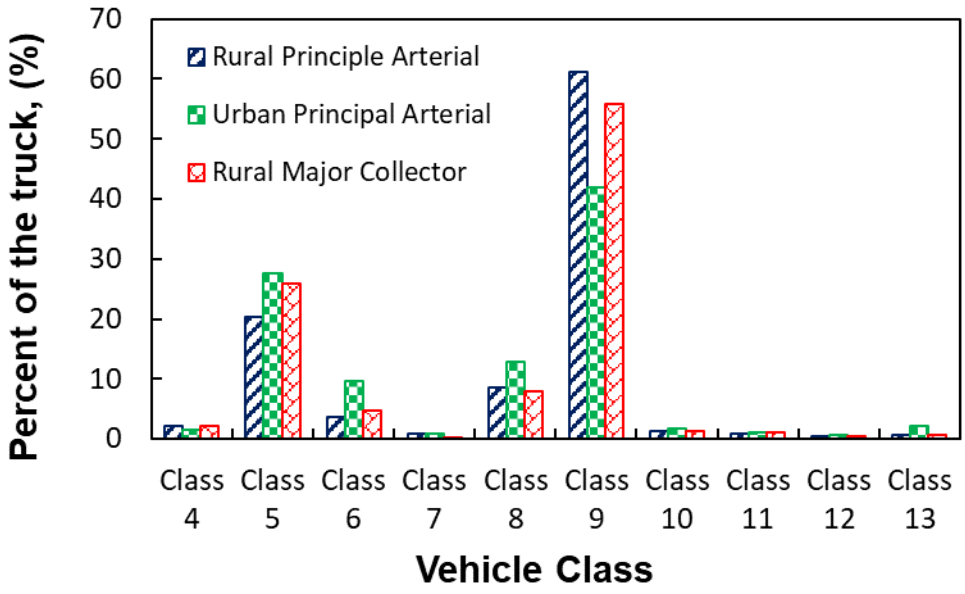

Figure 23- Truck class distribution factors for different road types in Oklahoma

The traffic varies each month throughout a year. Truck traffic monthly adjustment factors represent the proportion of annual truck traffic for a given truck class that occurs in a specific month. The sum of monthly factors for all the months in a year for each vehicle class must be equal to 12.

One of the Pavement ME design traffic inputs is axle load distribution for each class of trucks. Figure 24 through Figure 27 shows the average value of single, tandem, tridem, and quad-axle load distribution for each class of trucks in the state of Oklahoma. Level 2 inputs are the statewide average values determined from traffic analyses of data from various LTPP sites in the state.

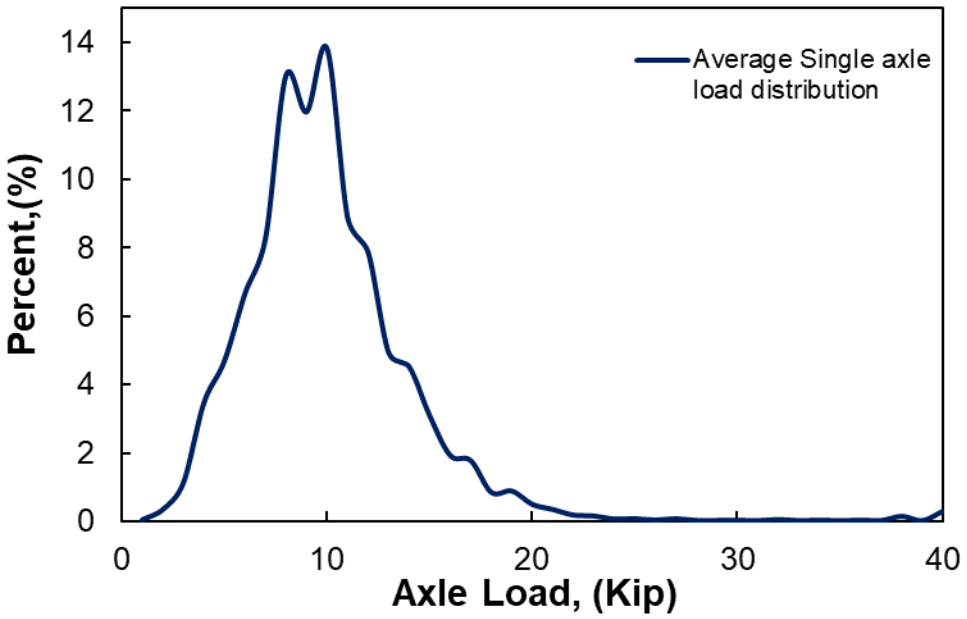

Figure 24 - Average single axle load distribution factors for truck traffic in Oklahoma

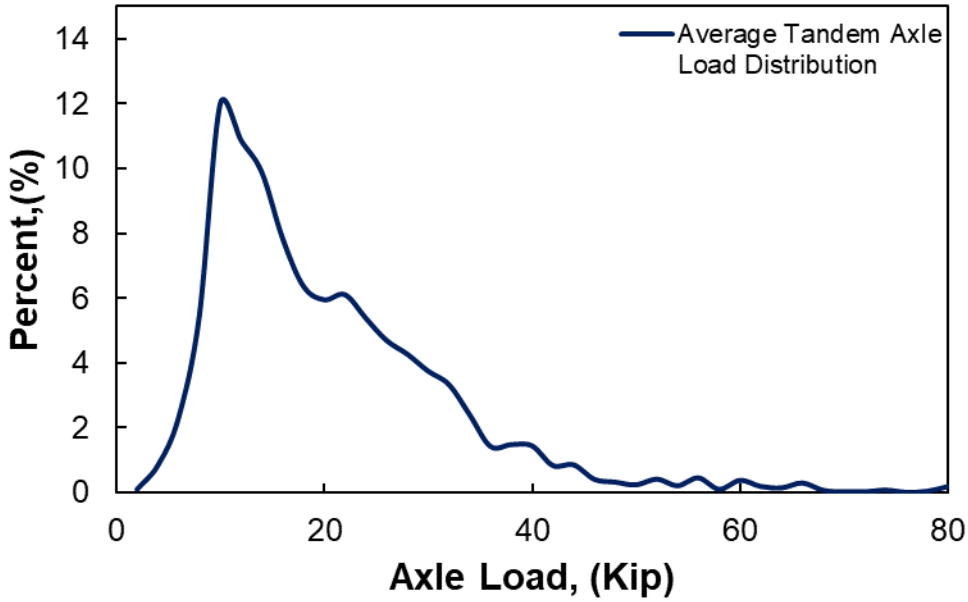

Figure 25 - Average tandem axle load distribution factors for truck traffic in Oklahoma

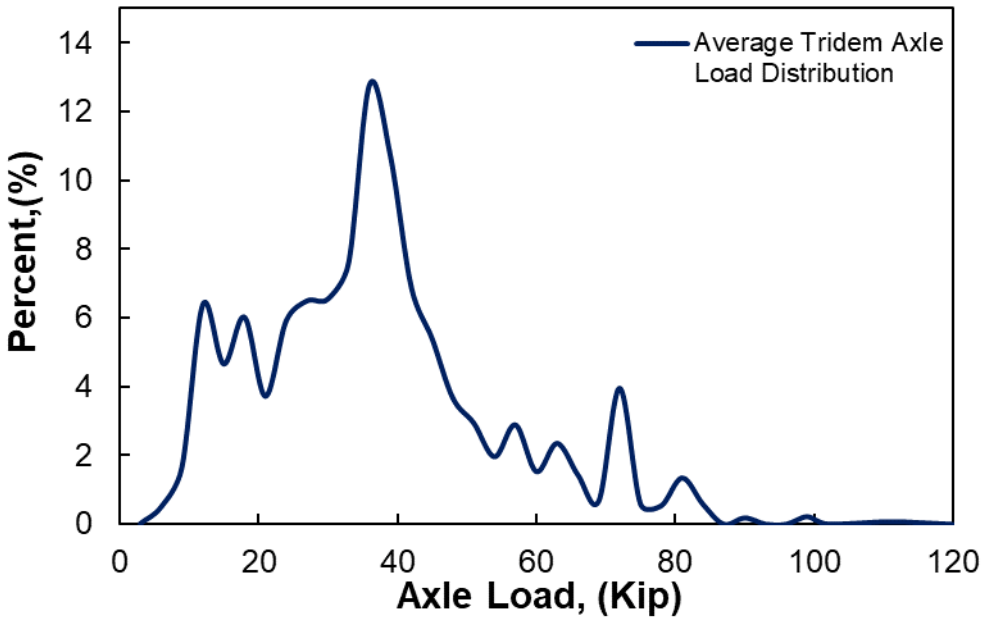

Figure 26 - Average tridem axle load distribution factors for truck traffic in Oklahoma

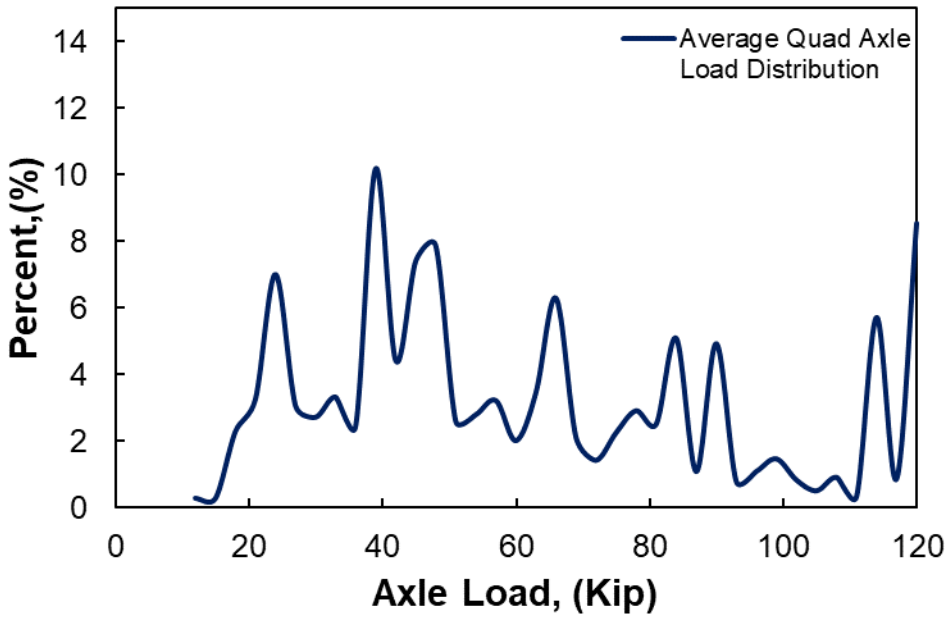

Figure 27 - Average quad-axle load distribution factors for truck traffic in Oklahoma

Climate Data

Environmental conditions play a significant effect on the performance of both flexible and rigid pavements. The performance of a pavement depends on both temperatures and moisture contents of its structural layers (e.g., surface, base, and subgrade, etc.).

Based on the climate data, the mean annual temperature ranges from 62 °F along the Red River to about 58 °F along the northern border. Then it decreases westward to 56 °F in

Cimarron County (*40*). Figure 28 shows the average annual temperature for the state of Oklahoma.

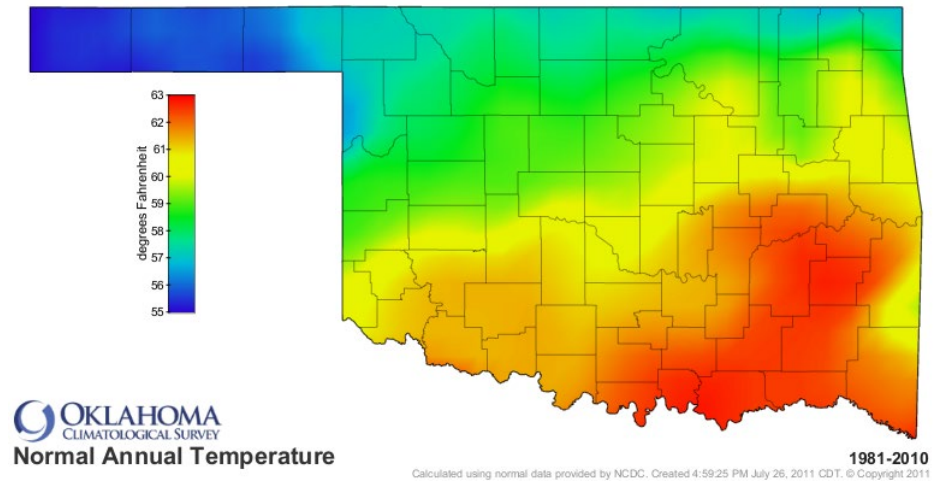

Figure 28- Map of average annual temperature for Oklahoma (*40*)

There is a sharp decrease in rainfall from east to west, as presented in Figure 29. The average annual precipitation ranges from about 17 inches in the far western panhandle to about 56 inches in the far southeast.

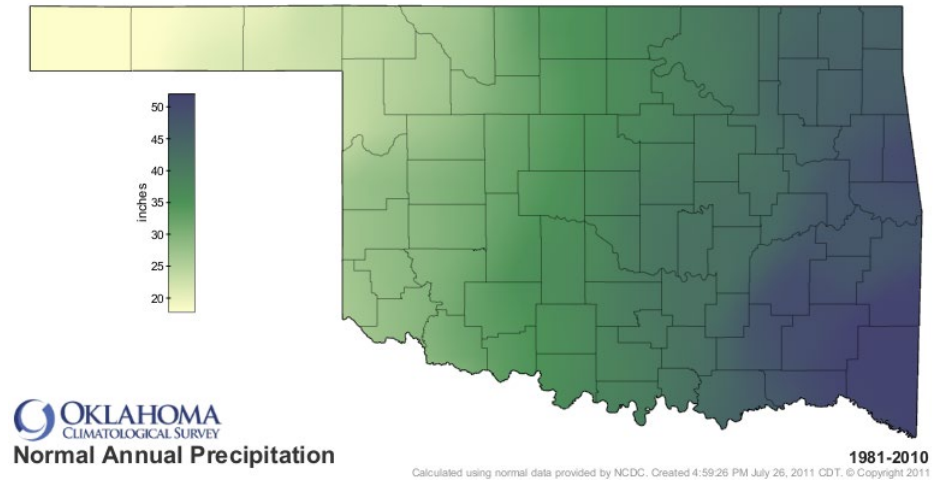

Figure 29- Map of average annual precipitation for Oklahoma (*40*)

Annual average relative humidity ranges from about 60 percent in the panhandle to over 70 percent in the east and southeast. On average, cloudiness increases from west to east across the state. The annual fraction of possible observed sunshine ranges from about 45 percent in eastern Oklahoma to near 65 percent in the panhandle (*40*).

The Modern-Era Retrospective analysis for Research and Applications (MERRA) dataset was used as the input for climate data in the calibration effort. Figure 30 shows the location of the selected weather stations. For each calibration design effort, the closest station or interpolation of information for two or three stations was used as climate input data.

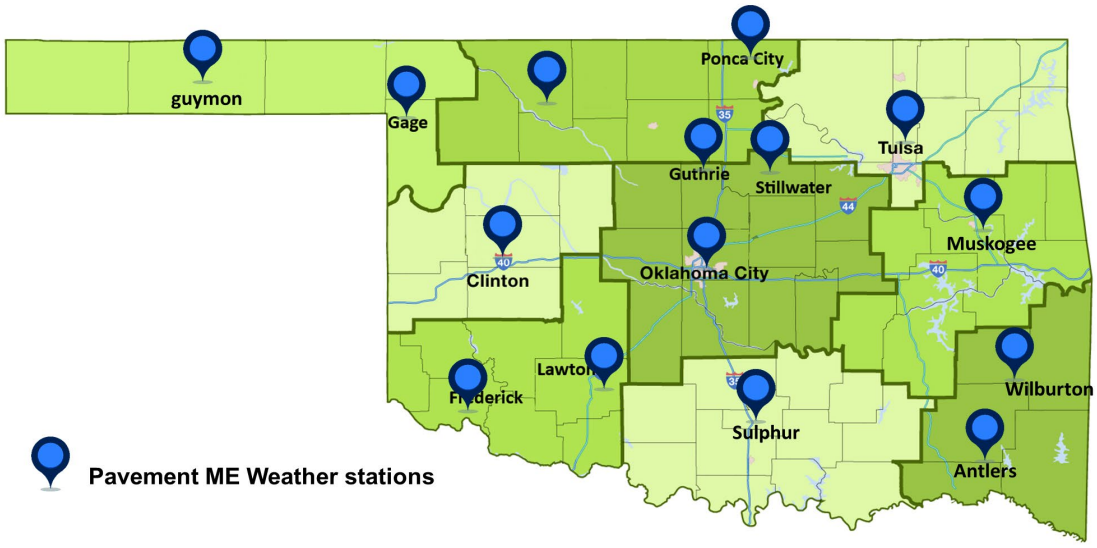

Figure 30 – Location of the Pavement ME weather stations

Groundwater table depth is an important parameter because it plays a significant role in the overall accuracy of the foundation/pavement moisture contents and, hence, equilibrium modulus values. The groundwater table depth is intended to be either the best estimate of annual average depth or seasonal average depth. The groundwater depth information was collected from the Oklahoma Water Resource Board (32) used as input to Pavement ME Design. Figure 31 shows the distribution of water depth in LTPP sections.

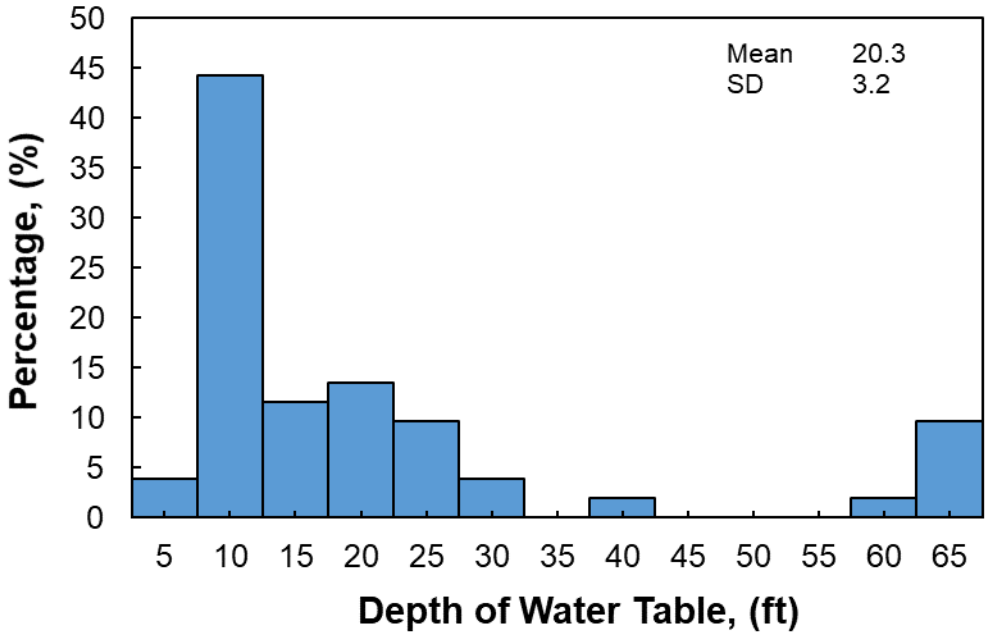

Figure 31 – Depth of water table for LTPP sections in Oklahoma

Pavement Performance and Distress Data

The magnitudes of time-series distress and IRI data from the identified LTPP projects were extracted and compared with design threshold values for each distress type and IRI. Figure 32, through Figure 35, summarizes the distribution of measured distresses from the LTPP sections in Oklahoma.

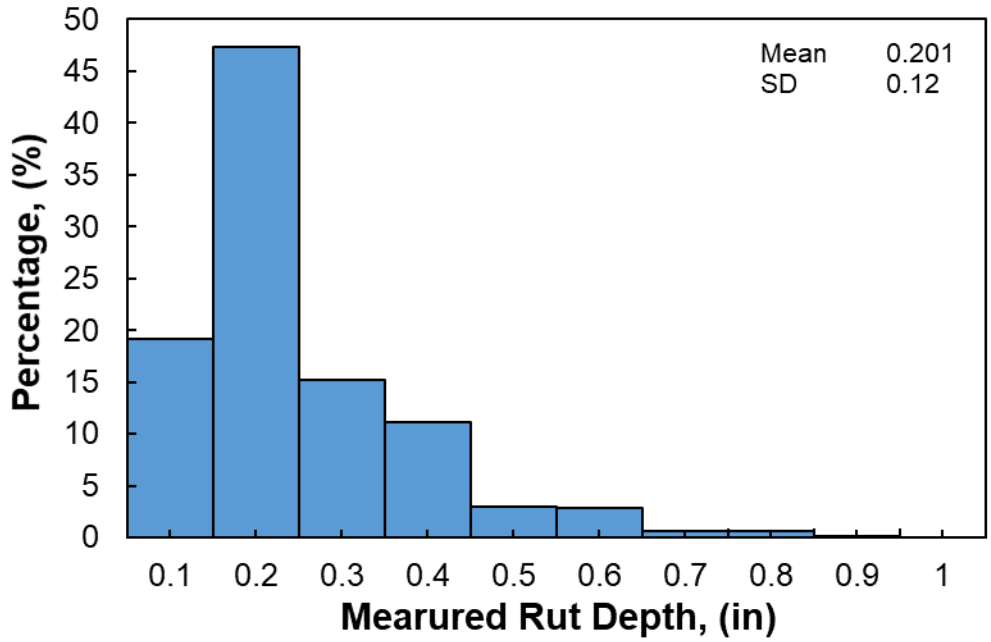

Figure 32 - Measured rutting of LTPP sections for new HMA and HMA overlay projects in Oklahoma

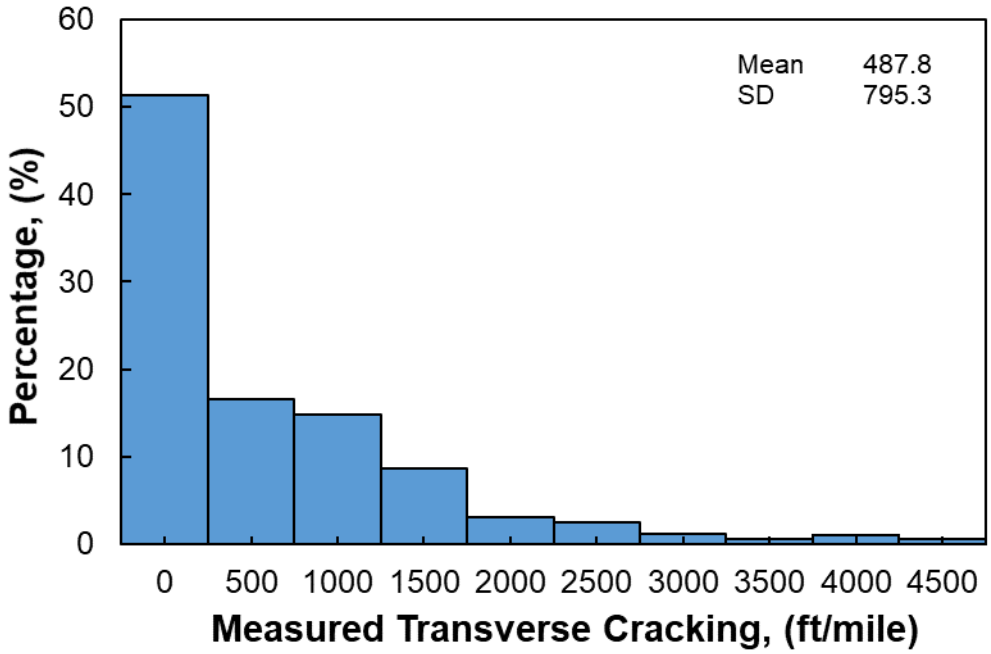

Figure 33 - Measured transverse cracking of LTPP sections for new HMA and HMA overlay projects in Oklahoma

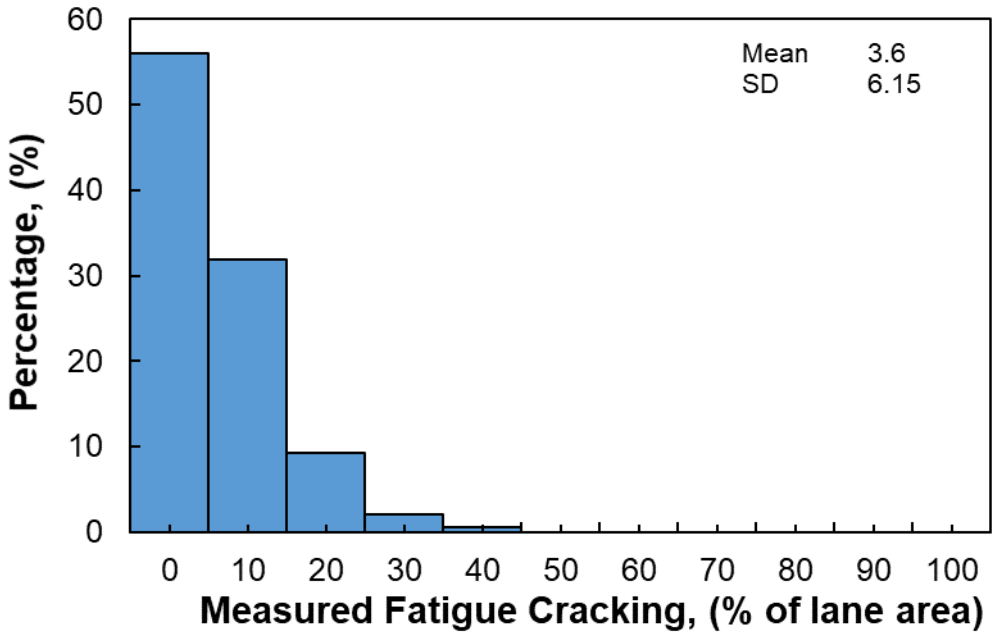

Figure 34 - Measured fatigue cracking of LTPP sections for new HMA and HMA overlay projects in Oklahoma

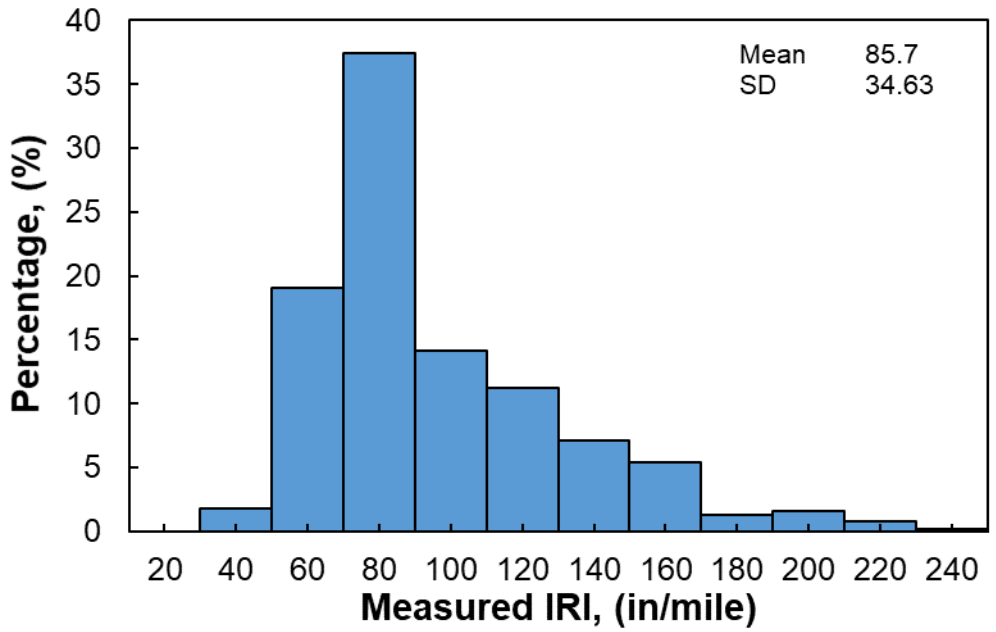

Figure 35 - Measured IRI in LTPP sections for new HMA and HMA overlay projects in Oklahoma

For all the distress types and IRI, the average value are lower than the design threshold values and range from 18 to 77 percent. Transverse cracking and rutting are commonly two severe types of distress in Oklahoma LTPP sections. Table 16 presents the comparison between measured distress/IRI from Oklahoma LTPP sections and the threshold values.

Table 16 - Comparison of distress and IRI values with design criteria or threshold values

Performance Prediction Models	Design Criteria	Average Value of LTPP Project	Percentage of Design Criteria
Alligator Cracking	20% lane area	3.6	18.00
Transverse Cracking	630 ft/mi	487.8	77.43
Rut Depth	0.4 inch	0.201	50.25
IRI	169 inch/mi	85.7	50.71

Pavement ME Analysis

The collected information for LTPP and non-LTPP sections were used in Pavement ME. The software was run to analyze different pavement sections in the different construction stages. Each section was considered as new construction project until before the rehabilitation or reconstruction activities. After this stage, the pavement was analyzed as an overlay project, and the related models were calibrated. After running the program for all the sections in each construction stage, the predicted distress/IRI values was extracted and compared with measured ones.

In this step, the accuracy of national calibration coefficients will be determined as well. The aim of the calibration process is to reduce the bias and standard error of estimate (SEE) of the measured values versus predicted ones. This was done by changing the calibration coefficients of each model and finding the best set of coefficients suitable for the condition of selected pavements in Oklahoma. Table 17 shows the accuracy of nationally calibrated distress models for newly constructed flexible pavements in Oklahoma.

Table 17- Accuracy of nationally calibrated distress models for flexible pavements in Oklahoma

Statistics parameter	Rutting (in)	Bottom-up Cracking (% of the lane)	Top-Down Cracking (ft/mile)	Transverse Cracking (ft/mile)	IRI (in/mile)
R-squared (%)	25	Poor	poor	poor	48.15
SEE (Distress Unit)	0.096	21.3	3054	1325	14.7
Se/Sy	0.88	6.31	1.23	1.26	0.4

Comparing the measured values of distress\IR, I in Oklahoma with Pavement ME nationally calibrated predictions shows a variance that affirms the need for local calibration of analytical models. Rutting and IRI predictions demonstrate better performance compared to other distresses. In most cases, the measured fatigue cracking from the field is higher than the predicted values. However, the predictions from Pavement ME show the very low amount of thermal cracking, which is very different than the observed values from the field.

Local Calibration Coefficient

A local calibration effort involves an investigation of the causes for the poor goodness of fit and bias in Pavement ME nationally calibrated models and modification of the calibration coefficients of distress/IRI models. The aim of the calibration process is to reduce the bias and standard error of estimate (SEE) of the measured values versus predicted ones by changing the calibration coefficients of each model and finding the best set of coefficients suitable for the condition of selected pavements in Oklahoma.

Calibration coefficients can be divided into two groups. A portion of coefficients causes the reduction in the bias of local calibration effort and another portion causes the reduction in the standard error and an increase in the precision of estimates. Figure 36 shows the elimination of bias and an increase in the precision of prediction by the local calibration process.

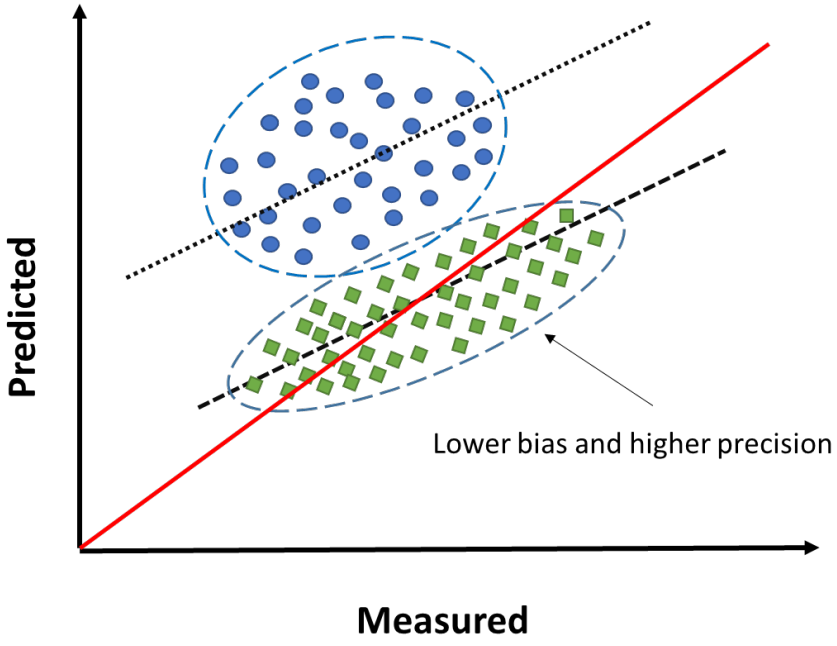

Figure 36- Improvement of bias and precision after local calibration

Table 18 shows the role of each coefficient in distress\IRI models. In addition, it shows the range of locally calibrated coefficients derived from previous studies that have been done for the calibration of MEPDG or Pavement ME models.

Table 18 – Coefficient's role in the calibration process and its local calibrated ranges

Distress Type	Role in the Calibration Process	Calibration Coefficient	Global Value	Lower Limit	Upper Limit
Rutting	Eliminate bias	K_r1	-3.35412	-3.35	-3.36
Rutting	Eliminate bias	B_r1	1	0.5	5
Rutting	Eliminate bias	B_s1	1	0.5	1.5
Rutting	Reduce standard error	K_r2	1.56	NA	NA
Rutting	Reduce standard error	K_r3	0.4791	NA	NA

Distress Type	Role in the Calibration Process	Calibration Coefficient	Global Value	Lower Limit	Upper Limit
Rutting	Reduce standard error	B_r2	1	0.5	2.5
Rutting	Reduce standard error	B_r3	1	0.5	2.5
Fatigue Cracking	Eliminate bias	B_f1	1	0.5	3.5
Fatigue Cracking	Eliminate bias	C_2	1	0.1	2
Fatigue Cracking	Reduce standard error	B_f2	1	0.5	1.5
Fatigue Cracking	Reduce standard error	B_f3	1	0.5	1.5
Fatigue Cracking	Reduce standard error	C_1	1	0	1.5
Top-Down Cracking	Eliminate bias	K_f1	0.007566	NA	NA
Top-Down Cracking	Eliminate bias	C_2	1	0.2	5
Top-Down Cracking	Reduce standard error	B_f2	1	0.5	1.5
Top-Down Cracking	Reduce standard error	B_f3	1	0.5	1.5
Top-Down Cracking	Reduce standard error	C_1	1	0	1.5
Transverse Cracking	Eliminate bias and reduce standard error	B_t3	1	NA	NA
Transverse Cracking	Eliminate bias and reduce standard error	K_t3	1.5	NA	NA
IRI	Eliminate bias	C_4	0.015	0.01	0.03
IRI	Reduce standard error	C_1	40	5	50
IRI	Reduce standard error	C_2	0.4	0.1	1.5
IRI	Reduce standard error	C_3	0.008	0.002	0.015

For the rutting and fatigue damage model, a narrow down iterative approach was used to reduce the standard error. In this approach, a different combination of calibration coefficients was applied in the Pavement ME analysis for all sections, and the distress results were evaluated. In the end, a set of calibration coefficients with minimum SEE were introduced. Figure 37 shows a schematic procedure for the calibration approach for the rutting model. This approach consists of finding the minimum SEE by using a wide range of the calibration coefficients' combination; then, increasing the precision of the coefficients by narrowing down the coefficients' range and finding the best Calibration coefficients. The set of coefficients that

correspond to eliminate bias were calibrated outside of the Pavement ME through Microsoft Excel Solver.

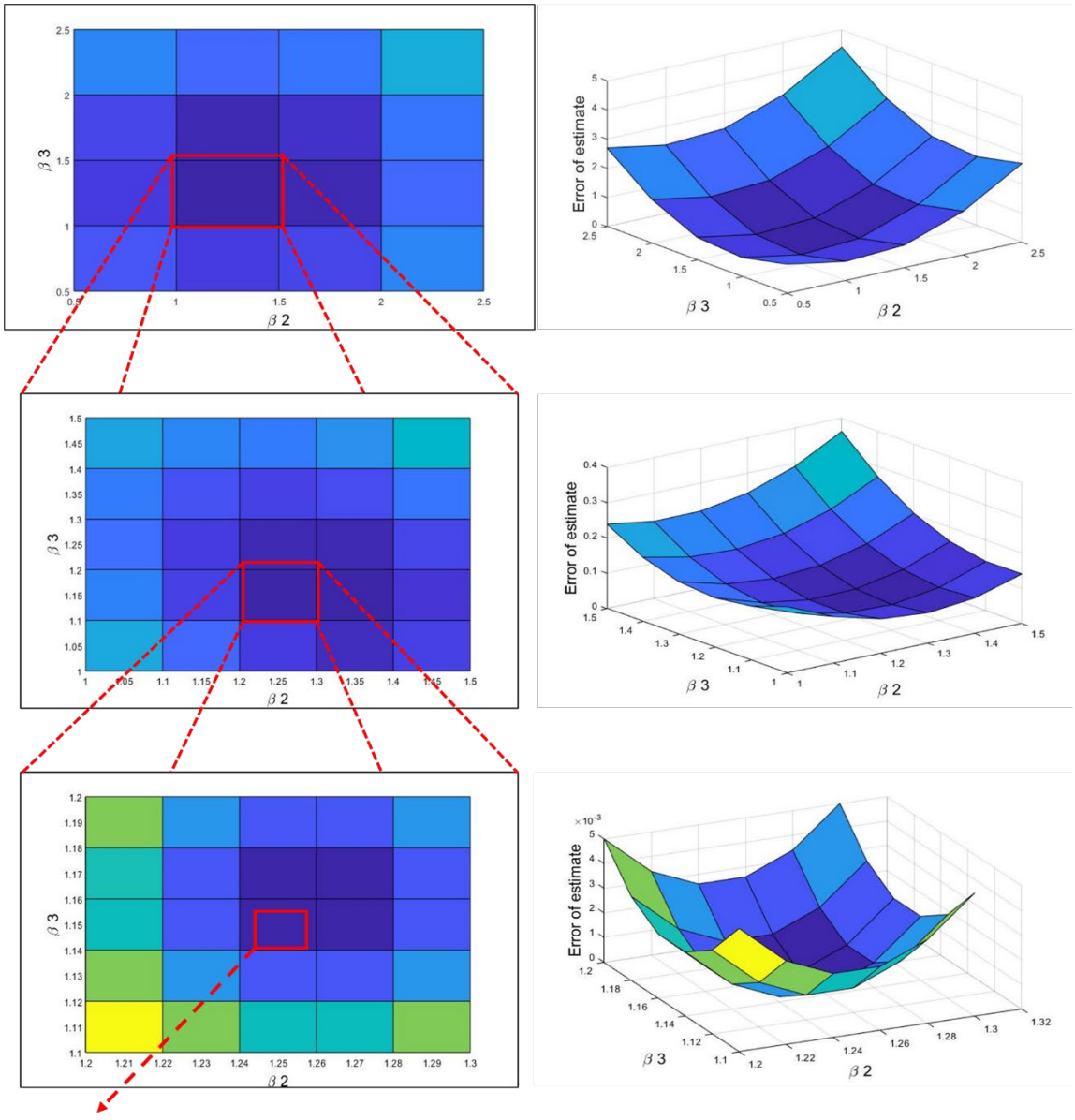

Figure 37 – A schematic narrow down procedure for distress calibration coefficients

Rutting Model

Among the five calibration coefficients affecting the rutting models,*βr1*, *βgb*, and *βsb* correspond to the AC layer, granular base, and subgrade rutting amount and were calibrated outside of the Pavement ME software by using the Microsoft Excel Solver. Calibration coefficients of *βr2* and *βr3* correspond to the effect of temperature and traffic on the AC layer, which was calibrated by numerous runs of the Pavement ME using the narrow down approach.

After running the Pavement ME by each set of calibration coefficients, the predicted values of rutting versus measured values from LTPP and non-LTPP sections were evaluated, and the best combination was chosen. In the next step, the other three calibration coefficients were determined through the optimization effort. Figure 38 shows the measured versus predicted values of rutting before and after calibration according to the material, temperature, and traffic conditions for the state of Oklahoma.

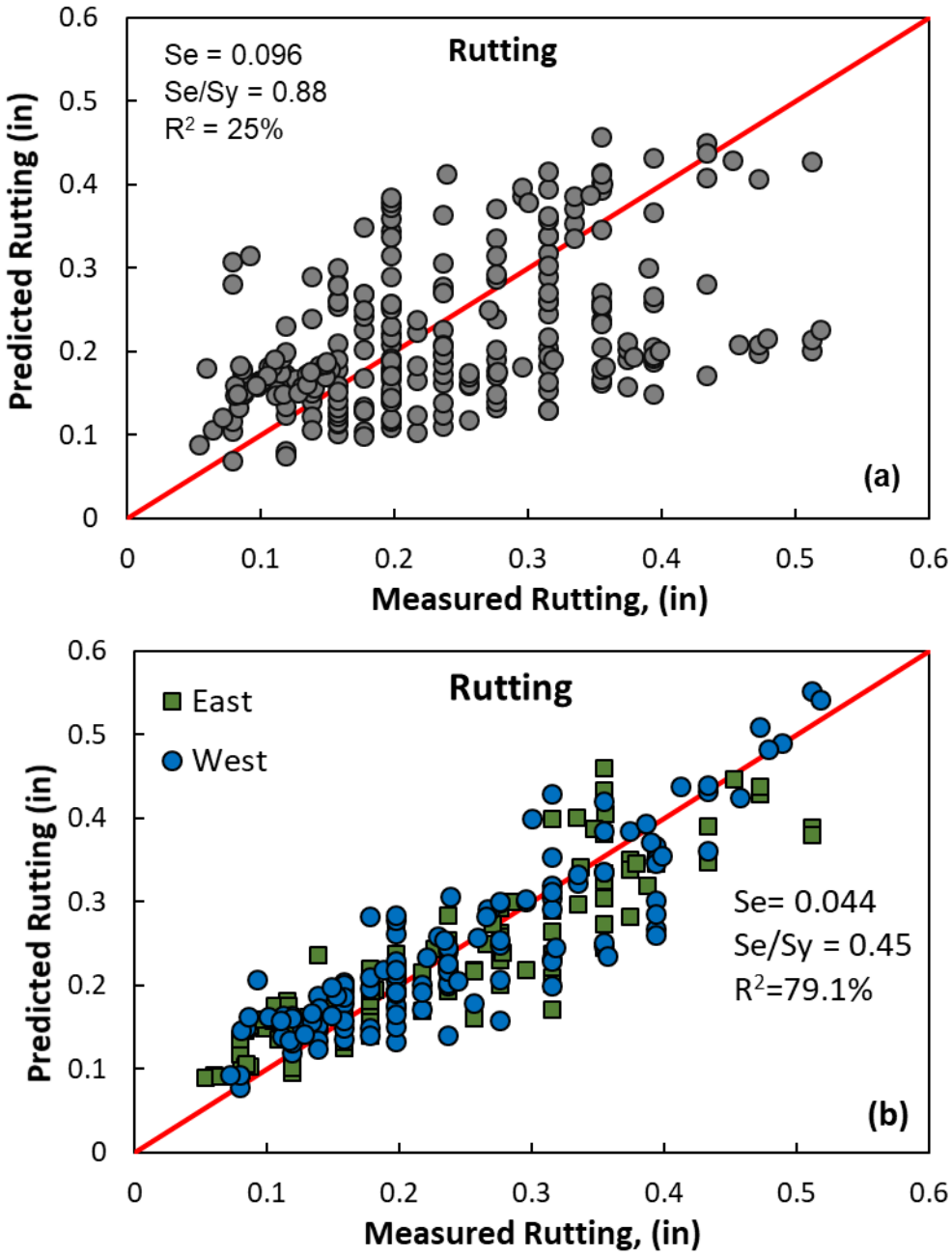

Figure 38- Total rut depth (a) before calibration, (b) after calibration.

Table 19 shows the recommended calibration values for the state of Oklahoma before and after the calibration effort.

Table 19- Rutting model coefficients before and after calibration effort for the state of Oklahoma

Layer	Parameter	National Coefficients	Calibrated Coefficients East	Calibrated Coefficients West
AC layer	k_1	-2.45	-2.45	-2.45
AC layer	k_2	1.565	1.565	1.565
AC layer	k_3	0.299	0.299	0.299
AC layer	β_1	0.4	0.79	0.21
AC layer	β_2	1	0.53	0.74
AC layer	β_3	1	1.48	1.03
Granular Base	k_1	0.965	0.965	0.965
Granular Base	β_{gb}	1	0.15	0.23
Subgrade	k_1- Coarse Grain	0.965	0.965	0.965
Subgrade	k_1 - Fine Grain	0.675	0.675	0.675
Subgrade	k_1 - A_3	0.635	0.635	0.635
Subgrade	β_{sg}	1	1.29	1.03

Table 20 shows the statistical analysis for the rutting model before and after calibration.

Table 20- Goodness of fit and bias test statistics for final locally calibrated rutting model

Model Calibration Status	Number of Observation	R^2 (%)	Se (in)	Se/Sy	p-value (paired t-test)	p-value (slope) (β=0)
National values	278	25%	0.096	0.88	0.0108	<0.0001
local calibrated values	278	79.1%	0.044	0.45	0.0501	<0.0001

Fatigue Cracking

Top-down and bottom-up cracking are both a function of fatigue damage. The calibration coefficients correspond to the fatigue damage (i.e. *βf1*, *βf2,* and *βf3*) were calibrated by the iteration process and the coefficients of C_1, C_2, and C_3 were optimized through Microsoft excel solver. Figure 39 shows the measured versus predicted values of top-down cracking before and after calibration according to the material, temperature, and traffic conditions for the state of Oklahoma.

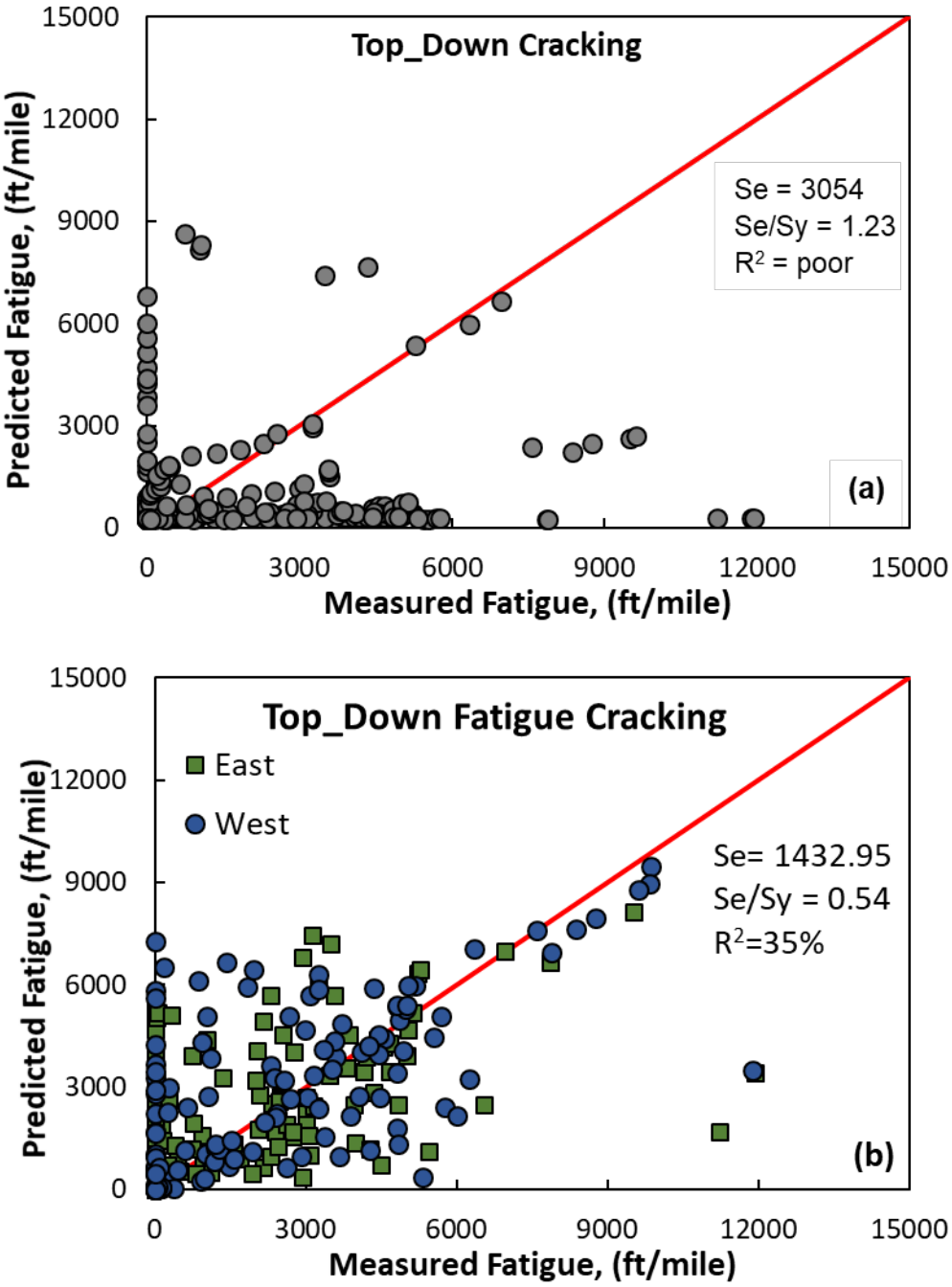

Figure 39- Total top-down fatigue cracking (a) before and (b) after the calibration process

Figure 40 shows the measured versus predicted values of top-down cracking before and after calibration according to the material, temperature, and traffic conditions for the state of Oklahoma.

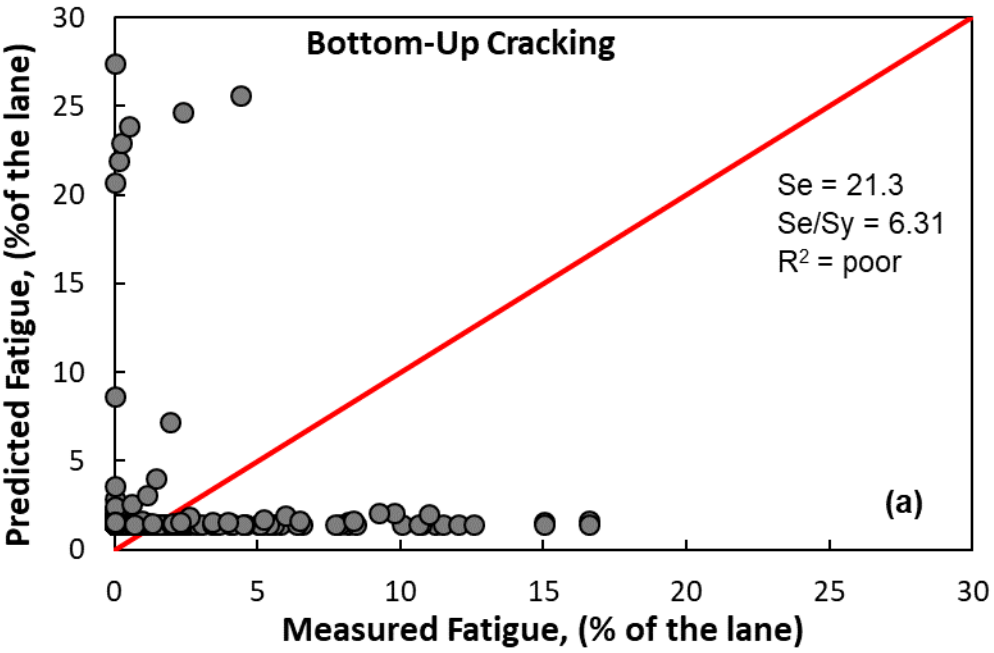

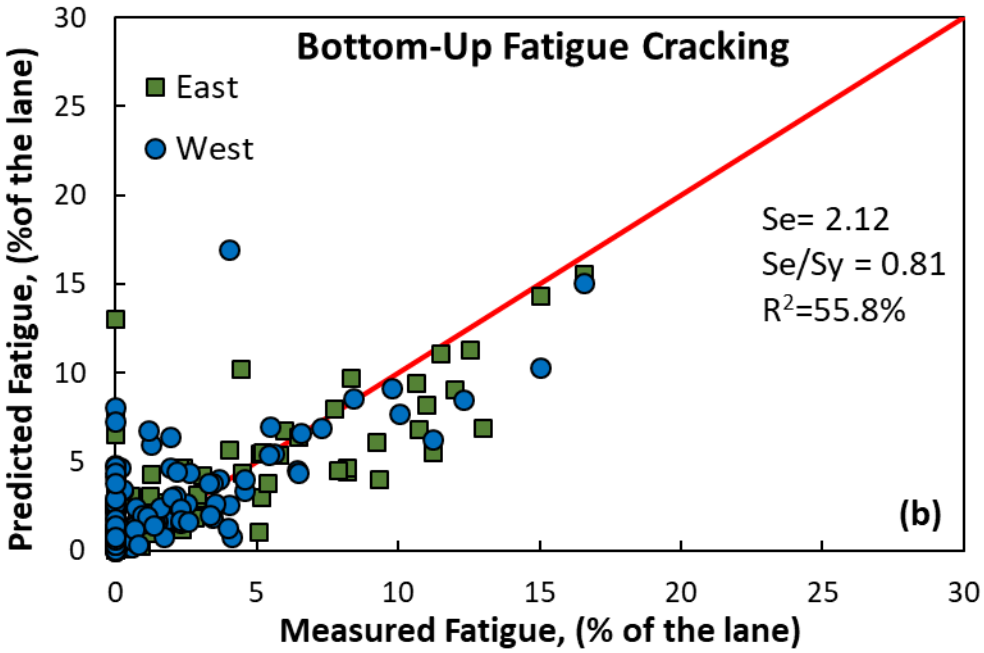

Figure 40 -Total bottom-up fatigue cracking (a) before calibration, (b) after calibration

Table 21 shows the recommended calibration values for fatigue top-down and bottom-up cracking for the state of Oklahoma before and after calibration effort.

Table 21- Fatigue models coefficients' before and after calibration effort for the state of Oklahoma

Model	Parameter	National Coefficients	Local Coefficients East	Local Coefficients West
Fatigue Damage (%)	β_{f1} h_{AC}<5 in	0.00205	0.00205	0.00205
Fatigue Damage (%)	β_{f1} 5 in< h_{AC} <14 in	(0.5014* h_{AC}-3.416)	(0.5014* h_{AC}-3.416)	(0.5014* h_{AC}-3.416)
Fatigue Damage (%)	β_{f1} h_{AC} >14 in	0.000065	0.000065	0.000065
Fatigue Damage (%)	β_{f2}	1	1	1
Fatigue Damage (%)	β_{f3}	1	1.35	1.23
Fatigue Damage (%)	k_1	3.75	4.2	3.56
Fatigue Damage (%)	k_2	3.961	3.62	4.18
Fatigue Damage (%)	k_3	1.285	1.4	2.2
Top-down Cracking (ft/mile)	C_1	7	6.6	6.1
Top-down Cracking (ft/mile)	C_2	3.5	4.5	4.23
Top-down Cracking (ft/mile)	C_4	1000	723	874
Bottom-up Cracking (%)	C_1	7	3.26	4.12
Bottom-up Cracking (%)	C_2 h_{AC} <5 in	2.16	2.16	2.16
Bottom-up Cracking (%)	C_2 5 in< h_{AC} <14 in	0.867+0.2583 * h_{AC}	0.867+0.2583* h_{AC}	0.867+0.2583* h_{AC}
Bottom-up Cracking (%)	C_2 h_{AC} >14 in	4.5	4.5	4.5
Bottom-up Cracking (%)	C_3	6000	6000	6000

Table 22 and Table 23 shows the statistical analysis for the top-down cracking model before and after calibration.

Table 22- Goodness of fit and bias test statistics for final locally calibrated top-down cracking

Model calibration status	Number of observation	R^2 (%)	Se (ft/mile)	Se/Sy	*p*-value (paired t-test)	*p*-value (slope), (β=0)
National values	342	poor	3054.135	0.88	<0.0001	0.777
local calibrated values	342	35%	1432.95	0.54	<0.0001	0.021

Table 23 - Goodness of fit and bias test statistics for final locally calibrated bottom-up cracking

Model calibration status	Number of observation	R^2 (%)	Se (% of the lane)	Se/Sy	*p*-value (paired t-test)	*p*-value (slope), (β=0)
National values	322	poor	21.3	6.31	<0.0001	0.14
local calibrated values	322	55.8%	2.12	0.81	<0.0001	<0.0001

Thermal Cracking

The thermal cracking showed poor performance before the calibration effort. In the previous Pavement ME version (i.e., referred to the as old version in the report), the thermal cracking calibration coefficients were depended on the hierarchical level of input data. In the new version released in Jun 2018, the thermal cracking coefficients are functions of the mean annual average temperature (MAAT). These coefficients are calibrated based on the climate condition in the state of Oklahoma. The equation (51) shows the locally calibrated coefficients for the thermal cracking using inputs for the state of Oklahoma.

$$\begin{cases} MAAT \le 57°F & K = \left(3*10^{-7}\right)*MAAT^{4.0319} \\ MAAT > 57°F & K = 0.13*MAAT^2 - 11.68*MAAT + 244.14 \end{cases} \quad (51)$$

Table 24 shows the standard deviation of thermal cracking for each level of input data. These standard deviations are used in the calculation of thermal cracking at each reliability level.

Table 24- Calibrated thermal cracking standard deviation

MAAT	National Coefficients	East Coefficients	West Coefficients
MAAT≤57 °F	$3 * 10^{-7} * MAAT^{4.0319}$	$3*10^{-7}*MAAT^{4.0319}-54$	$3 * 10^{-7} * MAAT^{4.0319} - 23$
MAAT>57 °F	$0.13 * MAAT^2 - 11.68 * MAAT + 244.14$	$0.13 * MAAT^2 - 11.68 * MAAT + 100$	$0.13 * MAAT^2 - 11.68 * MAAT + 78$

After running the Pavement ME using calibrated coefficients, the predicted values of thermal cracking versus measured values were evaluated. Figure 41 shows the measured versus predicted values of thermal cracking before and after calibration according to the material, temperature, and traffic conditions in Oklahoma.

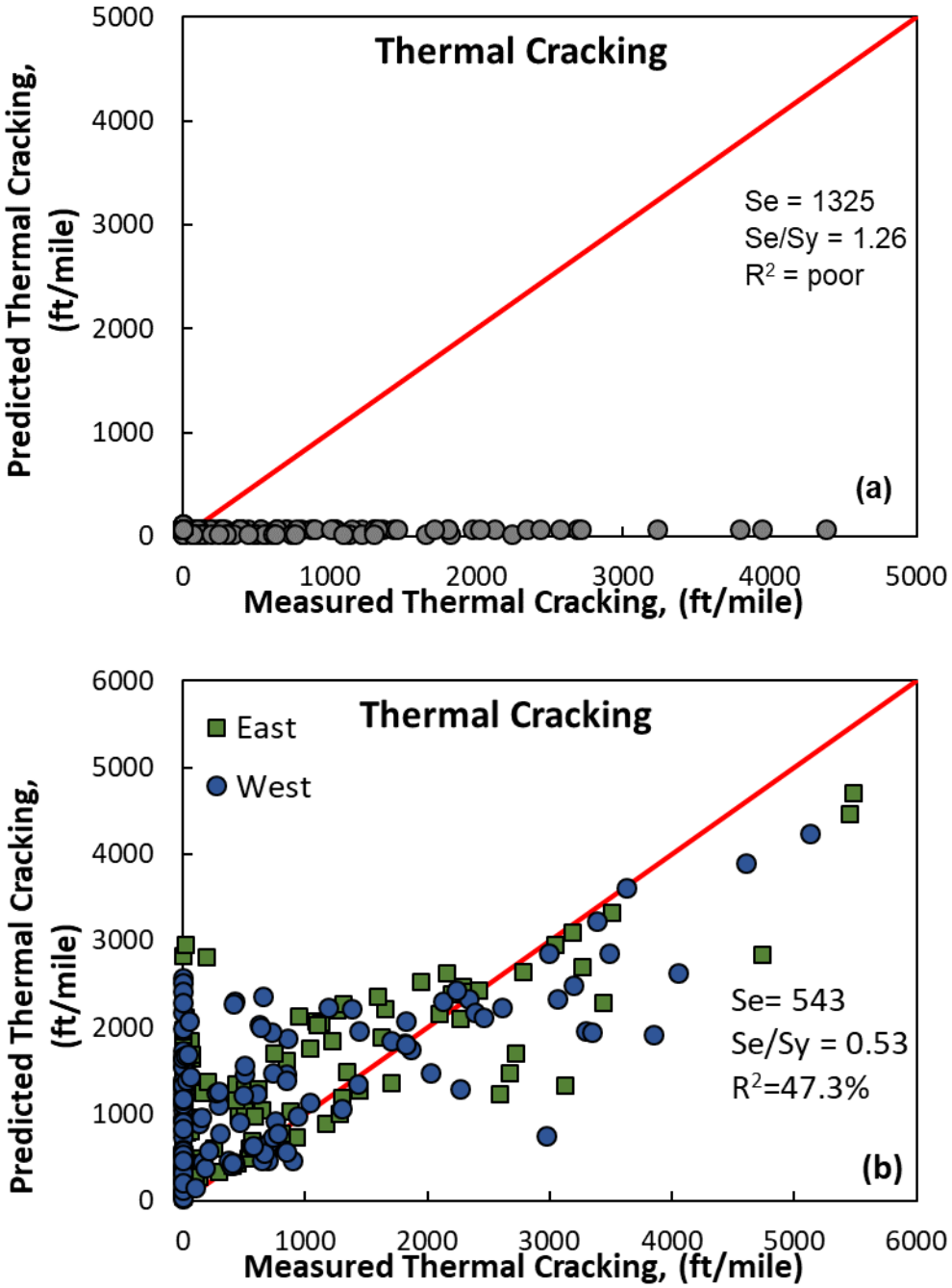

Figure 41- Total transverse cracking (a) before calibration, (b) after calibration

Table 25 shows the statistical analysis for the thermal cracking model before and after calibration.

Table 25- Goodness of fit and bias test statistics for final locally calibrated thermal cracking model

Model Calibration Status	Number of Observation	R^2 (%)	Se (ft/mile)	Se/Sy	p-value (paired t-test)	p-value (slope) (β=0)
National Values	278	Poor	1325	1.26	<0.0001	0.653
Local Calibrated Values	278	47.3%	543	0.53	<0.0001	0.011

IRI

To calibrate the IRI model, the research team investigated the causes of the poor goodness of fit and bias of the Pavement ME nationally calibrated models and modified the local calibration coefficients of the IRI model as needed based on the information derived from distress calibrations. First, for this model, the site factors for each section were calculated, and then by using Microsoft Excel Solver, the coefficients were calibrated, and the best combination was obtained. Figure 42 shows the measured vs. predicted IRI model before and after the calibration effort.

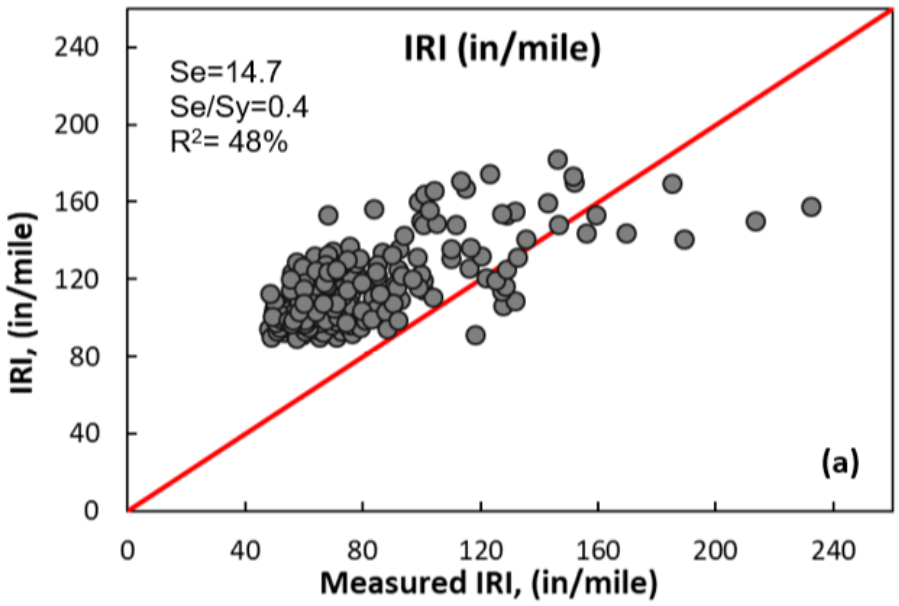

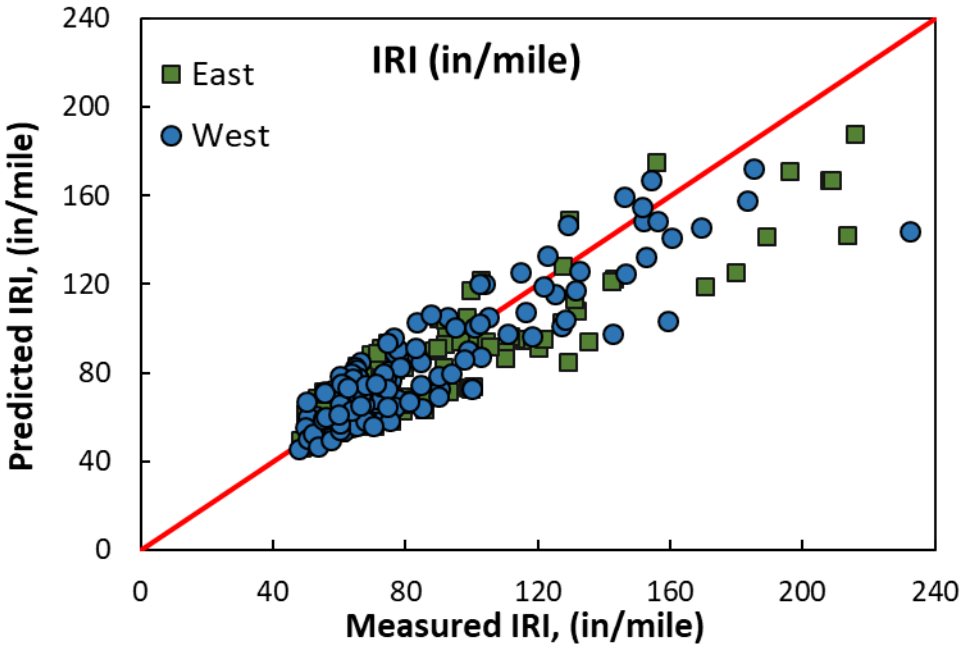

Figure 42 - Total IRI (a) before calibration, (b) after calibration

Table 26 shows the recommended calibration values for the IRI model for the state of Oklahoma before and after calibration effort.

Table 26- IRI models coefficients' before and after calibration effort for the state of Oklahoma

Parameter	National Coefficients	Local Coefficients East	Local Coefficients West
C_1	40	5.23	6.46
C_2	0.4	0.127	0.187
C_3	0.008	0.013	0.0098
C_4	0.015	0.0128	0.023

Table 27 shows the statistical analysis for the top-down cracking model before and after calibration.

Table 27 - Goodness of fit and bias test statistics for final locally calibrated IRI model

Model Calibration Status	Number of Observation	R^2 (%)	Se (in/mile)	Se/Sy	p-value (paired t-test)	p-value (slope) (β=0)
National values	366	48%	14.7	0.4	0.0095	<0.0001
local calibrated values	366	79.7%	10.23	0.23	0.0531	<0.0001

Discussion

Pavement ME models show improvement in all the distress/IRI models after calibration. Rutting and IRI models have a lower error and higher accuracy compared to the fatigue and transverse

cracking models. The accuracy and bias of the prediction models are inconsistent by MEPDG and Pavement ME calibration efforts for the states of Arizona, Colorado, Iowa, and Arkansas (*41*) (*42*, *43*) (*44*-*46*). Robbins et al. (*47*) gathered a summary of the Mechanistic empirical design calibration efforts in the US. Fatigue Cracking models generally underestimate the observed fatigue distresses before the calibration. After the calibration, these models show better performance. Pavement ME thermal cracking results are not inconsistent with Oklahoma's measured values. Even after the calibration, the thermal-cracking model cannot properly predict the measured values.

Figure 43 shows the rutting model prediction error versus the asphalt concrete depth of pavement sections before and after the calibration effort. The calibration effort reduced the error of estimate for all the sections; however, the error reduction decreases by increasing the AC layer thickness.

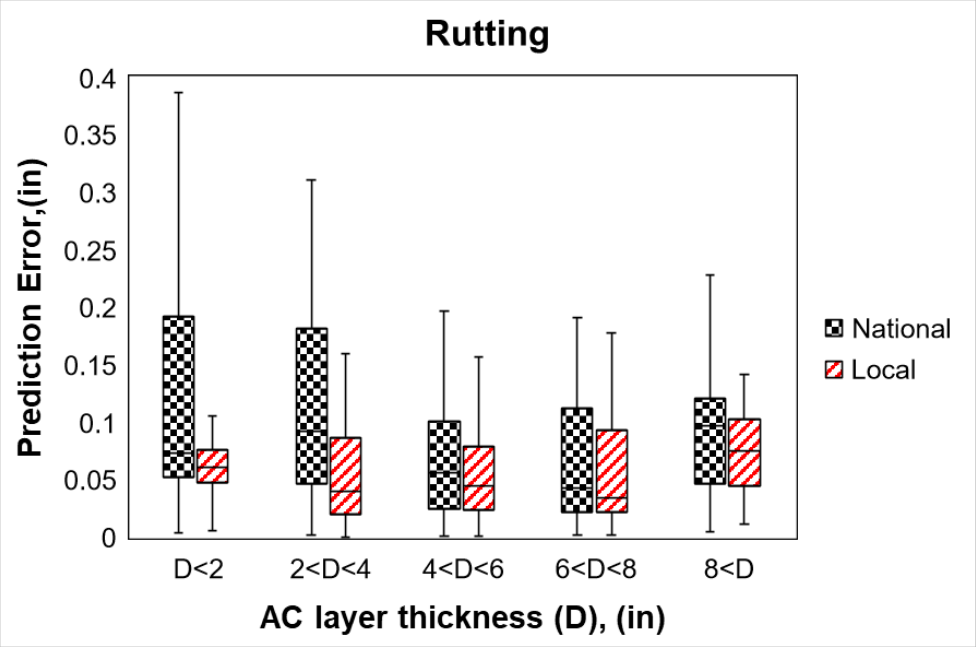

Figure 43- Error of estimate of rutting model vs. AC layer thickness of pavements before and after calibration

The rutting model shows a higher error for the roads with moderate traffic. The calibration effort effect was high for this type of road (Figure 44).

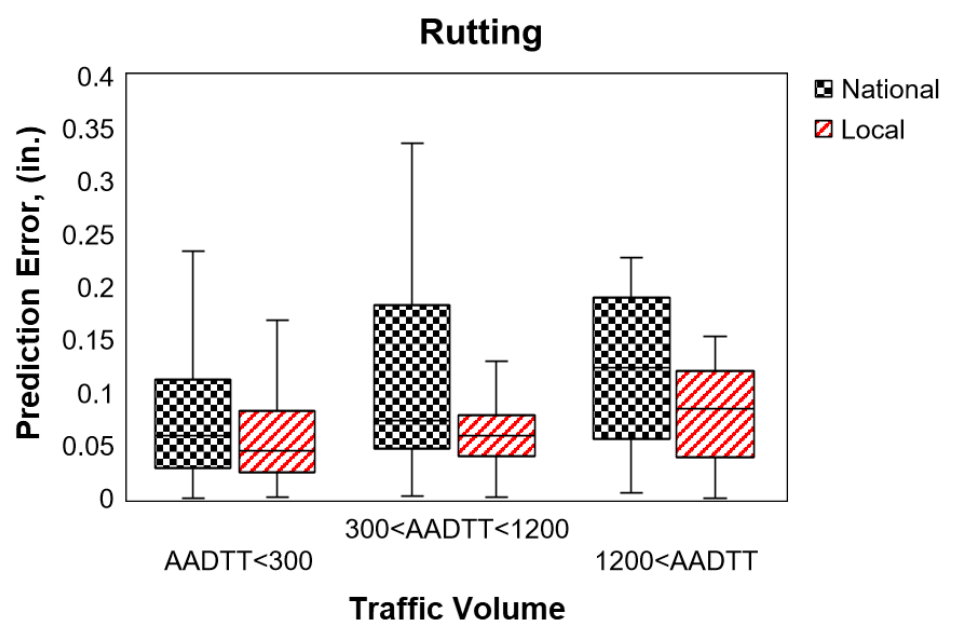

Figure 44- Error of estimate of rutting model vs. pavement's traffic level

Figure 45 shows the prediction error of the bottom-up fatigue cracking model versus the thickness of asphalt concrete pavement sections before and after the calibration effort. The calibration effort reduced the error of estimate for all the sections; however, the fatigue-cracking model shows a higher error before and after calibration for the pavement sections with a 4 to 8 inch AC layer. This model shows a good prediction for the thin pavements. Figure 46 shows the bottom-up fatigue cracking prediction error vs. the pavement age before and after the calibration effort. The prediction model shows low error at the early age of the pavements. The calibration efforts improved the prediction for the pavements before the age of 15 years, but it does not decrease the error of the estimate for the older pavements.

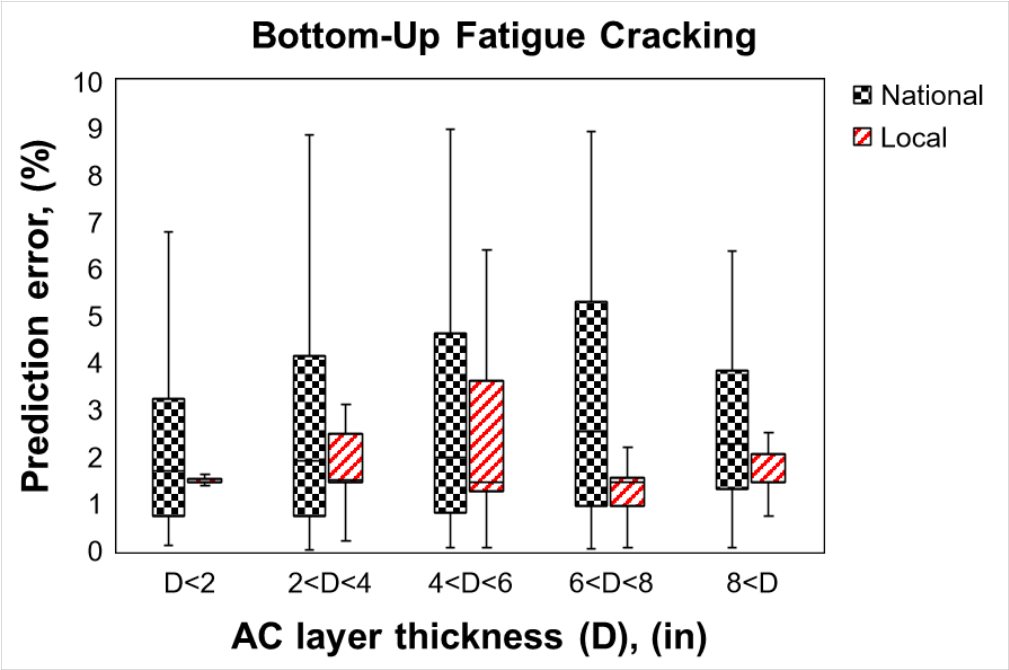

Figure 45- Error of estimate for bottom-up fatigue cracking model versus the layer thickness of AC pavements

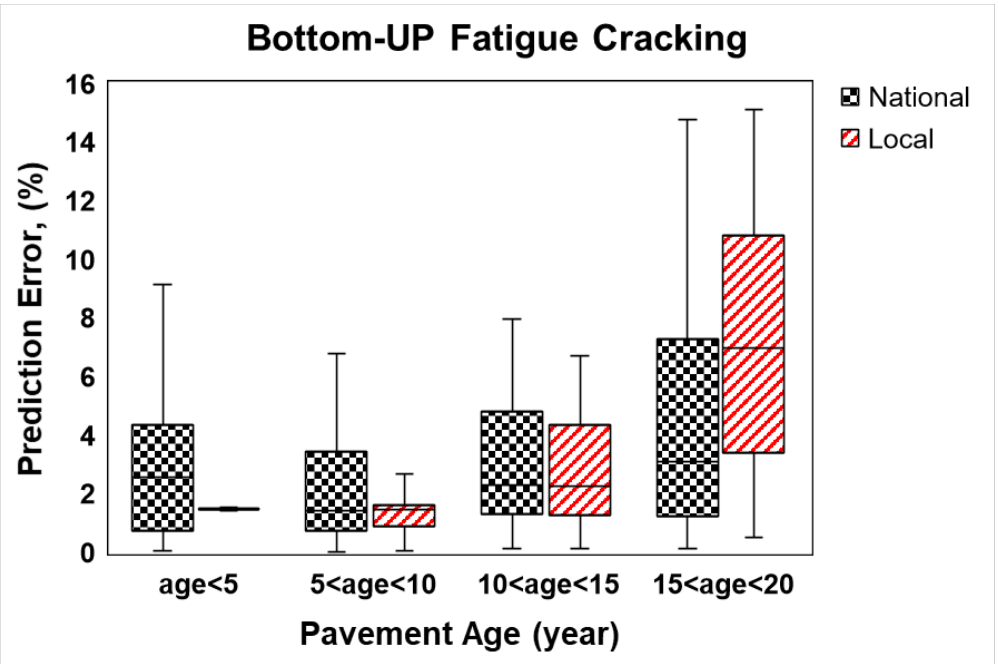

Figure 46 - Error of estimate of bottom-up fatigue cracking model vs. pavement age

Figure 47 shows the top-down fatigue cracking model's prediction error versus the asphalt concrete thickness before and after the calibration effort. This model shows a high error before and after calibration. The top-down fatigue cracking models show an insignificant sensitivity to the thickness of the AC layer. Figure 48 shows the prediction error of top-down fatigue cracking versus the pavement age before and after the calibration effort. This model, contrary to the

bottom-up cracking model, shows higher error at early ages and lower error for older pavements.

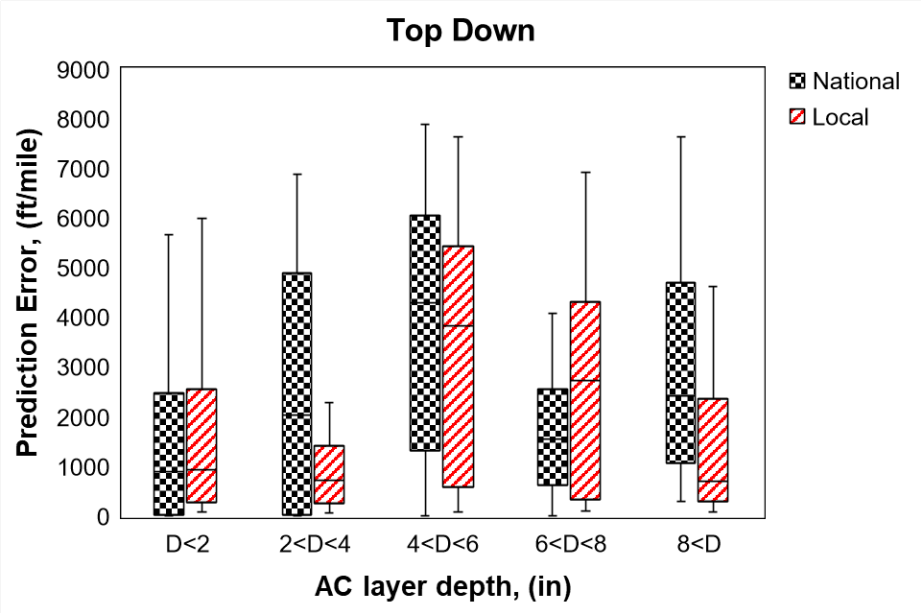

Figure 47- Error of estimate of top-down fatigue cracking model vs. AC layer thickness

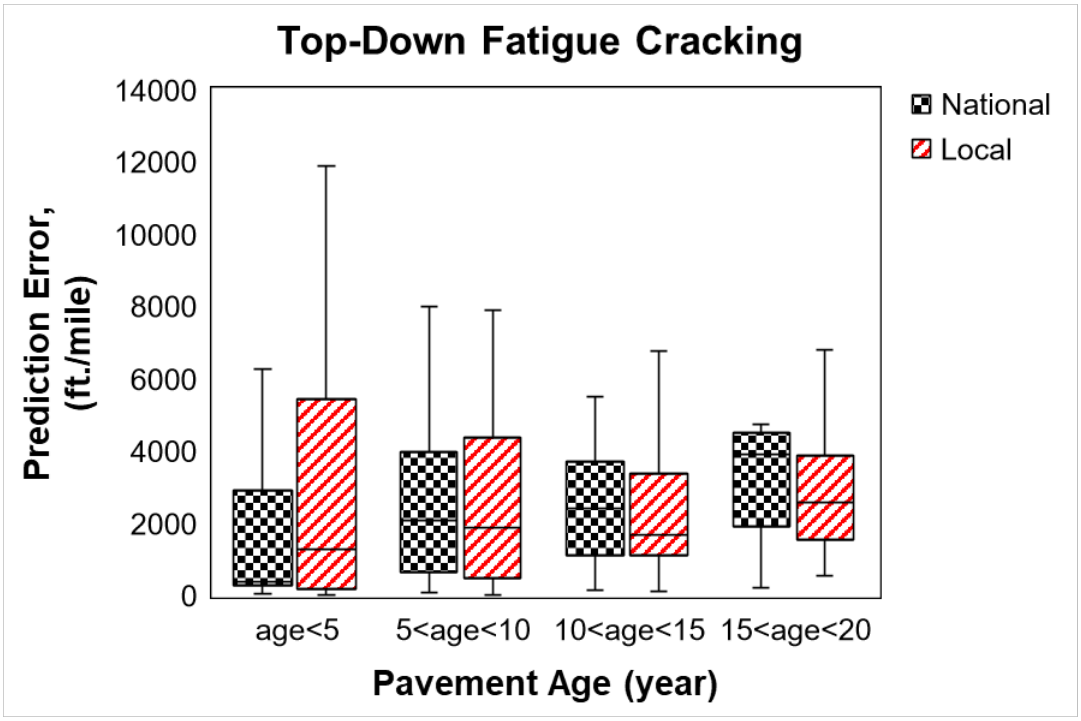

Figure 48- Error of estimate of top-down fatigue cracking model vs. pavement age

Figure 49 shows the prediction error of the thermal cracking model versus the asphalt concrete thickness in pavement sections before and after the calibration effort. This model shows a high error before and after the calibration. The calibration effort improved the thermal cracking prediction accuracy for the thicker pavements. However, the calibration effort was not much

effective for the thin pavements. Figure 50 shows the prediction error of the thermal cracking model versus the pavement age before and after the calibration effort. The thermal cracking model overpredicts the distress at the older age of the pavement life, and by increasing the pavement life, the error increase. But after the calibration, the prediction model improved at older ages and showed higher error at the early age of the pavement.

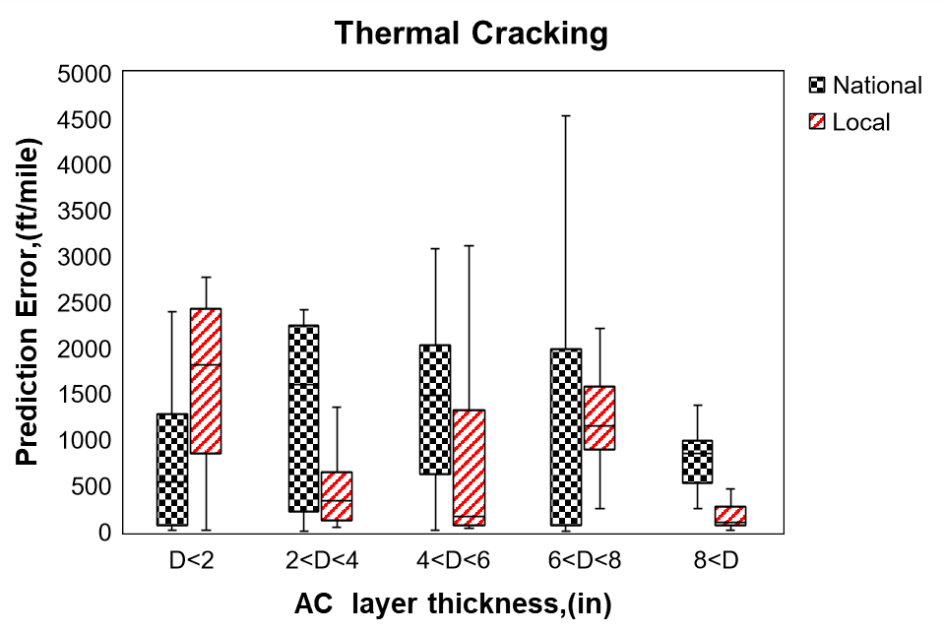

Figure 49 - Error of estimate of thermal cracking model vs. AC layer thickness

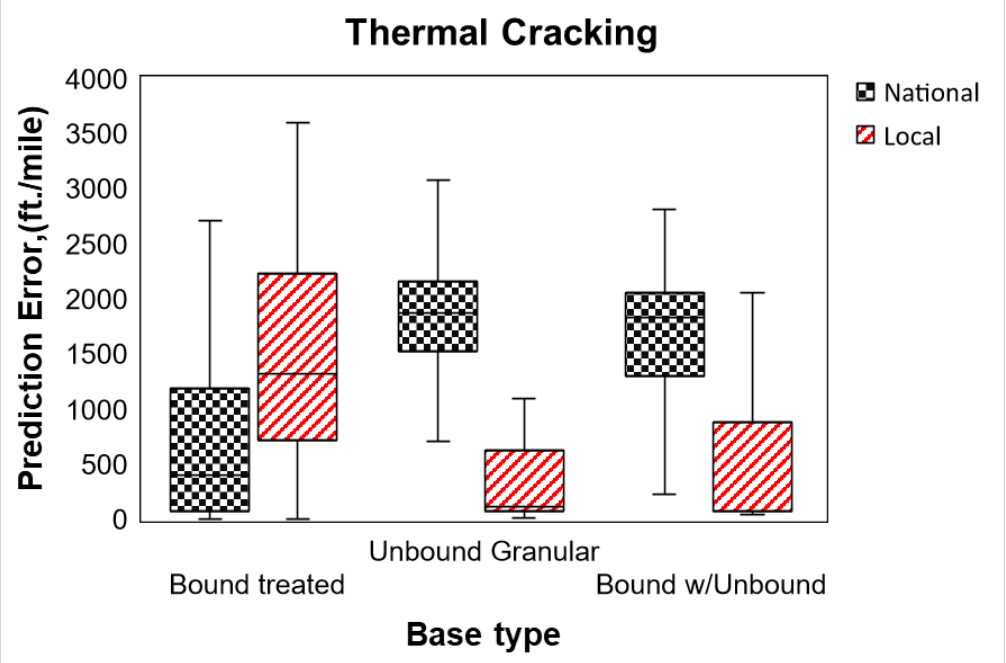

Figure 50- Error of estimate of thermal cracking model vs. pavement age

Figure 51 shows the prediction error for the thermal cracking model vs. the base type in the pavement before and after the calibration effort. The thermal cracking is dependent on the type

of the base. For unbound and granular base, the prediction model shows a lower error; conversely, for the bound treated base, the model shows a high error before and after the calibration. The calibration effort improves the prediction for all types of pavements except the pavements with bound treated bases.

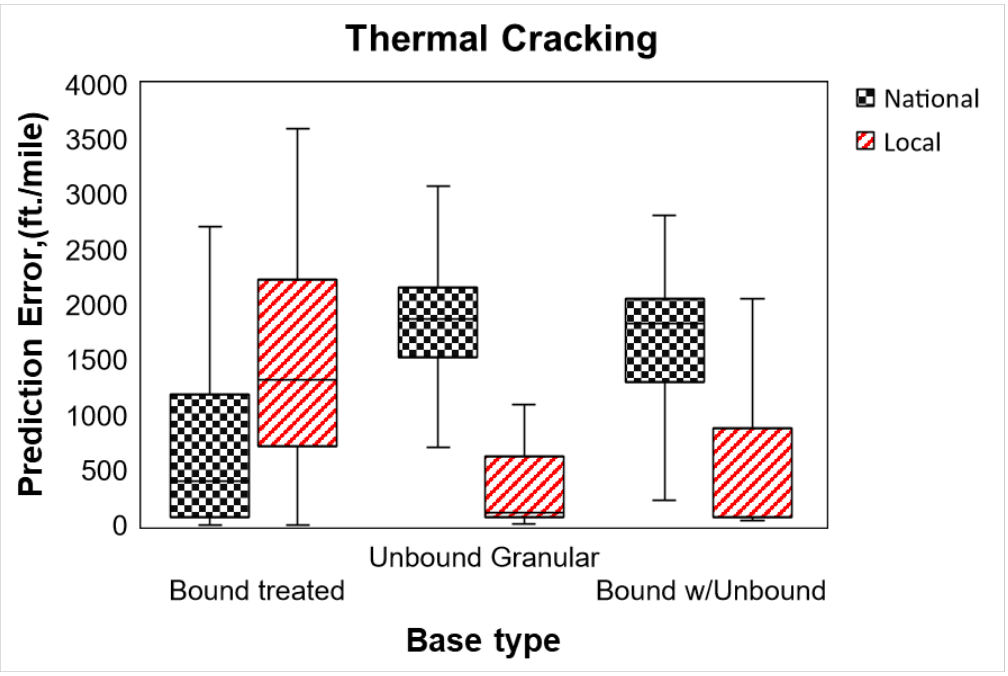

Figure 51 - Error of estimate of thermal cracking model vs. pavement base type

Figure 52 shows the prediction error of the IRI model versus the asphalt concrete thickness of pavement sections before and after the calibration effort. The calibration effort reduced the error of estimate for all the sections; however, the error reduction increases by increasing the AC layer thickness. The IRI model shows higher accuracy for the thick pavements.

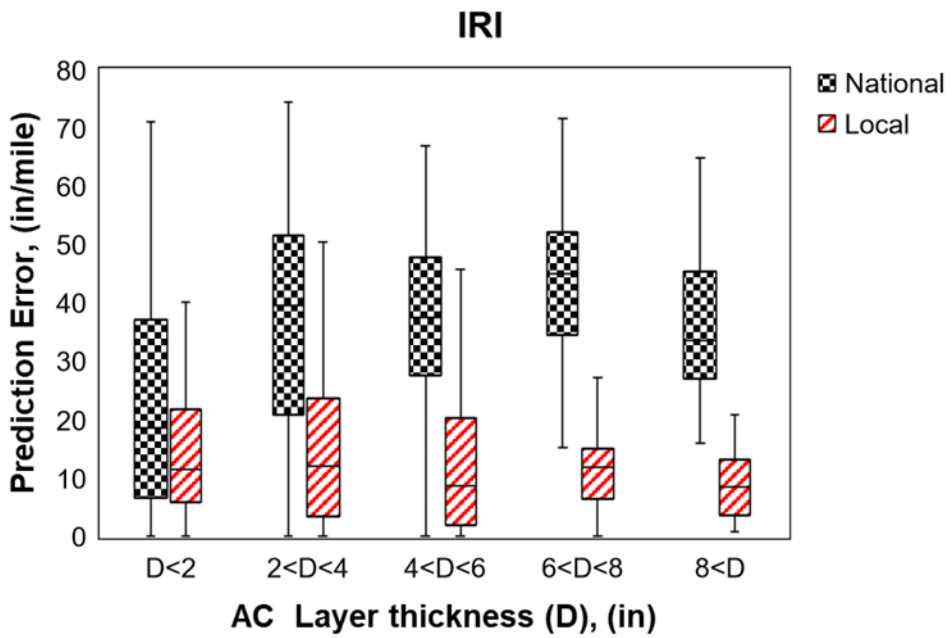

Figure 52- Error of estimate of the IRI model vs. AC layer thickness

Figure 53 shows the prediction error of the IRI model versus the pavement age before and after the calibration effort. Before the calibration, the IRI model error increases for the older pavements. However, after the calibration, the IRI model accuracy improved, and it is almost insensitive to the age of the pavement.

Figure 53 - Error of estimate of the IRI model vs. pavement age

Impact of Local Calibration of Pavement ME on Flexible Pavement Design

After completing the local calibration of the Pavement ME, it is essential to consider taking the next step of the implementation process, which is to adopt the locally calibrated models for some routine pavement designs. For this reason, the Pavement ME was used to design the asphalt pavements using the typical material and design parameters of the state of Oklahoma. Three types of conventional flexible pavement design, as well as one perpetual design, were compared in this study. Figure 54 shows the cross-section of the flexible pavement designs used in this study.

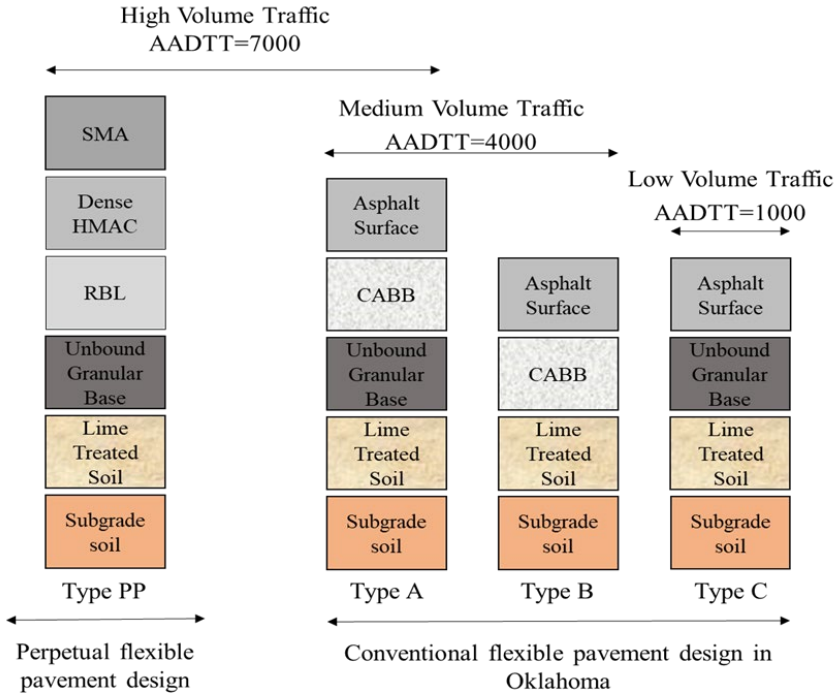

Figure 54- Cross section of flexible pavement design types

Typical material properties of the Oklahoma flexible pavement were selected for calibration impact analysis. Table 28 shows the material properties data used for conventional pavement, and Table 29 shows the material properties data used for perpetual pavement.

Table 28- Material Properties of the Conventional pavement

Layer	Properties
Asphalt Surface	Mix type: S4 Binder type: PG 64-22 Binder content: 5% Air voids: 4.4%
Coarse Aggregate Bituminous base (CABB)	Mix type: S3 Binder type: PG 64-22 Binder content: 6% Air voids: 5%
Unbound Granular Base	Type: Crushed stone Modulus: 21000 (psi)

Layer	Properties
Lime treated Base	Type: A-7-6 soil + 9% lime Modulus: 41000 (psi)
Subgrade soil	Type: A-7-6 Modulus: 13000 (psi)

Table 29- Material Properties of the perpetual pavement

Layer	Properties
Stone Matrix Asphalt (SMA)	Mix type: SMA Binder type: PG 76-22 Binder content: 6 % Air voids: 4%
Dense HMAC	Mix type: Stone-Filled HMAC Binder type: PG 76-22 Binder content: 6% Air voids: 5%
Rich Bottom Layer (RBL)	Mix type: RBL Binder Type: PG 64-22 Binder content: 5% Air voids: 5%
Unbound Granular Base	Type: Crushed stone Modulus: 21000 (psi)
Lime treated Base	Type: A-7-6 soil + 9% lime Modulus: 41000 (psi)
Subgrade soil	Type: A-7-6 Modulus: 13000 (psi)

A reliability level of 90% and AASHTO recommended performance criteria were selected for the design. A minimum life span of 30 years for the conventional and 40 years for the perpetual pavement design types were selected. To illustrate the impact of local calibration on pavement design, local calibration models, and global calibration models were used, and by changing thicknesses and material properties, the appropriate design was determined. Figure 55 shows the design thicknesses for each layer of the conventional flexible pavement designs with local and global calibration coefficients. Using the Oklahoma calibration coefficients results in decreasing the pavement thicknesses, particularly the surface layers.

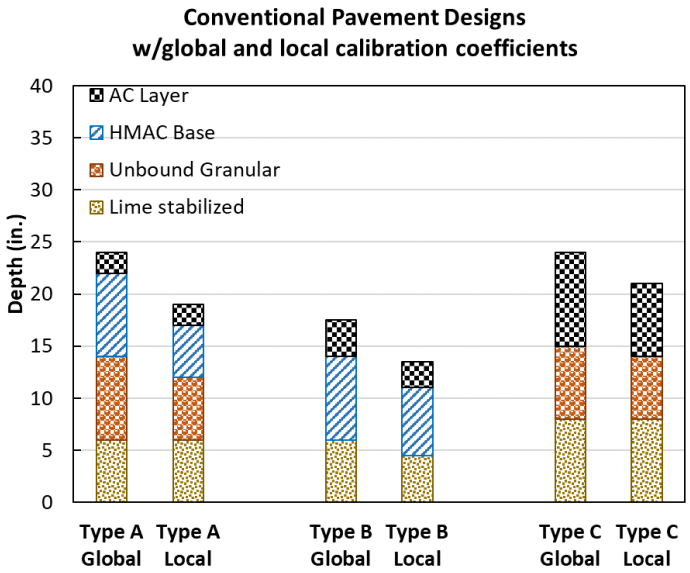

Figure 55- Pavement layer thicknesses for the Oklahoma conventional pavement designs with global and local calibration coefficients

Figure 56 shows the design thicknesses for each layer of the perpetual flexible pavement designs with local and global calibration coefficients. Using the Oklahoma calibration coefficients results in decreasing the pavement thicknesses, particularly the surface layers.

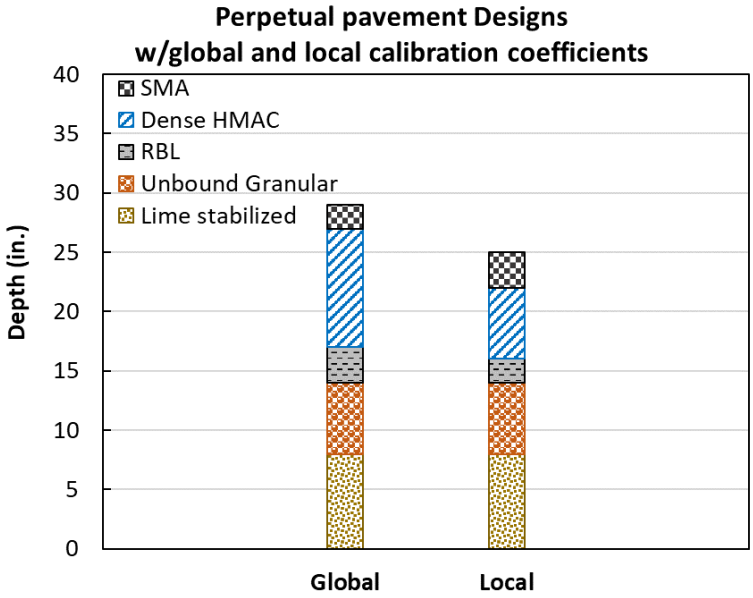

Figure 56- Pavement layer thicknesses for the Oklahoma perpetual pavement designs with global and local calibration coefficients

Generally, using local calibration coefficients leads to the prediction of lower rutting and higher fatigue cracking. However, the pavement roughness at the end of design life is lower by using the Oklahoma calibration coefficients. Figure 57 shows the IRI during the design life for the conventional and perpetual flexible pavement designs.

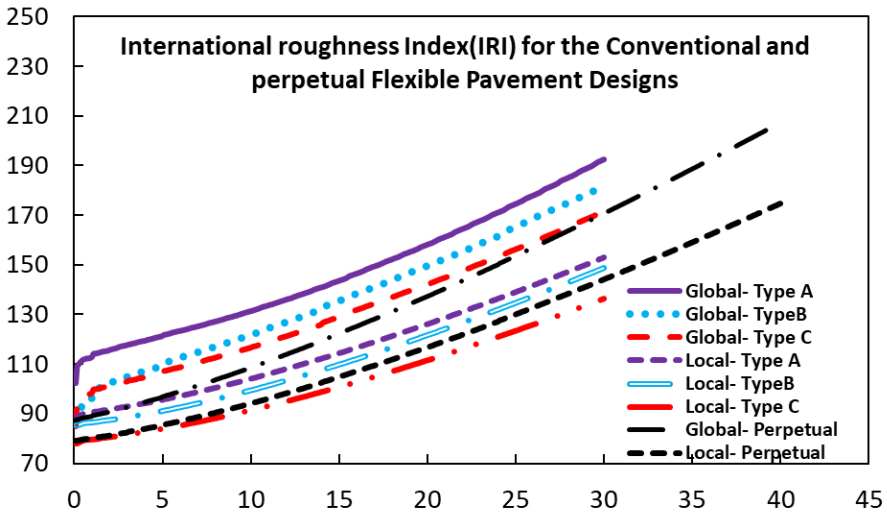

Figure 57- International roughness index for the conventional and perpetual pavement designs

LOCAL CALIBRATION OF RIGID PAVEMENT

This part discusses the updates on the pavement ME calibration for the rigid pavement sections in Oklahoma. The following sections of this part summarize the work that was completed by the Texas A&M Transportation Institute (TTI) between October 1st, 2017 and September 30th, 2018. The main goal of this section is to facilitate the calibration process of the rigid pavement sections in Oklahoma. The rigid pavement calibration process in Oklahoma is limited to the Jointed Plain Concrete Pavement (JPCP) and the Continuously Reinforced Concrete Pavement (CRCP). It is well known that the rigid pavement is a durable pavement type which reduces the number and extent of distresses in the LTPP survey records. Thus, the researchers investigated new ways for developing distress-time relationships that can help to evaluate and estimating the performance of the existing rigid pavements from the LTPP data without relying totally on the existence of visible distresses. This section discusses extensively the following items:

1- Extraction and evaluation of the LTPP data of JPC and CRC rigid pavement sections
2- Development of analysis methodology for falling weight deflectometer (FWD) data to evaluate the performance of the rigid pavement sections and predict the development of distresses
3- Application of the new methodology in analyzing the CRCP rigid pavement sections

Extract and Evaluate LTPP Data

The LTPP database is the most accurate source for information regarding the pavement conditions. It is also the best source for the pavement ME local calibration of rigid pavement. This is because it contains an ongoing project initiated since the 1990s which allow the specific and consistent way in the evaluation of pavement condition in terms of distresses. The LTPP monitors the performance of around 2500 pavement segments in North America (the US and Canada). Each LTPP section is 500 ft long in any direction of the road. Along with distresses records, the LTPP database stores important complementary information about the pavement

section, such as traffic, materials, destructive and non-destructive testing information, as well as pavement structure and maintenance and repair records.

Data Inventory

In this task, for the rigid pavement evaluation and data extraction, the research group has performed data inventory to look up for the number of rigid pavement sections, pavement surface types, pavement location, underneath surface layer types. The data inventory was performed employing the Long Term Pavement Performance- Information Management System User Guide *(48)*.

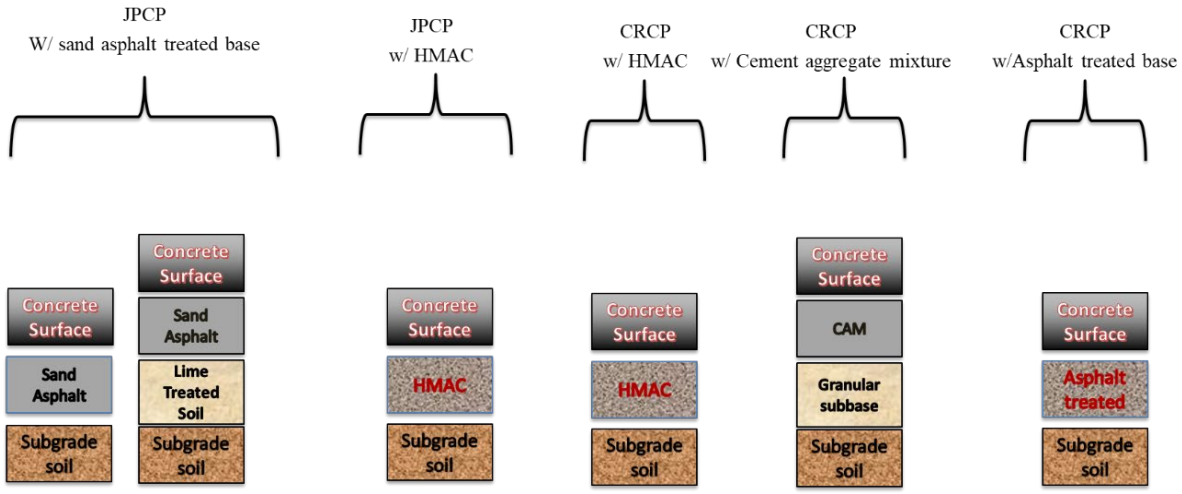

Figure 58- Representative rigid pavements' structures used in Oklahoma calibration effort

Oklahoma has 67 LTPP sections, among which 7 JPCP segments and 3 CRCP segments excluding any sections with an asphalt overlay. Figure 59 shows a representative rigid pavements' structures used in the Oklahoma calibration effort. For pavement ME local calibration, these LTPP sections are considered the backbone of the calibration process. Thus, it is important to gather detailed information about these sections and strive to obtain others. The LTPP JPCP sections were constructed before 1990 and were all non-doweled. Thus, the calibration process should consider taking into consideration current Oklahoma practice in using a doweled JPCP. Table 30 summarizes the JPCP and CRCP sections and their locations in Oklahoma, while Table 31 shows the rigid pavement structure and layer's material type.

Table 30- Oklahoma rigid pavement sections and locations

Sections	County	Route/ Direction	Pavement Type	Climatic Zone	GPS long. /lat	Construction Date	LTPP start date
40-3018	OKLAHOMA	Interstate-240 , WB	JPCP	Wet, Non-Freeze	35.39148 , -97.45124	01-Jun-1976	01-Jan-1987
40-4157	MAYES	U. S.-69 , NB	JPCP	Wet, Non-Freeze	36.07647 , -95.36436	01-Mar-1986	01-Jan-1987
40-4160	PONTOTOC	State-3 , WB	JPCP	Wet, Non-Freeze	34.75407,-96.68412	01-Jun-1979	01-Jan-1987
40-4162	COMANCHE	U. S.-62 , EB	JPCP	Wet, Non-Freeze	34.63091 , -98.48158	01-Jun-1985	01-Jan-1987

Sections	County	Route/ Direction	Pavement Type	Climatic Zone	GPS long. /lat	Construction Date	LTPP start date
40-A410	PONTOTOC	State-3 , WB	JPCP	Wet, Non-Freeze	34.75246 , -96.67735	01-Jun-1979	01-Jan-1987
40-A420	PONTOTOC	State-3 , WB	JPCP	Wet, Non-Freeze	34.75258 , -96.67919	1-Jun-1979	1-Jan-1987
40-A430	PONTOTOC	State-3 , WB	JPCP	Wet, Non-Freeze	34.75628 , -96.68823	1-Jun-1979	1-Jan-1987
40-4158	WASHINGTON	U. S.-75 , SB	CRCP	Wet, Non-Freeze	36.6185 , -95.9357	01-Jun-1989	31-May-1989
40-4166	PITTSBURG	U. S.-69 , NB	CRCP	Wet, Non-Freeze	35.03894 ,-95.71174	1-May-90	30-Apr-90
40-5021	MAYES	State-33 , WB	CRCP	Wet, Non-Freeze	36.17016, -95.38403	01-Oct-1987	30-Sep-1987

Table 31- Structure of Oklahoma's rigid pavement sections

Section No.	Pavement Type	Pavement Thickness	Base Layer	Base Thickness	Subgrade/ Subbase Layer	Subgrade Thick	LTPP Status
40-3018	JPCP	8.9	TB	3.6	B	6.1	Inactive
40-4157	JPCP	8.9	TB	3.8	U	41	Active
40-4160	JPCP	9.2	TB	2.2	UG	12	Inactive
40-4162	JPCP	9	TB	2.9	U	NA	Inactive
40-A410	JPCP	9.2	TB	2.2	UG	12	Inactive
40-A420	JPCP	9.2	TB	3.2	UG	12	Inactive
40-A430	JPCP	9.2	TB	4.2	UG	13	Inactive
40-4158	CRCP	10.3	TB	4.4	U	NA	Active
40-4166	CRCP	9.9	TB	4.1	UG	10.3	Active
40-5021	CRCP	9.4	TB	3.5	U	NA	Active

Note:
TB : treated base
B : Bound (treated) subbase or subgrade layer
U : Unbound subbase or subgrade layer
UG : Unbound granular subbase or subbase layer

In the above tables, 4 of the JPCP sections are General Pavement Studies (GPS), and 3 JPCP sections are Specific Pavement Studies (SPS). The difference between the GPS and SPS is that the GPS inspects the in-service pavement sections while the SPS inspects specific variables such as new construction, maintenance treatments, and rehabilitation activities. As the SPS section aged and a new rehabilitation was applied, the SPS can be reclassified as GPS. The LTPP does not keep frequent records for the SPS sections in terms of traffic, distresses, and testing data. Therefore, only the GPS sections were considered for further analysis.

Pavement ME Calibration-Key Data

Pavement ME calibration requires obtaining different information. Along with pavement structure and properties, the availability of the following data was checked before planning for calibration:

1. Traffic data
2. Falling weight deflectometer (FWD) data
3. Distress data

Traffic Data

The traffic data in the LTPP database is provided by the agency that supplies the traffic estimates or by the computation of raw traffic information. This information is specific for each test section. There are two groups of traffic data that are historical or monitored. The historical data refers to the traffic estimates of volume and loading for the time before the start of the LTPP (LTPP records started in 1990). Monitored traffic data refers to the annual traffic estimates provided by participating highway agencies or computed from raw data by the agency after 1990. In order to collect the most accurate traffic information, the research team concentrated on the monitored traffic data as the main source of the existing traffic condition. For traffic data of any section, availability of the following components is crucial: I) annual volumes of trucks and axles, II) truck and axle distribution, and III) annual estimate of the number of 80 kips equivalent of single axle load (ESAL).

Figure 59 below shows the number of sections with complete traffic records. It shows that traffic data is available in 7 sections out of 10. These sections are 40-3018, 40-4157, 40-4160, 40-4162 for JPCP and 40-4158, 40-4166 and 40-5021 for CRCP. All these sections are GPS, while SPS (i.e., 40-A410, 40-A420, and 40-A430) sections were not considered due to the unavailability of one or more traffic information. Figure 60 shows the Annual Average Daily Truck Traffic (AADTT) for all sections with the year. To group the traffic level based on the presented AADTT numbers, AADTT fewer than 750 is categorized as low traffic volume; between 750 and 1,200 are categorized as medium traffic volume, and AADTT higher than 1,200 are categorized as high traffic volume.

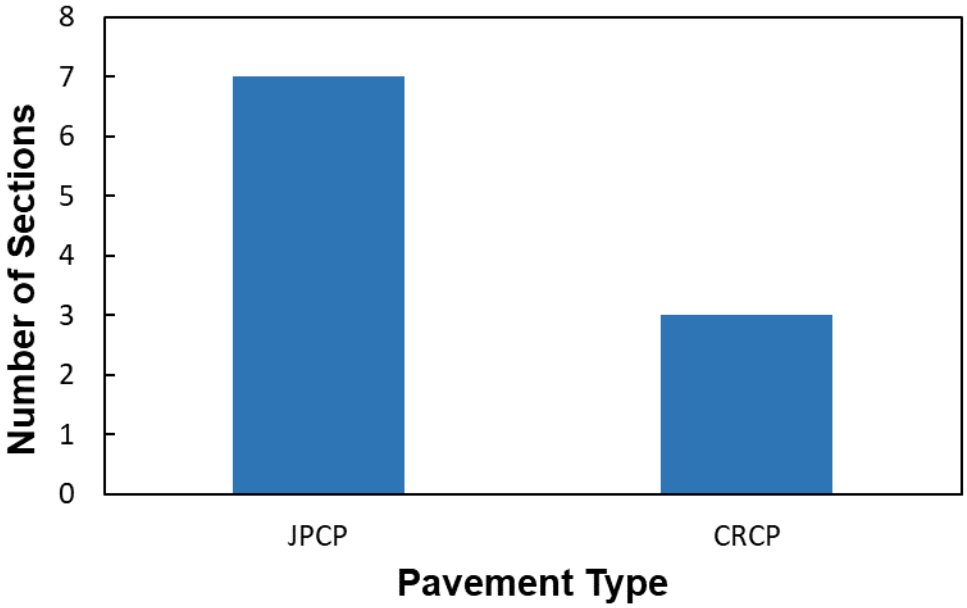

Figure 59- Traffic data availability

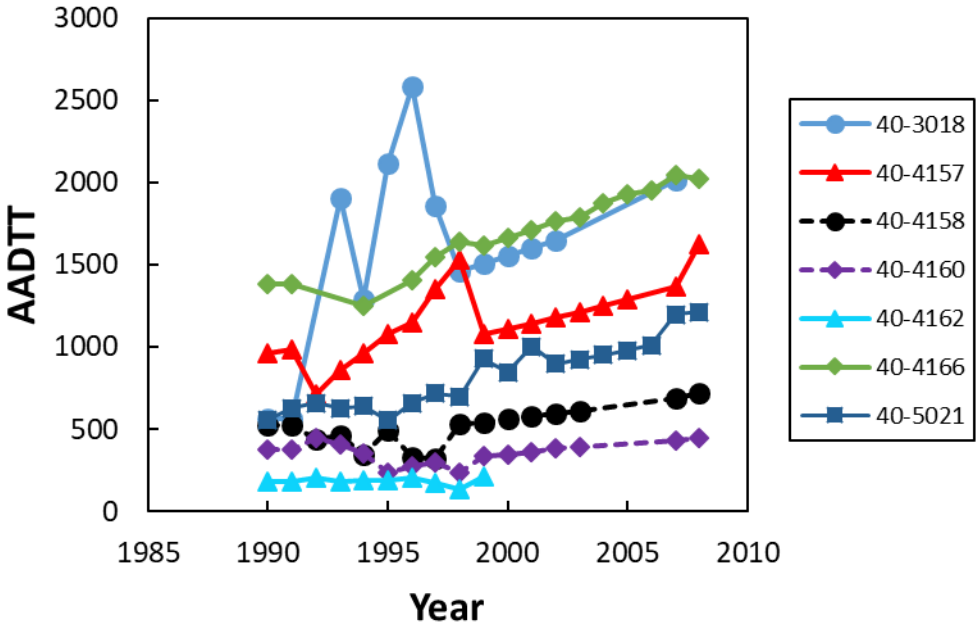

Figure 60 - The annual average daily truck traffic with years- all section

FWD Data

The PCC elastic modulus and k-value of the supporting subbase are important inputs for the pavement ME. Prior to start calibration, FWD data are used to back-calculate this parameter in order to evaluate the rigid pavement structure. In the FWD analysis, the structural condition of the PCC slab can be evaluated using the PCC elastic modulus, while the supporting layers can be evaluated using the K-value. The LTPP FWD data were also used to evaluate the load transfer efficiency (LTE), the degree of bonding and friction coefficient, and ultimately estimate the percent of erosion for faulting and punchout calibration. Thus, it is important to extract or obtain these non-destructive data for each rigid pavement section.Figure 61 below shows the availability of the FWD data for the LTPP sections. As shown in the figure, the FWD data are available for all for Oklahoma rigid pavement sections. The SPS sections were not considered for FWD data extraction because complete traffic records were not acquired for any of them.

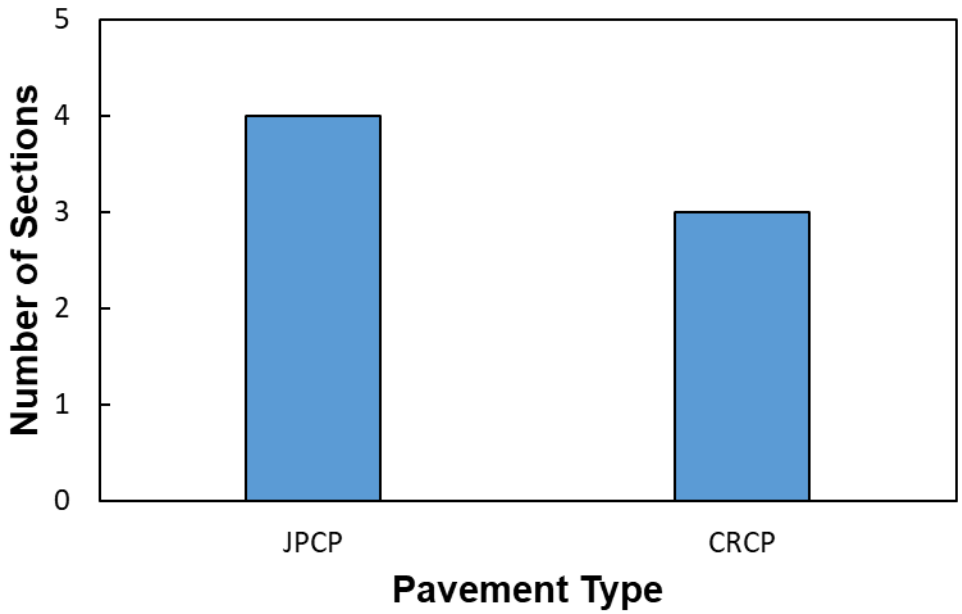

Figure 61- FWD Data Availability

Distress Data

The mechanistic-empirical procedure in pavement ME design uses engineering mechanics to calculate pavement mechanical responses such as stress, strain, and deflection along with the transfer functions of the empirical distress for pavement performance predictions. In pavement ME, the transfer functions used to predict the pavement performance are nationally calibrated using sections and distress data from the LTPP for different national locations. For local calibration, further calibration and validation of coefficients in the transfer function are encouraged by the NCHRP project 1-37 A as an essential step to implement a new design procedure that employs mechanical and environmental impacts.

In Oklahoma State, rigid pavement sections are represented by the 7 JPCP and 3 CRCP sections. In order to perform and validate the calibration of these sections, the availability of the main distress data from the LTPP for JPCP and CRCP is required. This distress is:

- Transverse cracking in the jointed plain concrete pavement (JPCP)
- Faulting in JPCP
- Punch-outs in the continuously reinforced concrete pavement (CRCP)

For transverse cracking in JPCP, Figure 62 shows that no JPCP sections are showing any transverse cracking records over the LTPP survey years. Thus, it is important to look for other sections that can be used to calibrate the transverse cracking for JPCP. Sections can be found in neighbor states, as will be discussed later. Figure 63 and Figure 64 show the average faulting of JPCP sections in Oklahoma. The average faulting is considerable and can be used for faulting calibration, especially in sections 40-3018 and 40-4160, where the faulting is increasing with time and reaches 5 mm (0.2 inches) level. Sections 40-4157 and 40-4162 can also be used considering any maintenance activities or/and section's inactive status. Figure 65 shows the number of punchouts in all three CRCP sections. As shown in the figure, the only CRCP section that shows the punchouts record is 40-4166, and it is the only one that can be used for calibration of punchouts. However, the erosion damage can be assessed for other CRCP

Oklahoma sections through FWD data analysis as well as the pavement ME analysis results. This step can be significant to determine and predict the starting point of punchouts in these sections. For punchout calibration, existing punchouts are required in the section under study. Therefore, other sections from other states can also be used to validate calibration for punchouts in Oklahoma's CRCP sections.

Table 32 shows the summary of all distresses recorded in all Oklahoma sections.

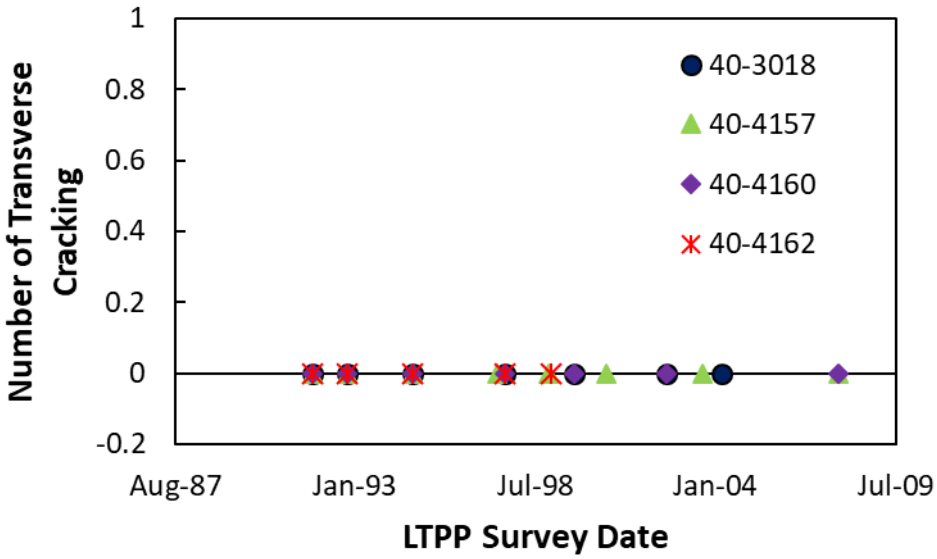

Figure 62- Number of transverse cracking in JPCP sections with LTPP survey date- Oklahoma

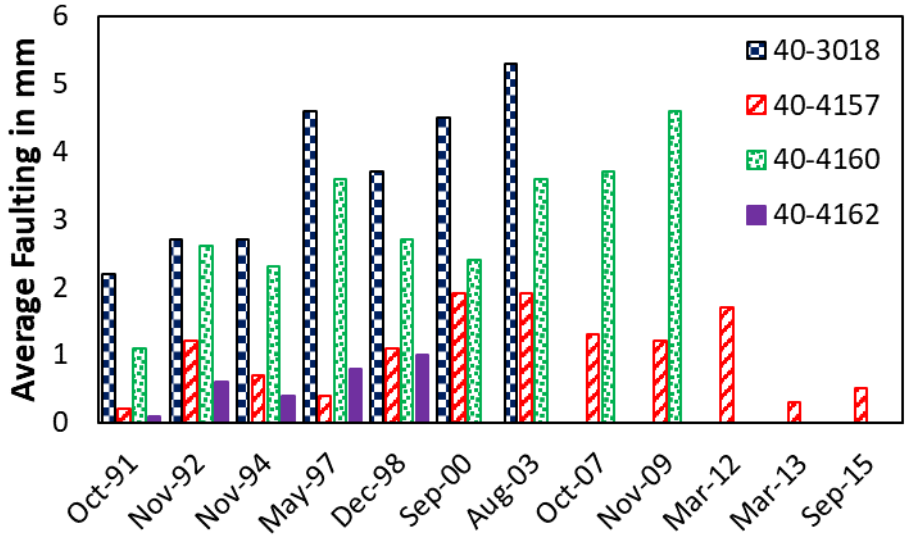

Figure 63- Average faulting at the edge in JPCP sections with LTPP survey date- Oklahoma

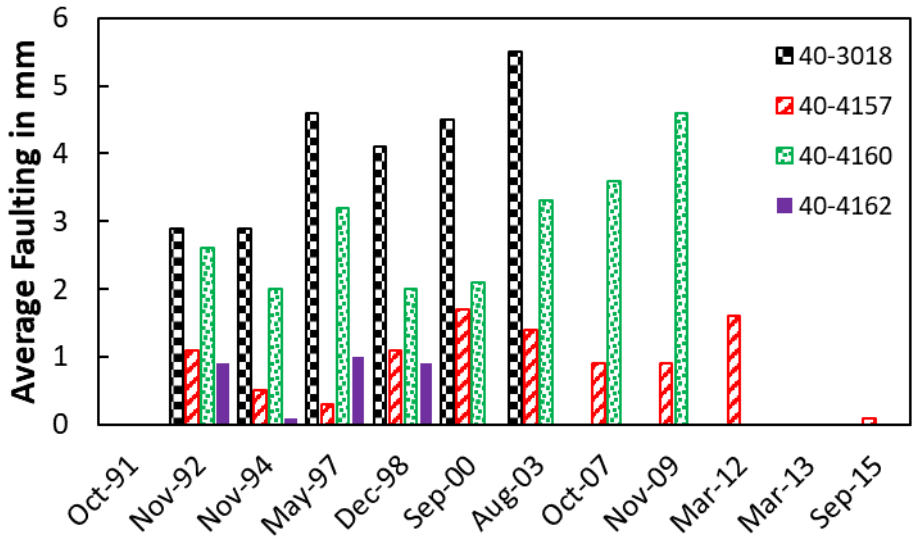

Figure 64 Average faulting at wheel path in JPCP sections with LTPP survey date- Oklahoma

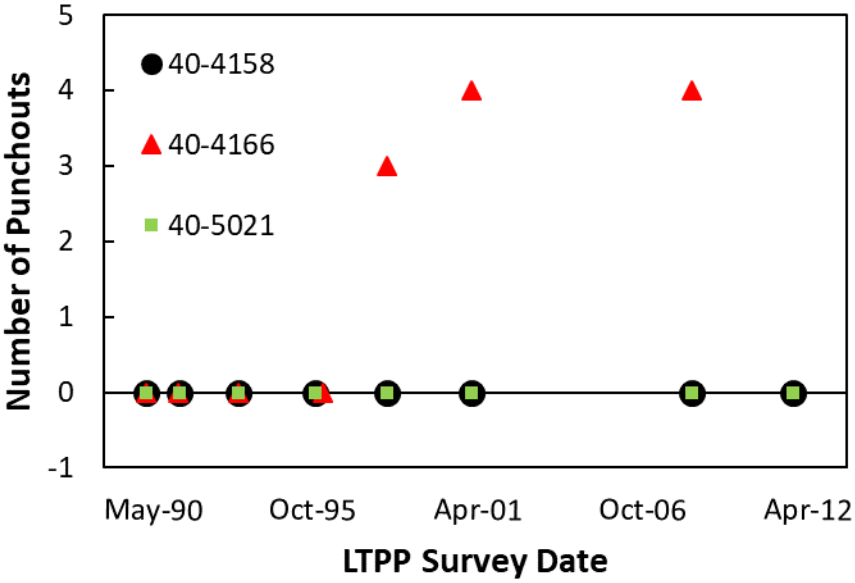

Figure 65- Number of Punchouts in CRCP sections- Oklahoma

Table 32- Summary of Oklahoma's rigid pavement performance

Sections	Pavement Type	Max. Faulting (year)	Max. Transverse cracking (year)	Max. Punchouts (year)	Latest distress records	LTPP status
40-3018	JPCP	5.5 mm (2004)	1 cracking (2001)	-	2004	Inactive
40-4157	JPCP	1.7 mm (2000)	0 (all years)	-	2015	Active
40-4160	JPCP	4.6 mm (2013)	0 (all years)	-	2013	Inactive

Sections	Pavement Type	Max. Faulting (year)	Max. Transverse cracking (year)	Max. Punchouts (year)	Latest distress records	LTPP status
40-4162	JPCP	1mm (1997)	0 (all years)	-	1999	Inactive
40-A410	JPCP	4mm (1997)	0 (all years)	-	2002	Inactive
40-A420	JPCP	3.1mm (1992)	0 (all years)	-	2002	Inactive
40-A430	JPCP	4 mm (1997)	1 (1991)	-	2002	Inactive
40-4158	CRCP	-	-	0 (all years)	2015	Active
40-4166	CRCP	-	-	4 (2002&2009)	2015	Active
40-5021	CRCP	-	-	0 (all years)	2015	Active

As shown in the previous table, maximum distress values correspond to the year where the distress was recorded. This means that the distress at the latest distress survey date might be lower than the maximum distress value due to the application of maintenance and repair. CRCP sections are in good condition, and this limits their use in CRCP calibration. Among the three CRCP sections, only Section 40-4166 can be used as it showed several punchouts as of 2009. On the other side, most JPCP sections have no transverse cracking, as shown in Figure 62. However, they can be used for calibration of faulting as they show a considerable amount of faulting. The main issue is the inactivity of most of the sections where some of them are inactive since 1999 and 2002.

Based on the previous table and figures, the research team had the following options to allocate distress data that can be used for calibration:

1. Perform distress survey and FWD testing on all inactive JPCP LTPP sections. This option includes only the three GPS sections, which are 40-3018, 40-4157, 40-4160, and 40-4162. The SPS sections do not have enough traffic information such as truck and axle distribution. For CRCP, sections from other states can be used for calibration

2. Locate and use concrete pavement sections in neighbor states such as Texas, Arkansas, and Kansas that meet the climatic and material conditions of Oklahoma.

3. Use distress records from Oklahoma PMS with performing FWD testing on selected sections. This option can have the following limitation:

    - The Oklahoma pavement survey protocol is not consistent with the protocol used by the LTPP. PMS data are collected every two years by an external contractor where the automatic survey vehicles that incorporate the Oklahoma pavement survey protocol.

    - The ODOT PMS, unlike LTPP, does not store supplementary section information such as traffic, pavement structure, and material testing.

    - Section locations in the PMS do not totally match with section locations in the LTPP. Thus, important information that can be found in the LTPP will not be used in the calibration and also will not be found in the Oklahoma DOT PMS.

Neighbor States- JPCP and CRCP Sections

After discussion with Oklahoma officials, the second option, which is locating other sections from neighbor states, was the best option for rigid pavement calibration. The main goal of this task was to locate JPCP and CRCP section candidates that can be incorporated in the calibration of rigid pavement in Oklahoma. To choose acceptable sections, the following factors were considered:

1. Sections should be located in the same climatic zone as Oklahoma, which is Wet, Non-Freeze.

2. JPCP and CRCP sections should have distress records for JPCP (transverse cracking and faulting) and CRCP (punchouts)

Additional factors such as using the same aggregate type in the concrete mix (which is usually crushed stone in states other than Texas) and availability of FWD data and traffic records.

Table 33 presents the potential list of JPCP, and CRCP sections existed in neighbor states. The considered states were Texas, Arkansas, and Kansas. As seen in the table, the JPCP sections were found in Arkansas, which has a state code of 05, while CRCP sections were located in Texas, which has a state code of 48. No sections in Kansas were selected due to not meeting one or more searching criteria. Although this list contains LTPP inactive or recently active sections, they have considerable distress records and can be beneficial invalidating the calibration of Oklahoma sections.

Table 33- List of JPCP and CRCP sections

Sections	County	Route/ Direction	Pavement Type	Climatic Zone	Construction Date	LTPP start date	LTPP status
05-0213	SALINE	Interstate-30, WB	JPCP	Wet, Non-Freeze	01-Oct-95	01-Sep-93	Inactive(11/15/2008)
05-0217	SALINE	Interstate-30, WB	JPCP	Wet, Non-Freeze	01-Oct-95	01-Sep-93	Inactive(08/20/2013)
05-0218	SALINE	Interstate-30, WB	JPCP	Wet, Non-Freeze	01-Oct-95	01-Sep-93	Inactive(08/20/2013)
05-0221	SALINE	Interstate-30, WB	JPCP	Wet, Non-Freeze	01-Oct-95	01-Sep-93	Inactive(08/20/2013)
48-3596	HOPKINS	Interstate-30 , WB	CRCP	Wet, Non-Freeze	01-Jun-1960	01-Jan-87	Inactive(06/01/2017)
48-5323	CARSON	Interstate-40, EB	CRCP	Wet, Non-Freeze	01-Sep-80	01-Jan-87	Inactive(09/16/2002)
48-5334	WHEELER	Interstate-40, EB	CRCP	Wet, Non-Freeze	01-Apr-70	1-Jan-87	Inactive(02/15/2001)

The main factor of selected JPCP sections is the existence of transverse cracking for calibration. Therefore, Figure 66, through Figure 69, shows the transverse cracking records for the out-state sections in relation to the LTPP survey date. For the faulting calibration, the records of Oklahoma sections can be used in calibration as they show good faulting records. In the CRCP sections, the main factor is the existence of punchouts, and this can be shown in Figure 70 through Figure 72.

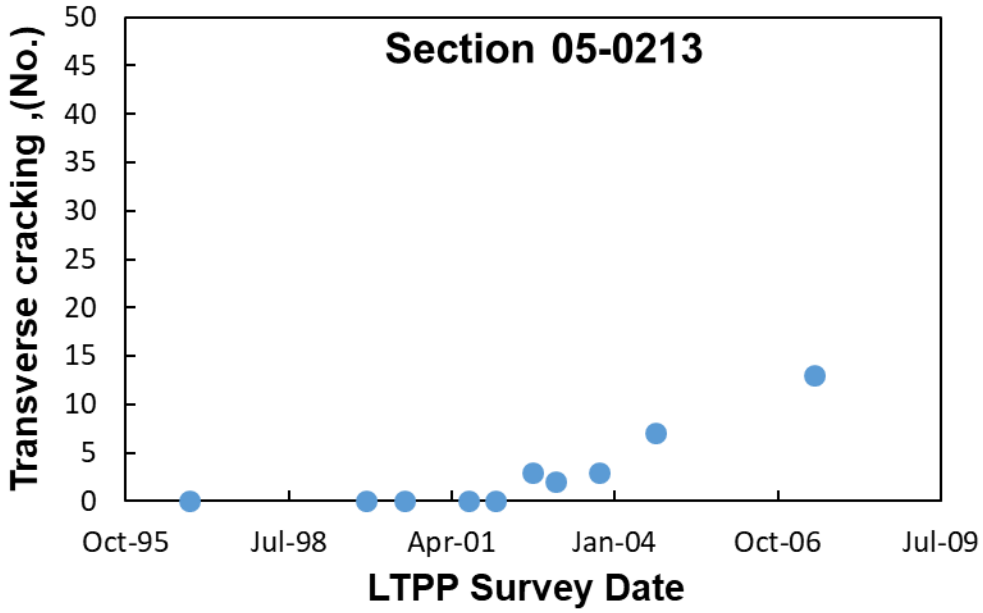

Figure 66- Number of transverse cracking with LTPP survey date for section 05-0213

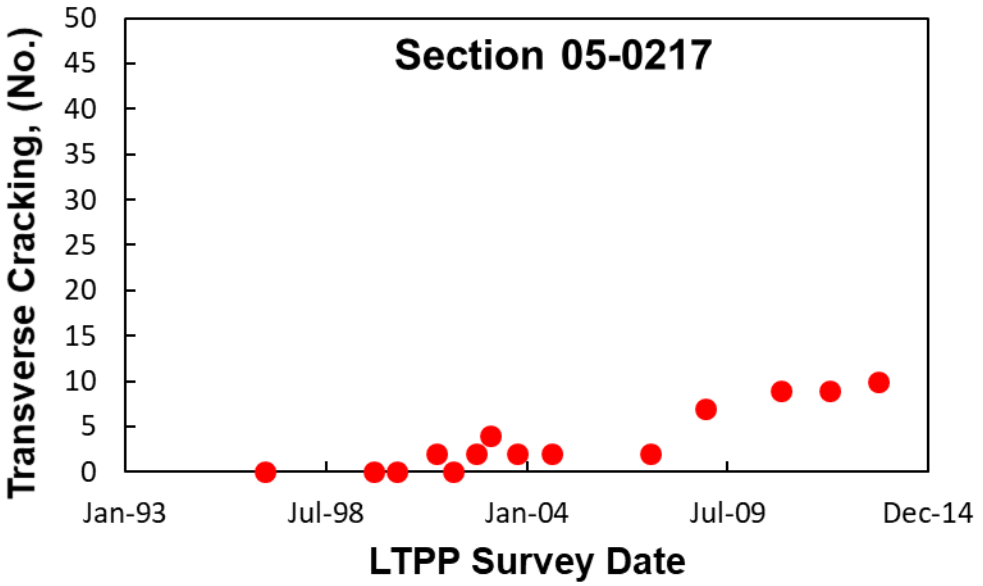

Figure 67- Number of transverse cracking with LTPP survey date for section 05-0217

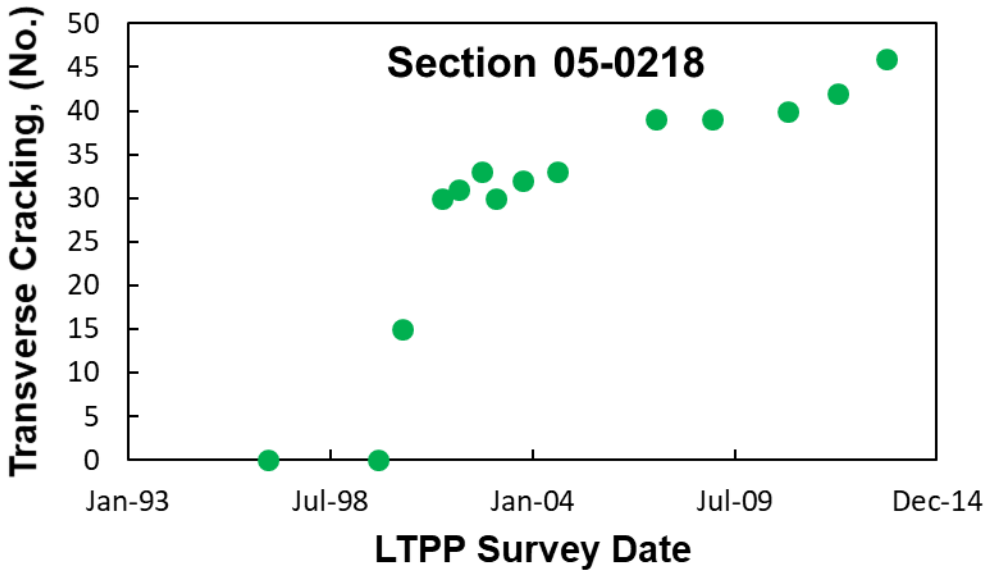

Figure 68- Number of transverse cracking with LTPP survey date for section 05-0218

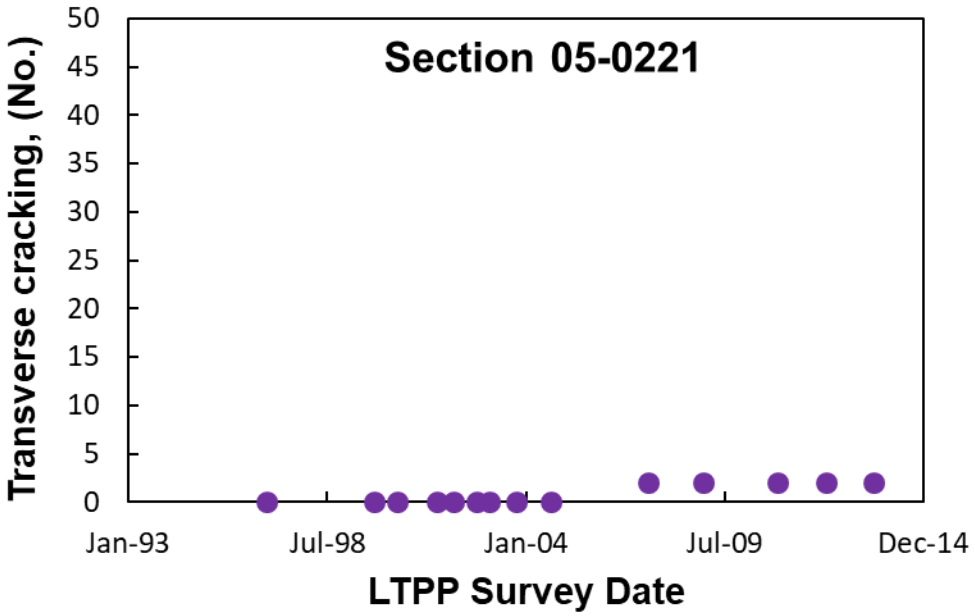

Figure 69- Number of transverse cracking with LTPP survey date for section 05-0221

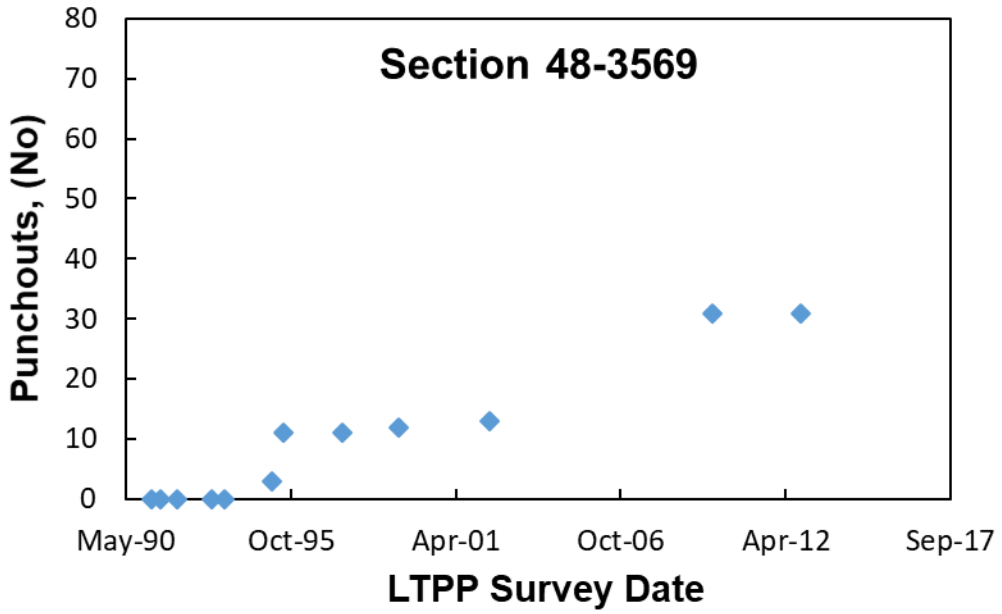

Figure 70- Number of Punchouts with LTPP survey date for section 48-3569

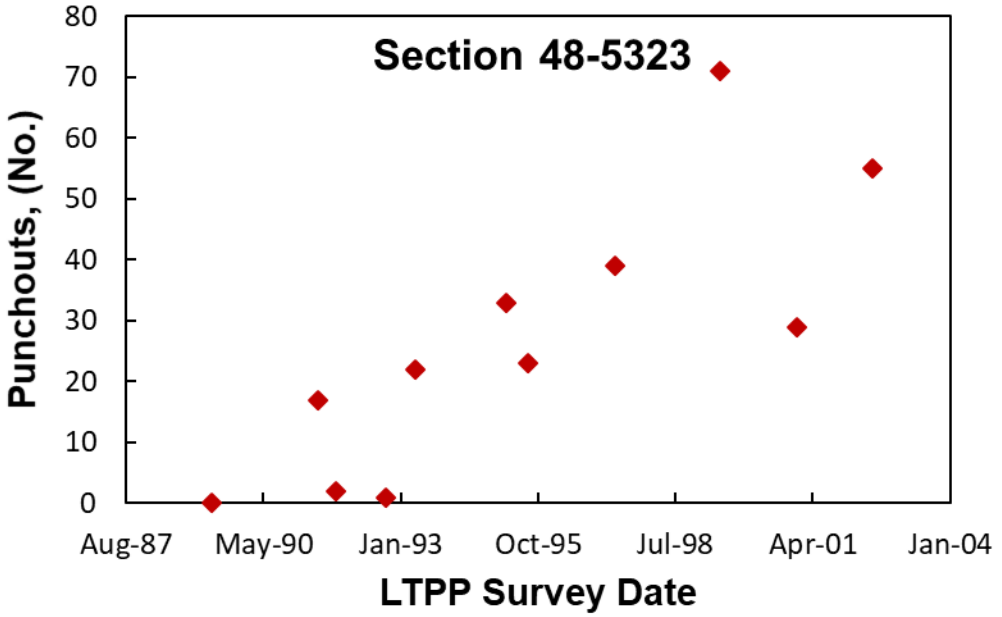

Figure 71- Number of Punchouts with LTPP Survey Date for Section 48-5323

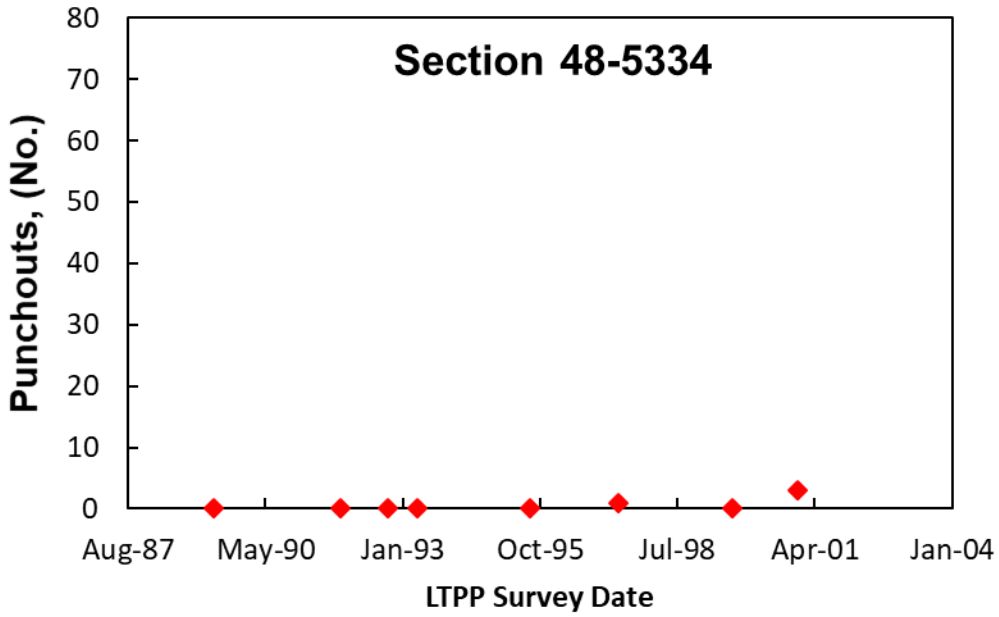

Figure 72- Number of Punchouts with LTPP Survey Date for Section 48-5334

LTPP Section Analysis

FWD Analysis Background

The deflection basin data from falling weight deflectometer (FWD) in concrete pavement focuses on the determination of the elastic layer properties as well as joint behavior in terms of slab deflection and load transfer efficiency (LTE). The Long-Term Pavement Performance (LTPP) program performs this deflection-testing program periodically on all General Pavement Study (GPS) and Specific Pavement Study (SPS) to obtain the load-related characteristics of pavement and underneath layers (i.e., base and subbase or subgrade). FWD testing is usually performed by the LTTP program every 2 years for the SPS projects and every 5 years for the GPS sites.

One of the most common methods for analyzing the deflection data is done by back-calculation of the elastic properties of each layer in the pavement structure. The back-calculation programs provide the elastic properties for the pavement to be used for pavement evaluation and rehabilitation. Interpretation of the deflection basin is made through the static-linear analysis, and there are many computer programs that can help in the calculation of the elastic modulus values or Young's modulus.

Back-Calculation Methods

The existing back-calculation methods can be categorized into i) Static Load Application with Linear (Material Characterization) Methods, ii) Static Load Application with Nonlinear (Material Characterization) Methods iii) Dynamic Load Application with Linear (Material Characterization) Methods, iv) Dynamic Load Application with Nonlinear (Material Characterization) Methods.

Through all four back-calculation methods, the main concept is to estimate the material response of each layer in the pavement structure using the FWD basin (deflection) measurement. The limitations of the back-calculation programs are represented by the

limitation on the thickness and number of layers in the pavement structure as well as the assumption of linear elasticity of the layers while the unbound materials and soil layers are nonlinear. However, the calculation of layer-modulus or effective Young's modulus is considered accurate because it can be adjusted for stress sensitivity, discontinuities such as variations in layer's thickness and cracking.

LTPP FWD Load Application and Material Response

ASTM D5858 suggests a procedure for analyzing deflection basin test results to determine layer elastic moduli (i.e., Young's modulus). This procedure is based on the static load application. On the other hand, there is no standardized procedure for material properties calculations using dynamic analysis, and also there are limited programs that can perform dynamic analysis of pavement structures. Thus, programs that use dynamic analyses were not considered in the back-calculation of elastic modulus. Only the static load application analysis was performed for use in a production mode where back-calculation of elastic layer modulus is required for mass deflection basins obtained from LTPP test sections.

In the material response model, the LTPP, as most of the back-calculation methods, adopted the elastic layer theory for back-calculation. Other methods using elastic theory were introduced to account for viscoelastic (time-dependent) and elastoplastic (inelastic) behaviors. However, these programs have not been used in mass back-calculation and have not been able to produce consistent and reliable solutions (*49, 50*). Studies by SHRP and others were performed for available back-calculation procedures to select a reliable method for prediction of flexible and rigid pavement performance (*7, 24*) Based on these studies, the program entitled "MODULUS 4.0" was used for flexible and composite pavements, whereas a new procedure was developed for rigid pavements as part of the SHRP P-020 Data Analysis Project (*49, 50*). The main limitations of these programs can be summarized by the following: i) Number of layers and thickness of layers in the pavement structure. ii) The materials are considered linear-elastic. Thus, as mentioned above, the calculated layer modulus is considered an "effective" or "equivalent" elastic modulus that accounts for differences in stress states and any discontinuities or anomalies (such as variations in layer thickness, slippage between two adjacent layers, cracks, and the combinations of similar materials into a single layer).

FWD Back-Calculation Method and Consideration

In this project, additional effort is added to estimate the effectiveness of the rigid pavement section through the study of the bond between the pavement structure layers. In addition to elastic parameters such as thickness and modulus, this effort will allow the researchers to identify the percent of erosion in Jointed Plain Concrete Pavement (JPCP) and Continuously Reinforced Concrete Pavement (CRCP) and use this erosion percentage in calibration for faulting in the JPCP and for punchout in the CRCP sections.

The bond between a concrete slab and its substrate has been a key component in the stiffness and longevity that a slab displays when subjected to passing loads. Bond has long been thought to be separate from sliding friction in that it mainly resists tensile forces. However, upon careful reflection, it's clear that bond also has shear as well as sliding friction components. Interfacial bond for certain base types such as those made from asphalt concrete can actually serve to maintain contact between a slab and a base as long as the tendencies for the slab to curl and warp are not too great. Maintenance of the slab/base interfacial contact helps to preserve the adhesive nature of the bond, which affords the interface the capability to resist both the tensile and shear forces that result from loads applied to a pavement structure.

Furthermore, the interfacial bond is comprised of both chemical and mechanical components, adhesion being the chemical and sliding friction being the mechanical portion. The degree of either one or both acting on the interface determines the extent a slab will be either bonded, unbonded, or partially bonded.

It is important to model bonds in design since it has a significant effect on performance as the number of bonds affects how thick the slab effectively is. In other words, a slab bonded to an HMA layer is effectively thicker than a slab that is unbonded to the same layer. However, the Pavement ME program presently only represents the extremes of the effective-thickness spectrum as either bonded or unbonded thicknesses; experience with Pavement ME software calibration has reinforced that most slabs are likely partially bonded especially along slab edges and corners where most of the change in bond occurs during the lifetime of a concrete slab. The cause of the variation in bond in these areas is principally from two effects:

1. Differential slip between the slab and the base layer due to loading, and
2. Vertical separation of the slab from the base layer due to climatic effects.

Vertical separation essentially eliminates the chemical composition from the interfacial resistance. However, the friction component is still in play whenever the bottom of the slab comes in contact (due to climatic or external loading) with the surface of the base layer. Nonetheless, the probability that the chemical composition will be diminished but can be expressed in terms of the degree of the bond (xb) as:

$$Xb = \frac{h_p - h_u}{h_b - h_u} \tag{52}$$

Where
hb = bonded slab thickness
h_u = unbonded slab thickness
h_p = partially bonded slab thickness

As discussed further below, the quantities of h_b and h_u are calculated values and hp measured. In order to characterize or model the full range of bond (f_e) strength, including partially bonded conditions, it will be important to address chemical and mechanical components as:

$$f_e = (x_b)[f_b] = \cos^2\phi\,(f_\tau + f_F) = \cos^2\phi\,(f_\tau + \sigma_v \tan\phi) \tag{53}$$

Where

f_e= effective interfacial frictional resistance or bond strength =$\sigma_v \mu_e$
f_τ= adhesive bond
f_F = mechanical or frictional bond
σ_v= normal loaded pressure
ϕ= friction angle

Assessment of Interfacial Bond Strength
When a load is placed on a rigid pavement – particularly near a joint or crack, the slabs on either side of the joint will deflect in the form of a basin. The deflected shape of the basin is a function of several variables, including the thickness and stiffness of the slab, the stiffness of

the underlying materials (which is indirectly affected by the interlayer bond or frictional resistance), and the magnitude of the load. Other factors that affect the shape of the basin area are the thickness and types of subbase materials, nature of load transfer devices, the texture of the aggregate interlock, and the magnitude of joint openings. Basin area gives an indication of the deflection profiles measured using FWD and may be calculated from sensor deflections as:

$$BA = \frac{SS}{2 \times D_1}[D_1 + 2(D_1 + D_2 + ... + D_{j-1}) + D_j] \quad (54)$$

Where
Area = basin area, inches
Di = measured sensor deflection
n = number of the sensor (at 0.3m (12 in) spacing) on one side of the load plate

This area concept combines all measured deflections in the basin into a single parameter. The area is determined is essentially ½ of the cross-sectional area of the deflection basin taken through the center of the load. Each deflection reading is normalized with respect to the maximum deflection D_o. Thus, the basin area has the units of length and is a function of the number and location of the sensors. For any given sensor arrangement, a relationship between the basin area and the radius of relative stiffness (ℓ) exists in concept as illustrated in Figure 73.
Figure 73 forms the basis of the representation of different load transfer conditions and stiffness conditions in an existing slab.

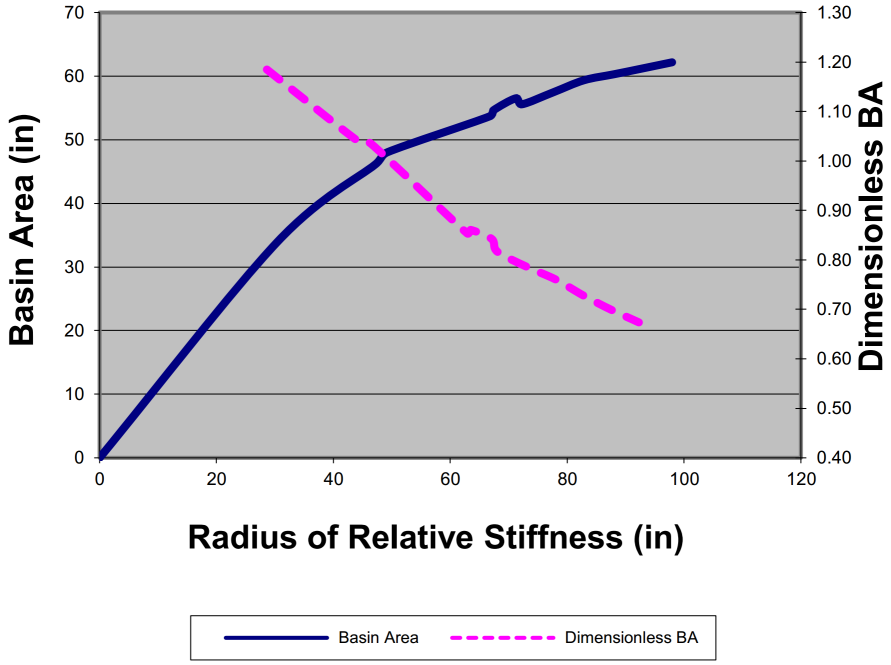

Figure 73- Variation of deflection Basin Area with ℓ

A concrete pavement slab deforms under load depending upon the position, magnitude, and area of contact of the load on the pavement surface. The resistance to deformation depends upon the stiffness of the supporting medium, the pavement thickness, opening of the joint or crack, as well as the interlayer bond. One parameter that characterizes this combined resistance to deformation is called the radius of relative stiffness (ℓ), and it depends upon the above characteristics. As previously noted, the relative stiffness is defined by the following equation:

$$\ell_e = \sqrt[4]{\frac{E_c h_e^3}{12(1-\nu^2)k}} \quad (55)$$

where
E_c= concrete modulus of elasticity
h_e= slab thickness
v = Poisson's ratio
k = foundation modulus

In terms of load transfer, representations of load transfer factors and mechanisms are reflected in measured ℓ -values as determined by an FWD basin area. It is also noted that the principle pavement distress types associated with a crack can be tied to a reduction in them, as related to the loss of support through subbase erosion or faulting in jointed concrete pavements.

Many studies have clearly indicated the important factors of load transfer, which continually reminds us of a need for a systematic relationship between them and the pavement design process. Such a relationship will be subsequently described, as well as details of a load transfer model that addresses both dowel bars (or similar load transfer devices) and aggregate interlock mechanisms. Elements of the following approach (*48*) were incorporated into the latest version of the AASHTO Pavement ME software.

Slab Effective Thickness and Interlayer Friction Stiffness Determination Field evaluation of concrete pavement using a Falling Weight Deflectometer (FWD) focus on the loaded behavior of a joint in terms of slab deflections and deflection load transfer efficiency (LTE_δ). Falling weight deflectometer (FWD) test results provide a primary way of characterizing in-place conditions. Results of FWD testing may be described in part with respect to the plate deflection (D_o) and the LTE. Load transfer efficiency may be defined as the deflection on the unloaded side of the joint divided by the deflection on the loaded side of a joint:

$$LTE\ \% = \frac{\delta_u}{\delta_l} * 100 \quad (56)$$

Where
δ_u = unloaded deflection
δ_L = loaded deflection

The load transfer efficiency of a joint or crack has an important effect on the composite stiffness manifested by a concrete pavement, and therefore on the level of stress developed in the pavement structure. Slab thickness and interlayer friction are components that have an indirect, yet the important effect on slab stiffness, particularly in the vicinity of a joint that can be demonstrated through consideration of slab bending behavior. This is accomplished through the application of theoretically sound, mechanistic structural evaluation concepts to slab behavior in the vicinity of a joint or crack. A rational characterization of this nature allows for consideration of the degree of bond or interlayer friction while under load on the overall joint stiffness. There are two different extremes that will arise when considering friction effects on slab stiffness. The slab interface friction condition may range from bonded to unbonded. In the analysis of this range, the subbase is a part of the pavement system rather than part of the pavement support. The two-layer analysis may be used for an unbonded condition, whereas in a bonded slab, each layer is combined as one equivalent layer. In both cases, the layers are combined to form a composite, single layer thickness. The characterization of the composite slab bending moment (Me) (especially in the vicinity of a joint) effectively involves the

composite sum of the bending moment within the concrete and the subbase layer. A variation of medium-thick plate theory suggests that the composite or partially-bonded bending stress ($\sigma_{e\text{-}p}$) in the composite section can be related to the wheel load stress of an unbonded slab ($\sigma_{e\text{-}u}$) where the frictional restraint (τ_f) afforded by the base layer as:

$$M_{e-p} = \frac{h_{e-p}^2}{6}\sigma_{e-p} = \frac{h^2}{6}(\sigma_{e-u} - \tau_f) \quad (57)$$

Where,

$$h_{e-p}^3 = \ell_e{}^4 * 12(1-\nu^2)\frac{k_{dyn}}{E_c} \quad (58)$$

and ℓ_e = radius of relative stiffness corresponding to the basin area measured at the slab edge or corner across a joint

It is argued that ℓ_e represents an in-place pavement stiffness at a joint as affected by the measured load transfer efficiency and the effective interlayer bond exhibited by the pavement structural response. As such, the ℓ_e term can represent a partially bonded condition where the composite slab thickness ($h_{e\text{-}p}$) may be determined or associated with ℓ_e as noted above. The partially bonded condition between the slab and subbase is created by a certain amount of slippage due to frictional restraint that can occur under load but still makes a contribution to the load transfer or the stiffness at a joint. This restraint is also formulated relative to the degree of bonding (x_b – a parameter that ranges between zero and 1.0) as:

$$h_{e-p} = (1-x)h_{e-u} + (x)h_{e-b} \quad (59)$$

The previous equation can be rearranged to solve for the degree of bonding as:

$$X_b = \frac{h_{e-p} - h_{e-u}}{h_{e-b} - h_{e-u}} \quad (60)$$

The value of he-p will vary between the conditions of unbonded to bonded - depending, of course, upon the degree of the bond. The composite or effective thickness for fully bonded layers:

$$h_{e-b} = \left\{h_1^3 + \frac{E_2}{E_1}h_2^3 + 12\left[\left(x_{na} - \frac{h_1}{2}\right)^2 + \frac{E_2}{E_1}\left(h_1 - x_{na} + \frac{h_2}{2}\right)^2 h_2\right]\right\}^{1/3} \quad (61)$$

And

$$x_{na} = \frac{E_1 h_1 \frac{h_1}{2} + E_2 h_2 (h_1 + \frac{h_2}{2})}{E_1 h_1 + E_2 h_2} \quad (62)$$

The effective thickness for unbonded layers

$$h_{e-u} = \left[\left(h_1^3 + \frac{E_2}{E_1}h_2^3\right)\right]^{1/3} \quad (63)$$

where

E_c = Elastic modulus of the PCC layer ;
$h_{e\text{-}b}$ = Effective thickness of the bonded PCC layer ;
$h_{e\text{-}u}$ = Effective thickness of the unbonded PCC layer ;
υ = Concrete Poisson's ratio;
E_1 or E_2 = Elastic modulus for layer 1 or 2 ;
h_1 or h_2 = Thickness for layer 1 or 2 , and
ℓ_e = Radius of relative stiffness .

Figure 74 depicts the relationships between the partially bonded and unbonded effective thicknesses and stresses; using simple proportioning, the effective partially bonded stress (σ_{e-p}) can be found as:

$$\sigma_{e-p} = \sigma_e \left[\frac{2h_{e-u}}{h_{e-p}} - 1\right] \quad (64)$$

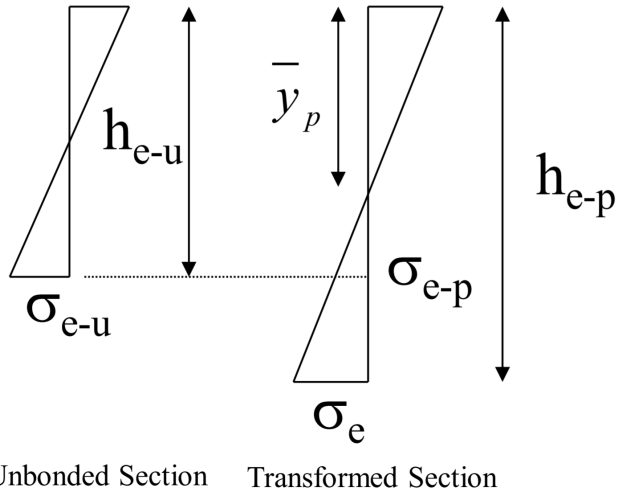

Figure 74 - Stress pattern of the unbonded and partially bonded transformed section of a concrete slab

In order to formulate a relationship for the effective interlayer friction coefficient (μe – since it includes both mechanical and cohesive effects), the effective bonded bending stress (σ_e) is equated to the difference between the unbonded bending stress (σ_{e-u}) and the effective frictional restraint (f_e) at the bottom of the slab as:

$$\sigma_e = \sigma_{e-u} - f_e = \frac{S_{e-u}P}{h_{e-u}} - f_e = \frac{S_{e-u}P}{h_{e-u}} - \sigma_v\mu_e \quad (65)$$

The previous equations can be rearranged to develop an expression for μ_e to be determined from FWD data as:

$$\mu_e = \frac{f_e}{\sigma_v} = \frac{\sigma_{e-u} - \sigma_e}{\sigma_v} \quad (66)$$

Where for FWD plate loading:

$\sigma_e = \frac{S_e P}{h_e^2}$; $S_e = a + b\ell_e + c{\ell_e}^2$

S_e = Effective dimensionless stress (for the composite pavement section);
P = Applied FWD load (F) a, b, c = 0.0006, 0.0403, and -0.0002 (for FWD plate loading);
h_c = Concrete slab thickness (L);
σ_v = Load induced vertical pressure (≈ 1.0 psi) =k_{dyn}*D_1; and
D_1 = Center plate deflection (L).

The interlayer effective frictional restraint is determined from the difference between the stress at the bottom of the concrete layer (σ_{e-u}) and the effective bending stress (σ_e). The interlayer

bond restraint is related to the coefficient of friction (μ_e) between the subbase layer and the concrete layer.

Findings of FWD Analysis

By applying the concepts discussed in the previous section, a sample of the type of analysis being carried out is shown below with respect to the calibration of CRC pavement performance. From these values, the degree of bonding (xb) between the surface and base layer can be determined and compared against the effective coefficient of friction (μe). The relationship between xb and μe is used to determine the percent of erosion. Figure 75 illustrates the relationship between the interfacial degree of bond and the effective friction as determined for the interior of the CRC pavement section 40-4166.

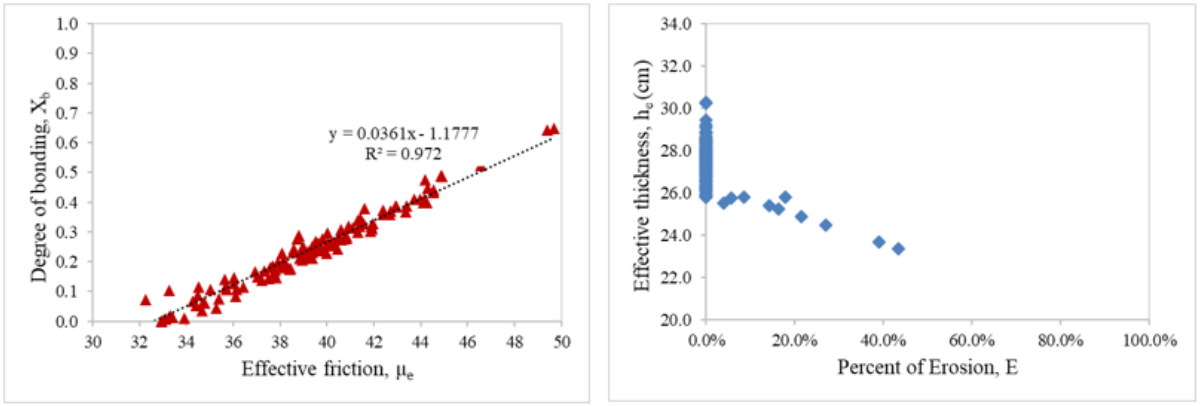

(a) (b)

Figure 75 Composite Section- Characteristic Degree of Bond and Effective Friction Relationship

This relationship is best defined for the interior position of a pavement slab since this position represents the greatest amount of contact between the slab and the base support and thus serves well as a point of reference for erosion development determinations. Early in the life of a concrete pavement section, the effective thicknesses are high, and the damage due to erosion is low, but this changes over time. Furthermore, since the degree of the bond is a function of the effective slab thickness, it is subject to change over time and traffic as well, but the rate of deterioration takes over all areas of a concrete slab but more so along the slab edges and corners. In many cases, the set in a concrete slab is a principal contributor to erosion damage of the slab interface resulting in significant losses in slab stiffness. Set is a consequence of irreversible drying shrinkage that occurs mainly at the surface due to the high rate of drying that occurs at that location during and hours after the placement of the slab. The development of set is countered by improved management of the curing process but ultimately is a factor in the long-term performance of the slab and thus should be accounted for in the calibration process. As shown in Figure 75, the expression for the degree of the bond (x_b) is established for the interior portions of a CRC pavement where m and b are regression coefficients.

$$x_b = m\mu_e + b \tag{67}$$

For each effective thickness determination, a value of μ_e is determined and used to compute a value of x_b. The erosion damage is then determined as:

$$\%E = 0 \; if \; x_{b_i} > 0; \; or \; \%E_i = \left| x_{b_i} + \alpha b \right| \le 100; if \; x_{b_i} < 0 \tag{68}$$

The parameter α is found from the calibration process as:

$$\alpha = \left(\frac{\left(1 - \frac{f_{e_i}}{f_b}\right) - \left|x_{b_i}\right|}{b} \right) \text{ and } \frac{1}{f_b} = \frac{b}{f_e} + \frac{m}{\sigma_v} \tag{69}$$

Figure 76 to Figure 78 illustrate the trends over time in values of equivalent thickness and the percent of erosion that results from the implementation of the above expressions. The following figures are associated with FWD data along with location C-3, which is the edge of the panel in the middle of the slab. Clearly, the deterioration process that leads to punchout distress is represented and provides the means to related damage to punchouts in CRC pavement once the trends in Figure 76 through Figure 78 are associated with the applied levels of traffic.

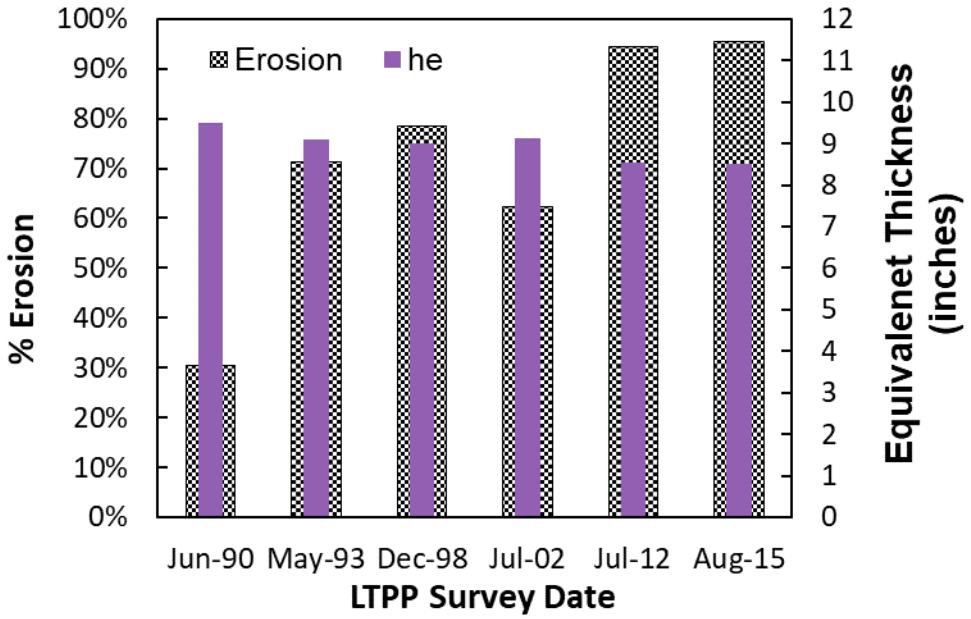

Figure 76- Trend in the Effective Thickness and the Development of Erosion Damage over Time for Position C-2 in Section 40-4158

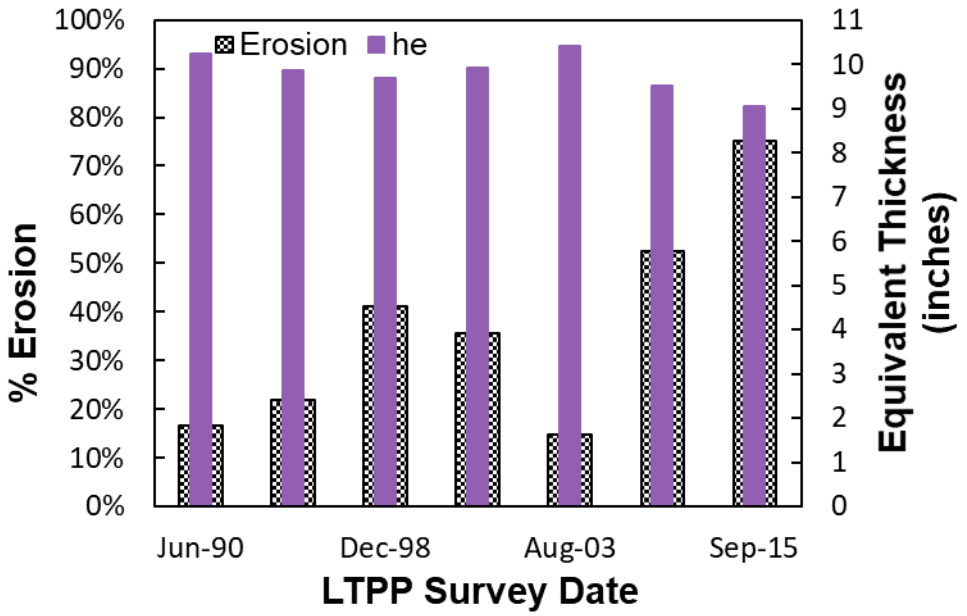

Figure 77- Trend in the Effective thickness and the development of erosion damage over time for position C-2 in section 40-4166

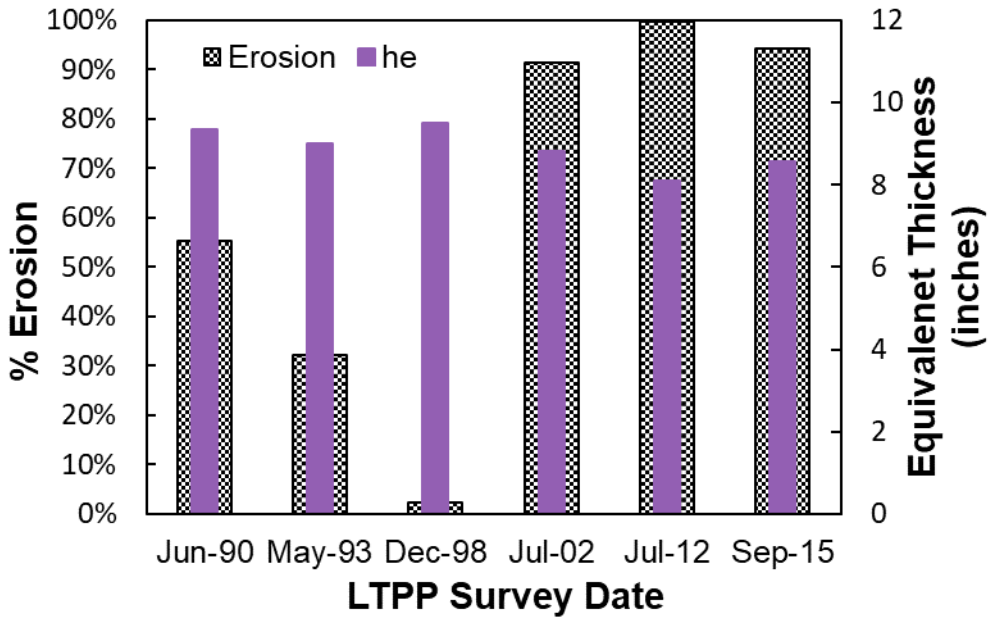

Figure 78-Trend in the effective thickness and the development of erosion damage over time for position C-3 in section 40-5021

The previous figures represent the CRCP sections in the state of Oklahoma. As shown, the general erosion trend increases with time, while the general equivalent thickness trend decreases with time. As mentioned before, only section 40-4166 shows punchout distress among all three Oklahoma CRCP sections (Figure 65). Thus, other sections from out of Oklahoma are important to study the development of the punchout distress and validate the calibration coefficient of transfer function regarding punchouts in the CRCP pavement.

Therefore, the same procedure was also applied to sections from Texas. Figure 79, through Figure 81, exhibits the trends over time in values of equivalent thickness and the percent of erosion for sections 48-3569, 48-5323, and 48-5334 along with J3 location.

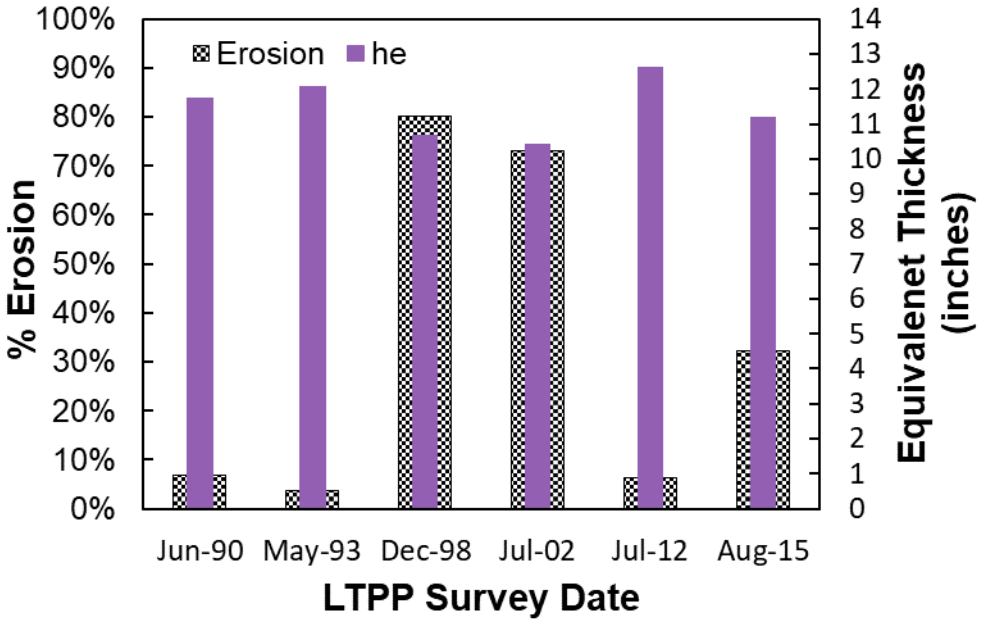

Figure 79-Trend in the Effective Thickness and the Development of Erosion Damage Over Time for Position C-3 in Section 48-3569

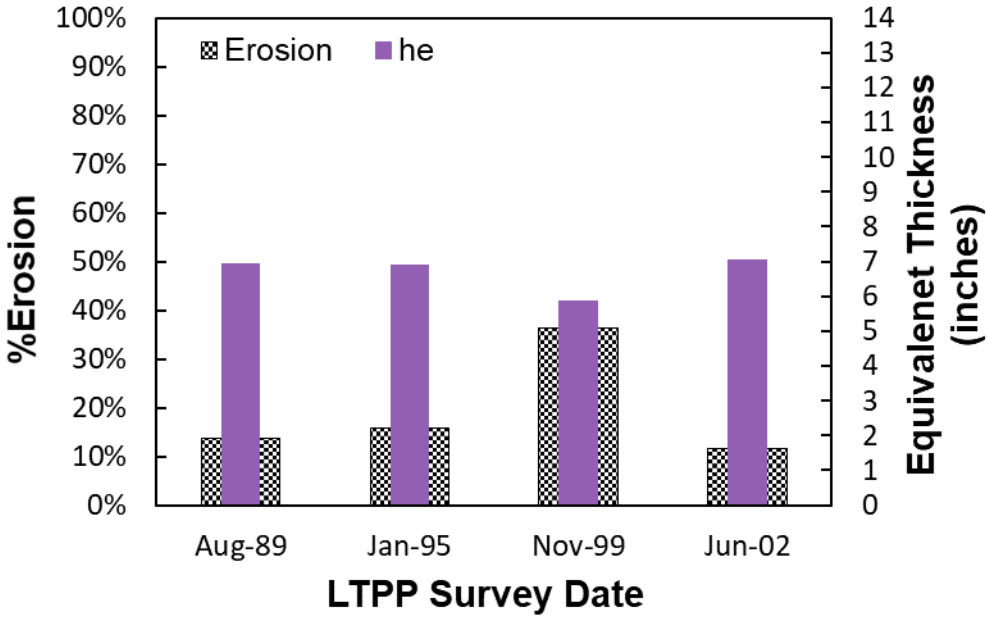

Figure 80-Trend in the Effective Thickness and the Development of Erosion Damage Over Time for Position C-3 in Section 48-5323

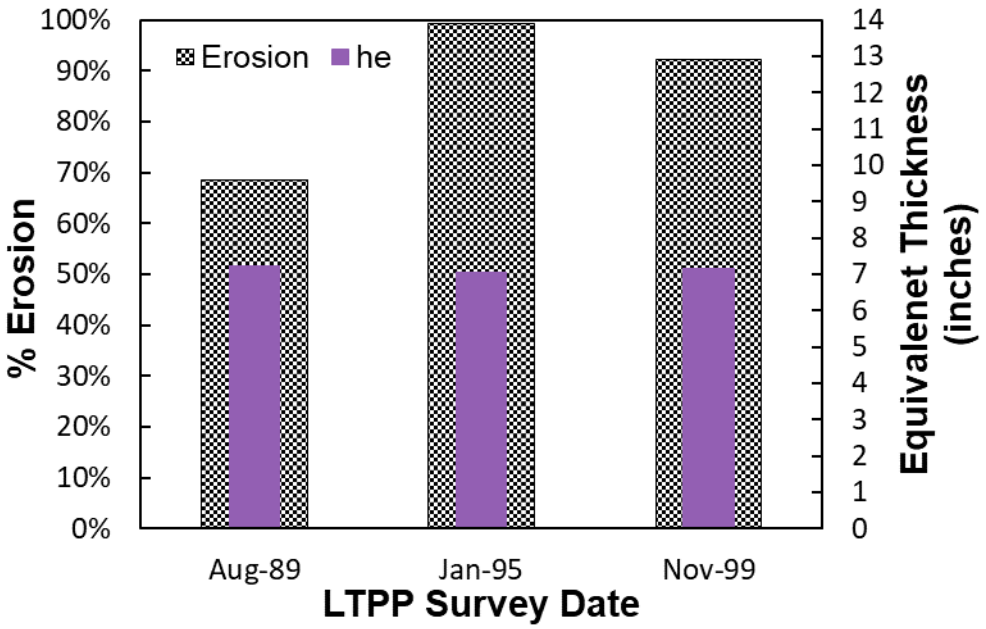

Figure 81-Trend in the Effective Thickness and the Development of Erosion Damage Over Time for Position C-3 in Section 48-5334

As shown in the previous figures, the general trend of thickness is decreasing overtime while erosion percentage is increasing. The erosion percentage is generally related to the effective thickness. However, other factors such as maintenance and repair activities, different base and subbase type and thicknesses as well as FWD test time might cause inconsistent equivalent thickness to erosion percentage relationships at some LTPP survey dates. To make a better sense of this relationship, damage calculation using pavement ME is required and planned for all sections considering traffic, climate, and pavement sections and properties.

One-step further was taken by comparing the percent of erosion with the percent of punchouts of the CRCP sections. The punchout records in LTPP sections are represented by the number of punchouts in the surveyed section. The punchout records in LTPP sections are represented by a number. Also, the area of each punchouts is not recorded. Therefore, a methodology to calculate the percent of punchout based on the number of punchouts was used. The methodology depends on calculating the maximum possible number of punchouts for any given section. Based on the LTPP definition, a common type of punchout can be defined as the area bordered by two transverse cracks (spaced < 2 ft), a longitudinal crack, and a longitudinal joint or the edge of the CRC pavement (*51*). Therefore, the LTPP records of transverse crack numbers can be used to calculate the maximum (ultimate) possible number of punchouts for each section. The ultimate punchout number was calculated by dividing the length of the section (i.e., 500 ft) by the average spacing of transverse cracks, as shown in equation (70). The average spacing of transverse cracks can be found by dividing the length of the section by the number of transverse cracks, as shown in equation (71). The recorded punchouts number was then divided by the ultimate number of punchout to yield the percent of punchout in each CRCP section, as shown in the equation (72). Figure 82, through Figure 85, shows the comparison between the percent of punchout and the percent of erosion calculated from the FWD data along location C-1.

$$Upunchouts = \frac{L_s}{S_{tc}} \quad (70)$$

where

$$S_{tc} = \frac{L_s}{N_{tc}} \quad (71)$$

and

$$\%Po = \frac{N_{puchouts}}{U_{punchouts}} x100\% \quad (72)$$

where,

$U_{punchouts}$ = Ultimate punchout number for any given section
L_s = Length of CRCP section (500 ft for LTPP sections)
S_{tc} = Average spacing of LTPP transverse cracks
N_{tc} = Number of transverse cracks in a given survey date
%Po = Percent of punchouts for a given section and survey date
$N_{punchouts}$ = LTPP records of punchout number for each survey date

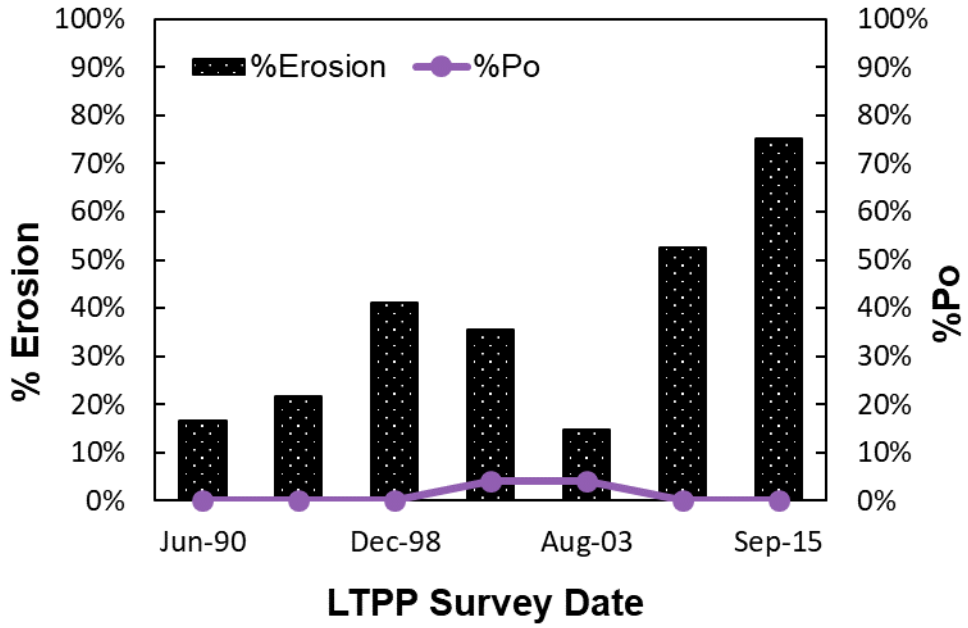

Figure 82 -The Percent of Punchouts and the Development of Erosion Damage Over Time Along Position C-3 in Section 40-4166

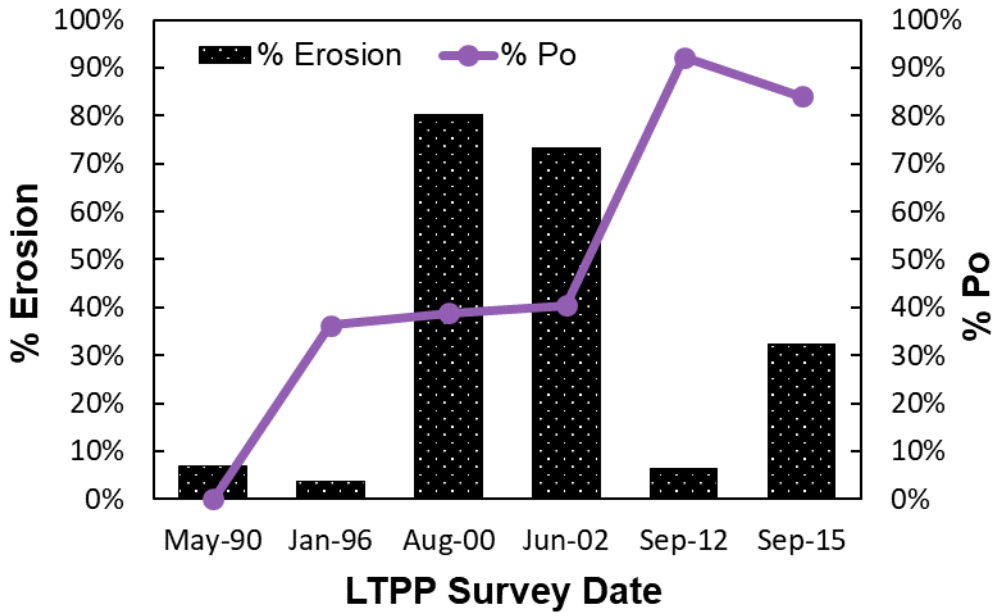

Figure 83-The Percent of Punchouts and the Development of Erosion Damage Over Time Along Position C-3 in Section 48-3569

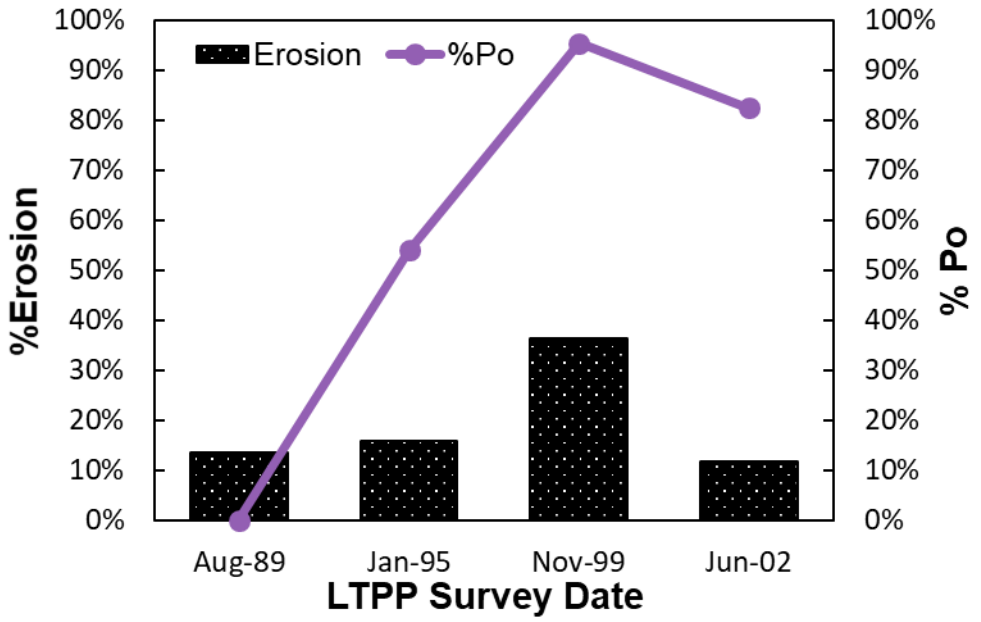

Figure 84- The Percent of Punchouts and the Development of Erosion Damage Over Time Along Position C-3 in Section 48-5323

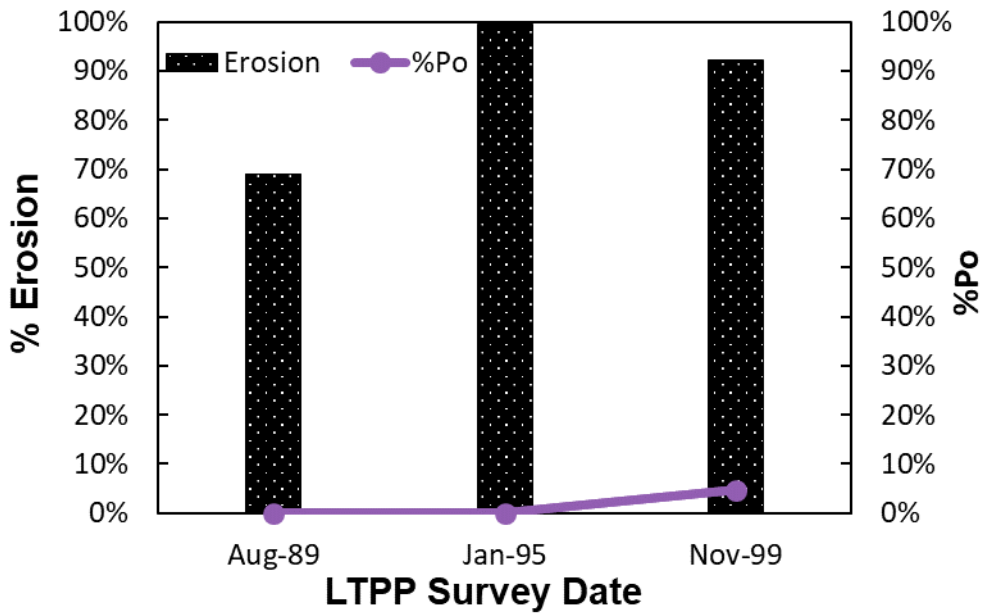

Figure 85-The Percent of Punchouts and the Development of Erosion Damage Over Time Along Position C-3 in Section 48-5334

In the previous figures, the percent of punchouts in CRCP pavement increases as the erosion damage increases. The erosion damage is not cumulative as it is based on the FWD data, which depends on factors such as pavement structure, time of testing, and maintenance, and repair activities. On the other hand, the punchout percentage is cumulative, which explains a high percent of punchouts with low erosion damage percentage in section 40-4166. The punchout percent in sections 48-3569 and 48-5323 match with the calculated percent of erosion where it increases whenever erosion percentage increases and vice versa. In section 48-3569, a maintenance activity of grinding surface in June 2015 has reduced the number of punchouts recorded in the September 2015 survey date and thus reduced the percent of punchout even though the erosion was higher than the previous LTPP survey date (September 2012). However, forming punchouts in CRC pavement might require a high level of erosion damage in some cases, such as section 48-5334. In this case, the 5.8 inches asphalt treated base layer might have a major role in reducing the development of punchouts. Because the calculation of punchout percentage depends on the ultimate punchout number, which depends mainly on the number of transverse cracks, additional effort was made to compare the number of transverse cracking with the percent of erosion.

Figure 86, through Figure 89, shows the comparison between the LTPP number of transverse cracks and percent of erosion calculated from the FWD data along location C-3. The figures show that the number of transverse cracks increases as erosion damage percent increases and as survey time advances. In section 48-5323, the number of transverse cracks decreases in 2015 because of maintenance activities of 5-full depth patching of other than at joint and 6-partial depth patching other than at joint was applied in 2001. As mentioned before, a longitudinal crack is required to connect two closely spaced transverse cracks to form punchouts in CRCP. Thus, comparing the percent of punchouts with the number of transverse cracks suggests investigating the effect of traffic, climate, and pavement structure on the development of transverse and longitudinal cracking as well as punchouts.

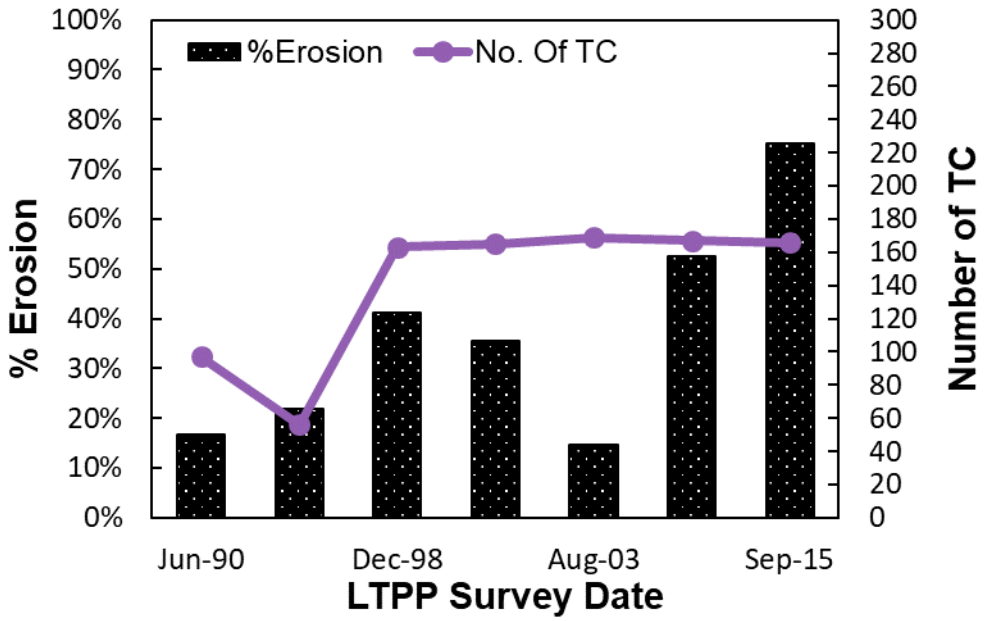

Figure 86-The Number of Transverse Cracks and the Development of Erosion Damage Over Time Along Position C-3 in Section 40-4166

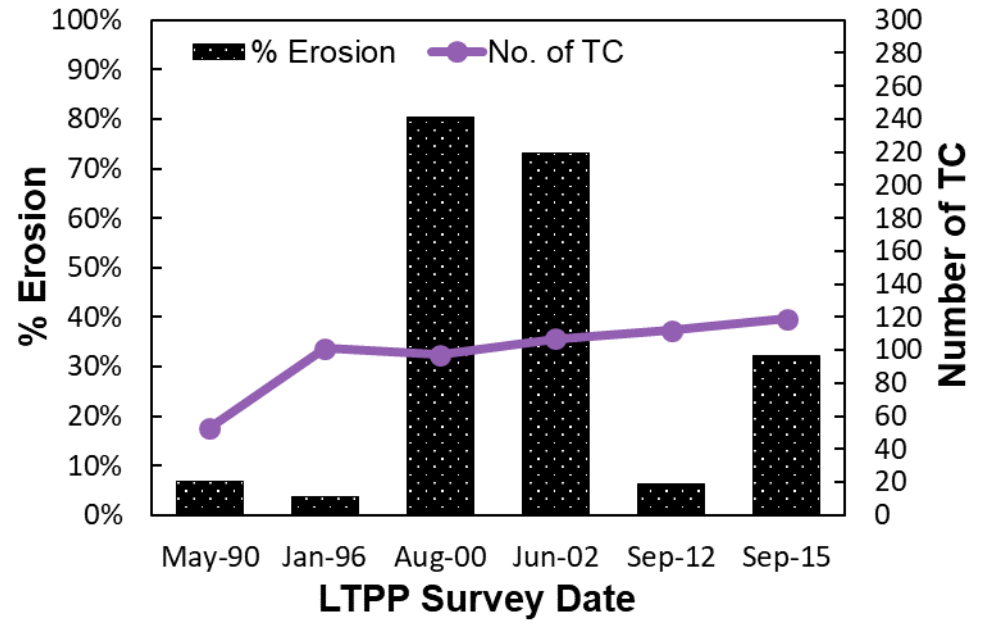

Figure 87-The Number of Transverse Cracks and the Development of Erosion Damage Over Time Along Position C-3 in Section 48-3569

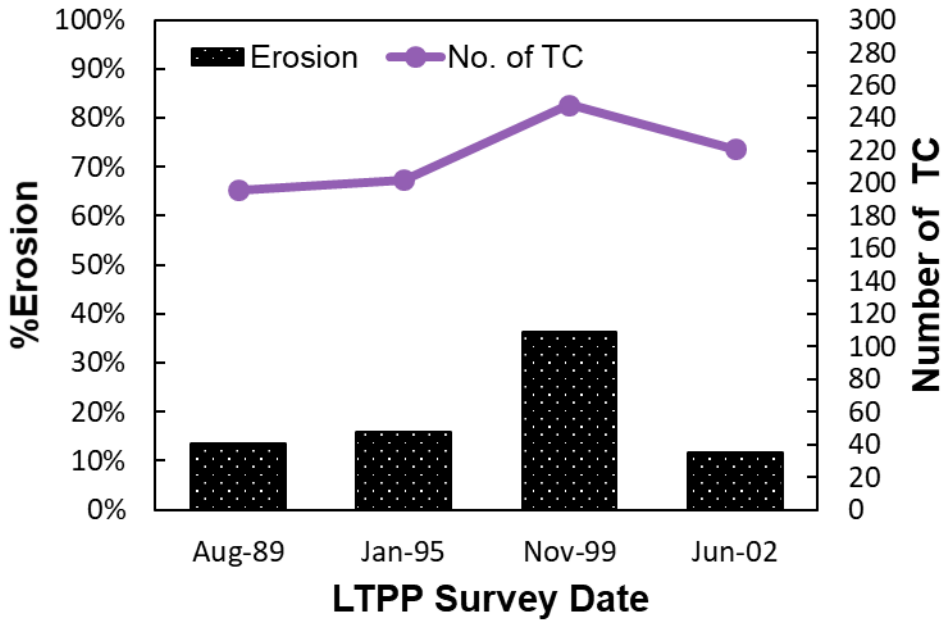

Figure 88 -The Number of Transverse Cracks and the Development of Erosion Damage Over Time Along Position C-3 in Section 48-5323

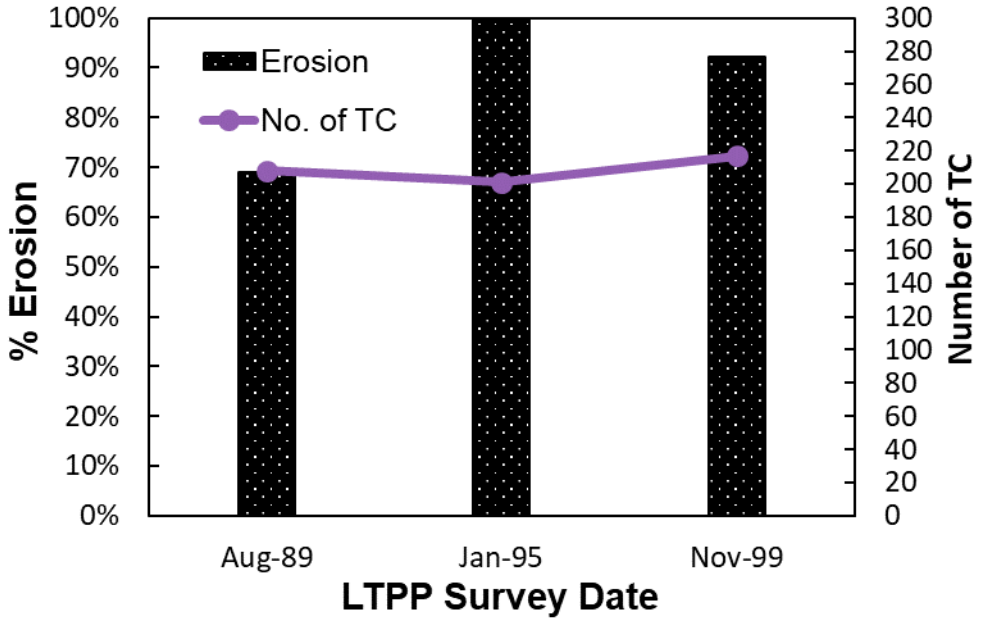

Figure 89 -The Number of Transverse Cracks and the Development of Erosion Damage Over Time Along Position C-3 in Section 48-5334

The same concept was also applied to the JPCP sections in Oklahoma. One step further was taken by comparing the percent of erosion with the average faulting from the LTPP database of each JPCP section. Figure 82 through Figure 85 shows the trends over time in values of equivalent thickness and the percent of erosion for all JPCP sections in Oklahoma. Similarly, the following figures are associated with FWD data along location J-3, which is the edge of the panel at the middle of the slab.

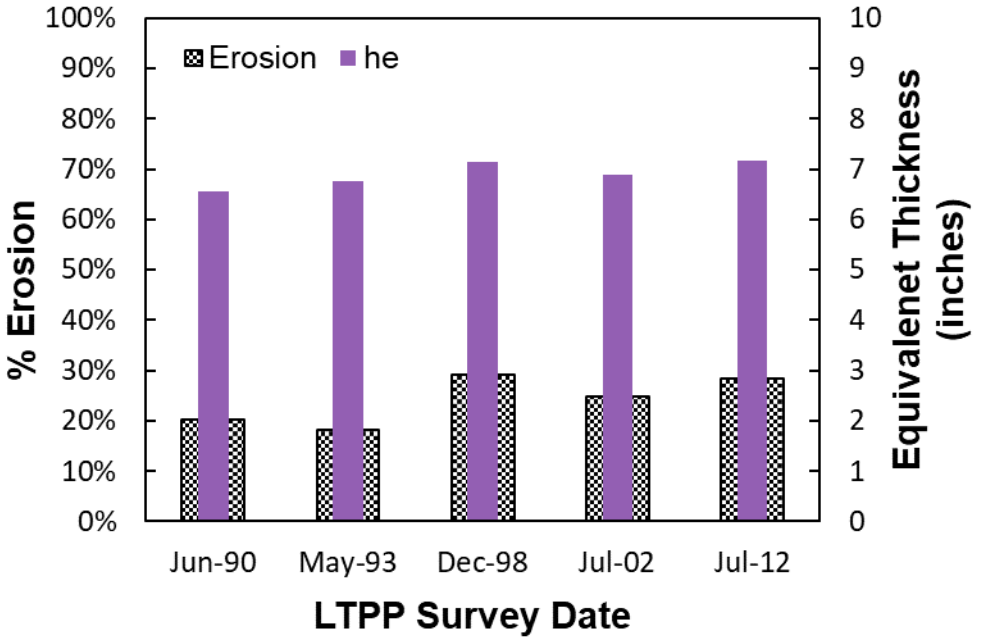

Figure 90 -Trend in the Effective Thickness and the Development of Erosion Damage Over Time for Position J-3 in Section 40-3018

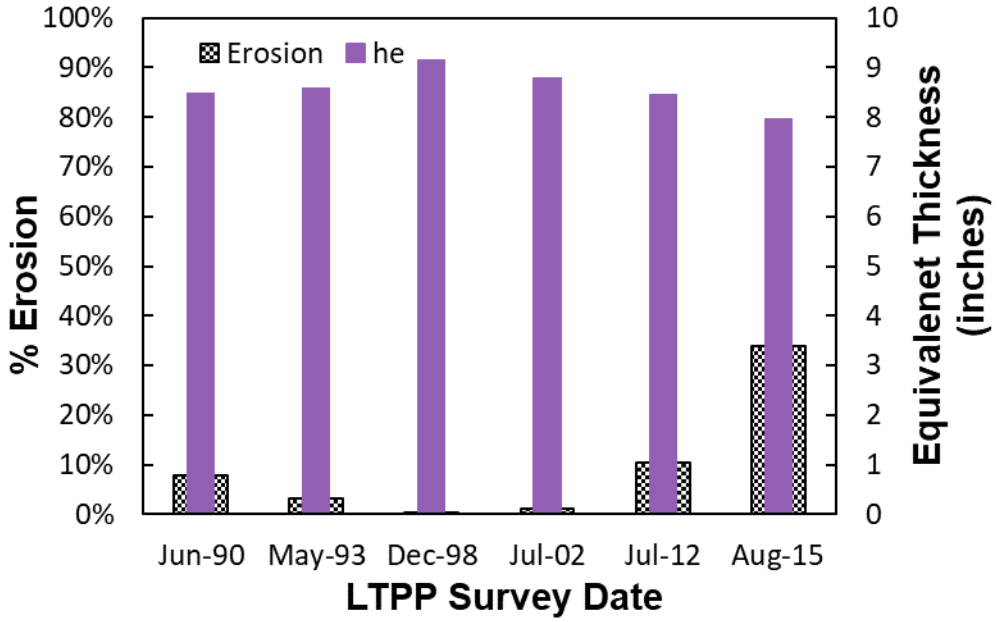

Figure 91 -Trend in the Effective Thickness and the Development of Erosion Damage Over Time for Position J-3 in Section 40-4157

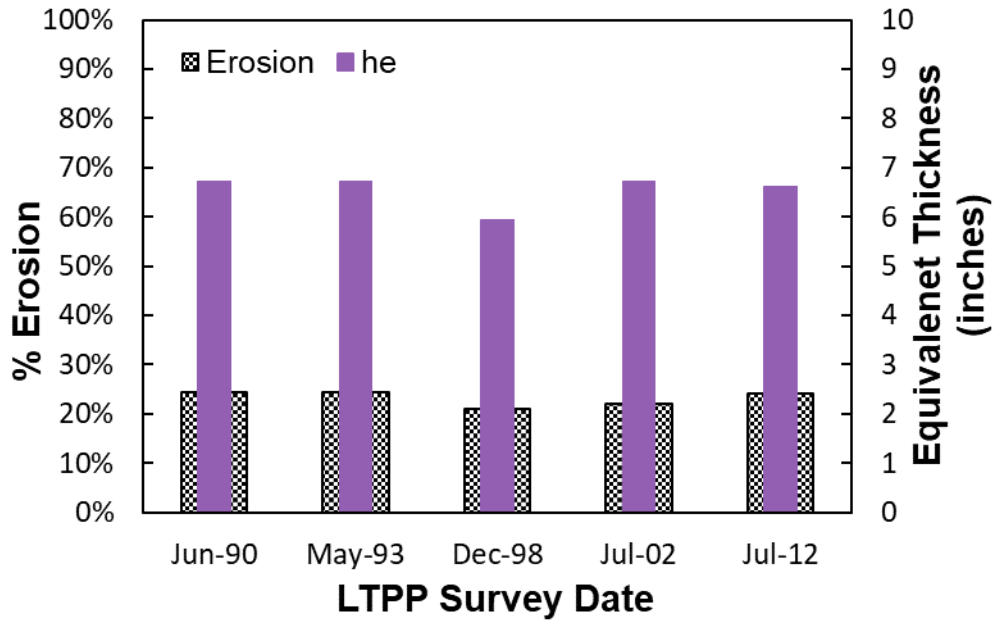

Figure 92 -Trend in the Effective Thickness and the Development of Erosion Damage Over Time for Position J-3 in Section 40-4160

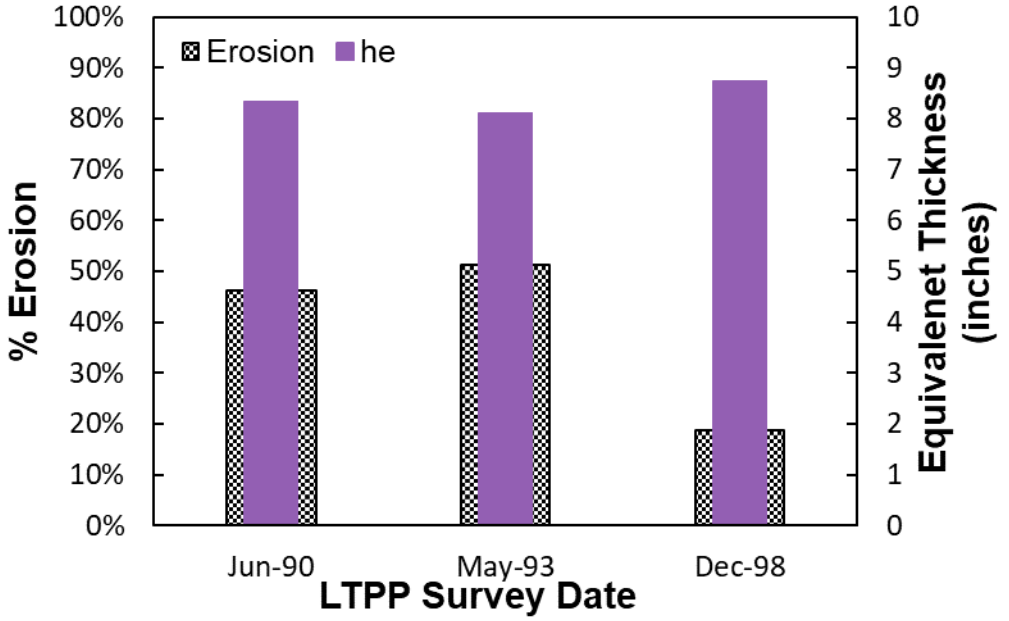

Figure 93 -Trend in the Effective Thickness and the Development of Erosion Damage Over Time for Position J-3 in Section 40-4162

From the previous figures, the erosion percent is trending up with time, while the equivalent thickness trend is going down with time. However, the relationship between the equivalent thickness and the percent of erosion seems to have other factors controlling the FWD records and hence providing unexpected equivalent thickness and/or percent of erosion. In addition, the equivalent thickness is more sensitive to erosion in JPCP than in CRCP sections. To evaluate the erosion calculations in JPCP sections, a comparison has been made between the percent of erosion and the average faulting over time. Figure 94, through Figure 97, shows the

comparison between the LTPP faulting values and percent of erosion calculated from the FWD data along location J-3.

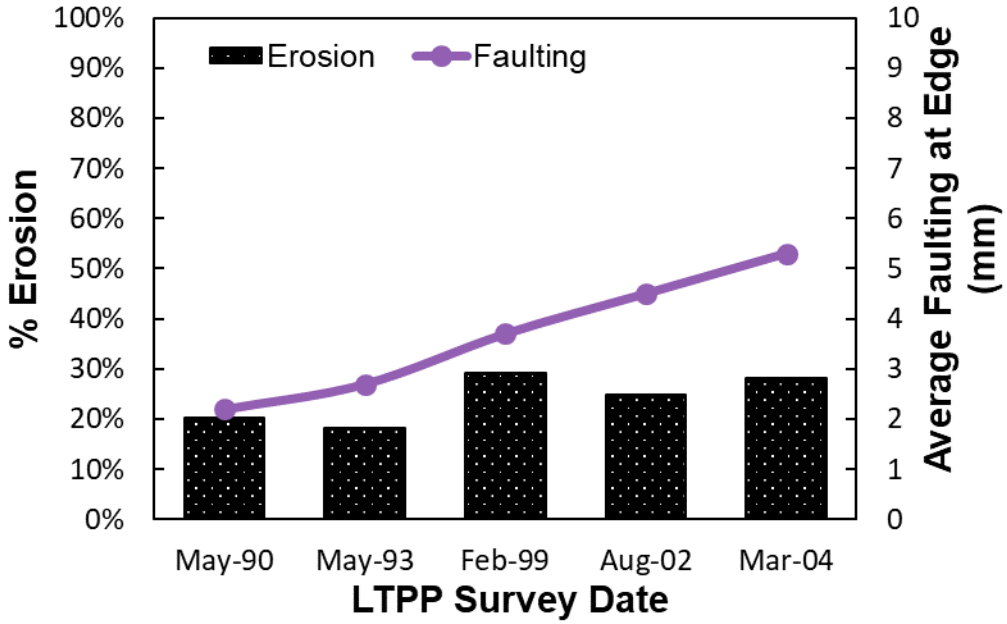

Figure 94 - Comparison Between the Average Faulting at Edge and the Development of Erosion Damage Over Time for Position J-3 in Section 40-3018

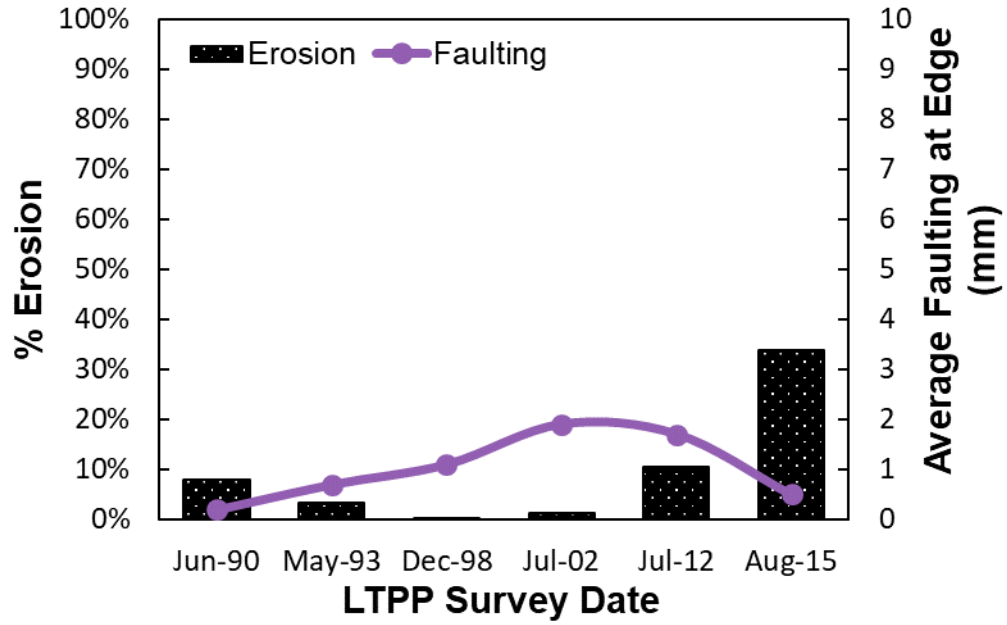

Figure 95- Comparison Between the Average Faulting at Edge and the Development of Erosion Damage Over Time for Position J-3 in Section 40-4157

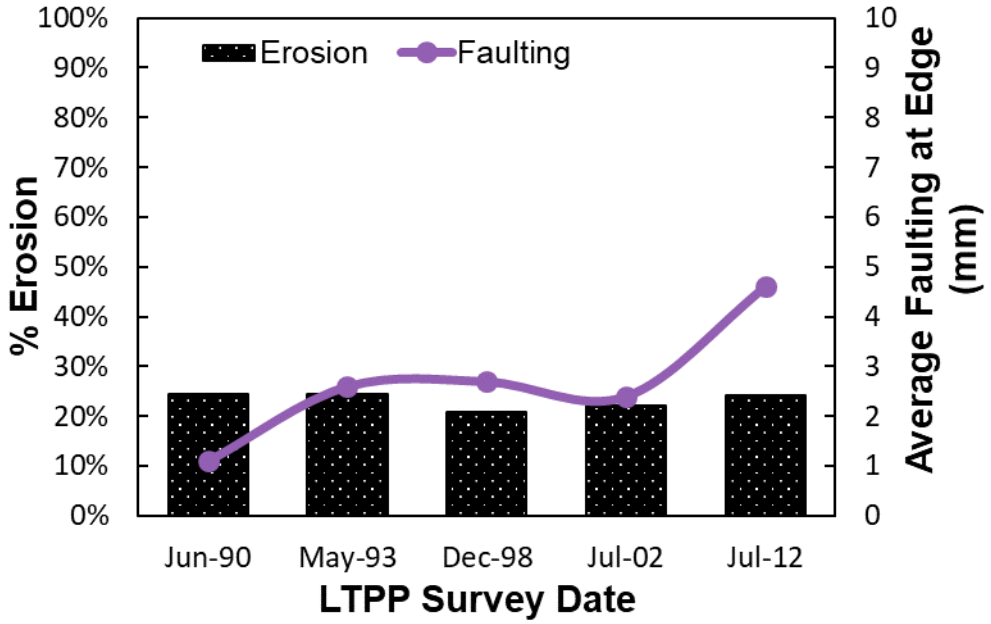

Figure 96- Comparison Between the Average Faulting at Edge and the Development of Erosion Damage Over Time for Position J-3 in Section 40-4160

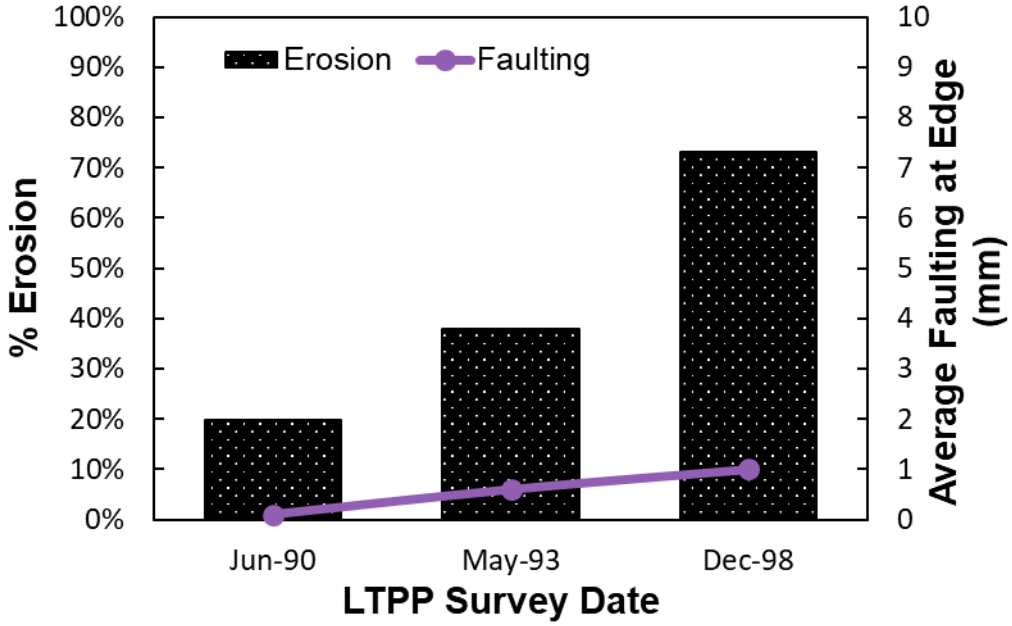

Figure 97- Comparison Between the Average Faulting at Edge and the Development of Erosion Damage Over Time for Position J-3 in Section 40-4162

In the previous figures, the faulting at edge and percent of erosion is generally increasing with time. The faulting values show that the damage is cumulative as expected, while the calculated erosion is not. This is because erosion calculation depends on the FWD records, which might be affected by many other factors mentioned earlier. However, the faulting increase matches the erosion development at the edge of the JPCP sections. In section 40-4157, the erosion is decreasing significantly in 2015 because a joint load transfer restoration and some transverse

and longitudinal joint sealant were applied in May and September 2012, respectively. Additional analysis of the JPCP sections using the pavement ME program will be conducted to evaluate the erosion damage under the existing traffic and climate.

Calibration of CRCP Sections

Local calibration of the punchout model in the Pavement ME software is a vital step in achieving performance predictability for the design of Continuously Reinforced Concrete (CRC) pavement. In Oklahoma, there was only limited performance data available in the General Pavement Studies (GPS) database for CRC pavement. This set of circumstances required a different approach as to the type of data used for calibration. The type of data originally utilized in NCHRP 1-37A essentially represented visually evident damage that is clearly observable at the surface of the pavement structure. Non-observable damage, however, is actually of greater value as a source of calibration data since it represents the deteriorative conditions that lead to the visual manifestation of the damage process. Since visually validated distress is the end result of the distress cycle, the traffic level associated with it is often subject to a considerable amount of error. In this regard, non-observable data such as erosion damage is shown to be a good indicator of and a substitute for actual punchout data since it represents the deterioration of the slab subbase interface that has been found to closely aligned with the punchout process. The amount of erosion is evaluated based on FWD data and is shown to be a reliable way to determine the calibration coefficients for the punchout model. This report proposes an approach for calibrating local coefficients for CRC pavements based on non-observable performance data. The main process of this methodology requires estimating erosion percentage damage using Falling Weight Deflectometer data (FWD), determining the percentage of punchout from the Long-Term Performance Program (LTPP) records, and establishing the relationship between both components to estimate the existing punchout distresses. This relationship can be used to calculate the actual damage, including erosion damage, and to calibrate the local coefficients used in the pavement ME punchout model. This methodology was carried out on one section from Oklahoma and one section from Texas in order to validate its applicability and conclude on the pavement ME punchout model and its ability to predict punchout distress in the field.

One component of the pavement ME design procedure focuses on constitutive relations to calculate load-induced responses such as stress, strain, and deflection while another component focuses on the use of empirical distress models to estimate pavement performance over time and traffic. These models are nationally calibrated using performance and distress related data from the Long-Term Pavement Performance (LTPP) database for different national locations. The NCHRP project 1-37A encourages further calibration and validation of coefficients in the transfer function as a key step in implementing a new design that considers mechanical and environmental impacts for local calibration.

Punchout development is the main type of distress in CRC pavements, and the model for that must be calibrated to achieve a precise design of Pavement ME software. Efforts have been made by the Oklahoma Department of Transportation (DOT) to perform local CRCP calibration. However, due to the limitation of the number of sections and the punchout records, there was insufficient information to validate the applicability of the CRC pavement punchout model as NCHRP 1-37A requires at least 20 sections to validate the suitability of the calibration coefficients (7). Therefore, it is desirable to develop a modified methodology which can be used with a limited number of sections and yield to a reliable local punchout model calibration coefficients.

The NCHRP 1-37A approach of modeling punchout distress in CRC pavement is based on the development of longitudinal crack between closely spaced transverse cracks (*49*) due to accumulated fatigue damage from the flexural bending of the slab segment in the transverse direction (*52-55*). Researchers have carried out local calibration of the pavement ME software punchout model using recorded punchout, traffic, and materials data to facilitate the performance prediction process (*56-58*). However, due to the limited number of CRC pavement performance sections in the LTPP database, in some cases, local pavement management systems (PMS) have been used to provide distress data for local calibration and validation(*59, 60*).

As previously noted, the development of punchout distress is related to not only bending fatigue but also erosion induce voiding(*61*). In the Pavement ME software, the effect of erosion in the design of a CRC pavement is only considered through adjustment of the bending stresses relative to the potential of material erodibility in the subbase layer (*62*). However, the process of erosion is not directly addressed in the assessment of subbase erodibility in the ME design procedure. The erosion process gradually degrades support conditions that contribute, alongside with a reduction of transverse cracking stiffness and loss of load transfer efficiency, to the formation of punchout distress. The erosion damage is dependent upon the presence of water and the rate of water that water infiltrates the subbase interface, the number and magnitude of repeated loads, and the amount of deflection (*63-66*). The key to the integral incorporation of the erosion damage process in the design of CRC pavement, an applicable materials model, was developed (*48, 67*). Besides the material modeling, erosion damage can be assessed by considering the structural behavior of the pavement and its relationship to the shear stress development between layers. Degradation of shear strength between layers decreases the degree of bonding, which can resemble the erosion damage along with the slab-subbase interface. Therefore, the use of FWD test data to determine the degree of bonding and the erosion damage is key to initiating a relationship between the in-situ erosion damage with punchout distress. The local calibration and validation can be performed for any number of sections based on such a relationship.

Selection of LTPP CRCP sections

Employing the LTPP - Information Management System User Guide(*7*), data inventory of the GPS-CRCP sections in Oklahoma was conducted. The GPS-CRCP sectional data used in the calibration with respect to traffic was consistent and complete. This, along with FWD and distress data, was considered essential for calibration. In this respect, relevant SPS sections were not considered since essential data was found to be missing in that database. Although traffic and FWD data was present for 3 GPS-CRCP sections in Oklahoma, only section 40-4166 showed punchout distress. Therefore, only one section from Oklahoma was considered for calibration. To validate the calibration methodology, the CRC pavement section from Texas as a neighbor state was chosen. Along with the availability of required basic data, the Texas section 48-5323 met the requirement of the climatic zone of Oklahoma, which is wet, non-freeze. Figure 98 shows the pavement structure information.

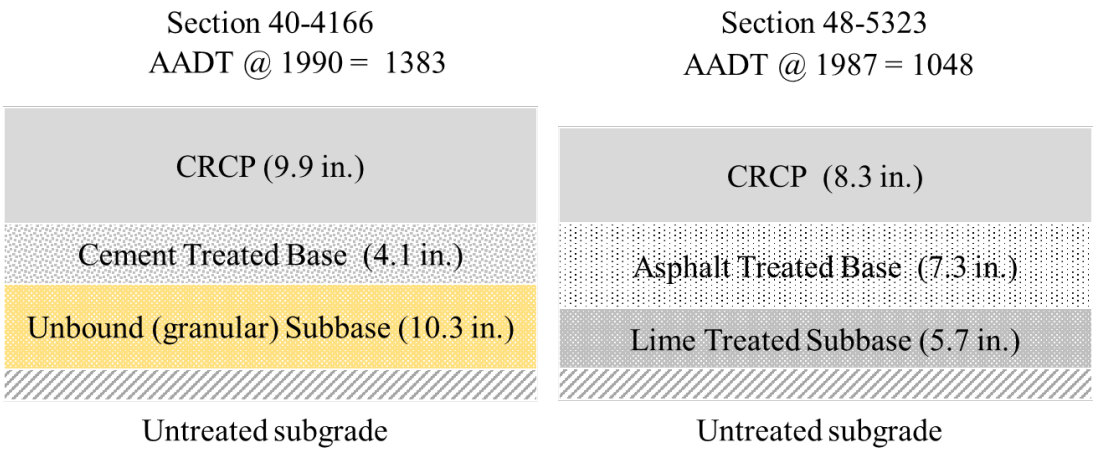

Figure 98 - CRCP pavement Sections- Cross Section Details.

The source of the traffic data in the LTPP database is typically the same agency that supplies the traffic estimates. In order to obtain the most accurate traffic information, efforts concentrated on the monitored traffic data as the main source of the existing traffic condition for any given CRC pavement section. The monitored traffic data consisted of the annual traffic estimates that were either provided by participating highway agencies or computed from raw data by the agency after 1990 (*60*). The traffic data was used as input in the Pavement ME software and obtain computed damage levels.

The FWD data is usually used to back-calculate the elastic modulus and the composite coefficient of subgrade reaction (K). In the FWD analysis, the structural condition of the Portland Cement Concrete (PCC) slab can be evaluated using the PCC elastic modulus, while the supporting layers can be evaluated using the K-value. Prior to start calibration, FWD data were analyzed to back-calculate these parameters and then was used to estimate the degree of bonding, friction coefficient and eventually estimate the percent of erosion underneath the surface CRCP layer(*68*).

In most sections, the punchout records exhibited increasing punchout number trends through the pavement life. The maximum number of punchouts for section 40-4166 was recorded in 2009 with 4 punchouts, while the maximum number of punchout for section 48-5323 was recorded in 1999 with 71 punchouts.

The methodology of Punchout Calibration

In this project, a methodology for the calibration of the Pavement ME punchout model was carried out as a function of the erosion data generated from the analysis of FWD LTPP data towards developing a relationship to field performance. To initiate an erosion-punchout relationship, the following steps are required:

1. Determine the percent of erosion by analysis of FWD LTPP data.
2. Develop a relationship between the percent erosion with pavement age
3. Develop the relationship between the percent erosion (%E) and the percent punchouts (%PO). Percent punchouts is the ratio of the number of punchout to the ultimate number of punchouts in any section. The ultimate number of punchouts is a function of the cracking pattern.
4. Calibrate the coefficients (A, α, and β) in the following performance model:

$$P.O. = \frac{A}{1 + \alpha . FD^{\beta}} \quad (73)$$

where P.O. is the predicted number of punchouts per mile, FD is the total accumulated fatigue damage at the end of yth year and A,α, β are calibration constants (defaulted to 107.73, 2.475, -0.785, respectively)

Erosion Analysis Using FWD Data

The erosion analysis in this project was carried out using the FWD data obtained from the LTPP database. The main concept of the erosion analysis is studying the interfacial bond between the concrete and the subbase layers. This study helped the researchers to evaluate the degree of bonding between pavement layers and formulate the erosion percent mechanically. The details of the erosion analysis procedure and its outcomes are discussed in earlier sections.

Erosion Relationship with Pavement Age

Since the dates of the distress surveys were different from the dates of the FWD testing, it was important to interpolate the percent erosion (%E) for different years to facilitate its relationship with the percent punchouts (%PO). The number of punchouts in pavement ME is determined solely on the calculation of bending fatigue damage. Ultimately, the percent of erosion was related to the pavement damage indirectly. This relationship was established through nonlinear regression, which yields into the use of the sigmoidal model presented in many works of literature (*69, 70*), as shown in the equation(74). The values of R^2 for each LTPP section were larger than 0.89 indicating a very good fit for the model that can be used to interpolate erosion data over the pavement life.

$$\%E = e^{-\left(\frac{\rho}{N}\right)^{\beta}} \quad (74)$$

Where E is the percent of erosion, N is the age of the pavement or the damage, ρ is a coefficient that controls the prolongation period or the location of the inflection point on the curve, B is a slope factor, and it was set as 1.0.

Figure 99 (a) and (b) show the relationship between %E with the pavement age for section 40-4166 in Oklahoma, which is placed on the cement-treated base and for section 48-5323 in Texas, which is placed on an asphalt treated mixture. Table 35 shows the fitting coefficients of the above equation as well as the R^2 value for each relationship.

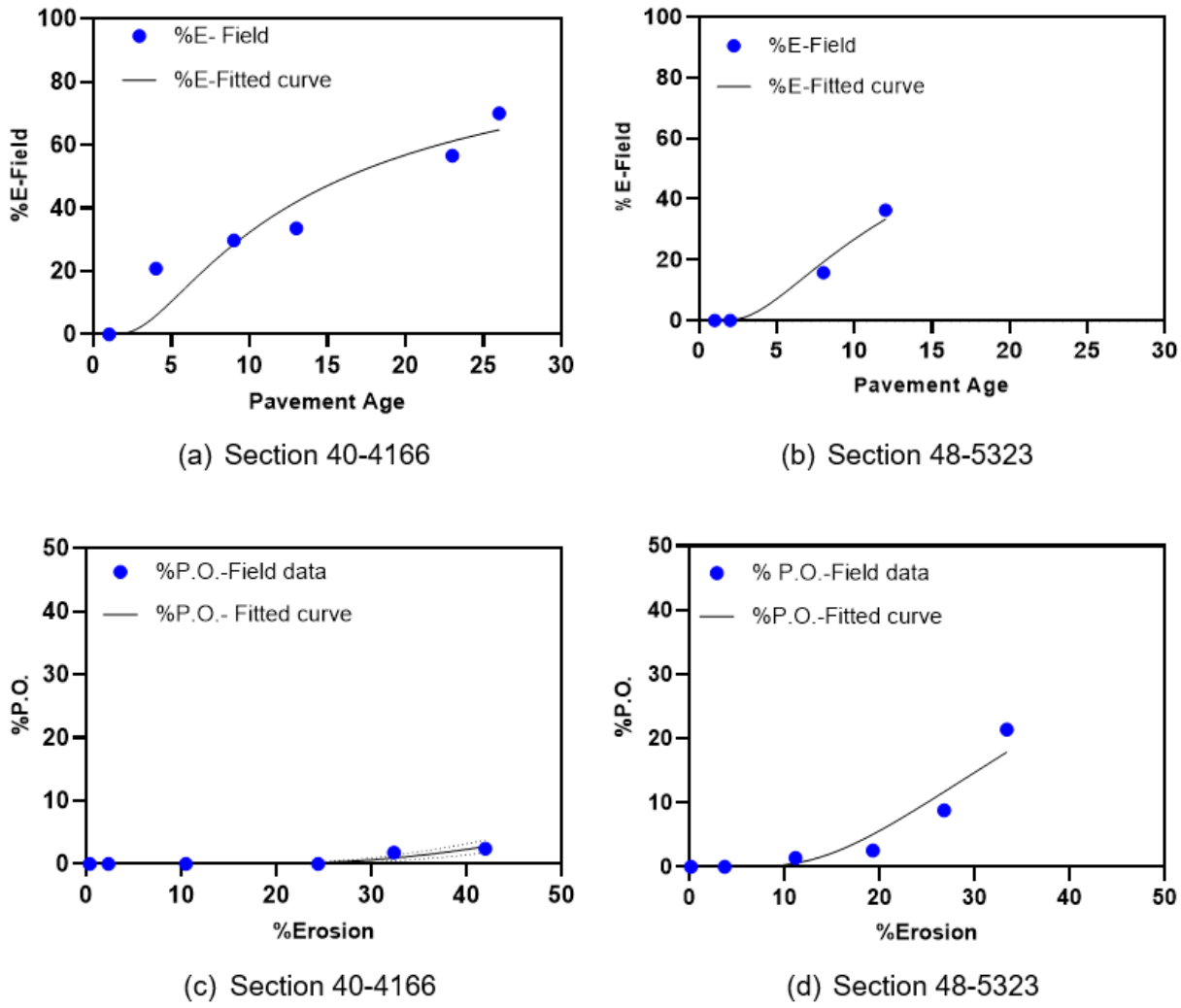

Figure 99- Curve fitting for Oklahoma and Texas sections

Erosion and Punchout Relationship

The relationship between %E, obtained from the FWD analysis, and the pavement age was interpolated for the corresponding yearly punchout data, which was used to establish the relationship with the %PO data. The %PO provides a way to consider the number of transverse cracks and the associated cracking pattern presented in the LTPP field data. This was done via the average crack spacing, which was determined by dividing the LTPP section length by the number of transverse cracks. The length of the LTPP section (i.e., 500 ft) was subsequently divided by the average crack spacing to represent the ultimate number of punchouts. The number of punchouts obtained from the LTPP survey was subsequently divided by the ultimate punchouts to find %PO. Table 34 shows the field number of punchouts and the associated %PO calculated using equation(75) and equation(76) below.

$$\%Po = \frac{N_{P.O.}}{U_{P.O.}} \times 100\% \qquad (75)$$

$$U_{P.O.} = \frac{L_s}{\left(\frac{L_s}{N_{tc}}\right)} \quad (76)$$

Where %Po is the Percent of punchouts for at each survey date, $N_{P.O.}$ is the LTPP records of punchout number at each survey date, $U_{P.O.}$ is the ultimate punchout number at each survey date, L_s is the length of the LTPP section, which is 500 ft, and N_{tc} is the LTPP records of the number of transverse cracks at each survey date.

Table 34-The LTPP number of punchouts and the associated %PO

Section Number	Survey date	Punchouts/section	%PO
40-4166	October 9, 1991	0	0.00%
40-4166	November 3, 1992	0	0.00%
40-4166	November 1, 1994	0	0.00%
40-4166	August 18, 1997	0	0.00%
40-4166	September 27, 1999	3	1.82%
40-4166	July 22, 2002	4	2.42%
40-4166	November 18, 2009	4	2.42%
40-4166	March 21, 2013	0	0.00%
40-4166	September 4, 2015	0	0.00%
48-5323	June 11, 1991	0	0%
48-5323	May 19, 1993	5	1.39%
48-5323	August 10, 1995	6	2.55%
48-5323	May 14, 1997	22	8.82%
48-5323	June 16, 1999	54	21.93%
48-5323	June 25, 2002	38	17.65%

The data in Table 34 was used to establish the relationship between %PO and %E using equation(74) for sections 40-4166 and 48-5323. Unlike the damage generated from the Pavement ME software, which is based on the bending fatigue damage, the %PO calculated from the relationship with the %E accounts for the erosion damage underneath the CRC pavement. Figure 99 (c) and (d) show the relationship between the %PO with the %E for each section. Table 35 shows the fitting coefficients and the R2 value for each section.

The fitted equations were then used to determine the existing %PO with respect to the actual pavement life. These %PO determinations are sensitive to not only the effects of repeated traffic loading but also erosion damage as an improved reflection of field performance. Nonetheless, this sensitivity could not be translated into the coefficients used in the Pavement ME punchout model due to its inherent limitations and insensitivity to the erosion process.

Table 35-Fitting coefficients for the %E vs. Age, %E vs. %P.O. and %P.O.- ME vs. %P.O.- Field relationships

Coefficient	Section 40-4166 %E vs. Age	Section 40-4166 %E vs. %P.O.	Section 48-5323 %E vs Age	Section 48-5323 %E vs. %P.O.
ρ	11.29	150.40	13.17	57.46
B	1.00	1.00	1.0	1.0
R^2	0.89	0.85	0.98	0.77

Calibration of Pavement ME Punchout Model

The calibration of the pavement ME punchout model was carried out by considering the damage generated from the Pavement ME software and correlating it to the field punchout data to obtain the coefficients A, α, and β in equation(73).The punchout model calibration was conducted in two steps. The first step was to calibrate the A value, which is in the numerator of the equation (73). The A value in the punchout equation was set to be the ultimate number of punchout in any section. Therefore, the percent of punchout can be represented by equation (77) . The second step is to fit the Pavement ME punchout equation with the field punchout number to calibrate α, β. In this step, the A value was set as a constant.

$$\%P.O. = \frac{PO}{A} = \frac{1}{(1+\alpha.FD^{\beta})} \tag{77}$$

For the calibration of A, the least squared method in EXCEL SOLVER was used to minimize the squared error between the field punchout percent calculated from its relationship with percent of erosion and the calculated percent of punchout (PO/A) in equation(77). By applying the mentioned procedure, Figure 100- (a) and (b) show the relationships between the pavement ME damage with the %PO from the field data and the calculated PO/A.
As shown in the figure, the data exhibit some differences in the damage in the range of 0 to 0.001 for sections 40-4166 and 48-5323. As fatigue damage increases, the difference between the two damages decrease, and it is obvious in the data associated with the fatigue damage range of 0.001 and above for sections 40-4166 and 48-5323.

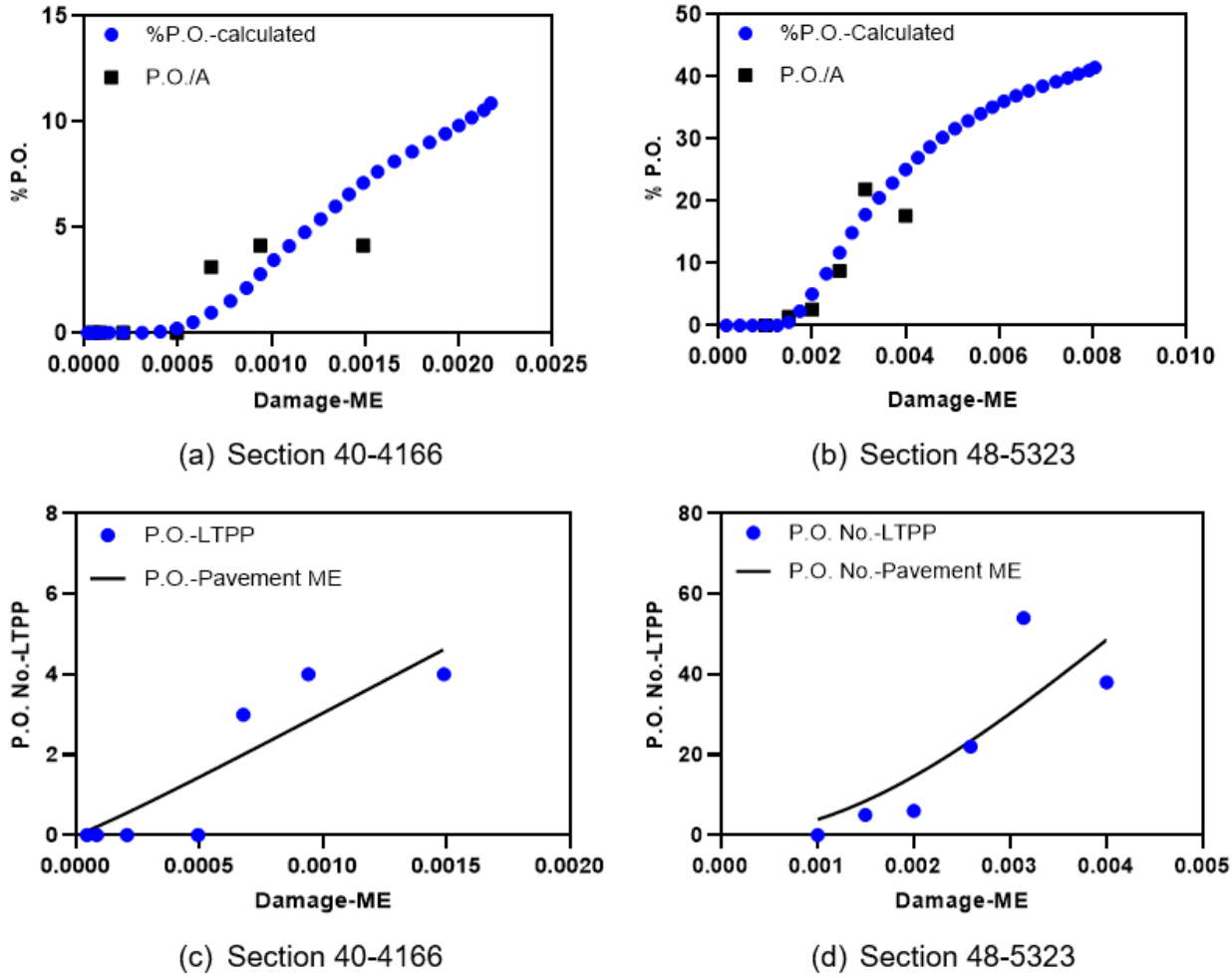

Figure 100-Punchout model calibrated coefficients representation

After determining the A coefficient, the punchout number determined from the fitting curve of punchout number vs. pavement age was used to fit the Pavement ME punchout model for the number of punchouts. In the pavement ME equation, the A coefficient was set as a constant, and α, β coefficients were calibrated.

Table 36-Pavement ME P.O. number equation- calibrated coefficients for punchout model

Calibration Coefficient	Pavement ME	Section 40-4166	Section 48-5323
A	107.73	96.76	222.00
α	2.475	0.016	6.03*10-5
β	-0.785	-1.095	-2.00
R^2	-	0.78	0.70

As shown from Figure 100 and Table 36, that punchout performance depends, in part, on the type and quality of the base and subbase layers. Section 40-4166, which is a CRC pavement on a cement-treated base, shows a lower number of punchout and associated fatigue damage throughout the analyzed pavement life. On the other hand, Section 48-5323 shows a much higher amount of punchout distress at a much lower fatigue damage level, in comparison.

Prediction of Punchouts in Other Oklahoma Sections

FWD data for sections 40-4158 and 40-5021 was analyzed to estimate the amount of erosion damage that had occurred over the life of the pavement. Section 40-4158 consisted of a hot mix asphalt (HMA) base, while section 40-5021 consisted of an asphalt treated base. Both sections show no punchout distress based on LTPP records. The annual average daily traffic (AADT) for section 40-4158 at the start year was 4200, with 14% trucks. Similarly, section 40-5021 had 2959 AADT with 17% trucks. Both sections had no significant growth in traffic over their service lives to date; this, along with the low traffic level, may explain why these sections had not yielded any punchout distress. However, estimates of the existing erosion damage in these sections can be utilized to estimate when punchouts are expected to develop based on the performance of section 40-4166.

This analysis was performed in the following steps:

1. Obtain the %E - pavement age relationship (equation(74)) for sections 40-4158 and 40-5021 shown in Figure 101.

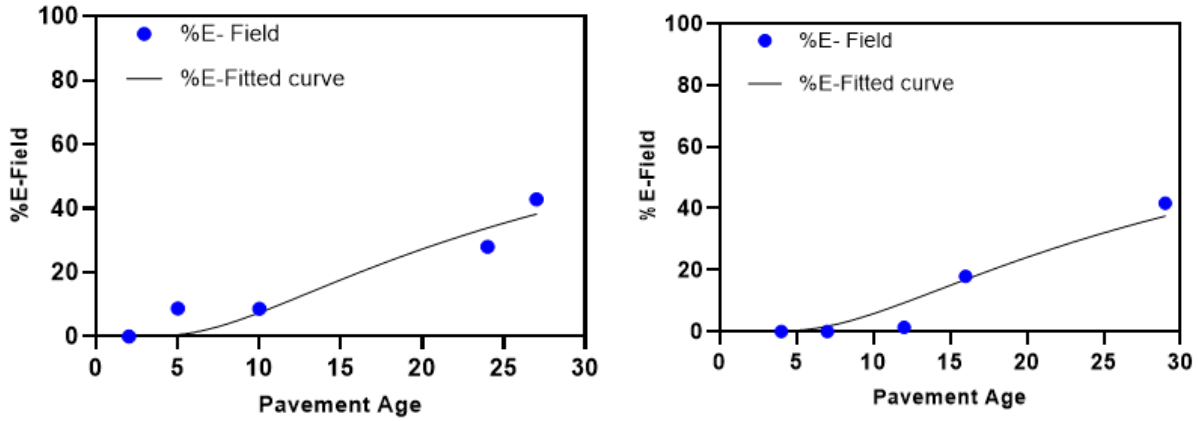

(a) Section 40-4158 (b) Section 40-5021

Figure 101-Percent of erosion with pavement age relationships

Table 37-Fitting Coefficients for the %E vs. Age

Coefficients	Section 40-4158 %E vs. Age	Section 40-5021 %E vs. Age
A	100.0	100.0
ρ	25.95	28.46
B	1.00	1.00
R^2	0.89	0.94

2. Determine the critical damage from Figure 99 (a) and associate it with the pavement age when that amount of damage is generated in sections 40-4158 and 40-5021. This determination is conveniently found from the damage accumulation (D) generated from Pavement ME analysis of the traffic (and associated pavement age) that occurred in those sections.

Using the results for section 40-4166 shown in Figure 100 (c), the damage accumulation in both sections could also be associated with the %E. Both relationships (D vs. %E and D vs. Age) were linear. Slope and y-intercept of the linear relation are shown in Table 38 below.

Table 38- Linear equations coefficients

Coefficients	Section 40-4158 D vs %E	Section 40-4158 D vs Age	Section 40-5021 D vs %E	Section 40-5021 D vs Age
m	$8.390*10^{-6}$	$1.403*10^{-5}$	$1.143*10^{-5}$	$1.804*10^{-5}$
y-intercept	$3.485*10^{-5}$	$-2.419*10^{-5}$	$6.237*10^{-5}$	$-2.975*10^{-5}$

3. Using the coefficients in Table 38 and the damage value of 0.0005, estimate the time to punch-out and associated %E.

Time to punchouts is calculated from the end of the 30 years analysis period, which ended in 2018 for section 40-4158 and 2016 for section 40-5021 and shown in Table 39.

Table 39-Predicted time and %E to punchouts

Section	Predicted time to punchout (yrs)	Predicted %E to punchout
40-4158	7	55
40-5021	0	38

As shown in Table 39, section 40-4158 is predicted to have punchout distress within 7 years after the end of the analysis period, while section 40-5021 is supposed to have punchout distress by the end of the analysis period. For section 40-5021, the latest LTPP distress survey date was conducted in 2015, which means that there is a high possibility of having punchouts recorded in the upcoming performance survey. The equivalent thicknesses in this section diminished nearly an inch from 2002 to 2012.

Conclusions

This study developed a new calibration approach for the CRC pavement punchout model applicable, incorporating sections that have shown little or no distress. Relating the punchout distress with erosion damage to validate calibration coefficients was found to be feasible and applicable for a different type of base and subbase materials.

The proposed methodology revealed the following points about the punchout formation and model calibration:

1. Erosion development is a factor in punchout distress, and its relationship to the incidence of punchout distress appears to be represented by a sigmoidal relationship.
2. The time required for punchout formation and the number of punchout depends on the base and subbase layers' inherent resistance to erosion.
3. Assuming that the A factor in the Pavement ME model is equivalent to the ultimate number of punchouts in a given length of CRC pavement appears to be reasonable.
4. The extension of the performance between sections showing distress and those not showing distress was based upon the applicability of extending the %E vs. %PO relationship for the non-distressed pavement sections, which should be further validated in future performance studies of CRC pavement.

The calibration methodology required improving upon FWD analysis to assess the degree of bonding by determining the degradation of shear strength over time as well as estimating the percent of erosion. The percent erosion data provided a useful relationship with the LTPP punchout data. The punchout records were also used to calculate the percent of punchout, which played a crucial role in incorporating field transverse cracking and spacing into the

erosion-punchout relationship. The calibration process assumed the C1 and C2 coefficients in the allowable loads to failure model were sufficient for calibration purposes.

Calibration of JPCP Sections

The fatigue mid-span transverse cracking and faulting of edge joints are considered the main distresses in JPCP. The two distresses are presented in the pavement ME software and must be calibrated to achieve an accurate design output. As mentioned before, the main challenge in the pavement ME performance model's calibration is the validation of the calibrated coefficients, which requires having at least 20 sections with considerable distress data. This challenge was resolved in the CRC pavement by introducing a new calibration methodology that depends on the erosion analysis using the FWD data. On the other hand, the JPC pavements calibration process faces other issues that limit the ability to calibrate the Oklahoma sections. the main issues in the calibration of the JPC pavements in Oklahoma can be summarized as:

1. An insufficient number of JPC pavement sections in Oklahoma. The GPS LTPP sections are only 4.

2. All the GPS LTPP sections do not show fatigue distress, which magnifies the problem of not having enough sections.

3. Unlike the punchout model in CRC pavement, which considers erosion in the material characterization of the pavement sections but does not account for it in the cumulative damage calculations, the pavement ME cracking model for JPC pavement depends solely on the mechanical loading. Therefore, the ability to develop a methodology that depends on erosion analysis is inaccurate for the case of the Pavement ME cracking model.

4. The faulting records from the LTPP show some of the data. However, the faulting model uses an incremental approach that requires calibrating 7 coefficients. additionally, it depends on many factors such as base/subbase erodibility factor, set gradient for curling and warping deflection calculations, and base freezing index, which vary from a base type to another. Therefore, it is only possible to calibrate these coefficients through sensitivity analysis of determinant factors. This cannot be achieved without the existence of multiple pavement sections with the same pavement structure in order to accurately estimate these factors and validate the new calibration coefficients.

Assessing Pavement ME Cracking Model

As mentioned before, due to the limitation of sections with considerable distress in the Oklahoma sections, the research team identified out-state sections that can be used to validate national calibration coefficients for JPC pavement performance models. The main criteria for the selection of these sections are the availability of traffic data and the climatic zone. In this part, three sections in Arkansas were used to validate the pavement ME JPCP cracking model and its coefficients for the state of Oklahoma sections. This validation was performed in the following steps.

1. Determine the transverse cracking number from the LTPP database for sections 05-0213, 05-0217, and 05-0218 . Section 05-0221 was not selected due to the low number of transverse cracking presented. The number of transverse cracking is shown in Table 40.

2. Calculate the cracking fraction for each section. The cracking fraction was calculated by dividing the number of cracked panels over the total number of panels, as shown in the equation(79). The total number of panels in the 1-mile section (L_s) was found by dividing the section length by joint spacing, which was set as 15 ft as shown in equation (78).

$$total\ number\ of\ panels = \frac{L_s}{JointSpacing} \quad (78)$$

$$\mathrm{CRK} = \frac{\mathrm{Panels_{crk}}}{\text{total number of panels}} \quad (79)$$

3. Calculate the number of cracked panels. The number of cracked panels was determined by (i) calculating the average spacing of the transverse cracking, as shown in equation(80). (ii) Using average crack spacing to calculate the cumulative distance from a reference point for a one-mile distance (iii) using the 15 ft joint spacing to calculate the cumulative distance from a reference point over a one-mile distance (iv) divide the 15 ft panel into 5 ft long sub-sections and use middle third to calculate the lower and upper cumulative distances from a reference point over a one-mile distance (v) match and count cumulative distance from step (ii) with cumulative distance from steps (iii) and (iv). The purpose of this procedure is to dismiss all joints and environmental cracking and count only for the Pavement ME mechanical induced transverse cracking that usually happens in the middle third of the panel. This procedure was applied mainly on section 05-0218, as it has 46 transverse cracks. Sections 05-0213 and 05-0217 have only 15 and 10 transverse cracks, respectively, and they were considered a mid-span transverse cracks.The cracking fractions for all sections were found, as shown in Table 40.

$$Average\ transverse\ cracking\ spacing = \frac{L_s}{N_{tc}} \quad (80)$$

Table 40-Cracking fraction calculations

Year	Transverse Crack 05-0213	Transverse Crack 05-0217	Transverse Crack 05-0218	CRK 05-0213	CRK 05-0217	CRK 05-0218
1993	0	0	0	0.00	0.00	0.00
1994	0	-	-	0.00	-	-
1995	0	0	0	0.00	0.00	0.00
1996	0	0	0	0.00	0.00	0.00
1997	-	2	8	-	0.0057	0.0227
1998	0	0	9	0.00	0.0000	0.0256
1999	0	2	11	0.00	0.0057	0.0313
2000	0	4	8	0.00	0.0114	0.0227
2001	0	2	10	0.00	0.0057	0.0284
2002	3	-	-	0.0085	-	-
2003	-	2	11	-	0.0057	0.0313
2004	2	-	-	0.0057	-	-
2005	3	2	17	0.0085	0.0057	0.0483
2006	-	7	17	-	0.0199	0.0483
2007	-	9	18	-	0.0256	0.0511

Year	Transverse Crack 05-0213	Transverse Crack 05-0217	Transverse Crack 05-0218	CRK 05-0213	CRK 05-0217	CRK 05-0218
2008	7	9	20	0.0199	0.0256	0.0568
2009	-	10	24	-	0.0284	0.0682
2010	13	-	-	0.0369	-	-

4. Calculate the fatigue damage. The ideal way to determine the fatigue damage is to run the LTPP acquired data inputs in the pavement ME.

5. Use the pavement ME cracking equation shown below to fit the field data, as shown in Figure 102. Table 41 shows the best fit for C4 and C5. The current national calibration is 0.52 for C4 and -2.17 for C5.

$$CRK = \frac{100}{1 + C4(D_F)^{C5}} \quad (81)$$

Where CRK is the predicted amount of bottom-up or bottom-down cracking as fraction and D_F is the cumulative fatigue damage.

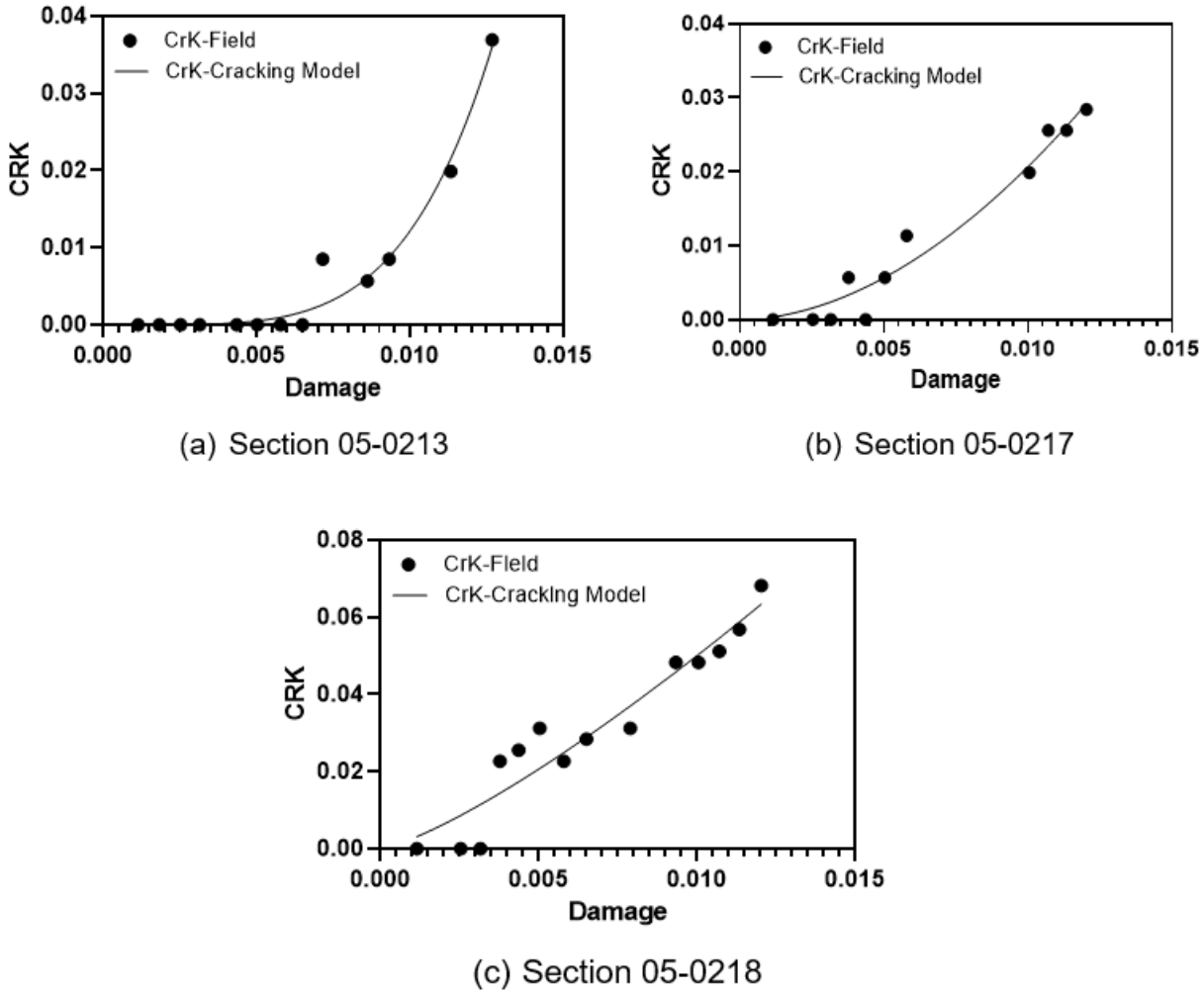

Figure 102-Pavement ME cracking model- field data fitting

Table 41-Pavement ME Cracking equation- best fit C4 and C5 for cracking model

Calibration Coefficient	Pavement ME	Section 05-0213	Section 05-0217	Section 05-0218
C4	0.52	5.6e-06	0.8835	5.593
C5	-2.17	-4.583	-1.869	-1.276
R^2	-	0.97	0.96	0.91

As shown in Figure 102 and Table 41, all sections showed a good fit between the pavement ME cracking model and the field data. However, due to the lack of JPCP sections as well as distress records in Oklahoma. Other practices can be embraced into the pavement ME software design by optimizing the gradient set for curling and warping stresses calculations (this gradient set is defaulted as -10° F in pavement ME). As shown in Figure 103, the pavement ME cracking model using the national coefficients shows the same trend for all sections. The nationally calibrated cracking model predicts the cracking fractions , especially at low damage levels, as presented in section 05-0213. It is worth to point out that the construction date for this section was December 1993, which explains the good fit between the cracking model with national coefficients and the field cracking data. This introduces the fact that the magnitude of the set gradient is significant to the equivalent temperature difference and to the set gradient stress. A "zero-stress" or "built-in" permanent gradient in pavement ME depends mainly on the input of the set gradient for curling and warping stresses calculations, which defaulted as -10°F in the pavement ME software.

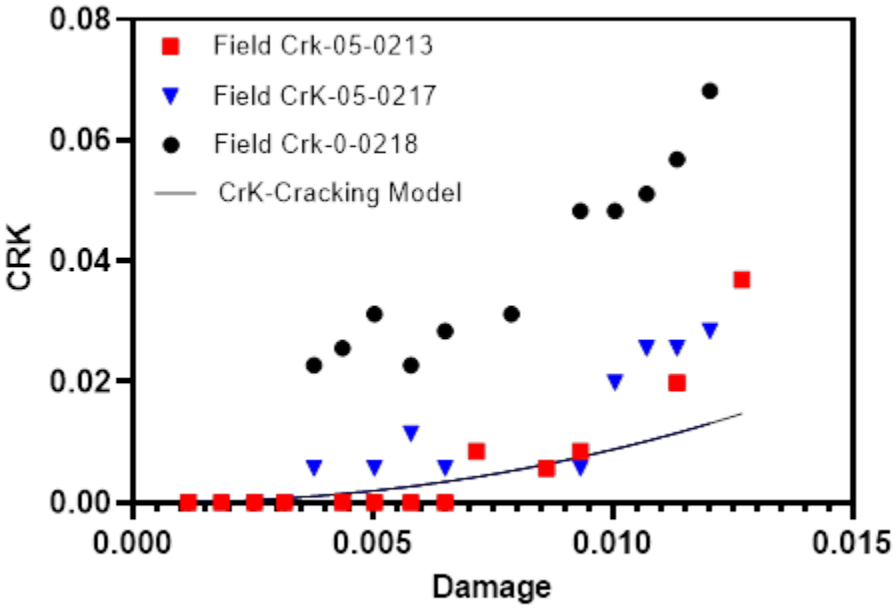

Figure 103-All sections cracking data comparison with the damage

Extra work has been conducted to determine the relationship between the C4 and C5 coefficients and the set gradient used in pavement ME software. The main goal of this step is to identify the importance of using the accurate set gradient in pavement design and its relation to the development of cracking in JPC pavements. To perform this work, determining the sum of the stress ratio of gradient set r_{-10^oF} and the stress ratio of the curling and warping stresses r_{cw} is significant. This value can be calculated by subtracting the stress ratio of mechanical loadings

($r_{mechanical}$) from the stress ratio (r) obtained from the Pavement ME analysis. The required value is presented in the equation below:

$$\Delta r = r_{pavement\ ME} - r_{mechanical} \quad (82)$$

Where,

$$\Delta r = r_{-10^{o}F} + r_{C.W.} \quad (83)$$

In order to estimate the stress ratio from the mechanical loadings, the Portland Cement Association (PCA) design procedure was incorporated. The PCA requires the subgrade reaction coefficients k and pavement thickness. The k value was taken as 50 psi. The stresses from single, tandem and tridem axle were calculated and aggregated. The modulus of rapture generated by the pavement ME over the analysis period was used to calculate the $r_{mechanical}$ as follows:

$$r_{mechanical} = \frac{\sigma_{mechanical}}{M.O.R} \quad (84)$$

Where,

$\sigma_{mechanical}$ are the stresses induced by single, tandem and tridem axles using PCA procedure
M.O.R is the modulus of the rapture of concrete over the pavement ME analysis period

After determining the $r_{mechanical}$ for each section, it was used to calculate the Δr by subtracting the $r_{mechanical}$ from the Pavement ME stress ratio (r). Table 42 shows the average Δr for each field section as well as for the pavement ME analyses of each section. Figure 104 and Figure 105 show the relationship between the average Δr and the C4 and C5 coefficients, respectively.

Table 42-Average Δr, C4 and C5 values

Section	Average Δr	C4	C5
Pavement ME	0.846	0.520	-2.170
05-0213	0.797	5.64E-06	-4.583
05-0217	0.805	0.884	-1.869
05-0218	0.887	5.593	-1.276

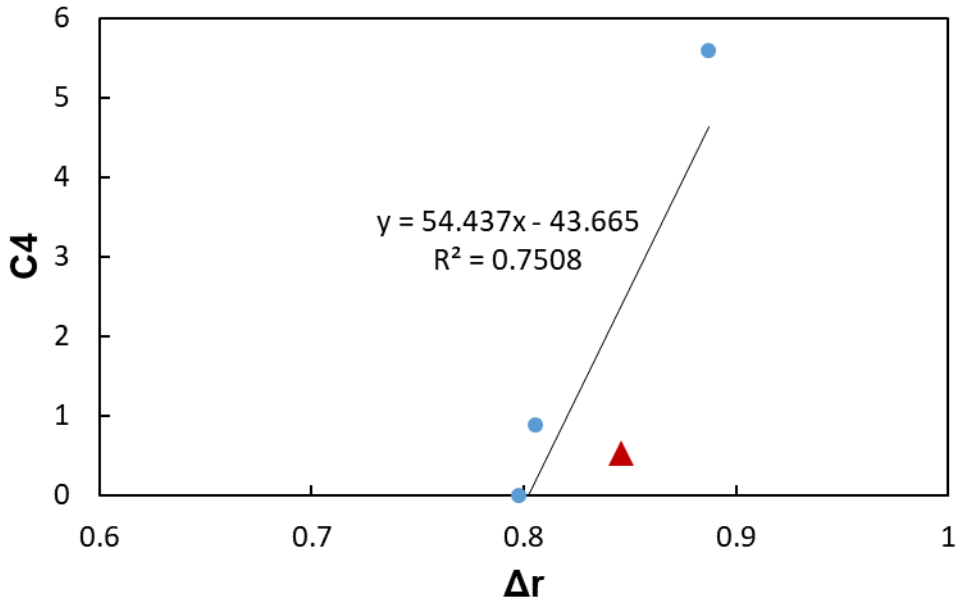

Figure 104-Average Δr and C4 relationship

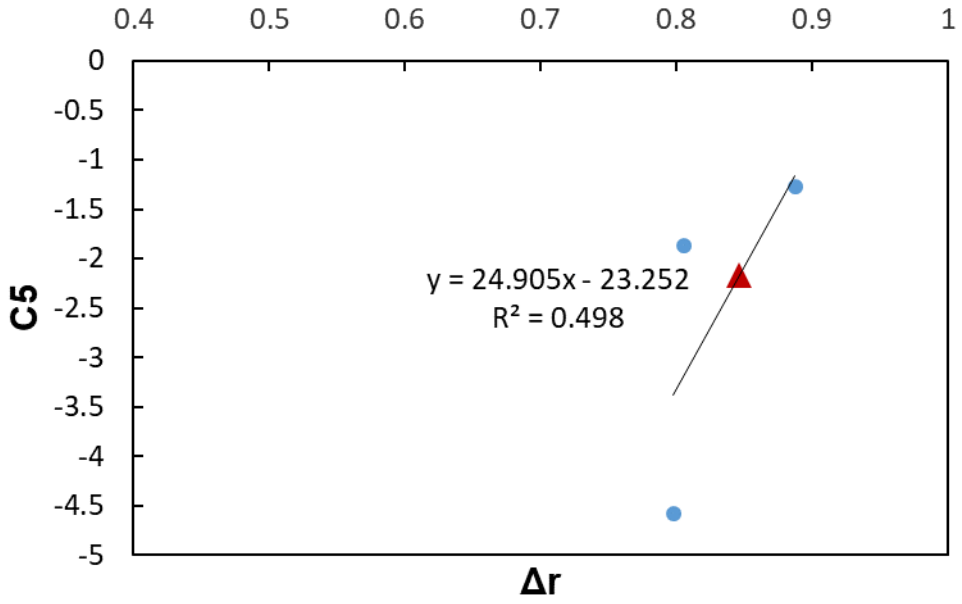

Figure 105-Average Δr and C5 relationship

In the figures above, the blue dots represent the field data while the marron dot represents the pavement ME national calibration. It is well accepted that the set gradient will vary with climatic and material factors that affect how the concrete sets during the hardening process. Analysis of the amount of heat and moisture transport that occurs during the setting of the concrete is a basis for anticipating the development of the set as it occurs throughout a paving operation. In these figures, it is shown that the pavement ME condition fits the plot and serves as an indication about the ability to introduce an accurate input for the gradient set during the design procedure as well as suggest the importance of curing during construction to preserve the set

gradient. Adopting these recommendations will allow dismissal of the need for local calibration for the JPC pavement cracking model.

Assessing pavement ME Faulting Model

The faulting model in pavement ME software determines transverse joint faulting using an incremental approach. This incremental approach requires determination of the faulting at each month, and it is dictated by the current faulting value. The main issue with the faulting model is the number of calibration coefficients (i.e., C1,….,C7) and other factors such as base/subbase erodibility factor, curling, and warping deflections and set gradient. Therefore, the local calibration of faulting for JPC pavements requires the presence of many JPC sections that can be used for calibration as well as for validation of new coefficients. Due to the limited number of JPC pavement sections in Oklahoma, this part of the report has only dealt with assessing the pavement ME faulting model for use in the Oklahoma sections. To achieve this goal, the field transverse joint faulting values were compared with the faulting values generated by pavement ME software.
Figure 106 below shows this comparison, as well as the R^2 value.

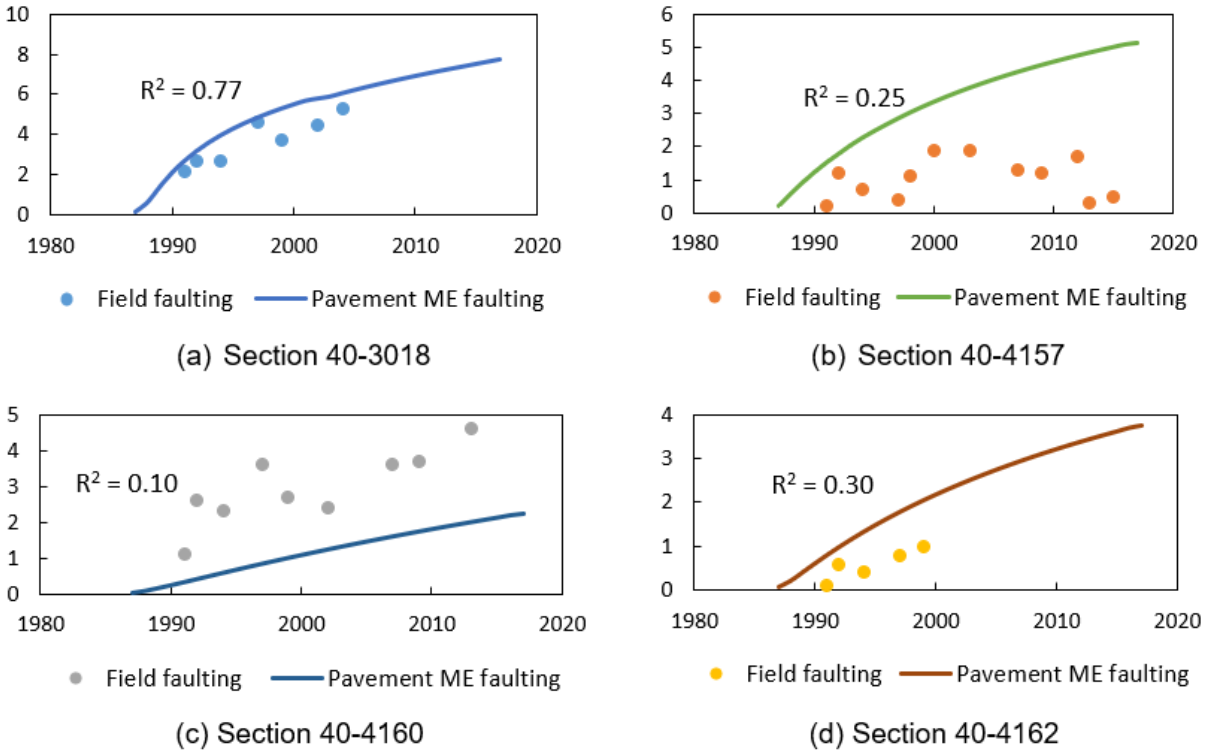

Figure 106-Pavement ME and field faulting comparison

As shown in Figure 106, the pavement ME faulting model slightly overestimate the field faulting, especially as indicated in sections 40-3018, 40-4157, and 40-4162. Moreover, section 40-4157 shows the fluctuation in field records, which indicate the existence of maintenance and rehabilitation activities such as the joint load transfer restoration in 2012. This overestimation can be due to many factors that dictate the faulting model. The main factors are the

base/subbase erodibility input as well as the curling and warping temperature set (which is defaulted as -10°C) that used to calculate the curling and warping stresses in Pavement ME software. On the other side, an onsite practice like proper curing techniques can have a significant impact on the faulting levels. Therefore, it is important to accurately input the set gradients and base/subbase erodibility during the design phase as well as establish proper curing practice in the construction site to reduce local conditions impact and eliminate calibration requirement for faulting. considering these two recommendations, the use of a faulting model with national calibration coefficients can be suitable for Oklahoma sections.

DEVELOPMENT OF INPUT-ME SOFTWARE

Pavement ME requires an extensive amount of input data. Availability and accuracy of input data is a serious concern of the designers. To facilitate using the Pavement ME, interface software was developed. This software provides Pavement ME input data based on the Oklahoma material, traffic, and climate properties. A database was provided from the Oklahoma Pavement materials, traffic, and climate data. INput-ME reads the required information from the database and generates an input compatible by Pavement ME. This software was developed by using QT creator. QT Creator provides a cross-platform, complete integrated development environment (IDE) based on C++ programing language and is a tool for application developers to create applications for multiple desktops, embedded, and mobile device platforms (*71*).

Input ME includes three modules: a) material; b) traffic; and c) calibration coefficients. Each module provides specified data for the corresponding Pavement ME inputs for designing pavements in Oklahoma. Figure 107 shows the main window of the INput-ME interface.

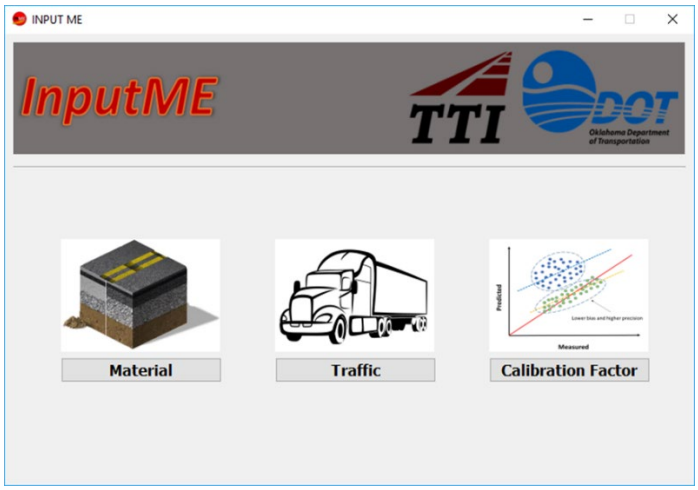

Figure 107- The Main window of INput-ME

Each dialog provides the information in the three levels of hierarchy. At level 1, the user inserts the essential measured values of properties for each parameter. At level 2, the Oklahoma-specified data collected from different sources will be shown. The user can edit the provided data and insert its own values for each parameter. At level 3, the software provides and locks the data, and the user is able to review and export it as an input file for Pavement ME. In the following, the application of each module will be explained.

Material Module

The material module classifies the materials according to the Pavement ME Design. This module enables the user to select materials for the subgrade soil, stabilized soil, unbound base material, bound treated base material, AC, and cement concrete materials. Figure 108 shows the material dialog. In the following, the application of each material dialog will be explained.

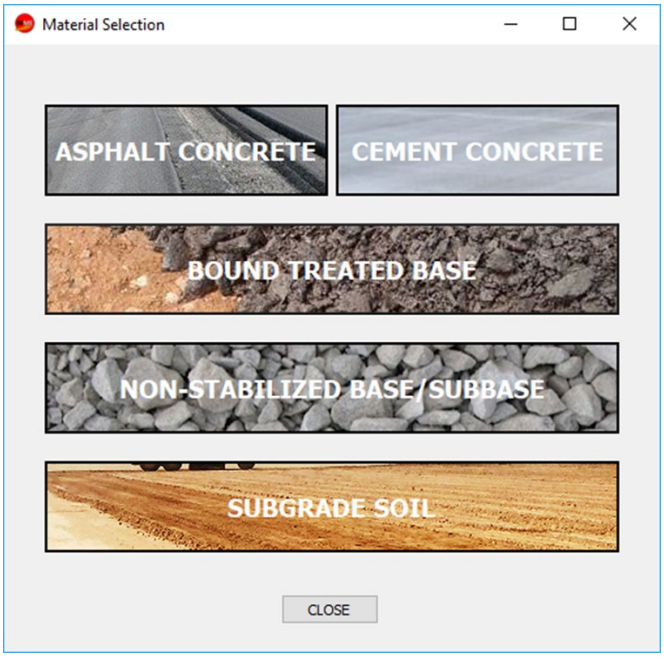

Figure 108- The material dialog

Subgrade Soil

The subgrade soil dialog consists of two tabs, which indicate the sources of the provided information. The hierarchical data tab provides the subgrade soil properties at three levels. The NCHRP 9-23 project provided some of the soil properties for the US. The NCHRP 9-23 tab provides information for the given latitude and longitude.

Hierarchical Data Tab

This tab provides information on the soil properties for the three levels of hierarchy. At level 1, the user inserts the essential measured values of properties for each parameter. Figure 109 shows the subgrade soil dialog for level 1 and Level 2 data.

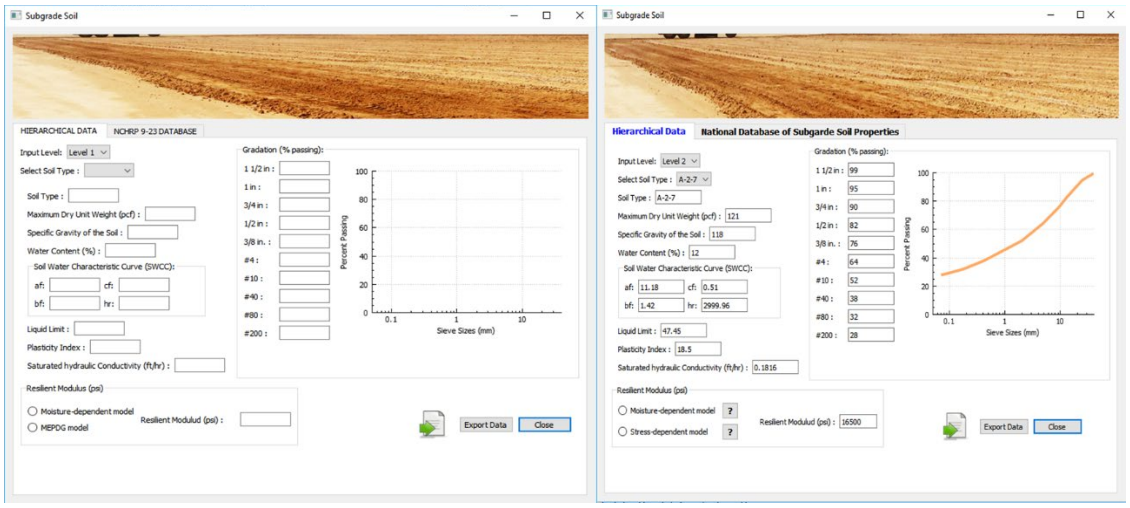

Figure 109-Hierarchical Data Tab – Level 1

At level 1, the user inserts the essential measured values of properties for each parameter. At level 2, the soil data collected from the state of Oklahoma for each soil type will be shown. The user can edit the provided data and insert its own values for each desired parameter. At level 3, the software provides and locks the data, and the user is able to review and extract it.

Subgrade Soil types include A-1-a, A-1-b, A-2-4, A-2-6, A-2-7, A-4, A-5, A-6, A-7-6. In addition, the properties of the soil will be modified by selecting the stabilizing agents such as lime 5%, 10%, fly ash 5%, 10%, Cement kiln dust (CKD) 5%, 10%. The provided subgrade soil properties in the hierarchical data tab include:

- Gradation
- SWCC properties and hydraulic conductivity
- Resilient Modulus
- LL and PI
- %WC and Unit weight
- Gs

In order to incorporate the moisture-dependent characteristic of the resilient modulus of unbound soil, a new constitutive model proposed by Lytton et al. for predicting the resilient modulus was provided (*29*). By selecting the “Moisture dependent Model,” the resilient modulus considering the moisture properties will be shown. This model incorporates the moisture dependency and stress dependency of the resilient modulus. In this model, the degree of saturation and the matric suction are proposed to discriminate the effect of moisture variations (*39*).The multiple regression analysis was performed to generate the predictive models for the constant coefficients in the resilient modulus model using a set of performance-related base course properties. The dry density, shape, angularity, and texture of the aggregates and the percent fine content are used in the predictive models. By clicking on “Export Data,” an XML version file will be generated, and the user is able to save the file wherever is desired. This file is readable by Pavement ME and can be imported as input to the desired layer.

NCHRP 9-23 Tab: The NCHRP 9-23 project provided a national database of pedologic soil families that contains the soil properties for subgrade materials needed as input to the Pavement ME. This database focuses upon the parameters describing the soil-water characteristic curves (SWCC), plasticity parameters of soil, gradation, and resilient modulus.

The NCHRP 9-23 tab provides this information for the given latitude and longitude. Figure 110 shows the NCHRP 9-23 database tab in the INput-ME interface.

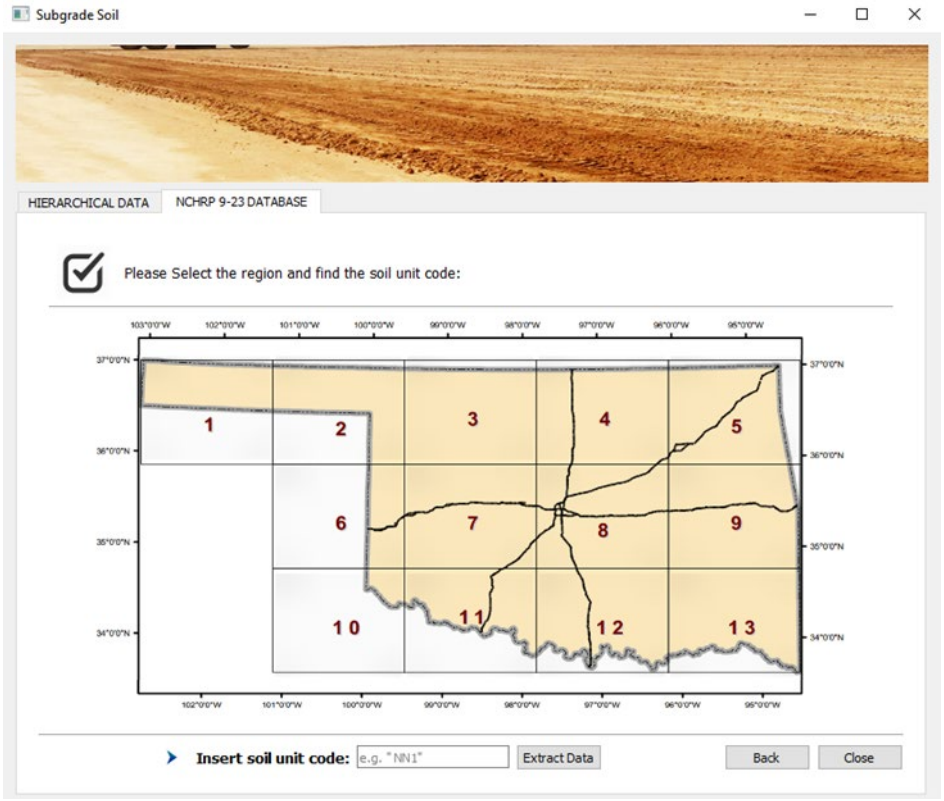

Figure 110- The NCHRP 9-23 database tab in INput-ME Software

The state of Oklahoma is divided into 13 regions surrounded by a wide range of coordinate legend. The appropriate section, based on the given latitude and longitude, should be selected by the user. By clicking on the section, the soil unit map will be shown. Figure 111 shows the soil unit map of region number 7. The soil unit code of the specific point can be selected from the given latitude and longitude, as well as a small legend of the selected region and its position. Also, a panning and zooming effect using mouse scrolling was enabled, So the user can easily see the soil unit code and the covered region by the soil types.

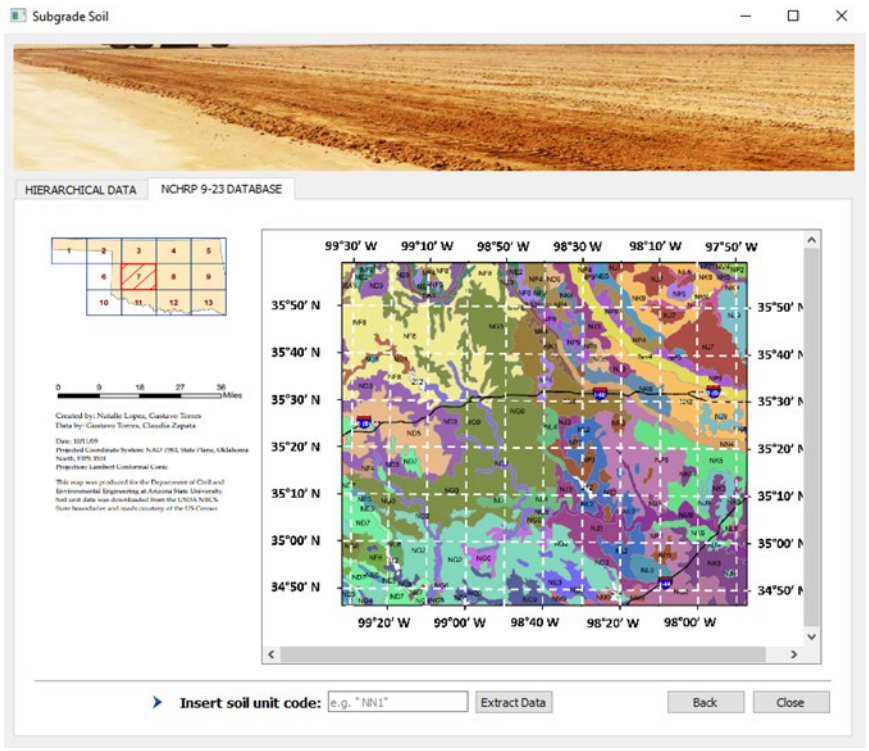

Figure 111- Soil unit map of region #7

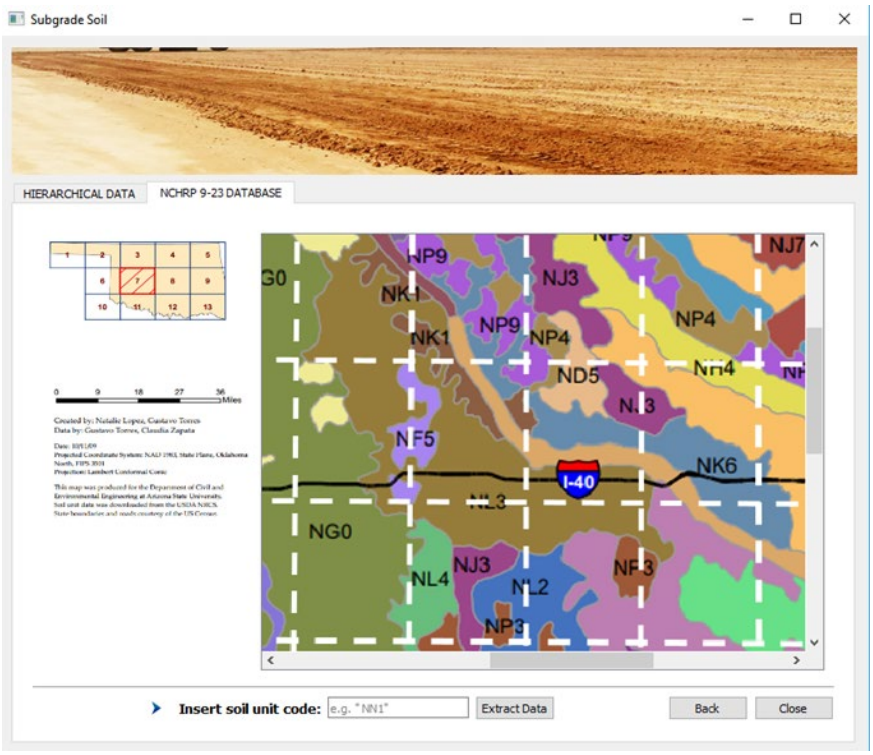

Figure 112- The zooming and panning in the soil unit map

After finding the appropriate soil unit code, the user can type in the text box at the bottom of the dialog. By clicking the “Extract Data” button, the properties of surface soil are extracted from the

NCHRP 9-23 database, and the results will be shown. Figure 113 shows the extracted soil properties for a sample soil unit.

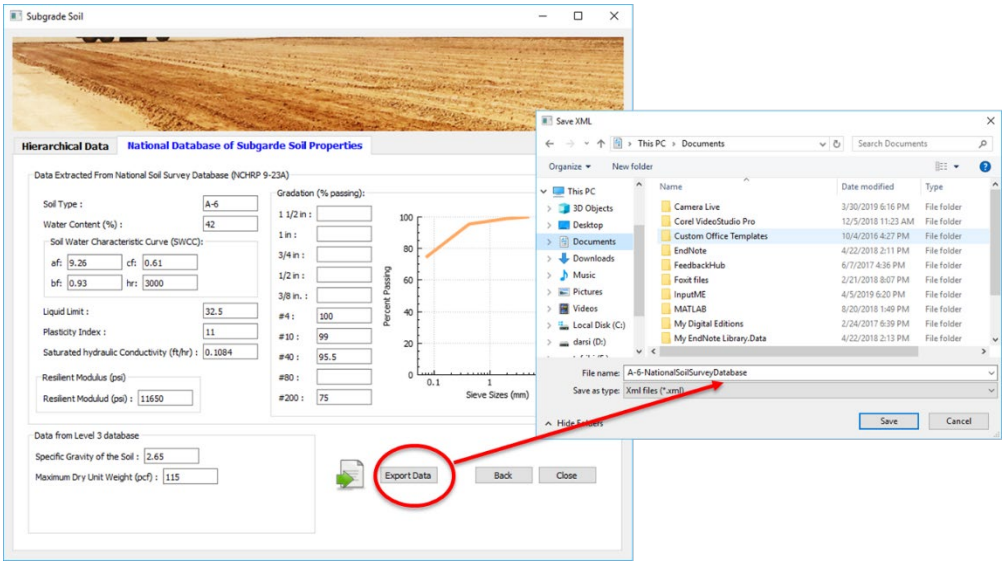

Figure 113- The extracted soil properties for Soil type of A-6

The provided subgrade soil properties in the NCHRP 9-23 Tab data tab include:

- Gradation
- SWCC properties and hydraulic conductivity
- Resilient Modulus
- LL and PI
- %WC and Unit weight
- Gs

By clicking the “Export Data,” a data file that is compatible with the Pavement ME input will be generated. The user can name and save the file in the desired directory.

Non-Stabilized Base/Subbase

This dialog provides the information for the unbound granular materials of base and subbase in three levels of hierarchy. At level 1, the user inserts the essential measured values of properties for each parameter. At level 2, the collected and classified data for each unbound granular type will be used. The user can edit the provided data and insert its own values for each parameter. Granular materials include A-1-a, A-1-b, A-2-4, A-2-6, A-2-7, crushed Stone, and crushed gravel. Figure 114 shows the non-stabilized base/subbase dialog for level 1 data. By clicking on the “Export Data” button, the data will be extracted in a format readable by Pavement ME.

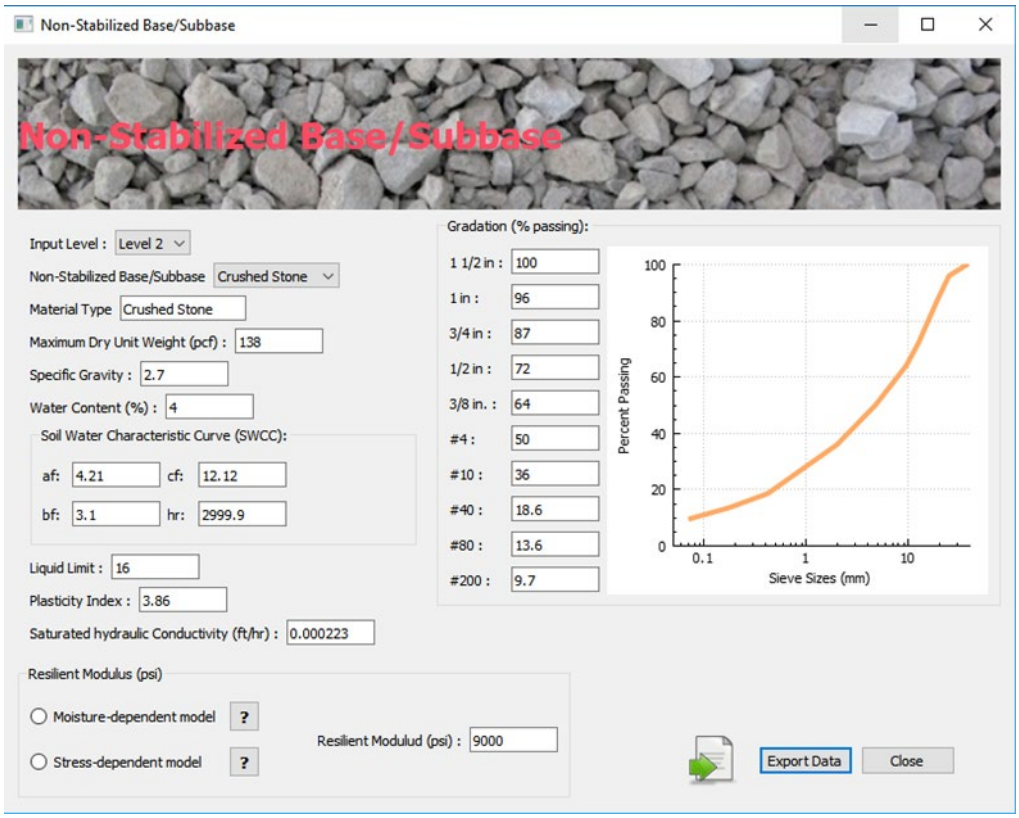

Figure 114- Unbound granular base material dialogue

Stabilized Base Material:

This dialog provides the required information for treated base and subbase materials in the three levels of hierarchy. Cement stabilized base types include cement-treated base, lean-concrete base, and cement-treated open-graded. The provided properties required for pavement ME design are unit weight, elastic modulus, Heat Capacity, and Thermal Conductivity. The unit weight and elastic modulus are gathered from the LTPP database from neighbor states together with the state of Oklahoma. The heat capacity and thermal conductivity are gathered from the Pavement ME database. By clicking on the “Export Data” button, the data will be extracted in a format readable by Pavement ME.

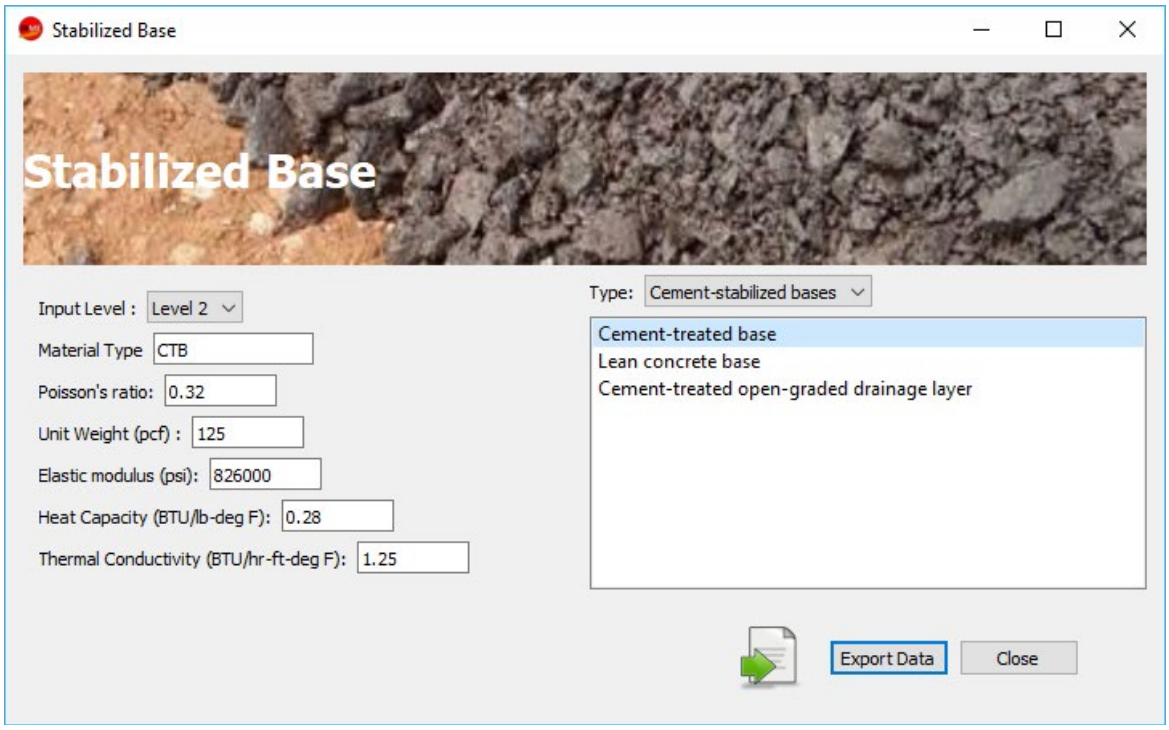

Figure 115- Stabilized base material dialogue

Asphalt Concrete

This dialog provides information for the asphalt concrete material in the three levels of hierarchy. At level 1, the user inserts the essential measured values of properties for each parameter. The mix designs used in the database include the common mixes used in the state of Oklahoma, and the provided Level 2 data are gathered from the dynamic modulus and the creep compliance test results reported in the previous ODOT research studies (*11*, *26*, *35*). There is a wide range for the sieve analysis and gradation for each asphalt concrete mix in the ODOT research. However, the most used gradation was provided as Level 2 in the Input-ME database. The binder properties include the PG 64-22, PG 70-22, and PG 76-22, which are the common binder types used in the asphalt concrete of the state of Oklahoma. At level 2, the shear modulus is gathered from the DSR test results reported by the ODOT research.

The intercept of temperature susceptibility relationship (A) and the slope of temperature susceptibility relationship (VTS) was provided in the NCHRP 1-37A effort. Figure 116 shows the binder properties and mix gradation in asphalt concrete dialog. By clicking on the “NEXT” button, dynamic modulus, and creep compliance data for the selected mix and binder type will be generated.

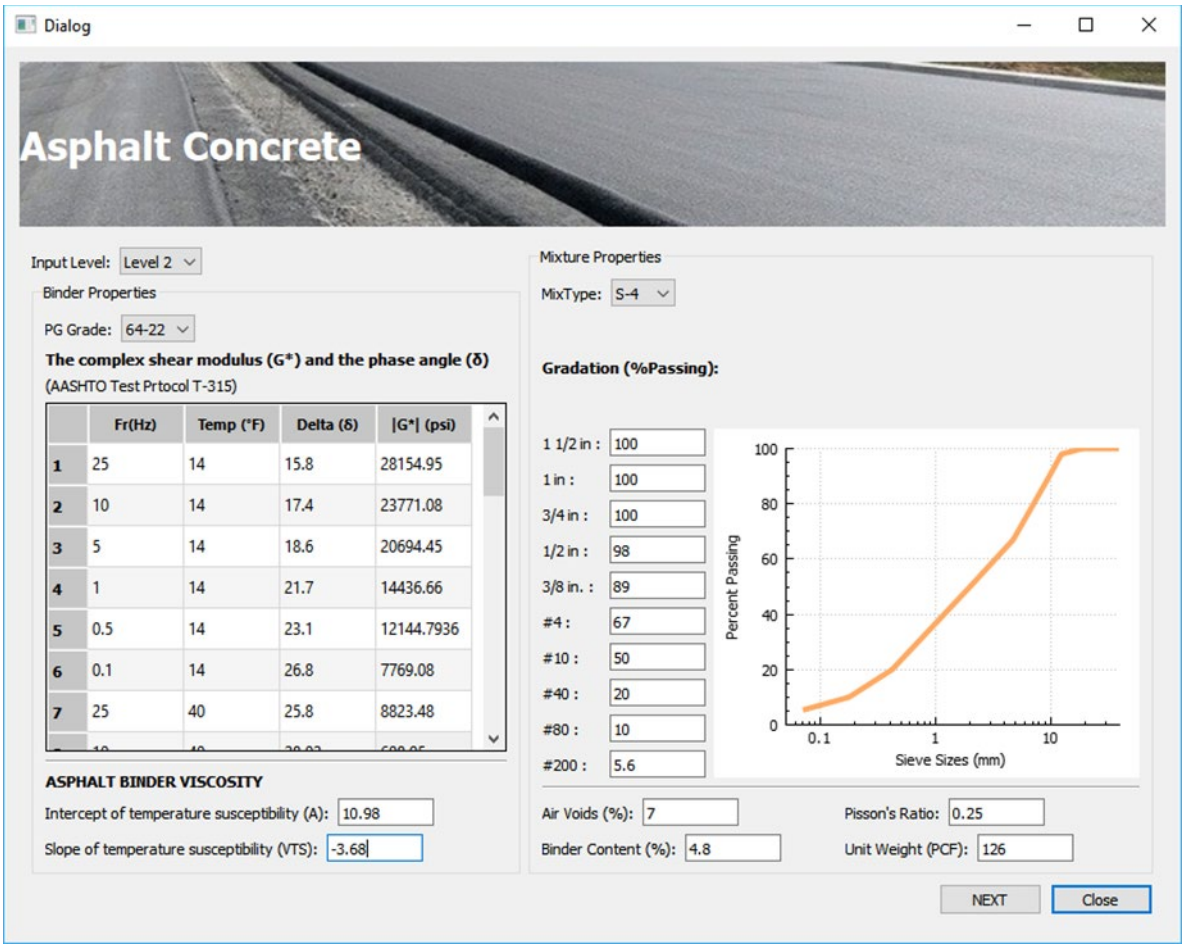

Figure 116- Binder properties and mix design gradation in asphalt concrete

Figure 117 shows the complex modulus and creep compliance in asphalt concrete dialog. In addition, the indirect tensile strength measured for each mix design is shown and provided in the INput-ME database. The heat capacity, thermal conductivity, and thermal contraction were provided in the NCHRP 1-37A effort and will be shown for the selected mix and binder type.

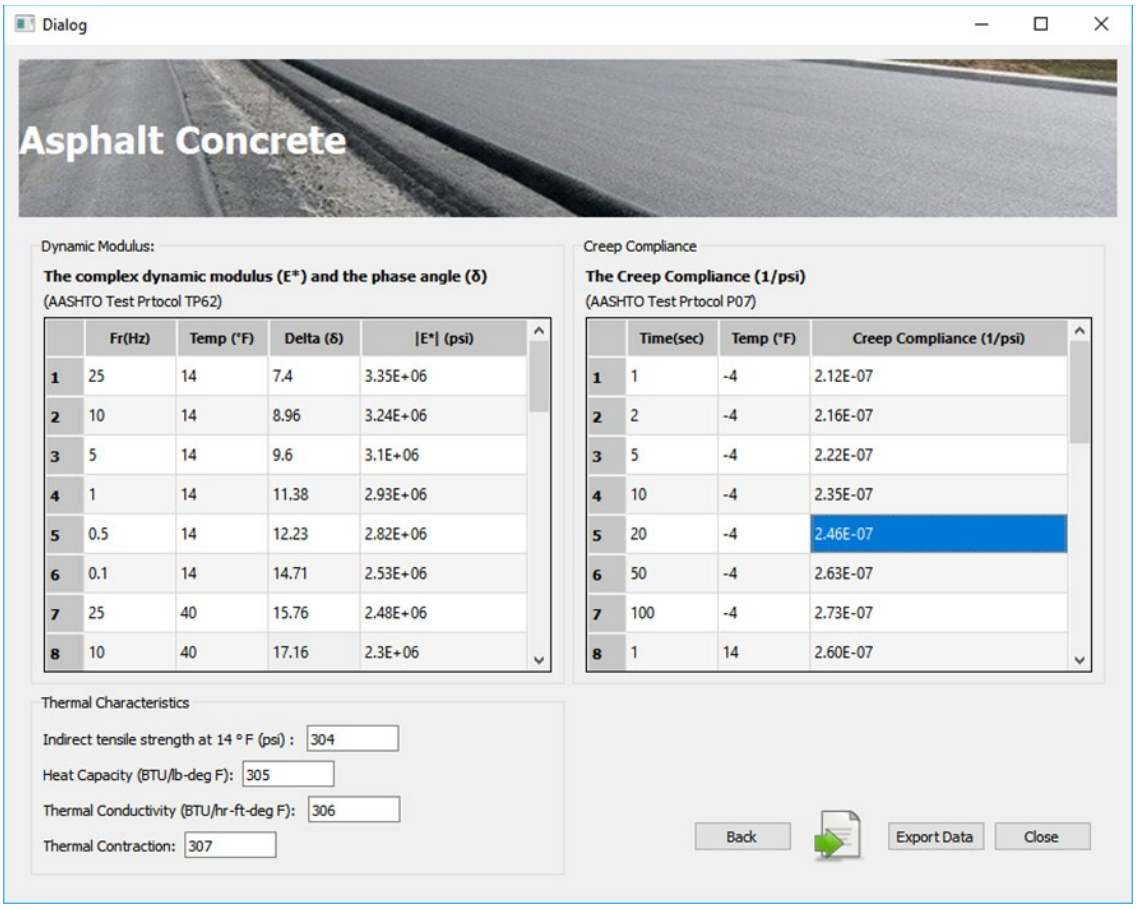

Figure 117- The complex modulus and creep compliance in asphalt concrete

By clicking on the “Export Data,” the asphalt concrete data for the selected mix and binder type as an XML file will be generated, and the user is able to import the generated file into the Pavement ME Design.

Traffic

This dialog provides information for the traffic data in three levels of hierarchy. At level 1, the user inserts the required measured properties for each parameter. At level 2, the typical traffic data for the selected road type will be shown, and the user is able to review and edit the provided data. At level 3, the user is able to review the data, but it is not editable. The level 2 data were provided for different road types, including Interstate urban principal arterial, non-interstate urban principal arterial, rural principal arterials, and major and minor rural collectors. These data were collected from the WIM data provided in the LTPP database for the state of Oklahoma and neighbor states.

Figure 118 shows the general traffic data and vehicle distribution for the selected road type. These data are common, typical values, and it can be edited by the user if needed. Figure 119 shows the axle per truck data tab in the traffic dialog.

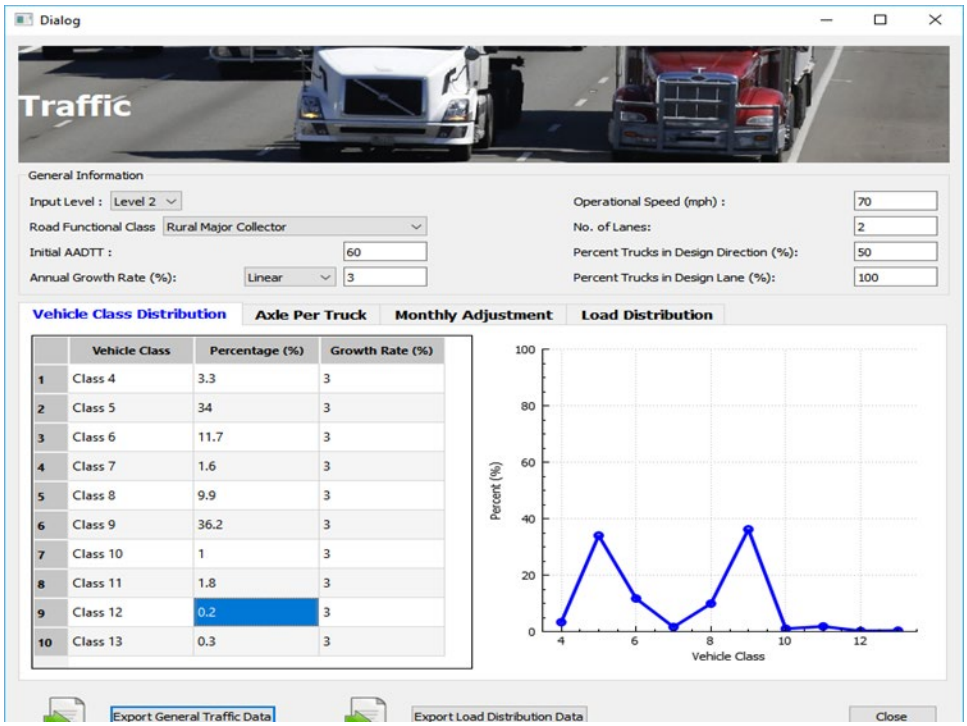

Figure 118- The general traffic and vehicle class distribution tab in the traffic module

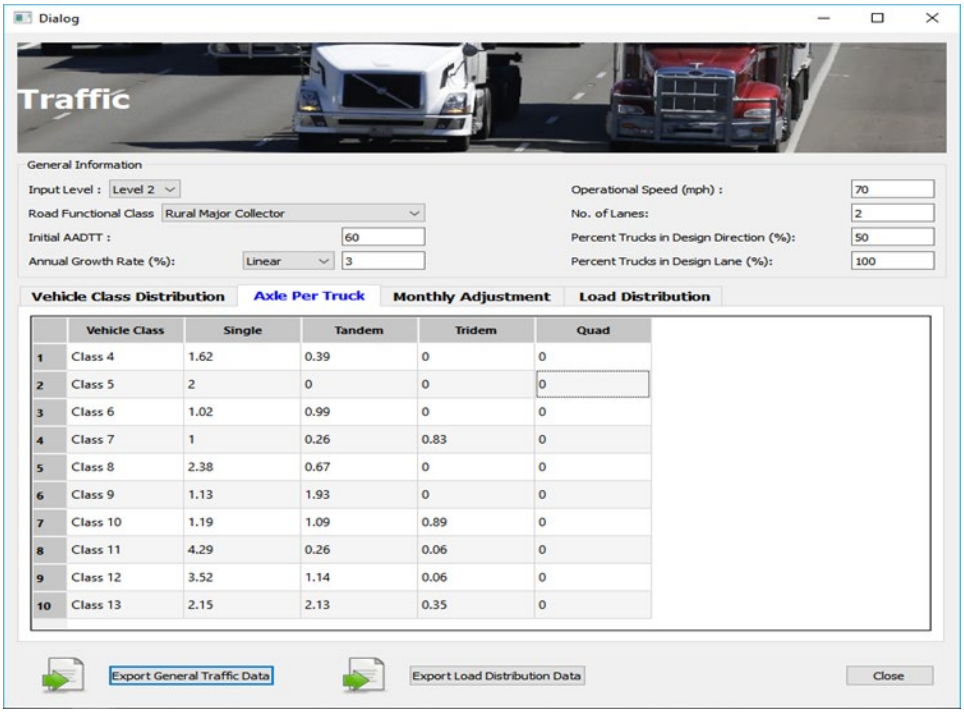

Figure 119- The axle per truck data tab in the traffic module

Figure 120 shows the load distribution tab in the traffic module. This tab provides the load distribution data collected from the WIM data analysis provided in the LTPP database. The load distribution is provided for the single axle, tandem axle, tridem axle, and the quad-axle trucks.

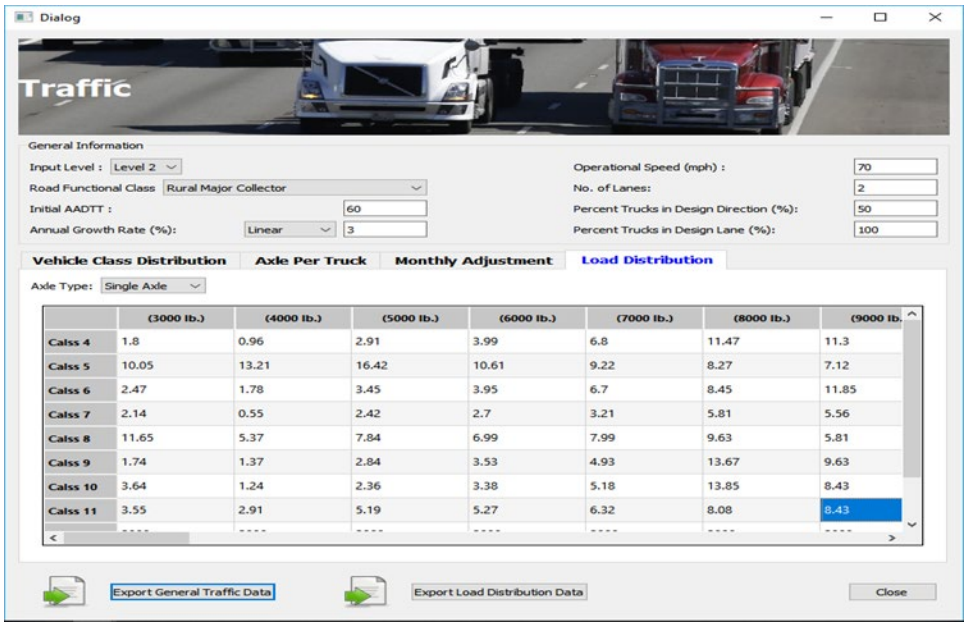

Figure 120- The load distribution tab in the traffic module

By clicking on the “Export General Traffic Data” button, AADTT, vehicle class distribution, axle per truck, and monthly adjustment will be generated. The Pavement ME gets the load distribution data in a different file. Thus these data will be generated separately by clicking on the “Export load distribution Data” button.

Calibration Coefficients

This module provides a summary of the results found in this project. The calibration coefficients were provided in this module for flexible pavement designs. The calibration effort in this study was determined for two sets of calibration coefficients for the east and west regions of the state of Oklahoma. Figure 121 shows the calibration coefficients of the rutting model for East Oklahoma flexible pavements. By clicking on the Export Data button, the calibration coefficients for the flexible and rigid pavements will be generated in an XML file format readable by the Pavement ME.

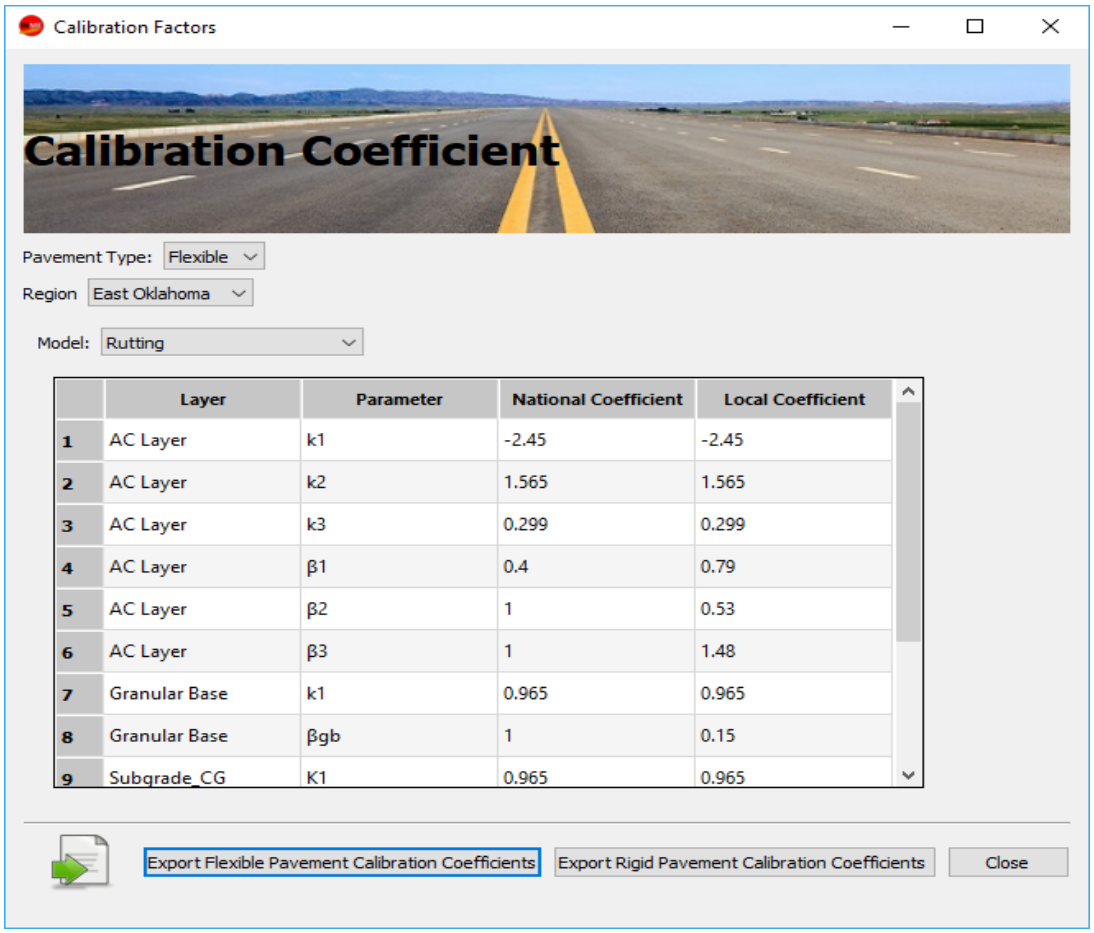

	Layer	Parameter	National Coefficient	Local Coefficient
1	AC Layer	k1	-2.45	-2.45
2	AC Layer	k2	1.565	1.565
3	AC Layer	k3	0.299	0.299
4	AC Layer	β1	0.4	0.79
5	AC Layer	β2	1	0.53
6	AC Layer	β3	1	1.48
7	Granular Base	k1	0.965	0.965
8	Granular Base	βgb	1	0.15
9	Subgrade_CG	K1	0.965	0.965

Figure 121- The calibration coefficient module

CONCLUSIONS AND RECOMMENDATIONS

The focus of this project is to calibrate and implement the Pavement ME Design for application in Oklahoma. The calibration and implementation process are systematically collect design, construction, maintenance and performance data for selected pavement sections, and use these data to adjust the calibration coefficients in the Pavement ME Design software to provide the best agreement between predicted and measured pavement performance.

The objectives of this report include:

- To compile information gathered from past studies relative to Oklahoma in a manner to be used to calibrate the Pavement ME Design;
- To develop material databases that are compatible with the Pavement ME Design software;
- To calibrate Pavement ME Design by adjusting the distress model coefficients to eliminate the bias between predicted and measured pavement performance;

In this study, the Pavement ME design prediction models were calibrated using local inputs and performance data for the state of Oklahoma. The selected projects are representatives of Oklahoma's flexible pavement construction practices and include various pavement conditions, construction age, and environmental conditions. The material, structural, and traffic data were gathered from LTPP, Oklahoma, and related national cooperative highway research program

(NCHRP) datasets. The material input data were evaluated, and the most accurate available datasets were selected. The prediction models were used to estimate level 2 and 3 material properties to generate the database.

After reviewing the input data and running a sensitivity analysis for each parameter, a master input database was developed. For each section, the Pavement ME design analysis was conducted. The predictions from distress and international roughness index (IRI) models were evaluated and compared with the measured distress values, and the accuracy and bias of each model were determined.

The nationally calibrated models show an improper performance and a significant bias, which asserts the need for local calibration. The rutting and IRI models show better performance compared to fatigue bottom-up and top-down and thermal cracking models. The reason for bias and error in the measured versus predicted distress values mainly comes from inaccurate input data, the error in the distress survey, and the accuracy of prediction models. In this effort, the error in prediction models was reduced through the calibration process. This process includes two steps for reducing bias and increasing accuracy. An iterative narrow-down approach was used to determine the calibration coefficient values corresponding to the minimum prediction bias. In this approach, starting from a wide range of coefficients combination, the best range was determined, and in the next steps, the identified ranges were narrowed down to the optimum combination of coefficients. In the next step, the standard error of prediction was decreased by optimizing the coefficients related to the accuracy of models. Finally, the locally calibrated coefficients for the distress and IRI models were determined for the Oklahoma pavement system. The distress and IRI models show that the calibrated coefficients improve the pavement ME predictions and design of flexible pavements in Oklahoma.

After completing the local calibration of the Pavement ME, it is essential to consider taking the next step of the implementation process, which is adopting the locally calibrated models for some routine pavement designs. For this reason, the Pavement ME was used to design the asphalt pavements using the typical material and design parameters of the state of Oklahoma. Three types of conventional flexible pavement design, as well as one perpetual design, were compared in this study. Generally, using calibration coefficients yields lower rutting and higher fatigue cracking. However, the pavement roughness at the end of design life is using the Oklahoma calibration coefficients.

A database of traffic data, climatic data, structure data, material property data, and the corresponding pavement performance/distress data were developed. In this database, the material property data has three hierarchical input levels based on the Pavement ME Design Guide. The INput-ME software program was developed to convert the traffic data, climatic data, structure data, and material property data from the developed ODOT database into the input format of the Pavement ME Design software.This software has a user-friendly interface, which facilitates using of Pavement ME for the pavement designers.

This report has provided the work completed on the rigid pavement part of the ODOT project “Compilation of Local Studies and Regional Calibration of Pavement ME Design for Rigid and Flexible Pavements in Oklahoma.” This document contains completed tasks in terms of extraction and evaluation of LTPP rigid pavement sections data, development of new FWD data analysis to accommodate the lack of visible distresses in the rigid pavement sections , the application of the new FWD data analysis methodology on the CRCP rigid pavement sections as well as the calibration methodology used for CRC and JPC pavements. The new FWD analysis led to the calculation of erosion damage, which was beneficial to establish the

relationship between punchout and erosion damages. This relationship led the research team to introduce a new and dynamic calibration methodology for the Pavement ME punchout model. Although erosion damage has an important role in inducing environmental transverse cracking and longitudinal cracking in JPC pavements, it was not applicable to use the new FWD data analysis for JPCP pavement because pavement ME cracking model considers the transverse cracking induced by mechanical loading and does not account for the erosion damage. The following subsections provide findings of CRC and JPC pavements calibration:

CRC pavement findings:

This study developed a new calibration methodology for the Pavement ME punchout model for CRC pavement applicable, incorporating sections that have shown little or no distress. Relating the punchout distress with erosion damage to validate calibration coefficients was found to be feasible and applicable for a different type of base and subbase materials.
The proposed methodology revealed the following points about the punchout formation and model calibration:

1- Erosion development is a factor in punchout distress, and its relationship to the incidence of punchout distress appears to be represented by a sigmoidal relationship.
2- The time required for punchout formation and the number of punchout depends on the base and subbase layers' inherent resistance to erosion.
3- Assuming that the A factor in the Pavement ME model is equivalent to the ultimate number of punchouts in a given length of CRC pavement appears to be reasonable.
4- The extension of the performance between sections showing distress and those not showing distress was based upon the applicability of extending the %E vs. %PO relationship for the non-distressed pavement sections, which should be further validated in future performance studies of CRC pavement.

The calibration methodology required improving upon FWD analysis to assess the degree of bonding by determining the degradation of shear strength over time as well as estimating the percent of erosion. The percent erosion data provided a useful relationship with the LTPP punchout data. The punchout records were also used to calculate the percent of punchout, which played a crucial role in incorporating field transverse cracking and spacing into the erosion-punchout relationship. The calibration process assumed the C1 and C2 coefficients in the allowable loads to failure model were sufficient for calibration purposes.

JPC Pavement Findings
This study assessed the transverse cracking and faulting models for the Pavement ME software for use in the Oklahoma sections. Unlike the analysis in the punchout model of CRC pavements, performance models of JPC pavements in pavement ME are not related to the erosion damage in the cracking model, while erosion damage is indirectly considered in the complicated faulting model. Therefore, it was not possible to introduce a new calibration methodology for both models. However, it was possible to assess the current models using the acquired field data. The JPC pavement calibration can be summarized as follows:

1. The cracking model with national calibration in pavement ME underestimates the cracking fraction, as it is shown in Figure 103. The national calibration coefficients are still valid to use in the Oklahoma sections. However, as shown in Figure 104 and Figure 105, an accurate set gradient temperature input in the pavement design phase is vital. Also, the use of suitable curing methodology in the site can reduce local conditions and eliminate cracking model coefficients calibration.

2. The national calibrated faulting model can also be used, especially if the erodibility factor of the base and the set gradient are accurately inputted in the design phase. The erodibility factor can control the faulting level while the set gradient is directly affecting the curling and warping deflections calculations. Inaccurate inputs of these factors can induce a significant variability in the Pavement ME faulting prediction.

The calibration of JPC pavements can be performed indirectly by studying the factors that affect model predictions. These factors are (i) the set gradient (which set as default -10ºC), (ii) the associated curling and warping stresses and deflections, and (iii) the proper curing techniques on site. Developing a methodology to determine these inputs as well as standardize the use of curing in on-site construction can effectively reduce the burden of calibration for JPC pavement ME performance models.

REFERENCES

1- Li, Q., et al.,(2011). *Mechanistic-Empirical Pavement Design Guide (MEPDG): a bird's-eye view.* Journal of Modern Transportation, 19(2): p. 114-133.

2- AASHTO,(2008). *Mechanistic-empirical pavement design guide: A manual of practice*. Washington, DC.

3- Brown, S.F., et al.,(2006). *Independent Review of the" Mechanistic-Empirical Pavement Design Guide" and Software.* NCHRP research results digest, (307).

4- AASHTO,(2015). *Mechanistic-empirical pavement design guide: A manual of practice*. Second ed. Washington, DC.

5- Sakhaeifar, M.S., Kim, Y.R. and,Kabir, P.,(2015). *New predictive models for the dynamic modulus of hot mix asphalt.* Journal of Construction Building Materials, 76: p. 221-231.

6- Kim, Y.R., et al.,(2011). *LTPP computed parameter: dynamic modulus*.

7- ARA, I., ERES Consultants Division,(2004). *Guide for Mechanistic-Empirical Design of New and Rehabilitated Pavement Structures*. Washington, DC.1-37A

8- Barksdale, R.D., et al.,(1997). *Laboratory determination of resilient modulus for flexible pavement design*.

9- Ceylan, H., Gopalakrishnan, K. and,Kim, S.,(2009). *Characterization of unbound materials (soils/aggregates) for mechanistic-empirical pavement design guide*.

10- Yau, A. andVon Quintus, H.L.,(2002). *Study of LTPP laboratory resilient modulus test data and response characteristics*.

11- Hossain, Z., et al.,(2011). *Development of flexible pavement database for local calibration of MEPDG*. Oklahoma Department of Transportation, Oklahoma City, OK.ODOT SPR 2209.

12- Kim, D. andSiddiki, N.Z.,(2006). *Simplification of resilient modulus testing for subgrades.*

13- George, K.,(2004). *Prediction of resilient modulus from soil index properties.*

14- Yeh, S.-T. andSu, C.-K.,(1989). *Resilient properties of Colorado soils*. Colorado Department of Highways.

15- Gu, F., et al.,(2014). *Estimation of resilient modulus of unbound aggregates using performance-related base course properties.* Journal of Materials in Civil Engineering, 27(6): p. 04014188.

16- Snethen, D.R., Miller, G.A. and,Cerato, A.B.,(2008). *Evaluation and field verification of strength and structural improvement of chemically stabilized subgrade soil*.

17- Li, J.Q., Wang, K.C. and,Lou, J.,(2016). *Impact of time coverage of traffic data collection on Pavement ME Design.* International Journal of Pavement Research Technology, 9(1): p. 1-13.

18- International, A.,(2017). *Standard Specification for Highway Weigh-In-Motion (WIM) Systems with User Requirements and Test Methods*. ASTM E1318-09: West Conshohocken, PA.

19- 2017). *CDOT M-E Pavement Design Manuals*. Colorado Department of Transportation.

20- Vandervalk-Ostrander, A.,(2009). *AASHTO Guidelines for Traffic Data Programs*. Washington, DC: AASHTO.

21- Von Quintus, H.L.,(2012). *Calibration of rutting models for structural and mix design*. Vol. 719. Transportation Research Board.

22- Kaloush, K. andWitczak, M.,(2000). *Development of a permanent to elastic strain ratio model for asphalt mixtures.* Development of the guide for the design of new rehabilitated pavement structures. NCHRP: p. 1-37.

23- Kosmatka, S. andPanarese, W.C.,(1988). *Design and control of concrete mixtures*.

24- Khazanovich, L., Tayabji, S.D. and,Darter, M.I.,(2001). *Backcalculation of layer parameters for LTPP test sections, Volume 1: Slab on elastic solid and slab on dense-liquid foundation analysis of rigid pavements.*

25- Pierce, L.M. andMcGovern, G.,(2014). *Implementation of the AASHTO mechanistic-empirical pavement design guide and software*.

26- Sakhaeifar, M.S., et al.,(2015). *Selection of Long Lasting Rehabilitation Treatment Using Life Cycle Cost Analysis and Present Serviceability Rating*. FHWA-OK-15-06. Oklahoma Department of Transportation, Materials and Research Division Oklahoma City, OK.

27- Federal Highway Administration—Office of Research, D., and Technology: Infrastructure R&D,(2015). *THE LONG-TERM PAVEMENT PERFORMANCE PROGRAM*. Washington, DC.FHWA-HRT-15-049.

28- Cross, S.A., Jakatimath, Y. and,KC, S.,(2007). *Determination of dynamic modulus master curves for Oklahoma HMA mixtures*. Oklahoma Department of Transportation, Oklahoma City, OK.ODOT SPR 2177.

29- Saha, S., et al.,(2018). *Use of an Artificial Neural Network Approach for the Prediction of Resilient Modulus for Unbound Granular Material.* Transportation Research Record: p. 0361198118756881.

30- *USDA soil survey*. 2018; Available from: https://websoilsurvey.sc.egov.usda.gov/App/HomePage.htm.

31- Witczak, M., Zapata, C. and,Houston, W.,(2006). *Models incorporated into the current enhanced integrated climatic model: NCHRP 9-23 project findings and additional changes after version 0.7*. Project NCHRP.

32- *The Oklahoma Water Resource Board*. 1998-2018; Available from: https://www.owrb.ok.gov/.

33- Cross, S.A., Jakatimath, Y. and,KC, S.,(2007). *Determination of dynamic modulus master curves for Oklahoma HMA mixtures*.

34- Schwartz, C.W., et al.,(2011). *Sensitivity evaluation of MEPDG performance prediction*. Transportation Research Board of the National Academies.NCHRP 1-47.

35- Cross, S.A., Gibbe, R. and,Aryal, N.,(2011). *Development of a Flexible Pavement Database for Local Calibration of the MEPDG, Part 2 Evaluation of ODOT SMA Mixtures*. Oklahoma Department of Transportation, Oklahoma City, OK.ODOT SPR 2209.

36- Singh, D., Zaman, M. and,Commuri, S.,(2011). *Evaluation of predictive models for estimating dynamic modulus of hot-mix asphalt in Oklahoma.* Transportation Research Record: Journal of the Transportation Research Board, (2210): p. 57-72.

37- Lekarp, F., Isacsson, U. and,Dawson, A.,(2000). *State of the art. I: Resilient response of unbound aggregates.* Journal of transportation engineering, 126(1): p. 66-75.

38- Fredlund, D.G. andXing, A.,(1994). *Equations for the soil-water characteristic curve.* Canadian geotechnical journal, 31(4): p. 521-532.

39- Saha, S., et al.,(2018). *Prediction of Soil-Water Characteristic Curve for Unbound Material Using Fredlund–Xing Equation-Based ANN Approach.* Journal of Materials in Civil Engineering, 30(5): p. 06018002.

40- *Oklahoma Climatological Survey*. Available from: https://climate.ok.gov/index.php/site/page/climate_of_oklahoma.

41- Darter, M.I., et al.,(2014). *Calibration and Implementation of the AASHTO Mechanistic-Empirical Pavement Design Guide in Arizona*. Arizona Department of Transportation.FHWA-AZ-14-606.

42- Wang, K.C., et al. *Pavement ME Design distress modeling for Oklahoma*. in *T&DI Congress: Planes, Trains, and Automobiles*. 2014. Orlando, Florida.

43- Mallela, J., et al.,(2013). *Implementation of the AASHTO mechanistic-empirical pavement design guide for Colorado*. Colorado. Dept. of Transportation. Research Branch, Denver, CO.CDOT-2013-4.

44- Ceylan, H., et al.,(2015). *Investigation of AASHTOWare Pavement ME Design/Darwin-ME™ Performance Prediction Models for Iowa Pavement Analysis and Design*. Iowa Department of Transportation, Ames, IA.Project 14-496.

45- Hall, K.D., Xiao, D.X. and,Wang, K.C.,(2011). *Calibration of the Mechanistic–Empirical Pavement Design Guidefor Flexible Pavement Design in Arkansas.* J Transportation Research Record, 2226(1): p. 135-141.

46- Muthadi, N. andKim, Y.,(2008). *Local calibration of mechanistic-empirical pavement design guide for flexible pavement design.* Transportation Research Record: Journal of the Transportation Research Board, (2087): p. 131-141.

47- Robbins, M.M., et al.,(2017). *Pavement ME Design–A Summary of Local Calibration Efforts for Flexible Pavements*.

48- Elkins, G., et al.,(2015). *Long-term pavement performance information management system user guide*. Publication No. FHWA-RD-03-088, Office of Infrastructure Research and Development, Federal Highway Administration, Washington, DC.

49- Kim, S., et al.,(2014). *Calibration of pavement ME design and mechanistic-empirical pavement design guide performance prediction models for Iowa pavement systems.* Journal of transportation engineering, 140(10): p. 04014052.

50- Yang, X., et al.,(2018). *Development and Implementation of an MEPDG for Rigid Pavements, Phase 3*.

51- Miller, J.S. andBellinger, W.Y.,(2014). *Distress identification manual for the long-term pavement performance program*.

52- Darter, M.I., LaCoursiere, S.A. and,Smiley, S.A.,(1979). *Structural Distress Mechanisms in Continuously Reinforced Concrete Pavement.* J Transportation Research Record, (715).

53- Selezneva, O., Zollinger, D. and,Darter, M. *Mechanistic analysis of factors leading to punchout development for improved CRCP design procedures*. in *Seventh International Conference on Concrete Pavements. The Use of Concrete in Developing Long-Lasting Pavement Solutions for the 21st Century. International Society for Concrete Pavements*. 2001.

54- Selezneva, O., et al.,(2004). *Development of a mechanistic-empirical structural design procedure for continuously reinforced concrete pavements.* J Transportation Research Record, 1896(1): p. 46-56.

55- Zollinger, D., et al.,(1998). *Performance of CRCP Volume 6-CRCP Design, Construction, and Performance.* J FHWA-RD-97-151, Report, Washington, DC.

56- Bustos, M., et al.,(2011). *Calibration of Distress Models from the Mechanistic–Empirical Pavement Design Guide for Rigid Pavement Design in Argentina.* Journal of the Transportation Research Board, 2226(1): p. 3-12.

57- Li, J., et al.,(2006). *Calibration of NCHRP 1–37A software for the Washington State Department of Transportation: Rigid pavement portion.* J Transportation research record, 1949(1): p. 43-53.

58- Rao, C., et al.,(2004). *Calibration of mechanistic-empirical performance model for continuously reinforced concrete pavement punch-outs.* J Transportation Research Record, 1896(1): p. 15-22.

59- Kim, S., et al.,(2010). *Use of Pavement Management Information System for Verification of Mechanistic–Empirical Pavement Design Guide Performance Predictions.* J Transportation Research Record, 2153(1): p. 30-39.

60- Smith, B. andNair, H.,(2015). *Development of local calibration factors and design criteria values for mechanistic-empirical pavement design*. FHWA, U.S. Department of Transportation.

61- Zollinger, D. andBarenberg, E.,(1990). *Continuously Reinforced Pavements: Punchouts and Other Distresses and Implications for Design*. Illinois Cooperative Highway Research Program, , University of Illinois at Urbana-Champaign.

62- Van Wijk, A.J. andLovell, C.W.,(1985). *Prediction of subbase erosion caused by pavement pumping.* Journal of the Transportation Research Board, (1099): p. 45-57.

63- Rauhut, J., Lytton, R. and,Darter, M.,(1984). *Pavement damage functions for cost allocation. vol 1: damage functions and load equivalence factors.*

64- Markow, M. andBrademeyer, B.,(1984). *EAROMAR VERSION 2. FINAL TECHNICAL REPORT*. FHWA, U.S. Department of Transportation.

65- Packard, R.G.,(1984). *Thickness design for concrete highway and street pavements.* Portland Cement Association, Skokie, Illinois.

66- Jeong, J.-H. andZollinger, D.,(2001). *Characterization of stiffness parameters in design of continuously reinforced and jointed pavements.* Transportation Research Record: Journal of the Transportation Research Board, (1778): p. 54-63.

67- Jung, Y., Zollinger, D. and,Ehsanul, B.,(2012). *Improved mechanistic-empirical continuously reinforced concrete pavement design approach with modified punchout model.* Transportation Research Record: Journal of the Transportation Research Board, (2305): p. 32-42.

68- Bari, M.E. andZollinger, D.G.,(2016). *New concepts for the assessment of concrete slab interfacial effects in pavement design and analysis.* J International Journal of Pavement Engineering, 17(3): p. 233-244.

69- Scullion, T. andSmith, R.,(1997). *TxDOT's pavement management information system: current status and future directions*. Texas. Dept. of Transportation.

70- Gharaibeh, N., et al.,(2012). *Evaluation and development of pavement scores, performance models and needs Estimates for the TxDOT Pavement Management Information System*. FHWA. U.S. Department of Transportation.

71- Company, T.Q.; Available from: https://www.qt.io/.

APPENDIX A. SUMMARY OF LTPP SECTION

LTPP Section Number	Experiment Number	Monitoring Status	County	Route	Direction	Longitude	Pavement Structure	Surface Type	Functional Class	No. of Lanes	Climatic Zone	Date of Const.	Data included in LTPP
40-0113	SPS-1	Out-of-study (15-JUN-08)	COMANCHE	U. S.62	EB	34.63446, -98.68509	Flexible	AC	RPA-O	2	Wet, Non-Freeze	35612	35065
40-0114	GPS-6S	ACTIVE	COMANCHE	U. S.62	EB	34.63196, -98.70585	Flexible	AC	RPA-O	2	Wet, Non-Freeze	35612	35065
40-0115	GPS-6S	ACTIVE	COMANCHE	U. S.62	EB	34.63367, -98.69167	Flexible	AC	RPA-O	2	Wet, Non-Freeze	35612	35065
40-0116	GPS-6S	ACTIVE	COMANCHE	U. S.62	EB	34.63339, -98.69431	Flexible	AC	RPA-O	2	Wet, Non-Freeze	35612	35065
40-0117	GPS-6S	ACTIVE	COMANCHE	U. S.62	EB	34.63405, -98.68867	Flexible	AC	RPA-O	2	Wet, Non-Freeze	35612	35065
40-0118	GPS-6S	ACTIVE	COMANCHE	U. S.62	EB	34.63307, -98.69695	Flexible	AC	RPA-O	2	Wet, Non-Freeze	35612	35065
40-0119	GPS-6S	ACTIVE	COMANCHE	U. S.62	EB	34.63559, -98.67521	Flexible	AC	RPA-O	2	Wet, Non-Freeze	35612	35065
40-0120	GPS-6S	ACTIVE	COMANCHE	U. S.62	EB	34.63599, -98.67161	Flexible	AC	RPA-O	2	Wet, Non-Freeze	35612	35065
40-0121	GPS-6S	ACTIVE	COMANCHE	U. S.62	EB	34.63655, -98.6673	Flexible	AC	RPA-O	2	Wet, Non-Freeze	35612	35065
40-0122	SPS-1	Out-of-study (15-JUN-08)	COMANCHE	U. S.62	EB	34.63476, -98.68243	Flexible	AC	RPA-O	2	Wet, Non-Freeze	35612	35065
40-0123	GPS-6S	ACTIVE	COMANCHE	U. S.62	EB	34.63691, -98.664	Flexible	AC	RPA-O	2	Wet, Non-Freeze	35612	35065
40-0124	GPS-6S	ACTIVE	COMANCHE	U. S.62	EB	34.63726, -98.66103	Flexible	AC	RPA-O	2	Wet, Non-Freeze	35612	35065
40-0160	GPS-6S	ACTIVE	COMANCHE	U. S.62	EB	34.63162, -98.70947	Flexible	AC	RPA-O	2	Wet, Non-Freeze	35612	35065
40-0501	SPS-5	Out-of-study (15-JUL-07)	COMANCHE	U. S.62	WB	34.63768, -98.65946	Flexible	AC	RPA-O	2	Wet, Non-Freeze	26846	31778

LTPP Section Number	Experiment Number	Monitoring Status	County	Route	Direction	Longitude	Pavement Structure	Surface Type	Functional Class	No. of Lanes	Climatic Zone	Date of Const.	Data included in LTPP
40-0502	GPS-6S	ACTIVE	COMANCHE	U. S.62	WB	34.63733, -98.66239	Flexible	AC	RPA-O	2	Wet, Non-Freeze	26846	31778
40-0503	GPS-6S	ACTIVE	COMANCHE	U. S.62	WB	34.63695, -98.66575	Flexible	AC	RPA-O	2	Wet, Non-Freeze	26846	31778
40-0504	GPS-6S	ACTIVE	COMANCHE	U. S.62	WB	34.63414, -98.69014	Flexible	AC	RPA-O	2	Wet, Non-Freeze	26846	31778
40-0505	GPS-6S	ACTIVE	COMANCHE	U. S.62	WB	34.63353, -98.6953	Flexible	AC	RPA-O	2	Wet, Non-Freeze	26846	31778
40-0506	GPS-6S	ACTIVE	COMANCHE	U. S.62	WB	34.6352, -98.68086	Flexible	AC	RPA-O	2	Wet, Non-Freeze	26846	31778
40-0507	GPS-6S	ACTIVE	COMANCHE	U. S.62	WB	34.63445, -98.68716	Flexible	AC	RPA-O	2	Wet, Non-Freeze	26846	31778
40-0508	GPS-6S	ACTIVE	COMANCHE	U. S.62	WB	34.63644, -98.67006	Flexible	AC	RPA-O	2	Wet, Non-Freeze	26846	31778
40-0509	GPS-6S	ACTIVE	COMANCHE	U. S.62	WB	34.63602, -98.67363	Flexible	AC	RPA-O	2	Wet, Non-Freeze	26846	31778
40-0560	GPS-6S	ACTIVE	COMANCHE	U. S.62	WB	34.63242, -98.70435	Flexible	AC	RPA-O	2	Wet, Non-Freeze	26846	31778
40-1015	GPS-2	Out-of-study (15-JUN-08)	SEMINOLE	State-3	NB	35.19324, -96.67488	Flexible	AC	RMA	2	Wet, Non-Freeze	28581	31778
40-1017	GPS-2	Out-of-study (01-MAY-96)	MUSKOGEE	U. S.-2	NB	35.79766, -95.40127	Flexible	AC	RPA-O	2	Wet, Non-Freeze	29860	31778
40-4086	GPS-6D	Out-of-study (01-MAR-16)	GRADY	U. S.-2	SB	35.07572, -97.96171	Flexible	AC	RMA	1	Wet, Non-Freeze	25720	31778
40-4087	GPS-6C	Out-of-study (15-JUN-07)	JACKSON	U. S.-2	EB	34.63757, -99.28864	Flexible	AC	RPA-O	2	Wet, Non-Freeze	31503	31778
40-4088	GPS-2	Out-of-study	KAY	U. S.-2	EB	36.68829, -97.26922	Flexible	AC	RPA-O	2	Wet, Non-Freeze	27546	31778

LTPP Section Number	Experiment Number	Monitoring Status	County	Route	Direction	Longitude	Pavement Structure	Surface Type	Functional Class	No. of Lanes	Climatic Zone	Date of Const.	Data included in LTPP
		(15-MAY-95)											
40-4154	GPS-6S	ACTIVE	GRADY	U. S.-2	SB	34.75062, -97.95845	Flexible	AC	RMA	2	Wet, Non-Freeze	32509	32508
40-4161	GPS-2	Out-of-study (01-MAY-98)	CARTER	U. S.-2	WB	34.11571, -97.0396	Flexible	AC	RPA-O	1	Wet, Non-Freeze	30773	31778
40-4163	GPS-6S	Out-of-study (15-JUL-09)	BLAINE	U. S.-2	WB	35.84163, -98.47516	Flexible	AC	RPA-O	2	Wet, Non-Freeze	31868	31867
40-4164	GPS-6B	Out-of-study (15-JUL-10)	MAJOR	U. S.-2	SB	36.3316, -98.47982	Flexible	AC	RMA	1	Wet, Non-Freeze	28611	31778
40-4165	GPS-2	Out-of-study (07-DEC-07)	MAJOR	U. S.-2	WB	36.39117, -98.2855	Flexible	AC	RPA-O	1	Wet, Non-Freeze	30834	31778
40-6010	GPS-6A	Out-of-study (30-SEP-99)	LE FLORE	State-3	EB	35.12531, -94.56988	Flexible	AC	RMC	1	Wet, Non-Freeze	25720	31778
40-A320	SPS-3	Out-of-study (16-SEP-97)	JACKSON	U. S.-2	EB	34.63757, -99.28348	Flexible	AC	RPA-O	2	Wet, Non-Freeze	31503	31778
40-A330	SPS-3	Out-of-study (16-SEP-97)	JACKSON	U. S.-2	EB	34.63758, -99.2811	Flexible	AC	RPA-O	2	Wet, Non-Freeze	31503	31778
40-A340	SPS-3	Out-of-study (16-SEP-97)	JACKSON	U. S.-2	EB	34.63755, -99.27875	Flexible	AC	RPA-O	2	Wet, Non-Freeze	31503	31778

LTPP Section Number	Experiment Number	Monitoring Status	County	Route	Direction	Longitude	Pavement Structure	Surface Type	Functional Class	No. of Lanes	Climatic Zone	Date of Const.	Data included in LTPP
40-A350	SPS-3	Out-of-study (16-SEP-97)	JACKSON	U. S.-2	EB	34.63756, -99.27617	Flexible	AC	RPA-O	2	Wet, Non-Freeze	31503	31778
40-AA01	SPS-10	ACTIVE	CANADIAN	State-3	WB	35.50806, -97.79262	Flexible	AC	UPA-O	2	Wet, Non-Freeze	42309	42064
40-AA02	SPS-10	ACTIVE	CANADIAN	State-3	WB	35.50802, -97.79927	Flexible	AC	UPA-O	2	Wet, Non-Freeze	42309	42064
40-AA03	SPS-10	ACTIVE	CANADIAN	State-3	WB	35.50798, -97.80479	Flexible	AC	UPA-O	2	Wet, Non-Freeze	42309	42064
40-AA61	SPS-10	ACTIVE	CANADIAN	State-3	WB	35.508, -97.80959	Flexible	AC	UPA-O	2	Wet, Non-Freeze	42309	42064
40-AA62	SPS-10	ACTIVE	CANADIAN	State-3	WB	35.508, -97.81493	Flexible	AC	UPA-O	2	Wet, Non-Freeze	42309	42064
40-AA63	SPS-10	ACTIVE	CANADIAN	State-3	WB	35.50797, -97.82235	Flexible	AC	UPA-O	2	Wet, Non-Freeze	42309	42064
40-B310	SPS-3	Out-of-study (30-JAN-06)	SEMINOLE	State-3	NB	35.19527, -96.67493	Flexible	AC	RMA	2	Wet, Non-Freeze	28581	31778
40-B320	SPS-3	Out-of-study (30-JAN-06)	SEMINOLE	State-3	NB	35.19747, -96.67486	Flexible	AC	RMA	2	Wet, Non-Freeze	28581	31778
40-B330	SPS-3	Out-of-study (30-JAN-06)	SEMINOLE	State-3	NB	35.19929, -96.67478	Flexible	AC	RMA	2	Wet, Non-Freeze	28581	31778
40-B350	SPS-3	Out-of-study (30-JAN-06)	SEMINOLE	State-3	NB	35.20702, -96.67484	Flexible	AC	RMA	2	Wet, Non-Freeze	28581	31778
40-B360	SPS-3	Out-of-study (30-JAN-06)	SEMINOLE	State-3	NB	35.20922, -96.67463	Flexible	AC	RMA	2	Wet, Non-Freeze	28581	31778

LTPP Section Number	Experiment Number	Monitoring Status	County	Route	Direction	Longitude	Pavement Structure	Surface Type	Functional Class	No. of Lanes	Climatic Zone	Date of Const.	Data included in LTPP
40-C310	SPS-3	Out-of-study (22-JUN-95)	KAY	U. S.-2	EB	36.68833, -97.27386	Flexible	AC	RPA-O	2	Wet, Non-Freeze	27546	31778
40-C320	SPS-3	Out-of-study (22-JUN-95)	KAY	U. S.-2	EB	36.68827, -97.26541	Flexible	AC	RPA-O	2	Wet, Non-Freeze	27546	31778
40-C330	SPS-3	Out-of-study (22-JUN-95)	KAY	U. S.-2	EB	36.68826, -97.26268	Flexible	AC	RPA-O	2	Wet, Non-Freeze	27546	31778
40-C350	SPS-3	Out-of-study (22-JUN-95)	KAY	U. S.-2	EB	36.68825, -97.26008	Flexible	AC	RPA-O	2	Wet, Non-Freeze	27546	31778